ISSN 2307-8960 (online)

World Journal of *Clinical Cases*

World J Clin Cases 2019 April 26; 7(8): 908-1005

Published by Baishideng Publishing Group Inc

World Journal of Clinical Cases

Contents

Semimonthly Volume 7 Number 8 April 26, 2019

REVIEW

MINIREVIEWS

ORIGINAL ARTICLE

Retrospective Study

Observational Study

CASE REPORT

World Journal of Clinical Cases
Volume 7 Number 8 April 26, 2019

Contents

NAME OF JOURNAL
World Journal of Clinical Cases

ISSN
ISSN 2307-8960 (online)

LAUNCH DATE
April 16, 2013

FREQUENCY
Semimonthly

EDITORS-IN-CHIEF
Dennis A Bloomfield, Sandro Vento

EDITORIAL BOARD MEMBERS
https://www.wjgnet.com/2307-8960/editorialboard.htm

EDITORIAL OFFICE
Jin-Lei Wang, Director

PUBLICATION DATE
April 26, 2019

INSTRUCTIONS TO AUTHORS
https://www.wjgnet.com/bpg/gerinfo/204

GUIDELINES FOR ETHICS DOCUMENTS
https://www.wjgnet.com/bpg/GerInfo/287

GUIDELINES FOR NON-NATIVE SPEAKERS OF ENGLISH
https://www.wjgnet.com/bpg/gerinfo/240

PUBLICATION MISCONDUCT
https://www.wjgnet.com/bpg/gerinfo/208

ARTICLE PROCESSING CHARGE
https://www.wjgnet.com/bpg/gerinfo/242

STEPS FOR SUBMITTING MANUSCRIPTS
https://www.wjgnet.com/bpg/GerInfo/239

ONLINE SUBMISSION
https://www.f6publishing.com

World Journal of Clinical Cases

Submit a Manuscript: https://www.f6publishing.com

World J Clin Cases 2019 April 26; 7(8): 908-916

DOI: 10.12998/wjcc.v7.i8.908

ISSN 2307-8960 (online)

REVIEW

Exosomes in esophageal cancer: A review on tumorigenesis, diagnosis and therapeutic potential

Lin-Lin Su, Xiao-Jing Chang, Huan-Di Zhou, Liu-Bing Hou, Xiao-Ying Xue

ORCID number: Lin-Lin Su (0000-0003-0488-618x); Xiao-Jing Chang (0000-0001-6277-3883); Huan-Di Zhou (0000-0002-2617-6157); Liu-Bing Hou (0000-0003-2018-8103); Xiao-Ying Xue (0000-0002-4934-2904).

Author contributions: All authors provided intellectual input for this manuscript; Su LL drafted the paper; Chang XJ and Hou LB revised and improved this article; Zhou HD and Xue XY proposed the idea and made critical revisions; All authors read and approved the final manuscript.

Supported by the Natural Science Foundation of Hebei Province, NO. H2018206307.

Conflict-of-interest statement: Authors declare no conflict of interests for this article.

Manuscript source: Unsolicited manuscript

Received: December 28, 2018

Lin-Lin Su, Xiao-Jing Chang, Huan-Di Zhou, Liu-Bing Hou, Xiao-Ying Xue, Department of Radiotherapy, The Second Hospital of Hebei Medical University, Shijiazhuang 050000, Hebei Province, China

Huan-Di Zhou, Liu-Bing Hou, Department of Central Laboratory, The Second Hospital of Hebei Medical University, Shijiazhuang 050000, Hebei Province, China

Corresponding author: Xiao-Ying Xue, MD, PhD, Professor, Department of Radiotherapy, The Second Hospital of Hebei Medical University, NO.215 Heping West Road, Shijiazhuang 050000, Hebei Province, China. xxy0636@163.com
Telephone: +86-311-66003709

Abstract

Exosomes are nanovesicles secreted from various types of cells and can be isolated from various bodily fluids, such as blood and urine. The number and molecular contents, including proteins and RNA of exosomes, have been shown to reflect their parental cell origins, characteristics and biological behaviors. An increasing number of studies have demonstrated that exosomes play a role in the course of tumorigenesis, diagnosis, treatment and prognosis, although its precise functions in tumors are still unclear. Moreover, owing to a lack of a standard approach, exosomes and its contents have not yet been put into clinical practice successfully. This review aims to summarize the current knowledge on exosomes and its contents in esophageal cancer as well as the current limitations/challenges in its clinical application, which may provide a basis for an all-around understanding of the implementation of exosomes and exosomal contents in the surveillance and therapy of esophageal cancer.

Key words: Exosome; Esophageal cancer; Tumorigenesis; Biomarker; Therapeutic potential

Core tip: The exosome is a popular area of current research. Numerous studies have shown that exosomes may play an important role in the progression of esophageal cancer, but have not yet been applied to the clinic. This review systemically summarized the current knowledge on exosomes and its contents in esophageal cancer and pointed out the current limitations in its clinical application. This paper may provide a basis for an all-around understanding of the implementation of exosomes in esophageal cancer.

Peer-review started: December 29, 2018
First decision: January 18, 2019
Revised: February 28, 2019
Accepted: March 8, 2019
Article in press: March 9, 2019
Published online: April 26, 2019

P-Reviewer: Aurello P, Khuroo MS
S-Editor: Wang JL
L-Editor: Filipodia
E-Editor: Wu YXJ

Citation: Su LL, Chang XJ, Zhou HD, Hou LB, Xue XY. Exosomes in esophageal cancer: A review on tumorigenesis, diagnosis and therapeutic potential. *World J Clin Cases* 2019; 7(8): 908-916
URL: https://www.wjgnet.com/2307-8960/full/v7/i8/908.htm
DOI: https://dx.doi.org/10.12998/wjcc.v7.i8.908

INTRODUCTION

Exosomes were first discovered by Johnstone and Pan while studying the transformation from reticulocyte to mature red blood cells in 1987. Originally, exosomes were considered a form of waste discharge in the process of reticulocytes differentiating into mature red blood cells. Interestingly, further studies found that exosomes from intracellular multivesicular bodies that fuse with cell membranes and then released into the extracellular matrix are membrane nanoscale vesicles with a diameter of 50-150 nm and have a lipid bilayer membrane structure[1]. Moreover, studies have found that exosomes can be secreted from a variety of cells including red blood cells, T cells, B cells, dendritic cells and tumor cells[2-5] and are widely distributed in various body fluids, such as blood, urine, saliva and milk.

Exosomes contain various types of biologically active substances, including proteins, lipids, DNA fragments and RNA, such as microRNA (miR), circular RNAs (circRNAs), long non-coding RNA and mRNA[6]. Researchers found that these biologically active substances contained within the exosomes may participate in the immune response, antigen presentation, intercellular communication, transport of proteins and RNA and many other physiological processes[7-9]. It suggested that exosomes are a crucial intercellular organelle and communication media. Thus, exosomes may play a pivotal role in the diagnosis and therapy of various diseases including tumors.

There were 455800 newly diagnosed esophageal cancer (EC) patients and 400200 deaths worldwide in 2012[10]. Just in China, there were approximately 477900 new cases and 375000 deaths in 2015[11]. Recent studies have shown that exosomes secreted from various cells including tumor cells, irradiated T cells[12] or tumor associated fibroblasts[13] and exosomal contents may play important roles in EC development. Therefore, exosomes may be of value as a diagnostic/prognostic tool and as a therapeutic target in EC (Figure 1).

PubMed, MEDLINE advanced search builder and Geenmedical was used for this review's literature search. The terms searched were "exosome" and "esophageal cancer," and the time period was restricted from 2008 to 2018. Then we further screened the retrieved articles according to (1) the formation and regulation of exosomes and (2) the research progress of exosomes in EC. Cross references were also screened for papers relevant to this paper. Here we reviewed relevant articles from the last 10 years with the aim of summarizing the function of exosomes in tumorigenesis, diagnosis and treatment of EC (Table 1).

EXOSOME AND ESOPHAGEAL CANCER TUMORIGENESIS

Recent studies found that exosomes derived from many cancer cell types, including glioblastoma[14], tongue cancer[15], thyroid carcinoma[15], breast cancer[17], EC[18], *etc*, may play a crucial part in the course of tumor formation and cancer metastasis by transfer of exo-miRNA, exo-circRNA, exo-DNA and exo-protein.

Promotion of tumor proliferation

Researchers have found that exosomes are involved in tumor proliferation by transferring exo-microRNA. MiR-93-5p[18] can be transferred between EC9706 cells by exosomes and may downregulate the expression of p21 and Cyclin D1 through the PTEN/PI3K/Akt pathway to promote the proliferation of EC cells. Ke *et al*[19] found that the overexpression of miR-25 and miR-210 in EV–Co-Cultured (EV: the extracellular vesicle secreted from esophageal adenocarcinoma (EA) cells) gastroids decreased the mRNA levels of PTEN and AIFM3, respectively, which are known tumor suppressor genes[20,21].

Promotion of invasion and metastasis of tumors

Exosomes and epithelial-mesenchymal transition: A large number of studies have

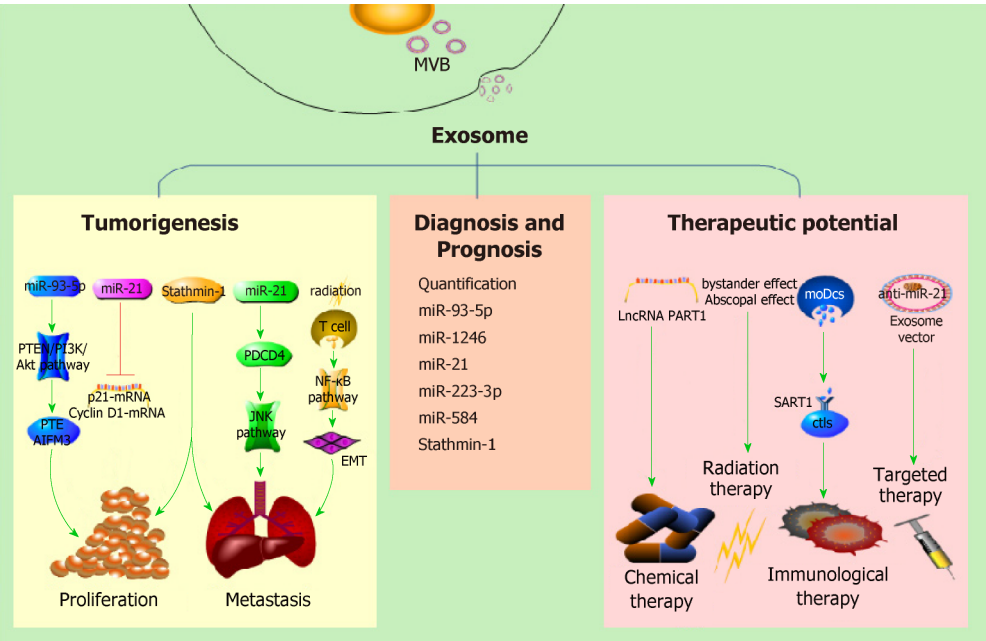

Figure 1 The role of exosomes in esophageal cancer. CTLs: Cytotoxic T lymphocytes; MVB: Intracellular multivesicular body. Red line and cross bar: Inhibit; Green arrow: Promote.

indicated that epithelial-mesenchymal transition (EMT) is closely related to cancer metastasis[22-26]. Recent studies found that exosomes may be involved in the course of tumor metastasis by EMT. Min *et al*[12] found that exosomes derived from irradiated T cells showed the potential role of promoting metastasis of TE13 cells *in vitro*, possibly by promoting EMT through regulating β-catenin and the NF-κB/snail pathway. A recent study demonstrated that overexpression of exosomal circPRMT5 in urothelial carcinoma of the bladder tissues could also promote the EMT process *in vivo* and *in vitro* through the miR-30c sponge[27]. However, exosomal circRNA has not been reported in the pathogenesis of EC. Thus, further studies on the relationship of exo-circRNA and EMT in tumors is needed.

MiR-21: A study has shown a high expression of miR-21 in EC cells and the exosomes secreted by them, and the expression of miR-21 is higher in exosomes than in their donor cells[28,29]. Exosome-shuttling miR-21 overexpression from parental cells could target programmed cell death 4 protein thus activating its downstream c-Jun N-terminal kinase signaling pathway and distinctly promote the migration and invasion of recipient cells.

Stathmin-1: Stathmin-1 is a microtubule-destabilizing cytosolic phosphoprotein that plays an important role in tumor cell proliferation and migration and may be regulated by miR-34a[30,31], miR-223[32] and miR-193b[33]. It is associated with cancer metastasis and poor prognosis in osteosarcoma[31,34], prostate cancer[35,36], head and neck squamous cell carcinoma[37], hepatocellular carcinoma[32], colorectal cancer[33,38], gallbladder carcinoma[39] and non-small-cell lung cancer[40]. In esophageal squamous cell carcinoma (ESCC), stathmin-1 is also vital for ESCC invasiveness and predicts a poor prognosis[41]. Knockdown stathmin-1 expression enhanced the sensitivity of ESCC cell line to docetaxel and radiation[42]. Stathmin-1 can be delivered by exosomes and then promote the division, growth, migration, and invasion of esophageal squamous cells[43].

Others: In addition, studies demonstrated that the downregulation of the *ECRG4* gene in serum exosomes of oral squamous cell carcinoma patients was closely related to tumor growth *in vitro* and *in vivo*[44]. MiR-221-3p from cervical squamous cell carcinoma exosomes transferred into human lymphatic endothelial cells to accelerate lymphangiogenesis and lymphatic metastasis *via* downregulating vasohibin-1[45], but their relationship in EC requires further research.

EXOSOMES AS BIOMARKERS FOR EARLY DIAGNOSIS AND PROGNOSTIC PREDICTION OF ESOPHAGEAL CANCER

Table 1 The function of exosomes in esophageal cancer

Function	Exosome or its cargo	Pathway	Expression	Ref.
Tumorigenesis	miR-93-5p	PTEN/PI3K/Akt	up	[15]
	miR-25	miR/PTEN mRNA	up	[16]
	miR-210	miR/AIFM3 mRNA		
	Ir-T cell-derived exosomes	NF-κB	up	[9]
	miR-21	JNK	up	[29,30]
	Stathmin-1			[44]
Diagnosis and prognosis	Quantification of exosomes			[50]
	miR-93-5p		up	[15]
	miR-1246		up	[55]
	miR-21		up	[29]
	miR-223-3p		down	[57,58]
	miR-584		down	[58]
	Stathmin-1		up	[44]
Therapy	lncRNA PART1		up	[12]
	moDcs-derived exosomes			[65]

Ir-T cell: Irradiated T cells; JNK: c-Jun N-terminal kinase; lncRNA: Long non-coding RNA; miR: MicroRNA; moDcs: Monocyte-derived dendritic cells.

Studies have confirmed that the number or contents (including RNA and proteins) of exosomes in the circulating blood are of use as a biomarker for cancers, such as lung cancer[46], prostate cancer[47], colorectal cancer[48], as well as EC[18,28,43,49].

Exosome quantification

Matsumoto *et al*[49] established mouse subcutaneous tumor models by injecting human ESCC cell line (TE2-CD63-GFP) and detected tumor-derived exosomes from the plasma in the mouse model. They also recruited 66 ESCC patients and 20 non-malignant patients to measure exosomes separated from 100 μL of each individual's plasma and analyzed the relationship between the prognosis of ESCC cases and the plasma exosome amount. Results showed that ESCC patients had more exosomes than in non-malignant patients. The 3-year overall survival rate of patients with higher levels of exosomes was 79.2%. However, the 3-year overall survival rate of patients with lower levels of exosomes was 47.2%. The molecular mechanism and the major donor cell require further research.

Exosome microRNA

MiRNAs, a large family of small, noncoding RNAs, are enriched in exosomes and could regulate the expression of their target genes. MiRNAs are relatively stable, which can in part represent the level of miRNAs in its donor cell. Numerous studies have indicated that aberrant expression levels of exosomal miRNAs are closely related to the onset of multiple diseases, including cancer. MiR-21, miR-25, miR-93, miR-192, and miR-210 are widely studied oncogenic miRNAs, and have been studied as biomarkers for some kinds of human cancers[50,51].

MiR-93-5p: MicroRNA-93-5p can be transferred between EC9706 cells by exosomes and promote the proliferation of recipient EC9706 cells. Liu *et al*[18] also found that the expression of miR-93-5p was statistically different (P = 0.035) between EC patients and healthy participants (the former being 1.39 times higher than the latter). The upregulation of plasma miR-93-5p in ESCC patients increased the risk of EC. The Cancer Genome Atlas data analysis also showed that miR-93-5p expression differs in tissues and is associated with patient survival. Therefore, miR-93-5p may be a plasma biomarker for the diagnosis and prognosis of EC.

MiR-1246: MiR-1246 is another cancer associated miRNA dysregulated in many malignant tumors[52,53]. Takeshita *et al*[54] used ESCC cell lines (including TE1, TE2, TE4, TE6 and TE11) to evaluate the diagnostic and prognostic values of the exo-miR-1246 and estimated the miR-1246 level in peripheral blood of ESCC patients. In the serum samples of ESCC patients, the sensitivity and specificity of miR-1246 were 57.4% and 67.4%, respectively. The area under the curve of receiver operating characteristic curve was 0.665 when setting the optimal cut-off value to 1.15 for squamous cell

carcinoma (SCC)-Ag. Furthermore, the miR-1246 expression level of the lymph nodes in adjacent stations was apparently higher than that of the distant lymph nodes.

MiR-21: One microarray data analysis[28] showed that a total of 15 miRNAs were upregulated in the plasma of ESCC patients compared with healthy control participants. They were hsa-miR-16-5p, hsa-miR-130a-3p, hsa-miR-15a-5p, hsa-miR-144-3p, hsa-miR-19b-3p, hsa-miR-5196-5p, hsa-miR-25a-3p, hsa-miR1914-3p, hsa-miR-93-5p, hsa-miR-107, hsa-miR-3911, hsa-miR-21-5p, hsa-let-7d-3p, hsa-let7i-5p and hsa-miR-1290. In contrast, four miRNAs including hsa-miR-1238-3p, hsa-miR-6069, hsa-miR-191-3p, hsa-miR-4665-3p and hsa-miR-937-5p were downregulated. One case-control study on the correlation between exosome-shuttling miR-21 and EC morbidity indicated that the relative expression of miR-21 was 2.95 times higher in EC patient plasma compared to healthy controls. Furthermore, conditional logistic regression analysis showed that the higher miR-21 was expressed, the higher the EC incidence risk was (odds ratio: 1.107; 95% confidence interval: 1.012-1.21; $P = 0.026$). The area under the curve value was 0.60 to show the diagnostic value of exosome-shuttling miR-21 in ESCC patients.

MiR-223-3p: Exo-miRNAs are also important biomarkers for EA diagnosis and progression[55]. Warnecke-Eberz *et al*[56] first isolated exosomes from serum of EA patients and compared exosomal miRNA profiles in matching primary tumors with adjacent tissues. Results showed that a total of eight miRNAs (miR-126-5p, miR-146a-5p, miR-192-5p, miR-196b-5p, miR-223-3p, miR-223-5p, miR-409-3p and miR-483-5p) were significantly overexpressed. Conversely, ten miRNAs (miR-22-3p, miR-23b-5p, miR-27b-3p, miR-149-5p, miR-203-5p, miR-224-5p, miR-452-5p, miR-671-3p, miR-944-5p and miR-1201-5p) were significantly downregulated. They also detected that miR-223-3p was overexpressed in T2-staged adenocarcinoma patients and was higher than that in T3 tumors. There was no statistical difference in the overexpression of miR-223-5p and miR-483-5p in EA and ESCC. This result is consistent with the research of Zhou *et al*[57].

MiR-584: A four-stage study[57] including screening, training, testing and validating identified that miR-106a, miR-18a, miR-20b, miR-486-5p and miR-584 were upregulated, but miR-223-3p was downregulated in the plasma of patients with ESCC. MiR-584 was also overexpressed in ESCC tissues. This result is consistent with the data in The Cancer Genome Atlas database. Furthermore, exosome miR-584 in plasma was consistently dysregulated. Therefore, miR-584 could play an important role in the early diagnosis of ESCC.

Exosome proteins

Stathmin-1 was abundant in exosomes and could enter peripheral blood loaded by exosomes[43]. Yan *et al*[43] found that the serum levels of stathmin-1 in ESCC patients with lymph node metastasis were significantly higher compared with the cases without lymph node metastasis. As the stage increased, its sensitivity improved accordingly. They also measured the serum levels of stathmin-1 in patients with various cancers. When setting the diagnostic critical value to 4.47ng/mL, the positive rates of stathmin-1 were 81.0% (295/364) for ESCC, 68.8% (33/48) for head and neck squamous cell carcinoma, 71.2% (37/52) for lung squamous cell carcinoma, 50.9% (27/53) for lung adenocarcinoma, 27.1% (16/59) for gastric cancer, 43.9% (25/57) for colorectal cancer and 45.3% (24/53) for hepatocellular carcinoma. The area under the curve value of stathmin-1 for SCC was over 0.8, but it was lower than 0.7 for other types of cancer. Thus, stathmin-1 showed excellent diagnostic capability for SCC and may be a serology biomarker for SCC in the clinic, especially for ESCC.

EXOSOMES AND ESOPHAGEAL CANCER THERAPEUTIC POTENTIAL

Chemotherapy

Kang *et al*[15] demonstrated that long non-coding RNA PART1, as a competitive endogenous RNA, regulated and transported by exosomes, took part in the formation of drug resistance in ESCC patients *via* the STAT1-long non-coding RNA PART-Bcl-2 pathway in a gefitinib drug-resistant cell line. We hypothesize that the level of PART1 in exosomes is a promising diagnostic serological biomarker to evaluate the clinical benefits of gefitinib therapy in ESCC patients.

Radiation therapy

Radiotherapy is one of the main treatment methods for EC. Several studies have

shown that exosomes derived from the exposed cells in the microenvironment could increase the curative effect of radiotherapy through the bystander effect and abscopal effect[58-61]. For example, exosomes derived from mesenchymal stem cells are the main determinant in enhancing radiation effects in the metastatic spread of melanoma cells. More often than not the reason might be that exosome-derived factors could be involved in the bystander and abscopal effects when combining radiotherapy with mesenchymal stem cells[62]. Recently, Bruton *et al*[63] presented an unusual case of the abscopal effect in EA with distant metastasis. After palliative radiation therapy to this patient, they observed a complete response of the irradiated tissues, the primary tumor and adjacent lymph nodes, as well as non-irradiated distant lymph nodes. One year later, the patient is still cancer-free. This case inspires the hope that advanced understanding of the abscopal effect of radiation therapy increases the effect of EA and improves patient outcomes.

Immunological therapy

An *in vitro* study[64] revealed that immunotherapy, which was based on dendritic cells, could generate monocyte-derived dendritic cells (moDcs). The moDcs were powerful enough to induce cytotoxic T lymphocytes. Advanced study demonstrated that SART1 peptide-specific cytotoxic T lymphocytes could be induced by moDcs-derived exosomes, which had antigen presenting ability. Therefore, exosomes may play a potent part in the immunotherapy of EC.

Targeted therapy

Targeted therapy, also known as bio-missile, is a treatment for established cancer-causing sites at the cellular and molecular level. As is well known, exosomes are cell-derived natural nanometric vesicles, widely existing in body fluids and participate in the processes of many diseases, including cancer. There are many advantages of exosome-based nanometric vehicles: non-toxic, safe, non-immunogenic and programmable to have a strong delivery capacity and targeting specificity. Therefore, some scholars proposed to make exosomes a biological carrier to deliver anti-cancer drugs and genes for cancer stem cell-targeted therapy[65,66]. Jc Bose *et al*[66] found that delivery of anti-miR-21 could inhibit the overexpression of endogenous oncogenic miR-21 in tumor cells. Exosome-mediated anti-miR-21 delivery attenuates doxorubicin resistance in breast cancer cells. This makes the killing-cell efficiency of doxorubicin three times higher than that with doxorubicin alone. They also verified the biodistribution *in vivo*, tumor specific accumulation of anti-miR-21 loaded TEV-GIONs (gold-iron oxide nanoparticles) and its theranostic property. In summary, exosomes are expected to be used as targeted therapeutic vectors for various cancers, including EC in the near future.

OTHER ROLES OF EXOSOME IN ESOPHAGEAL CANCER

A study[13] demonstrated that dysregulated miR-33a, miR-1, miR-326, miR-133a/b, miR-548h, miR-603, miR-141-5p, miR-429, miR-26a and miR-548k contained in exosomes from tumor associated fibroblasts next to EC cells were all involved with stromal remodeling including endocytosis, adhesion, gap and tight junction, focal adhesion, actin cytoskeleton regulation and ubiquitin-mediated proteolysis in tumor microenvironments through targeting different mRNA molecules.

CONCLUSION

Exosomes are another newly discovered vehicle of efficient cell communication in addition to classical intercellular communication (including signaling molecules, membrane binding, channels, *etc*.). It is an important component of the tumor microenvironment and plays a complex role in the progression and treatment of EC.

To date, the research on exosomes in EC has been successful, but some problems still need to be solved in the clinical diagnosis and treatment of EC. Although studies have shown that the number and molecular contents of exosomes in patients with EC may be helpful for the diagnosis, there are still some questions worth thinking about and require more efforts to solve. Which part of the blood or which content is more sensitive? Is the RNA and protein of the circulating exosomes more sensitive than the corresponding circulating RNA and protein? What should the diagnostic criteria related to exosomes be? Last but not least, the same miRNA plays the opposite role in different cancers. For example, miR-93-5p can promote the formation of EC, lacrimal adenoid cystic carcinoma[67,68] and hepatoma development[69], but it was proved that

miR-93-5P may inhibit epithelial ovarian carcinoma tumorigenesis and progression by targeting Ras homolog gene family member C[70]. Therefore, we should consider comorbidities when analyzing the cause of tumor formation. In conclusion, we need to analyze the role and specific mechanisms of exosomes in the formation, monitoring and treatment of EC in a multifaceted way.

REFERENCES

1 **Malla B**, Zaugg K, Vassella E, Aebersold DM, Dal Pra A. Exosomes and Exosomal MicroRNAs in Prostate Cancer Radiation Therapy. *Int J Radiat Oncol Biol Phys* 2017; **98**: 982-995 [PMID: 28721912 DOI: 10.1016/j.ijrobp.2017.03.031]

2 **Ibrahim SH**, Hirsova P, Tomita K, Bronk SF, Werneburg NW, Harrison SA, Goodfellow VS, Malhi H, Gores GJ. Mixed lineage kinase 3 mediates release of C-X-C motif ligand 10-bearing chemotactic extracellular vesicles from lipotoxic hepatocytes. *Hepatology* 2016; **63**: 731-744 [PMID: 26406121 DOI: 10.1002/hep.28252]

3 **Segura E**, Nicco C, Lombard B, Véron P, Raposo G, Batteux F, Amigorena S, Théry C. ICAM-1 on exosomes from mature dendritic cells is critical for efficient naive T-cell priming. *Blood* 2005; **106**: 216-223 [PMID: 15790784 DOI: 10.1182/blood-2005-01-0220]

4 **Regev-Rudzki N**, Wilson DW, Carvalho TG, Sisquella X, Coleman BM, Rug M, Bursac D, Angrisano F, Gee M, Hill AF, Baum J, Cowman AF. Cell-cell communication between malaria-infected red blood cells via exosome-like vesicles. *Cell* 2013; **153**: 1120-1133 [PMID: 23683579 DOI: 10.1016/j.cell.2013.04.029]

5 **Yu S**, Cao H, Shen B, Feng J. Tumor-derived exosomes in cancer progression and treatment failure. *Oncotarget* 2015; **6**: 37151-37168 [PMID: 26452221 DOI: 10.18632/oncotarget.6022]

6 **Valadi H**, Ekström K, Bossios A, Sjöstrand M, Lee JJ, Lötvall JO. Exosome-mediated transfer of mRNAs and microRNAs is a novel mechanism of genetic exchange between cells. *Nat Cell Biol* 2007; **9**: 654-659 [PMID: 17486113 DOI: 10.1038/ncb1596]

7 **Bang C**, Thum T. Exosomes: new players in cell-cell communication. *Int J Biochem Cell Biol* 2012; 2060-2064 [PMID: 22903023 DOI: 10.1016/j.biocel.2012.08.007]

8 **Miksa M**, Wu R, Dong W. Immature dendritic cell-derived exosomes rescue septic animals via milk fat globule epidermal growth factor-factor VIII [corrected]. *J Immunol* 2009; 5983-5990 [PMID: 19812188 DOI: 10.4049/jimmunol.0802994]

9 **Robbins PD**, Morelli AE. Regulation of immune responses by extracellular vesicles. *Nat Rev Immunol* 2014; 195-208 [PMID: 24566916 DOI: 10.1038/nri3622]

10 **Torre LA**, Bray F, Siegel RL, Ferlay J, Lortet-Tieulent J, Jemal A. Global cancer statistics, 2012. *CA Cancer J Clin* 2015; **65**: 87-108 [PMID: 25651787 DOI: 10.3322/caac.21262]

11 **Chen W**, Zheng R, Baade PD, Zhang S, Zeng H, Bray F, Jemal A, Yu XQ, He J. Cancer statistics in China, 2015. *CA Cancer J Clin* 2016; **66**: 115-132 [PMID: 26808342 DOI: 10.3322/caac.21338]

12 **Min H**, Sun X, Yang X, Zhu H, Liu J, Wang Y, Chen G, Sun X. Exosomes Derived from Irradiated Esophageal Carcinoma-Infiltrating T Cells Promote Metastasis by Inducing the Epithelial-Mesenchymal Transition in Esophageal Cancer Cells. *Pathol Oncol Res* 2018; **24**: 11-18 [PMID: 28132116 DOI: 10.1007/s12253-016-0185-z]

13 **Smith RA**, Lam AK. Liquid Biopsy for Investigation of Cancer DNA in Esophageal Adenocarcinoma: Cell-Free Plasma DNA and Exosome-Associated DNA. *Methods Mol Biol* 2018; **1756**: 187-194 [PMID: 29600371 DOI: 10.1007/978-1-4939-7734-5_17]

14 **Skog J**, Würdinger T, van Rijn S, Meijer DH, Gainche L, Sena-Esteves M, Curry WT, Carter BS, Krichevsky AM, Breakefield XO. Glioblastoma microvesicles transport RNA and proteins that promote tumour growth and provide diagnostic biomarkers. *Nat Cell Biol* 2008; **10**: 1470-1476 [PMID: 19011622 DOI: 10.1038/ncb1800]

15 **Kang M**, Ren M, Li Y, Fu Y, Deng M, Li C. Exosome-mediated transfer of lncRNA PART1 induces gefitinib resistance in esophageal squamous cell carcinoma via functioning as a competing endogenous RNA. *J Exp Clin Cancer Res* 2018; **37**: 171 [PMID: 30049286 DOI: 10.1186/s13046-018-0845-9]

16 **Mitomo S**, Maesawa C, Ogasawara S, Iwaya T, Shibazaki M, Yashima-Abo A, Kotani K, Oikawa H, Sakurai E, Izutsu N, Kato K, Komatsu H, Ikeda K, Wakabayashi G, Masuda T. Downregulation of miR-138 is associated with overexpression of human telomerase reverse transcriptase protein in human anaplastic thyroid carcinoma cell lines. *Cancer Sci* 2008; **99**: 280-286 [PMID: 18201269 DOI: 10.1111/j.1349-7006.2007.00666.x]

17 **Melo SA**, Sugimoto H, O'Connell JT, Kato N, Villanueva A, Vidal A, Qiu L, Vitkin E, Perelman LT, Melo CA, Lucci A, Ivan C, Calin GA, Kalluri R. Cancer exosomes perform cell-independent microRNA biogenesis and promote tumorigenesis. *Cancer Cell* 2014; **26**: 707-721 [PMID: 25446899 DOI: 10.1016/j.ccell.2014.09.005]

18 **Liu MX**, Liao J, Xie M, Gao ZK, Wang XH, Zhang Y, Shang MH, Yin LH, Pu YP, Liu R. miR-93-5p Transferred by Exosomes Promotes the Proliferation of Esophageal Cancer Cells via Intercellular Communication by Targeting PTEN. *Biomed Environ Sci* 2018; **31**: 171-185 [PMID: 29673440 DOI: 10.3967/bes2018.023]

19 **Ke X**, Yan R, Sun Z, Cheng Y, Meltzer A, Lu N, Shu X, Wang Z, Huang B, Liu X, Wang Z, Song JH, Ng CK, Ibrahim S, Abraham JM, Shin EJ, He S, Meltzer SJ. Esophageal Adenocarcinoma-Derived Extracellular Vesicle MicroRNAs Induce a Neoplastic Phenotype in Gastric Organoids. *Neoplasia* 2017; **19**: 941-949 [PMID: 28968550 DOI: 10.1016/j.neo.2017.06.007]

20 **Feng X**, Jiang J, Shi S, Xie H, Zhou L, Zheng S. Knockdown of miR-25 increases the sensitivity of liver cancer stem cells to TRAIL-induced apoptosis via PTEN/PI3K/Akt/Bad signaling pathway. *Int J Oncol* 2016; **49**: 2600-2610 [PMID: 27840896 DOI: 10.3892/ijo.2016.3751]

21 **Delettre C**, Yuste VJ, Moubarak RS, Bras M, Lesbordes-Brion JC, Petres S, Bellalou J, Susin SA. AIFsh, a novel apoptosis-inducing factor (AIF) pro-apoptotic isoform with potential pathological relevance in human cancer. *J Biol Chem* 2006; **281**: 6413-6427 [PMID: 16365034 DOI: 10.1074/jbc.M509884200]

22 **Krebs AM**, Mitschke J, Lasierra Losada M, Schmalhofer O, Boerries M, Busch H, Boettcher M, Mougiakakos D, Reichardt W, Bronsert P, Brunton VG, Pilarsky C, Winkler TH, Brabletz S, Stemmler MP, Brabletz T. The EMT-activator Zeb1 is a key factor for cell plasticity and promotes metastasis in pancreatic cancer. *Nat Cell Biol* 2017; **19**: 518-529 [PMID: 28414315 DOI: 10.1038/ncb3513]

23 **Fici P**, Gallerani G, Morel AP, Mercatali L, Ibrahim T, Scarpi E, Amadori D, Puisieux A, Rigaud M, Fabbri F. Splicing factor ratio as an index of epithelial-mesenchymal transition and tumor aggressiveness in breast cancer. *Oncotarget* 2017; **8**: 2423-2436 [PMID: 27911856 DOI: 10.18632/oncotarget.13682]

24 **Gibbons DL**, Creighton CJ. Pan-cancer survey of epithelial-mesenchymal transition markers across the Cancer Genome Atlas. *Dev Dyn* 2018; **247**: 555-564 [PMID: 28073171 DOI: 10.1002/dvdy.24485]

25 **Malek R**, Wang H, Taparra K, Tran PT. Therapeutic Targeting of Epithelial Plasticity Programs: Focus on the Epithelial-Mesenchymal Transition. *Cells Tissues Organs* 2017; **203**: 114-127 [PMID: 28214899 DOI: 10.1159/000447238]

26 **Okubo K**, Uenosono Y, Arigami T, Yanagita S, Matsushita D, Kijima T, Amatatsu M, Uchikado Y, Kijima Y, Maemura K, Natsugoe S. Clinical significance of altering epithelial-mesenchymal transition in metastatic lymph nodes of gastric cancer. *Gastric Cancer* 2017; **20**: 802-810 [PMID: 28247164 DOI: 10.1007/s10120-017-0705-x]

27 **Chen X**, Chen RX, Wei WS, Li YH, Feng ZH, Tan L, Chen JW, Yuan GJ, Chen SL, Guo SJ, Xiao KH, Liu ZW, Luo JH, Zhou FJ, Xie D. PRMT5 Circular RNA Promotes Metastasis of Urothelial Carcinoma of the Bladder through Sponging miR-30c to Induce Epithelial-Mesenchymal Transition. *Clin Cancer Res* 2018; **24**: 6319-6330 [PMID: 30305293 DOI: 10.1158/1078-0432.CCR-18-1270]

28 **Liao J**, Liu R, Shi YJ, Yin LH, Pu YP. Exosome-shuttling microRNA-21 promotes cell migration and invasion-targeting PDCD4 in esophageal cancer. *Int J Oncol* 2016; **48**: 2567-2579 [PMID: 27035745 DOI: 10.3892/ijo.2016.3453]

29 **Liao J**, Liu R, Yin L, Pu Y. Expression profiling of exosomal miRNAs derived from human esophageal cancer cells by Solexa high-throughput sequencing. *Int J Mol Sci* 2014; **15**: 15530-15551 [PMID: 25184951 DOI: 10.3390/ijms150915530]

30 **Chakravarthi BVSK**, Chandrashekar DS, Agarwal S, Balasubramanya SAH, Pathi SS, Goswami MT, Jing X, Wang R, Mehra R, Asangani IA, Chinnaiyan AM, Manne U, Sonpavde G, Netto GJ, Gordetsky J, Varambally S. miR-34a Regulates Expression of the Stathmin-1 Oncoprotein and Prostate Cancer Progression. *Mol Cancer Res* 2018; **16**: 1125-1137 [PMID: 29025958 DOI: 10.1158/1541-7786.MCR-17-0230]

31 **Vetter NS**, Kolb EA, Mills CC, Sampson VB. The Microtubule Network and Cell Death Are Regulated by an miR-34a/Stathmin 1/βIII-Tubulin Axis. *Mol Cancer Res* 2017; **15**: 953-964 [PMID: 28275089 DOI: 10.1158/1541-7786.MCR-16-0372]

32 **Imura S**, Yamada S, Saito YU, Iwahashi S, Arakawa Y, Ikemoto T, Morine Y, Utsunomiya T, Shimada M. miR-223 and Stathmin-1 Expression in Non-tumor Liver Tissue of Patients with Hepatocellular Carcinoma. *Anticancer Res* 2017; **37**: 5877-5883 [PMID: 28982915 DOI: 10.21873/anticanres.12033]

33 **Guo F**, Luo Y, Mu YF, Qin SL, Qi Y, Qiu YE, Zhong M. miR-193b directly targets STMN1 and inhibits the malignant phenotype in colorectal cancer. *Am J Cancer Res* 2016; **6**: 2463-2475 [PMID: 27904764]

34 **Zhao C**, Li H, Wang L, Sun W. An Immunohistochemical Study of Stathmin 1 Expression in Osteosarcoma Shows an Association with Metastases and Poor Patient Prognosis. *Med Sci Monit* 2018; **24**: 6070-6078 [PMID: 30169496 DOI: 10.12659/MSM.910953]

35 Correction: "miR-34a Regulates Expression of the Stathmin-1 Oncoprotein and Prostate Cancer Progression". *Mol Cancer Res* 2018; **16**: 1205-1206 [PMID: 29884744 DOI: 10.1158/1541-7786.MCR-18-0519]

36 **Aksoy A**, Artas G, Sevindik OG. Predictive value of stathmin-1 and osteopontin expression for taxan resistance in metastatic castrate-resistant prostate cancer. *Pak J Med Sci* 2017; **33**: 560-565 [PMID: 28811771 DOI: 10.12669/pjms.333.12559]

37 **Wu H**, Deng WW, Yang LL, Zhang WF, Sun ZJ. Expression and phosphorylation of Stathmin 1 indicate poor survival in head and neck squamous cell carcinoma and associate with immune suppression. *Biomark Med* 2018; **12**: 759-769 [PMID: 29847156 DOI: 10.2217/bmm-2017-0443]

38 **Tan HT**, Chung MCM. Label-Free Quantitative Phosphoproteomics Reveals Regulation of Vasodilator-Stimulated Phosphoprotein upon Stathmin-1 Silencing in a Pair of Isogenic Colorectal Cancer Cell Lines. *Proteomics* 2018; **18**: e1700242 [PMID: 29460479 DOI: 10.1002/pmic.201700242]

39 **Wang J**, Yao Y, Ming Y, Shen S, Wu N, Liu J, Liu H, Suo T, Pan H, Zhang D, Ding K, Liu H. Downregulation of stathmin 1 in human gallbladder carcinoma inhibits tumor growth in vitro and in vivo. *Sci Rep* 2016; **6**: 28833 [PMID: 27349455 DOI: 10.1038/srep28833]

40 **Zhang J**, Fu J, Pan Y, Zhang X, Shen L. Silencing of miR-1247 by DNA methylation promoted non-small-cell lung cancer cell invasion and migration by effects of STMN1. *Onco Targets Ther* 2016; **9**: 7297-7307 [PMID: 27942223 DOI: 10.2147/OTT.S111291]

41 **Ni PZ**, He JZ, Wu ZY, Ji X, Chen LQ, Xu XE, Liao LD, Wu JY, Li EM, Xu LY. Overexpression of Stathmin 1 correlates with poor prognosis and promotes cell migration and proliferation in oesophageal squamous cell carcinoma. *Oncol Rep* 2017; **38**: 3608-3618 [PMID: 29039594 DOI: 10.3892/or.2017.6039]

42 **Suzuki S**, Yokobori T, Altan B, Hara K, Ozawa D, Tanaka N, Sakai M, Sano A, Sohda M, Bao H, Fukuchi M, Miyazaki T, Kaira K, Asao T, Kuwano H. High stathmin 1 expression is associated with poor prognosis and chemoradiation resistance in esophageal squamous cell carcinoma. *Int J Oncol* 2017; **52**: 1184-1190 [PMID: 28350065 DOI: 10.3892/ijo.2017.3899]

43 **Yan L**, Dong X, Gao J, Liu F, Zhou L, Sun Y, Zhao X. A novel rapid quantitative method reveals stathmin-1 as a promising marker for esophageal squamous cell carcinoma. *Cancer Med* 2018; **7**: 1802-1813 [PMID: 29577639 DOI: 10.1002/cam4.1449]

44 **Mao L**, Li X, Gong S, Yuan H, Jiang Y, Huang W, Sun X, Dang X. Serum exosomes contain ECRG4 mRNA that suppresses tumor growth via inhibition of genes involved in inflammation, cell proliferation, and angiogenesis. *Cancer Gene Ther* 2018; **25**: 248-259 [PMID: 29983418 DOI: 10.1038/s41417-018-0032-3]

45 **Zhou CF**, Ma J, Huang L, Yi HY, Zhang YM, Wu XG, Yan RM, Liang L, Zhong M, Yu YH, Wu S, Wang W. Cervical squamous cell carcinoma-secreted exosomal miR-221-3p promotes lymphangiogenesis and lymphatic metastasis by targeting VASH1. *Oncogene* 2019; **38**: 1256-1268 [PMID: 30254211 DOI: 10.1038/s41388-018-0511-x]

46 **Fleitas T**, Martínez-Sales V, Vila V, Reganon E, Mesado D, Martín M, Gómez-Codina J, Montalar J, Reynés G. Circulating endothelial cells and microparticles as prognostic markers in advanced non-small cell lung cancer. *PLoS One* 2012; **7**: e47365 [PMID: 23077602 DOI: 10.1371/journal.pone.0047365]

47 **Tavoosidana G**, Ronquist G, Darmanis S, Yan J, Carlsson L, Wu D, Conze T, Ek P, Semjonow A, Eltze E, Larsson A, Landegren UD, Kamali-Moghaddam M. Multiple recognition assay reveals prostasomes as promising plasma biomarkers for prostate cancer. *Proc Natl Acad Sci U S A* 2011; **108**: 8809-8814 [PMID: 21555566 DOI: 10.1073/pnas.1019330108]

48 **Silva J**, Garcia V, Rodriguez M, Compte M, Cisneros E, Veguillas P, Garcia JM, Dominguez G, Campos-Martin Y, Cuevas J, Peña C, Herrera M, Diaz R, Mohammed N, Bonilla F. Analysis of exosome release and its prognostic value in human colorectal cancer. *Genes Chromosomes Cancer* 2012; **51**: 409-418 [PMID: 22420032 DOI: 10.1002/gcc.21926]

49 **Matsumoto Y**, Kano M, Akutsu Y, Hanari N, Hoshino I, Murakami K, Usui A, Suito H, Takahashi M, Otsuka R, Xin H, Komatsu A, Iida K, Matsubara H. Quantification of plasma exosome is a potential prognostic marker for esophageal squamous cell carcinoma. *Oncol Rep* 2016; **36**: 2535-2543 [PMID: 27599779 DOI: 10.3892/or.2016.5066]

50 **Kinoshita T**, Yip KW, Spence T, Liu FF. MicroRNAs in extracellular vesicles: potential cancer biomarkers. *J Hum Genet* 2017; **62**: 67-74 [PMID: 27383658 DOI: 10.1038/jhg.2016.87]

51 **Bigagli E**, Luceri C, Guasti D, Cinci L. Exosomes secreted from human colon cancer cells influence the adhesion of neighboring metastatic cells: Role of microRNA-210. *Cancer Biol Ther* 2016; **17**: 1-8 [PMID: 27611932 DOI: 10.1080/15384047.2016.1219815]

52 **Zhai LY**, Li MX, Pan WL, Chen Y, Li MM, Pang JX, Zheng L, Chen JX, Duan WJ. In Situ Detection of Plasma Exosomal MicroRNA-1246 for Breast Cancer Diagnostics by a Au Nanoflare Probe. *ACS Appl Mater Interfaces* 2018; **10**: 39478-39486 [PMID: 30350935 DOI: 10.1021/acsami.8b12725]

53 **Wei C**, Li Y, Huang K, Li G, He M. Exosomal miR-1246 in body fluids is a potential biomarker for gastrointestinal cancer. *Biomark Med* 2018; **12**: 1185-1196 [PMID: 30235938 DOI: 10.2217/bmm-2017-0440]

54 **Takeshita N**, Hoshino I, Mori M, Akutsu Y, Hanari N, Yoneyama Y, Ikeda N, Isozaki Y, Maruyama T, Akanuma N, Komatsu A, Jitsukawa M, Matsubara H. Serum microRNA expression profile: miR-1246 as a novel diagnostic and prognostic biomarker for oesophageal squamous cell carcinoma. *Br J Cancer* 2013; **108**: 644-652 [PMID: 23361059 DOI: 10.1038/bjc.2013.8]

55 **Bansal A**, Gupta V, Wang K. MicroRNA Expression Signatures During Malignant Progression From Barrett's Esophagus. *J Cell Biochem* 2016; **117**: 1288-1295 [PMID: 26808728 DOI: 10.1002/jcb.25497]

56 **Warnecke-Eberz U**, Chon SH, Hölscher AH, Drebber U, Bollschweiler E. Exosomal onco-miRs from serum of patients with adenocarcinoma of the esophagus: comparison of miRNA profiles of exosomes and matching tumor. *Tumour Biol* 2015; **36**: 4643-4653 [PMID: 25631748 DOI: 10.1007/s13277-015-3112-0]

57 **Zhou X**, Wen W, Zhu J, Huang Z, Zhang L, Zhang H, Qi LW, Shan X, Wang T, Cheng W, Zhu D, Yin Y, Chen Y, Zhu W, Shu Y, Liu P. A six-microRNA signature in plasma was identified as a potential biomarker in diagnosis of esophageal squamous cell carcinoma. *Oncotarget* 2017; **8**: 34468-34480 [PMID: 28380431 DOI: 10.18632/oncotarget.16519]

58 **Al-Mayah AH**, Irons SL, Pink RC, Carter DR, Kadhim MA. Possible role of exosomes containing RNA in mediating nontargeted effect of ionizing radiation. *Radiat Res* 2012; **177**: 539-545 [PMID: 22612287 DOI: 10.1667/RR2868.1]

59 **Al-Mayah A**, Bright S, Chapman K, Irons S, Luo P, Carter D, Goodwin E, Kadhim M. The non-targeted effects of radiation are perpetuated by exosomes. *Mutat Res* 2015; **772**: 38-45 [PMID: 25772109 DOI: 10.1016/j.mrfmmm.2014.12.007]

60 **Golden EB**, Demaria S, Schiff PB, Chachoua A, Formenti SC. An abscopal response to radiation and ipilimumab in a patient with metastatic non-small cell lung cancer. *Cancer Immunol Res* 2013; **1**: 365-372 [PMID: 24563870 DOI: 10.1158/2326-6066.CIR-13-0115]

61 **Reynders K**, Illidge T, Siva S, Chang JY, De Ruysscher D. The abscopal effect of local radiotherapy: using immunotherapy to make a rare event clinically relevant. *Cancer Treat Rev* 2015; **41**: 503-510 [PMID: 25872878 DOI: 10.1016/j.ctrv.2015.03.011]

62 **de Araujo Farias V**, O'Valle F, Serrano-Saenz S, Anderson P, Andrés E, López-Peñalver J, Tovar I, Nieto A, Santos A, Martín F, Expósito J, Oliver FJ, de Almodóvar JMR. Exosomes derived from mesenchymal stem cells enhance radiotherapy-induced cell death in tumor and metastatic tumor foci. *Mol Cancer* 2018; **17**: 122 [PMID: 30111323 DOI: 10.1186/s12943-018-0867-0]

63 **Bruton Joe M**, Truong PT. Abscopal Effect after Palliative Radiation Therapy for Metastatic Adenocarcinoma of the Esophagus. *Cureus* 2018; **10**: e3089 [PMID: 30333943 DOI: 10.7759/cureus.3089]

64 **Narita M**, Kanda T, Abe T, Uchiyama T, Iwafuchi M, Zheng Z, Liu A, Kaifu T, Kosugi S, Minagawa M, Itoh K, Takahashi M. Immune responses in patients with esophageal cancer treated with SART1 peptide-pulsed dendritic cell vaccine. *Int J Oncol* 2015; **46**: 1699-1709 [PMID: 25625346 DOI: 10.3892/ijo.2015.2846]

65 **Wang J**, Zheng Y, Zhao M. Exosome-Based Cancer Therapy: Implication for Targeting Cancer Stem Cells. *Front Pharmacol* 2017; **7**: 533 [PMID: 28127287 DOI: 10.3389/fphar.2016.00533]

66 **Jc Bose R**, Uday Kumar S, Zeng Y, Afjei R, Robinson E, Lau K, Bermudez A, Habte F, Pitteri SJ, Sinclair R, Willmann JK, Massoud TF, Gambhir SS, Paulmurugan R. Tumor Cell-Derived Extracellular Vesicle-Coated Nanocarriers: An Efficient Theranostic Platform for the Cancer-Specific Delivery of Anti-miR-21 and Imaging Agents. *ACS Nano* 2018; **12**: 10817-10832 [PMID: 30346694 DOI: 10.1021/acsnano.8b02587]

67 **Liang L**, Zhao L, Zan Y, Zhu Q, Ren J, Zhao X. MiR-93-5p enhances growth and angiogenesis capacity of HUVECs by down-regulating EPLIN. *Oncotarget* 2017; **8**: 107033-107043 [PMID: 29291009 DOI: 10.18632/oncotarget.22300]

68 **Hao J**, Jin X, Shi Y, Zhang H. miR-93-5p enhance lacrimal gland adenoid cystic carcinoma cell tumorigenesis by targeting BRMS1L. *Cancer Cell Int* 2018; **18**: 72 [PMID: 29760585 DOI: 10.1186/s12935-018-0552-9]

69 **Wang X**, Liao Z, Bai Z, He Y, Duan J, Wei L. MiR-93-5p Promotes Cell Proliferation through Down-Regulating PPARGC1A in Hepatocellular Carcinoma Cells by Bioinformatics Analysis and Experimental Verification. *Genes (Basel)* 2018; **9**: E51 [PMID: 29361788 DOI: 10.3390/genes9010051]

70 **Chen X**, Chen S, Xiu YL, Sun KX, Zong ZH, Zhao Y. RhoC is a major target of microRNA-93-5P in epithelial ovarian carcinoma tumorigenesis and progression. *Mol Cancer* 2015; 31 [PMID: 25649143 DOI: 10.1186/s12943-015-0304-6]

World Journal of Clinical Cases

Submit a Manuscript: https://www.f6publishing.com

World J Clin Cases 2019 April 26; 7(8): 917-927

DOI: 10.12998/wjcc.v7.i8.917

ISSN 2307-8960 (online)

MINIREVIEWS

Food additives can act as triggering factors in celiac disease: Current knowledge based on a critical review of the literature

Clara Mancuso, Donatella Barisani

ORCID number: Clara Mancuso (0000-0001-7464-1749); Donatella Barisani (0000-0003-4592-6221).

Author contributions: All authors equally contributed to this paper with conception and design of the study, literature review and analysis, drafting and critical revision and editing, and final approval of the final version.

Conflict-of-interest statement: There are no conflicts of interest arising from this work.

Manuscript source: Invited manuscript

Received: January 13, 2019
Peer-review started: January 14, 2019
First decision: January 30, 2019
Revised: March 11, 2019
Accepted: March 16, 2019
Article in press: March 16, 2019
Published online: April 26, 2019

P-Reviewer: Sergi C

Clara Mancuso, Department of Medicine and Surgery, University of Milano-Bicocca, Via Cadore 48, Monza 20900, Italy

Donatella Barisani, Department of Medicine and Surgery, University of Milano-Bicocca, Monza 20900, Italy

Corresponding author: Donatella Barisani, MD, Associate Professor, Department of Medicine and Surgery, University of Milano-Bicocca, Building U-8, Via Cadore 48, Monza 20900, Italy.
donatella.barisani@unimib.it
Telephone: +39-02-64488304

Abstract

Celiac disease (CeD) is an autoimmune disorder, mainly affecting the small intestine, triggered by the ingestion of gluten with the diet in subjects with a specific genetic status. The passage of gluten peptides through the intestinal barrier, the uptake by antigen presenting cells and their presentation to T cells represent essential steps in the pathogenesis of the disease. CeD prevalence varies in different populations, but a tendency to increase has been observed in various studies in recent years. A higher amount of gluten in modern grains could explain this increased frequency, but also food processing could play a role in this phenomenon. In particular, the common use of preservatives such as nanoparticles could intervene in the pathogenesis of CeD, due to their possible effect on the integrity of the intestinal barrier, immune response or microbiota. In fact, these alterations have been reported after exposure to metal nanoparticles, which are commonly used as preservatives or to improve food texture, consistency and color. This review will focus on the interactions between several food additives and the intestine, taking into account data obtained *in vitro* and *in vivo*, and analyzing their effect in respect to the development of CeD in genetically predisposed individuals.

Key words: Celiac disease; Food additives; Metallic nanoparticles; Gluten; Intestine; Immune system

Core tip: Celiac disease (CeD) is a common autoimmune disorder caused by the ingestion of gluten. Its frequency has been increasing, and several factors have been analyzed as possible triggers; among them also food additives should be taken into account. Several nanoparticles are used as food additives or preservatives, and they can

S-Editor: Dou Y
L-Editor: A
E-Editor: Wu YXJ

interact with the intestine or the immune system, increasing, in theory, the immune response towards gluten. The scope of this review is to analyze the data present in the literature with respect to the pathogenetic mechanisms involved in the development of CeD.

Citation: Mancuso C, Barisani D. Food additives can act as triggering factors in celiac disease: Current knowledge based on a critical review of the literature. *World J Clin Cases* 2019; 7(8): 917-927
URL: https://www.wjgnet.com/2307-8960/full/v7/i8/917.htm
DOI: https://dx.doi.org/10.12998/wjcc.v7.i8.917

CELIAC DISEASE PATHOGENESIS

Celiac disease (CeD) is a multifactorial disorder, characterized by the presence of an autoimmune response that mainly involves the small intestine, triggered by the ingestion of gluten from wheat, barley, and rye in genetically predisposed individuals. CeD genetic background is quite complex, and partially still unknown. About 40% of the genetic predisposition relies on genes localized in the human leukocyte antigen (HLA) region, mainly on those encoding for specific class II HLA molecules, namely DQ2.5 and DQ8 heterodimers. The combination of the HLA alleles DQA1*0501 and DQB1*0201 generates the HLA-DQ2.5 heterodimer, which is detected in more than 90% of Caucasian CeD patients (either in cis or in trans), whereas the remaining patients carry the HLA-DQ8 heterodimer, encoded by DQA1*03 (α chain) and DQB1*0302 (β chain). However, the presence of the DQ2 heterodimer is not sufficient for the development of CeD. In fact, the HLA-DQ2 haplotype is present in 30%-35% of the Caucasian population (in which CeD has a high prevalence), but only 2%-5% of gene carriers develop CeD[1]. Using the Genome Wide Association Study approach, several additional loci have been identified as predisposing to CeD, but in total they account for about 50% of the genetic component.

Although the genetic background is essential for the development of CeD, research has started to focus on the possible environmental factors (apart from gluten) that could trigger the disorder. This could be quite important, since several data suggest that the prevalence of CeD is increasing, and cases are now reported even in populations that were thought to have a negligible prevalence of this disease. A study performed in United Kingdom showed a four-fold increase in CeD incidence rate over a period of 22 years, but regional differences were present[2]. Even if this increased rate could be explained by a different awareness of the problem by physicians, or by the use of an easier serological diagnosis and a casefinding approach, there is still some evidence which suggests that this raise in the prevalence/incidence of the disease is a real phenomenon. Evaluation in a Scottish pediatric population revealed that, in two decades, the incidence of children with nonclassical CeD had increased dramatically (attributable to better diagnosis), but also the number of patients with classical manifestations had quadrupled (thus suggesting a real variation in CeD frequency)[3]. Moreover, similar data have been observed in Finland as well as in the United States[4-6].

To identify the possible additional environmental causes it is necessary to dissect the various steps involved in CeD pathogenesis. The ingested gluten undergoes digestion, which generates several small peptides, including the 33 mer peptide (residues 57 to 89 of α-gliadin), a celiac "superantigen" able to stimulate T cells[7], or the 31-43 peptide (from residues 31 to 43 of α-gliadin), which can have a toxic effect on intestinal mucosa[8]. However, in order to trigger the autoimmune response these peptides need to cross the gastrointestinal barrier and reach the lamina propria. This passage can take place using two different routes, namely the transcellular and the paracellular one. The first is a vesicle-mediated passage which involves endocytosis on the luminal side of enterocytes, followed by transcytosis and release on the basolateral side. Thus, in theory, substances which are able to make the gluten peptides more prone to be captured on the apical side and transported could play a role in the pathogenesis of CeD. Conversely, paracellular transport depends on tight junctions (TJ) and the correct expression/interaction of the proteins that maintain junction functionality. Therefore, agents able to induce inflammation and/or cytokine release could cause the rearrangement of proteins such as ZO-1 or occludin, causing a loss of function of TJ and, in turn, an increased paracellular passage of lumen

substances, such as gluten peptides.

Once gluten peptides have crossed the intestinal barrier, they are further processed in the submucosa; due to their high content in glutamine, proline and hydrophobic amino acid residues, these peptides are excellent substrates for transglutaminase 2 (TG2) which deamidates them. This processing increases negative charges, allowing the gluten peptides to bind more strongly to HLA-DQ2 (or HLA-DQ8). Better antigen presentation results in CD4+ Th1 T-cell activation that, in turn, will cause activation of intraepithelial lymphocytes, crypt hyperplasia and villus atrophy, as well as B cell stimulation and the production of auto-antibodies directed against deamidated gliadin peptides and TG2 (Figure 1A).

Given these data, food additives could have a role in triggering the development of CeD if they are able to alter the gastrointestinal barrier, antigen presentation or the activation of the immune system. Although there are currently few experimental published data that specifically address the interaction between food additives and CeD, there are at least three possible categories that should be analyzed, namely transglutaminase, gluten nanoparticles and metallic nanoparticles.

USE OF TRANSGLUTAMINASE IN FOOD PREPARATION

The use of transglutaminase in food processing belongs to the various techniques that industries in the field currently use to modify the proteins present in aliments. Microbial transglutaminases (mTGs), like human ones, catalyzes acyl transfer, deamidation and crosslinking between glutamine (acyl donor) and lysine (acceptor). These reactions can profoundly modify a large amount of proteins constituting food matrices and this, in turn, can improve several food properties such as texture and stability; more interestingly, these changes can take place without affecting other food characteristics like taste or nutritional value. For these reasons, the possible ingestion of microbial tranglutaminases, due to its use in food processing, has been recognized as safe by Food and Drug Administration[9].

Currently mTGs are is used in several processed foods since, among others, their use increases the water retention capacity of proteins, fact that could help to increase the juiciness of products such as meat, or emulsion properties that are important in food characterized by creamy texture (*e.g.*, yogurt)[10]. Moreover, bacterial transglutaminase treatment has also been applied to cereal proteins (including wheat protein); its use can improve stability, elasticity and water retention of the dough, and for this reason it has also been employed in the preparation of gluten-free food[11-12].

Due to the pivotal role of transglutaminase in the pathogenesis of CeD, its use in food preparation has raised some concern. Transglutaminases can act on gluten peptides, making them more immunogenic, but it must also be remembered that TG2 is itself an autoantigen, and the ingestion of mTGs could also generate an autoimmune response through a molecular mimicry mechanism. The comparison of the primary and tertiary structure of a commonly used mTGs with TG2 reveals little homology, although both are able to bind gluten peptides using similar aminoacids[13]. Moreover, mTGs can deamidate gluten peptides, making them more immunogenic, as assessed in an *in vitro* system that employed gluten-specific T cells isolated from the duodenum of celiac patients[14].

Few papers have tried to assess the possible correlation between the use of bacterial transglutaminase and CeD, but most of them are only based on peptide-patients' antibody interaction. An initial investigation performed using sera from nine celiac patients suggested that treatment of wheat with mTGs increases the IgA-based reactivity, and to a lesser degree when mTGs were used to treat gluten-free bread[15]. Matthias *et al*[16] evaluated the presence of antibodies directed against either human or bacterial transglutaminase (alone or bound to gluten peptides) in pediatric patients with or without CeD. In the serum of CeD patients, they could detect antibodies against mTGs, although prevalently IgG rather than IgA (as commonly observed against TG2), whereas they were not present in controls. The authors also found a correlation between serum levels of antibodies against mTG-peptides and TG2-peptides, as well as between these serum titer and intestinal damage, and they suggested a causal role of this food supplement in the development of CeD. Different results were observed by Ruh *et al*[17], who extracted gliadin from pasta treated or untreated with mTGs and employed it to assess possible reactivity with circulating antibodies present in CeD patients. The authors detected a huge variation among patients, but no difference in reactivity between the two types of gliadin. These results were also confirmed by Heil *et al*[18].

On the contrary, in theory, the use of mTGs could also be useful to decrease the immunogenicity of gluten, but in order to do so the enzyme has to be used in

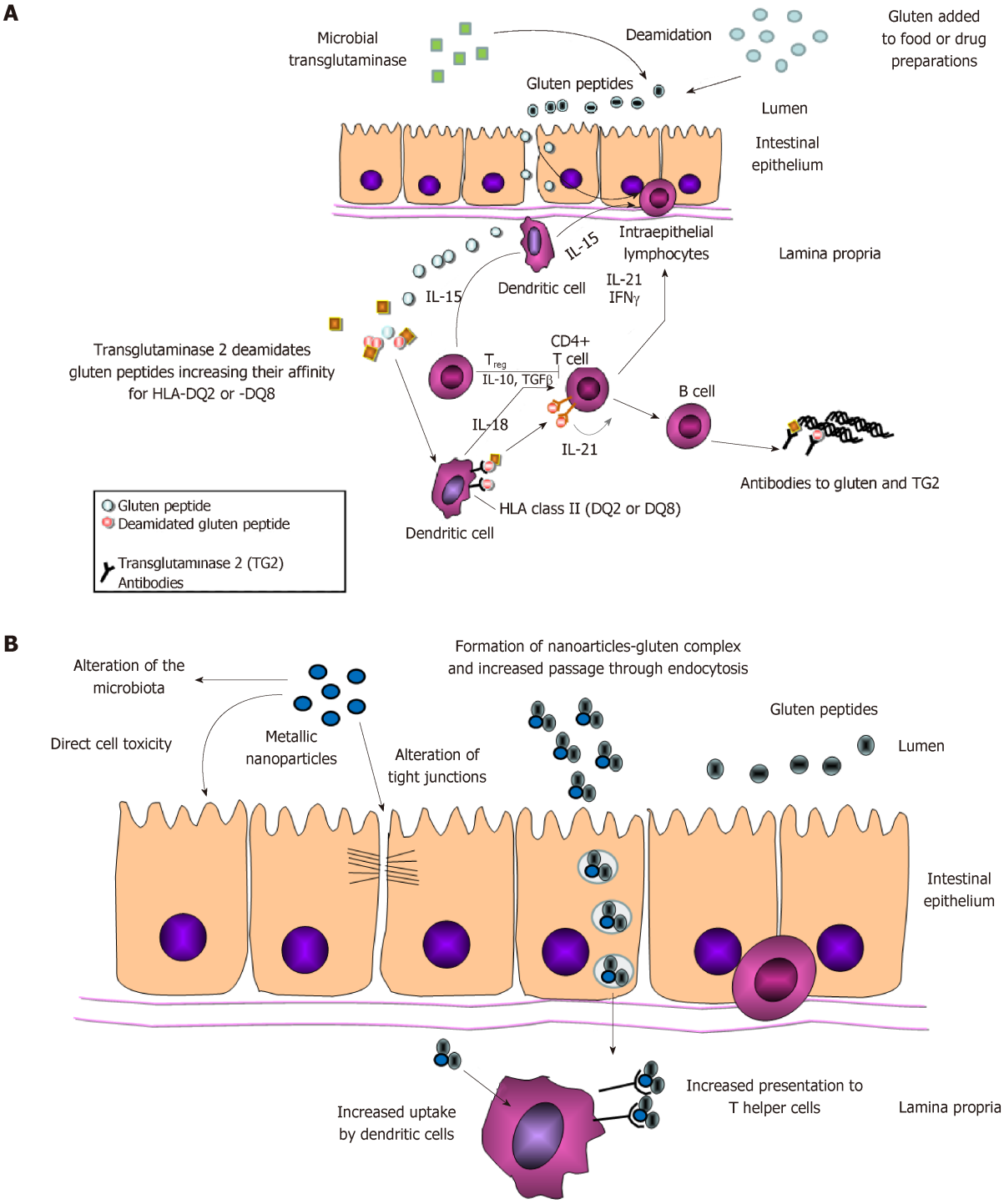

Figure 1 Role of Food additives in the pathogenesis of celiac disease. A: The pathogenesis of celiac disease involves the digestion of gluten in the gut lumen, the increased passage of gluten peptides through the intestinal epithelium, the deamination by the tissue transglutaminase 2 and the uptake by antigen-presenting cells. Once the gluten peptides are presented within the HLA class II molecule they activate CD4+ T cells, which in turn trigger the destruction of the tissue by CD8+ T cells and the production of autoantibodies by B cells. The increase amount of gluten or bacterial transglutaminase used as additive could increase this process; B: Metallic nanoparticles could affect both gluten passage through the epithelium (paracellularly or intracellularly) or the presentation of the antigen by dendritic bells. Moreover they can alter the microbiota, influencing gluten processing and/or immune response.

association with acyl-acceptor molecules such as lysine[19]. This pre-treatment of gluten could in fact block the aminoacids that are the usual target of TG2, thus preventing the modifications that increase the affinity of gluten peptides for the DQ2 molecule[13,20]. Moreover, experiments performed *ex vivo* on duodenal biopsies of CeD patients showed that the modification of gluten by mTGs with L-lysine prevented pro-inflammatory cytokine production[21,22]. Gluten transamidation by mTGs could thus be used to produce flour of bread with less immunoactive gluten peptides[23,24], but there are still some issues that need to be clarified, due to the affinity of mTGs for

the aminoacids usually targeted by TG2 and to the possibility that TG2 overcomes the modification induced by mTGs.

GLUTEN-BASED NANOPARTICLES

Gluten-based nanoparticles have been mainly developed as a tool for drug delivery, and have been tested in particular for hydrophobic drugs[25]. However, there is another use that could be potentially problematic, *i.e.*, the development of coating matrices for paper and cardboard used for food packaging. Plant-derived proteins have good film-forming properties, are biodegradable, and can be produced with moderate costs, facts that make them suitable for coating food containers. Some authors have also combined gluten with nanocellulose and titanium dioxide in order to obtain nanocomposites able to increase the resistance of paper. These nanocomposites also have an antibacterial activity, a quality that might be very attractive for food-preserving packages[26]. As will be mentioned later, the issue regarding these nanomaterials is that data about the possible release of nanoparticles in food are needed.

METALLIC NANOPARTICLES

Nowadays several nanoparticles (NPs) are intentionally added to food, beverages and their packages[27], mainly to preserve aliments[28,29] or to improve their organoleptic properties (such as taste, consistency and appearance). Consequently, in recent years, an increase of toxicological studies on food nanoparticles has been registered. Although NP can enter the body through several routes, according to the Nanotechnology Consumer Product Inventory (CPI) enlisted in 2014, one of the major NP points of entry is the gastrointestinal system[30]. They also reported that nanomaterials are particularly present in commercial food or food-related products under the form of metallic nanoparticles (mNP), of which Ag (E174), TiO2 (E171), ZnO, Au (E175) and SiO2 (E551) NPs are the most popular. Briefly, AgNPs are particularly used as antimicrobial agent in aliments/beverages, their packages and in agriculture[29]; ZnONPs are also used as strong antibacterial agents, but they can also be used as a dietary supplement; E171 is used as a whitening agent in pharmaceutical, dairy and pastry products; AuNP is mostly present as a contaminant from dental restoration material or agriculture-derived products (such as seeds)[31,32]; SiO2NP is employed to improve the organoleptic properties of food and its nutritional values.

In order to evaluate the possible effects of ingested NP, there are several factors that should be taken into account: (A) NP dimensions: several studies reported as the size of food mNP might alter their uptake from intestinal cells[33-35]. The smaller the mNP, the faster and easier will be its passage through the mucous layer and its passage into the mucosa either by transcellular or paracellular transport; (B) Core material: it could determine whether NPs remain intact or partially digested by the intestinal fluids. An important concern is in fact the propensity of NPs to be dissolved and release heavy metals, which in turn affects NP toxicity. In this sense, AgNP, ZnONP and CuONP are regarded as the most dangerous food nanoparticles[36,37]. NP core composition also determines the chemical reactivity, substance adsorption on NP surface, and possibly the epithelial translocation route[38,39]; (C) Aggregation/agglomeration state: NPs can arrive into the gut as single entities or in clusters (agglomerates or aggregates[40]). This feature depends on the NP composition, but also on the physiochemical properties of the environment. It has been reported that the degree of aggregation/agglomeration of SiO2-, Ag- and aluminium-NPs can change in artificial mouth, gastric and intestinal conditions[41-43]. At the same time, this factor also affects NP uptake and toxicity, as demonstrated by McCracken *et al*[44] and Albanese *et al*[45]; (D) Gastrointestinal environment and food: Physiochemical features of food, beverages, and the gut are important factors that influence NP stability, size, surface composition and aggregation/agglomeration state[41,43,44,46,47]. Wang *et al*[48] and Cao *et al*[49] demonstrated a higher oxidative stress-related toxicity exerted by ZnONP when associated with Vitamin C and palmitic oil, respectively; on the contrary the presence of flavonoids or quercetin seems to protect against AgNP toxicity[50,51].

Although the daily consumption of metallic NPs is usually thought to be trivial, this is not the case, in particular if TiO2 is taken into account. Early studies suggested that average daily human consumption of TiO2 was 5.4 mg per person[52], 0.035 mg/kg of body weight (b.w.)/d[53] and 5 mg/person[54]. More recent papers, however, estimated a daily intake of 1–2 mg TiO2/kg b.w. for United States children under 10 years of age, and 0.2-0.7mg TiO2/kg b.w. for other United States consumers[55],

whereas EFSA data reported a range between 0.2 and 0.4 mg/kg b.w. in infants and the elderly, and 5.5-10.4 mg/kg b.w. in children, depending on the exposure[56]. Although these data should be corrected for the percentage on TiO2 NPs present in the E171, it must be noted that these quantities are not far from the estimates for the lowest observed adverse effect level (LOAEL) of 5 mg/kg body weight/d derived for nano TiO2 by the European Commission's Scientific Committee on Consumer Safety[57].

The effects of mNP that could have a role in CeD development involve three different aspects, namely the impairment of the intestinal barrier, the interaction with the immune system and the possible effect on microbiota (Figure 1B).

Intestinal barrier impairment

The first layer of the small intestinal barrier is a very thin (approximately 20 micron) layer of mucus, composed of mucin glycoproteins and antimicrobial agents such as secretory IgA. The second layer is a continuous and tight epithelium, composed of several specialized cells: at the bottom of the crypts reside stem and Paneth cells, whereas enterocytes, goblet and enteroendocrine cells are mainly in the villi. What makes the epithelium a selective barrier is the presence of highly dynamic intercellular junctions, adherent junctions (AJ) and TJ being the most representative. AJ are composed of transmembrane proteins cadherine, which are connected between them extracellularly, and with the catenin proteins in the cells. Catenins are in turn linked to the acti-myosin complex. TJ are formed by occludins, claudins and JAM-A proteins that interact with zonula occludens proteins and catenins in the intracellular space. Therefore AJ, TJ and actin cytoskeleton form a complex that can regulate the permeability (paracellular route) of the intestinal barrier, following intracellular or extracellular signals.

A growing number of diseases have recently been associated with intestinal barrier alterations, particularly related to TJ dysfunction. This finding can be easily explained: gastrointestinal barrier permeability alterations can increase the cut-off of molecules passing into the submucosa. In physiological conditions, only small molecules with a molecular weight of about 600da can pass the barrier, but these alterations result in the passage of immunogenic molecules, the activation of the immune system and the establishment of an inflammatory state. Since inflammatory mediators are also known to affect the intestinal barrier, a mild inflammatory status could eventually lead to a stronger disruption of the barrier itself[58]. Particularly important in this sense is the association of a leaky barrier with inflammatory bowel diseases (IBD) and several autoimmune diseases, such as CeD[58-60]. To develop CeD, gluten peptides have to pass into the submucosa. Therefore, any factors which are able to alter the intestinal barrier permeability, allowing an higher passage of these peptides into the submucosa, may increase the number of predisposed subjects developing the disease.

In 2015 Lerner and Matthias[61] observed that the increase in the incidence of autoimmune diseases (considering also CeD among others) paralleled with the growing use of food additive in the industry. They therefore postulated that the permeability alterations induced by food additives could be associated with the increment in incidence of autoimmune diseases. Although the author did not refer directly to the mNP, several studies have been performed on their impact on the GI barrier. Results showed that mNP can alter the intestinal permeability both directly, by altering the TJ or inducing epithelial cell death[34,62-64], or indirectly, by inducing inflammation or oxidative stress that in turn can impair TJ and permeability[58,65]. In this context, the work of Ruiz *et al*[66] is interesting. It looked at the impact of TiO2NP both *in vivo* (mice with DSS-induced ulcerative colitis) and *in vitro* (intestinal epithelial cells and macrophages). TiO2NP oral administration worsened the already established colitis through inflammasome activation. Also, *in vitro* stimulations induced IL-1β and IL18 increment, as well as higher epithelial permeability driven by the activation of the inflammasome pathway. These results clearly associate the consumption of mNP with an increase of the intestinal permeability, but only when there is a pre-existent tendency to develop it.

However, even if the studied mNP does not induce permeability alteration, it has to be considered that the mNPs may absorb the protein itself on its surface and therefore behave as a "Trojan horse", increasing the amount of immunogenic molecules that arrive into the submucosa[67,68]. Thus, in the case of CeD, food NPs could bind gliadin peptides and help them to cross the intestinal barrier, probably using the endocytotic pathway. Several studies are needed to test this hypothesis, since no data are currently available on this topic. Moreover, it will be necessary to take into account the interaction with other food components[69,70], and with the intestinal mucus[71], since both components can alter NPs uptake by enterocytes.

On the other hand, it must be underlined that NPs can play a role in the pathogenesis of other gastroenterological disorders, and concerns have also been

raised for several evidences that linked NPs, particularly the whitening agent E171(TiO2NP), to IBD development[66,72,73].

mNPs and the immune system

mNPs can interact with cells involved in innate and adaptive immune response in several organs, altering cytokine production, activation of cell surface receptors and/or cell maturation (including the ability of cells to present antigens)[74-77]. Nanoparticles can be recognized as foreign materials and eliminated by the immune system, but they can also trigger an excessive activation of immune responses. This could be useful should NP be used as an adjuvant in vaccinations, but could be detrimental in case of autoimmune disorders. In particular, the binding of gliadin peptides to food NP could represent a way by which these specific antigens can be taken up in great quantity by antigen presenting cells, thus increasing the activation of the autoimmunity process. Several studies have been performed on macrophage-like cell lines to assess the effect of metallic NPs, analyzing the cytotoxicity as well as differences in cytokines production; AgNPs were able to increase the production of IL-8[78,79], which also depended on NP size[78] whereas TiO2 NPs increased the secretion of TNF-α and IL-6[80]. Interestingly, Au-NPs induced an alteration in phagocytosis without variation in cytotoxicity or cytokine gene expression[81], whereas a similar effect by TiO2 NPs was associated with an inflammatory response[82]. Transcription profiling on a macrophage cell line treated with different NPs revealed a particular expression pattern, thus suggesting that each metallic NP can trigger a specific response, also depending on the chemical characteristics of the nanoparticle itself[83]. Silver NPs have been demonstrated to be able to interact with human monocytes, increasing the production and release of IL-1β, even after the exposure to very low concentrations[84]. Ag-NP were also able to cause superoxide production, as well as the formation of inflammasome. Metallic NPs also altered the expression of adhesion molecules and chemokine receptor type 4 on the surface of human peripheral lymphocytes[85]; interestingly, these effects were independent from any sign of cytotoxicity, suggesting that the response to NP exposure can be more subtle and mainly related to gene expression variations. However, NPs can also interact with cells involved in adaptive immune response, and *in vitro* data showed that TiO2 NPs can induce maturation of dendritic cells through the activation of Nf-kB pathway[86], a process which is essential for antigen presentation to T helper cells. Again, this process could be important in CeD, since antigen presentation by dendritic cells represents an essential step for the activation of the autoimmune response.

Nanoparticles and microbiota

Microbiota plays an important role in maintaining the homeostasis of a healthy gut. Alterations in microbiota composition have been reported both in pediatric as well as adult CeD patients if compared to controls[87-89], although it is currently still unknown whether these changes are causative of the disease or a consequence of mucosal alterations.

However, microbiota can be altered by exposure to dietary mNP. *In vitro* experiments performed on a colon-like microbial community showed that exposure to small quantities of E171 (comparable to the amount present in two pieces of chewing gum) was sufficient to alter the phylogenetic composition[90]. Significant changes in the phyla were also observed in mice treated for 28 d with TiO2NP, with variations induced by both forms of TiO2NP, namely rutilium and anatase[91].

As already mentioned, silver nanoparticles are employed as antibacterial agents, and thus it should be expected that they can alter the microbiota composition. In fact, in mice exposed to increasing doses of AgNP for 28 d, a disturbed bacterial evenness (αdiversity) and populations (β-diversity) was detected by Next Generation Sequencing. This effect was also dose-dependent. Ag NP increased the ratio between Firmicutes (F) and Bacteroidetes (B) phyla, results similar to those observed in presence of inflammation[92]. Variation in microbiota composition were also observed by another group, although results were different regarding the phyla, possibly due to the different experimental design (rats treated for 14 d)[93].

Last but not least, it must be emphasized that within our gut there is also a viral component that interacts with the microbiota and the intestinal mucosa. Although studies evaluating the possible effect of food NP on this component are scanty, initial data obtained *in vitro* suggest that Ag-NP can alter the abundance of several viral species[94]. Since these species can be hosted by different categories of bacteria (commensal or pathogenic), changes in intestinal viriome can, in turn, cause alteration in the microbiota itself.

CONCLUSIONS

Food additives could play an important role in the pathogenesis of CeD, either altering gliadin peptides properties or interacting with the intestinal environment, at the barrier level or with the immune system. Moreover, the increasing use of prepared food and, in turn, the augmented ingestion of NPs, could be an additional factor in triggering the development of CeD in genetically predisposed individuals. For this reason, *in vitro* and *in vivo* studies to evaluate these possible interactions are needed.

REFERENCES

1 **Romanos J**, Rosén A, Kumar V, Trynka G, Franke L, Szperl A, Gutierrez-Achury J, van Diemen CC, Kanninga R, Jankipersadsing SA, Steck A, Eisenbarth G, van Heel DA, Cukrowska B, Bruno V, Mazzilli MC, Núñez C, Bilbao JR, Mearin ML, Barisani D, Rewers M, Norris JM, Ivarsson A, Boezen HM, Liu E, Wijmenga C; PreventCD Group. Improving coeliac disease risk prediction by testing non-HLA variants additional to HLA variants. *Gut* 2014; **63**: 415-422 [PMID: 23704318 DOI: 10.1136/gutjnl-2012-304110]

2 **West J**, Fleming KM, Tata LJ, Card TR, Crooks CJ. Incidence and prevalence of celiac disease and dermatitis herpetiformis in the UK over two decades: population-based study. *Am J Gastroenterol* 2014; **109**: 757-768 [PMID: 24667576 DOI: 10.1038/ajg.2014.55]

3 **White LE**, Merrick VM, Bannerman E, Russell RK, Basude D, Henderson P, Wilson DC, Gillett PM. The rising incidence of celiac disease in Scotland. *Pediatrics* 2013; **132**: e924-e931 [PMID: 24019416 DOI: 10.1542/peds.2013-0932]

4 **Lohi S**, Mustalahti K, Kaukinen K, Laurila K, Collin P, Rissanen H, Lohi O, Bravi E, Gasparin M, Reunanen A, Mäki M. Increasing prevalence of coeliac disease over time. *Aliment Pharmacol Ther* 2007; **26**: 1217-1225 [PMID: 17944736 DOI: 10.1111/j.1365-2036.2007.03502.x]

5 **Riddle MS**, Murray JA, Porter CK. The incidence and risk of celiac disease in a healthy US adult population. *Am J Gastroenterol* 2012; **107**: 1248-1255 [PMID: 22584218 DOI: 10.1038/ajg.2012.130]

6 **Almallouhi E**, King KS, Patel B, Wi C, Juhn YJ, Murray JA, Absah I. Increasing Incidence and Altered Presentation in a Population-based Study of Pediatric Celiac Disease in North America. *J Pediatr Gastroenterol Nutr* 2017; **65**: 432-437 [PMID: 28151767 DOI: 10.1097/MPG.0000000000001532]

7 **Shan L**, Molberg Ø, Parrot I, Hausch F, Filiz F, Gray GM, Sollid LM, Khosla C. Structural basis for gluten intolerance in celiac sprue. *Science* 2002; **297**: 2275-2279 [PMID: 12351792 DOI: 10.1126/science.1074129]

8 **Picarelli A**, Di Tola M, Sabbatella L, Anania MC, Di Cello T, Greco R, Silano M, De Vincenzi M. 31-43 amino acid sequence of the alpha-gliadin induces anti-endomysial antibody production during in vitro challenge. *Scand J Gastroenterol* 1999; **34**: 1099-1102 [PMID: 10582760]

9 **Food and Drug Administration**. Transglutaminase GRAS Notification, Washington, DC, 2001. Available from: https://www.fda.gov/Food/IngredientsPackagingLabeling/GRAS/NoticeInventory/ucm154631.htm

10 **Romeih E**, Walker G. Recent advances on microbial transglutaminase and dairy application. *Trends in Food Science & Technology* 2017; **62**: 133e140 [DOI: 10.1016/j.tifs.2017.02.015]

11 **Gharibzahedi SMT**, Yousefi S, Chronakis IS. Microbial transglutaminase in noodle and pasta processing. *Crit Rev Food Sci Nutr* 2017; 1-15 [PMID: 28857615 DOI: 10.1080/10408398.2017.1367643]

12 **Mazzeo MF**, Bonavita R, Maurano F, Bergamo P, Siciliano RA, Rossi M. Biochemical modifications of gliadins induced by microbial transglutaminase on wheat flour. *Biochim Biophys Acta* 2013; **1830**: 5166-5174 [PMID: 23891939 DOI: 10.1016/j.bbagen.2013.07.021]

13 **Gianfrani C**, Siciliano RA, Facchiano AM, Camarca A, Mazzeo MF, Costantini S, Salvati VM, Maurano F, Mazzarella G, Iaquinto G, Bergamo P, Rossi M. Transamidation of wheat flour inhibits the response to gliadin of intestinal T cells in celiac disease. *Gastroenterology* 2007; **133**: 780-789 [PMID: 17678925 DOI: 10.1053/j.gastro.2007.06.023]

14 **Dekking EHA**, Van Veelen PA, de Ru A, Kooy-Winkelaar EMC, Gröneveld T, Nieuwenhuizen WF, Koning F. Microbial transglutaminases generate T cell stimulatory epitopes involved in celiac disease. *J Cereal Sci* 2008; **47**: 339-346 [DOI: 10.1016/j.jcs.2007.05.004]

15 **Cabrera-Chávez F**, Rouzaud-Sández O, Sotelo-Cruz N, Calderón de la Barca AM. Transglutaminase treatment of wheat and maize prolamins of bread increases the serum IgA reactivity of celiac disease patients. *J Agric Food Chem* 2008; **56**: 1387-1391 [PMID: 18193828 DOI: 10.1021/jf0724163]

16 **Matthias T**, Jeremias P, Neidhöfer S, Lerner A. The industrial food additive, microbial transglutaminase, mimics tissue transglutaminase and is immunogenic in celiac disease patients. *Autoimmun Rev* 2016; **15**: 1111-1119 [PMID: 27640315 DOI: 10.1016/j.autrev.2016.09.011]

17 **Ruh T**, Ohsam J, Pasternack R, Yokoyama K, Kumazawa Y, Hils M. Microbial transglutaminase treatment in pasta-production does not affect the immunoreactivity of gliadin with celiac disease patients' sera. *J Agric Food Chem* 2014; **62**: 7604-7611 [PMID: 24998318 DOI: 10.1021/jf501275c]

18 **Heil A**, Ohsam J, van Genugten B, Diez O, Yokoyama K, Kumazawa Y, Pasternack R, Hils M. Microbial Transglutaminase Used in Bread Preparation at Standard Bakery Concentrations Does Not Increase Immunodetectable Amounts of Deamidated Gliadin. *J Agric Food Chem* 2017; **65**: 6982-6990 [PMID: 28721717 DOI: 10.1021/acs.jafc.7b02414]

19 **Zhou L**, Kooy-Winkelaar YMC, Cordfunke RA, Dragan I, Thompson A, Drijfhout JW, van Veelen PA, Chen H, Koning F. Abrogation of Immunogenic Properties of Gliadin Peptides through Transamidation by Microbial Transglutaminase Is Acyl-Acceptor Dependent. *J Agric Food Chem* 2017; **65**: 7542-7552 [PMID: 28771001 DOI: 10.1021/acs.jafc.7b02557]

20 **Lombardi E**, Bergamo P, Maurano F, Bozzella G, Luongo D, Mazzarella G, Rotondi Aufiero V, Iaquinto G, Rossi M. Selective inhibition of the gliadin-specific, cell-mediated immune response by transamidation with microbial transglutaminase. *J Leukoc Biol* 2013; **93**: 479-488 [PMID: 23108099 DOI: 10.1189/jlb.0412182]

21 **Elli L**, Roncoroni L, Hils M, Pasternack R, Barisani D, Terrani C, Vaira V, Ferrero S, Bardella MT. Immunological effects of transglutaminase-treated gluten in coeliac disease. *Hum Immunol* 2012; **73**: 992-997 [PMID: 22836039 DOI: 10.1016/j.humimm.2012.07.318]

22 **Mazzarella G**, Salvati VM, Iaquinto G, Stefanile R, Capobianco F, Luongo D, Bergamo P, Maurano F, Giardullo N, Malamisura B, Rossi M. Reintroduction of gluten following flour transamidation in adult celiac patients: a randomized, controlled clinical study. *Clin Dev Immunol* 2012; **2012**: 329150 [PMID: 22899947 DOI: 10.1155/2012/329150]

23 **Heredia-Sandoval NG**, Islas-Rubio AR, Cabrera-Chávez F, Calderón de la Barca AM. Transamidation of gluten proteins during the bread-making process of wheat flour to produce breads with less immunoreactive gluten. *Food Funct* 2014; **5**: 1813-1818 [PMID: 24917417 DOI: 10.1039/c4fo00118d]

24 **Ribeiro M**, Nunes FM, Guedes S, Domingues P, Silva AM, Carrillo JM, Rodriguez-Quijano M, Branlard G, Igrejas G. Efficient chemo-enzymatic gluten detoxification: reducing toxic epitopes for celiac patients improving functional properties. *Sci Rep* 2015; **5**: 18041 [PMID: 26691232 DOI: 10.1038/srep18041]

25 **Gulfam M**, Kim JE, Lee JM, Ku B, Chung BH, Chung BG. Anticancer drug-loaded gliadin nanoparticles induce apoptosis in breast cancer cells. *Langmuir* 2012; **28**: 8216-8223 [PMID: 22568862 DOI: 10.1021/la300691n]

26 **El-Wakil NA**, Hassan EA, Abou-Zeid RE, Dufresne A. Development of wheat gluten/nanocellulose/titanium dioxide nanocomposites for active food packaging. *Carbohydr Polym* 2015; **124**: 337-346 [PMID: 25839828 DOI: 10.1016/j.carbpol.2015.01.076]

27 **Groh KJ**, Geueke B, Muncke J. Food contact materials and gut health: Implications for toxicity assessment and relevance of high molecular weight migrants. *Food Chem Toxicol* 2017; **109**: 1-18 [PMID: 28830834 DOI: 10.1016/j.fct.2017.08.023]

28 **Yang FM**, Li HM, Li F, Xin ZH, Zhao LY, Zheng YH, Hu QH. Effect of nano-packing on preservation quality of fresh strawberry (Fragaria ananassa Duch. cv Fengxiang) during storage at 4 degrees C. *J Food Sci* 2010; **75**: C236-C240 [PMID: 20492272 DOI: 10.1111/j.1750-3841.2010.01520.x]

29 **Kim JS**, Kuk E, Yu KN, Kim JH, Park SJ, Lee HJ, Kim SH, Park YK, Park YH, Hwang CY, Kim YK, Lee YS, Jeong DH, Cho MH. Antimicrobial effects of silver nanoparticles. *Nanomedicine* 2007; **3**: 95-101 [PMID: 17379174 DOI: 10.1016/j.nano.2006.12.001]

30 **Vance ME**, Kuiken T, Vejerano EP, McGinnis SP, Hochella MF, Rejeski D, Hull MS. Nanotechnology in the real world: Redeveloping the nanomaterial consumer products inventory. *Beilstein J Nanotechnol* 2015; **6**: 1769-1780 [PMID: 26425429 DOI: 10.3762/bjnano.6.181]

31 **Arora S**, Sharma P, Kumar S, Nayan R, Khanna PK, Zaidi MGH. Gold-nanoparticle induced enhancement in growth and seed yield of Brassica juncea. *Plant Growth Regul* 2012; **66**: 303-310 [DOI: 10.1007/s10725-011-9649-z]

32 **Kumar V**, Guleria P, Kumar V, Yadav SK. Gold nanoparticle exposure induces growth and yield enhancement in Arabidopsis thaliana. *Sci Total Environ* 2013; **461-462**: 462-468 [PMID: 23747561 DOI: 10.1016/j.scitotenv.2013.05.018]

33 **Yao M**, He L, McClements DJ, Xiao H. Uptake of Gold Nanoparticles by Intestinal Epithelial Cells: Impact of Particle Size on Their Absorption, Accumulation, and Toxicity. *J Agric Food Chem* 2015; **63**: 8044-8049 [PMID: 26313743 DOI: 10.1021/acs.jafc.5b03242]

34 **Hanley C**, Thurber A, Hanna C, Punnoose A, Zhang J, Wingett DG. The Influences of Cell Type and ZnO Nanoparticle Size on Immune Cell Cytotoxicity and Cytokine Induction. *Nanoscale Res Lett* 2009; **4**: 1409-1420 [PMID: 20652105 DOI: 10.1007/s11671-009-9413-8]

35 **Imai S**, Morishita Y, Hata T, Kondoh M, Yagi K, Gao JQ, Nagano K, Higashisaka K, Yoshioka Y, Tsutsumi Y. Cellular internalization, transcellular transport, and cellular effects of silver nanoparticles in polarized Caco-2 cells following apical or basolateral exposure. *Biochem Biophys Res Commun* 2017; **484**: 543-549 [PMID: 28130106 DOI: 10.1016/j.bbrc.2017.01.114]

36 **Karlsson HL**, Cronholm P, Hedberg Y, Tornberg M, De Battice L, Svedhem S, Wallinder IO. Cell membrane damage and protein interaction induced by copper containing nanoparticles--importance of the metal release process. *Toxicology* 2013; **313**: 59-69 [PMID: 23891735 DOI: 10.1016/j.tox.2013.07.012]

37 **McShan D**, Ray PC, Yu H. Molecular toxicity mechanism of nanosilver. *J Food Drug Anal* 2014; **22**: 116-127 [PMID: 24673909 DOI: 10.1016/j.jfda.2014.01.010]

38 **Lichtenstein D**, Ebmeyer J, Meyer T, Behr AC, Kästner C, Böhmert L, Juling S, Niemann B, Fahrenson C, Selve S, Thünemann AF, Meijer J, Estrela-Lopis I, Braeuning A, Lampen A. It takes more than a coating to get nanoparticles through the intestinal barrier in vitro. *Eur J Pharm Biopharm* 2017; **118**: 21-29 [PMID: 27993735 DOI: 10.1016/j.ejpb.2016.12.004]

39 **Yang D**, Liu D, Qin M, Chen B, Song S, Dai W, Zhang H, Wang X, Wang Y, He B, Tang X, Zhang Q. Intestinal Mucin Induces More Endocytosis but Less Transcytosis of Nanoparticles across Enterocytes by Triggering Nanoclustering and Strengthening the Retrograde Pathway. *ACS Appl Mater Interfaces* 2018; **10**: 11443-11456 [PMID: 29485849 DOI: 10.1021/acsami.7b19153]

40 **Sokolov SV**, Tschulik K, Batchelor-McAuley C, Jurkschat K, Compton RG. Reversible or not? Distinguishing agglomeration and aggregation at the nanoscale. *Anal Chem* 2015; **87**: 10033-10039 [PMID: 26352558 DOI: 10.1021/acs.analchem.5b02639]

41 **Peters R**, Kramer E, Oomen AG, Rivera ZE, Oegema G, Tromp PC, Fokkink R, Rietveld A, Marvin HJ, Weigel S, Peijnenburg AA, Bouwmeester H. Presence of nano-sized silica during in vitro digestion of foods containing silica as a food additive. *ACS Nano* 2012; **6**: 2441-2451 [PMID: 22364219 DOI: 10.1021/nn204728k]

42 **Walczak AP**, Fokkink R, Peters R, Tromp P, Herrera Rivera ZE, Rietjens IM, Hendriksen PJ, Bouwmeester H. Behaviour of silver nanoparticles and silver ions in an in vitro human gastrointestinal digestion model. *Nanotoxicology* 2013; **7**: 1198-1210 [PMID: 22931191 DOI: 10.3109/17435390.2012.726382]

43 **Sieg H**, Kästner C, Krause B, Meyer T, Burel A, Böhmert L, Lichtenstein D, Jungnickel H, Tentschert J, Laux P, Braeuning A, Estrela-Lopis I, Gauffre F, Fessard V, Meijer J, Luch A, Thünemann AF, Lampen A. Impact of an Artificial Digestion Procedure on Aluminum-Containing Nanomaterials. *Langmuir* 2017; **33**: 10726-10735 [PMID: 28903564 DOI: 10.1021/acs.langmuir.7b02729]

44 **McCracken C**, Zane A, Knight DA, Dutta PK, Waldman WJ. Minimal intestinal epithelial cell toxicity in response to short- and long-term food-relevant inorganic nanoparticle exposure. *Chem Res Toxicol* 2013; **26**: 1514-1525 [PMID: 24028186 DOI: 10.1021/tx400231u]

45 **Albanese A**, Chan WC. Effect of gold nanoparticle aggregation on cell uptake and toxicity. *ACS Nano* 2011; **5**: 5478-5489 [PMID: 21692495 DOI: 10.1021/nn2007496]

46 **Bellmann S**, Carlander D, Fasano A, Momcilovic D, Scimeca JA, Waldman WJ, Gombau L, Tsytsikova L, Canady R, Pereira DI, Lefebvre DE. Mammalian gastrointestinal tract parameters modulating the integrity, surface properties, and absorption of food-relevant nanomaterials. *Wiley Interdiscip Rev Nanomed Nanobiotechnol* 2015; **7**: 609-622 [PMID: 25641962 DOI: 10.1002/wnan.1333]

47 **Walczak AP**, Kramer E, Hendriksen PJ, Helsdingen R, van der Zande M, Rietjens IM, Bouwmeester H. In vitro gastrointestinal digestion increases the translocation of polystyrene nanoparticles in an in vitro intestinal co-culture model. *Nanotoxicology* 2015; **9**: 886-894 [PMID: 25672814 DOI: 10.3109/17435390.2014.988664]

48 **Wang Y**, Yuan L, Yao C, Ding L, Li C, Fang J, Sui K, Liu Y, Wu M. A combined toxicity study of zinc oxide nanoparticles and vitamin C in food additives. *Nanoscale* 2014; **6**: 15333-15342 [PMID: 25387158 DOI: 10.1039/c4nr05480f]

49 **Cao Y**, Roursgaard M, Kermanizadeh A, Loft S, Møller P. Synergistic effects of zinc oxide nanoparticles and Fatty acids on toxicity to caco-2 cells. *Int J Toxicol* 2015; **34**: 67-76 [PMID: 25421740 DOI: 10.1177/1091581814560032]

50 **Martirosyan A**, Bazes A, Schneider YJ. In vitro toxicity assessment of silver nanoparticles in the presence of phenolic compounds--preventive agents against the harmful effect? *Nanotoxicology* 2014; **8**: 573-582 [PMID: 23738887 DOI: 10.3109/17435390.2013.812258]

51 **Martirosyan A**, Grintzalis K, Polet M, Laloux L, Schneider YJ. Tuning the inflammatory response to silver nanoparticles via quercetin in Caco-2 (co-)cultures as model of the human intestinal mucosa. *Toxicol Lett* 2016; **253**: 36-45 [PMID: 27113704 DOI: 10.1016/j.toxlet.2016.04.018]

52 **Ministry of Agriculture Fish and Food**. Dietary intake of food additives in the UK: initial surveillance (food surveillance paper 37). London, UK: MAFF; 1993;

53 **Fröhlich E**, Roblegg E. Models for oral uptake of nanoparticles in consumer products. *Toxicology* 2012; **291**: 10-17 [PMID: 22120540 DOI: 10.1016/j.tox.2011.11.004]

54 **Powell JJ**, Faria N, Thomas-McKay E, Pele LC. Origin and fate of dietary nanoparticles and microparticles in the gastrointestinal tract. *J Autoimmun* 2010; **34**: J226-J233 [PMID: 20096538 DOI: 10.1016/j.jaut.2009.11.006]

55 **Weir A**, Westerhoff P, Fabricius L, Hristovski K, von Goetz N. Titanium dioxide nanoparticles in food and personal care products. *Environ Sci Technol* 2012; **46**: 2242-2250 [PMID: 22260395 DOI: 10.1021/es204168d]

56 **EFSA ANS Panel (EFSA Panel on Food Additives and Nutrient Sources added to Food)**. Re-evaluation of titanium dioxide (E 171) as a food additive. *EFSA Journal* 2016; **14**: e04545 [DOI: 10.2903/j.efsa.2016.4545]

57 **SCCS (Scientific Committee on Consumer Safety)**. Opinion on titanium dioxide (nano form), 22 July 2013, revision of 22 April 2014. Available from: http://ec.europa.eu/health/scientific_committees/consumer_safety/docs/sccs_o_136.pdf

58 **Turner JR**. Intestinal mucosal barrier function in health and disease. *Nat Rev Immunol* 2009; **9**: 799-809 [PMID: 19855405 DOI: 10.1038/nri2653]

59 **Schumann M**, Siegmund B, Schulzke JD, Fromm M. Celiac Disease: Role of the Epithelial Barrier. *Cell Mol Gastroenterol Hepatol* 2017; **3**: 150-162 [PMID: 28275682 DOI: 10.1016/j.jcmgh.2016.12.006]

60 **Wapenaar MC**, Monsuur AJ, van Bodegraven AA, Weersma RK, Bevova MR, Linskens RK, Howdle P, Holmes G, Mulder CJ, Dijkstra G, van Heel DA, Wijmenga C. Associations with tight junction genes PARD3 and MAGI2 in Dutch patients point to a common barrier defect for coeliac disease and ulcerative colitis. *Gut* 2008; **57**: 463-467 [PMID: 17989107 DOI: 10.1136/gut.2007.133132]

61 **Lerner A**, Matthias T. Changes in intestinal tight junction permeability associated with industrial food additives explain the rising incidence of autoimmune disease. *Autoimmun Rev* 2015; **14**: 479-489 [PMID: 25676324 DOI: 10.1016/j.autrev.2015.01.009]

62 **Brun E**, Barreau F, Veronesi G, Fayard B, Sorieul S, Chanéac C, Carapito C, Rabilloud T, Mabondzo A, Herlin-Boime N, Carrière M. Titanium dioxide nanoparticle impact and translocation through ex vivo, in vivo and in vitro gut epithelia. *Part Fibre Toxicol* 2014; **11**: 13 [PMID: 24666995 DOI: 10.1186/1743-8977-11-13]

63 **Williams KM**, Gokulan K, Cerniglia CE, Khare S. Size and dose dependent effects of silver nanoparticle exposure on intestinal permeability in an in vitro model of the human gut epithelium. *J Nanobiotechnology* 2016; **14**: 62 [PMID: 27465730 DOI: 10.1186/s12951-016-0214-9]

64 **Koeneman BA**, Zhang Y, Westerhoff P, Chen Y, Crittenden JC, Capco DG. Toxicity and cellular responses of intestinal cells exposed to titanium dioxide. *Cell Biol Toxicol* 2010; **26**: 225-238 [PMID: 19618281 DOI: 10.1007/s10565-009-9132-z]

65 **Sheth P**, Basuroy S, Li C, Naren AP, Rao RK. Role of phosphatidylinositol 3-kinase in oxidative stress-induced disruption of tight junctions. *J Biol Chem* 2003; **278**: 49239-49245 [PMID: 14500730 DOI: 10.1074/jbc.M305654200]

66 **Ruiz PA**, Morón B, Becker HM, Lang S, Atrott K, Spalinger MR, Scharl M, Wojtal KA, Fischbeck-Terhalle A, Frey-Wagner I, Hausmann M, Kraemer T, Rogler G. Titanium dioxide nanoparticles exacerbate DSS-induced colitis: role of the NLRP3 inflammasome. *Gut* 2017; **66**: 1216-1224 [PMID: 26848183 DOI: 10.1136/gutjnl-2015-310297]

67 **Fasano A**. Leaky gut and autoimmune diseases. *Clin Rev Allergy Immunol* 2012; **42**: 71-78 [PMID: 22109896 DOI: 10.1007/s12016-011-8291-x]

68 **Howe SE**, Lickteig DJ, Plunkett KN, Ryerse JS, Konjufca V. The uptake of soluble and particulate antigens by epithelial cells in the mouse small intestine. *PLoS One* 2014; **9**: e86656 [PMID: 24475164 DOI: 10.1371/journal.pone.0086656]

69 **Lichtenstein D**, Ebmeyer J, Knappe P, Juling S, Böhmert L, Selve S, Niemann B, Braeuning A, Thünemann AF, Lampen A. Impact of food components during in vitro digestion of silver nanoparticles on cellular uptake and cytotoxicity in intestinal cells. *Biol Chem* 2015; **396**: 1255-1264 [PMID: 26040006 DOI: 10.1515/hsz-2015-0145]

70 **Bajka BH**, Rigby NM, Cross KL, Macierzanka A, Mackie AR. The influence of small intestinal mucus structure on particle transport ex vivo. *Colloids Surf B Biointerfaces* 2015; **135**: 73-80 [PMID: 26241918 DOI: 10.1016/j.colsurfb.2015.07.038]

71 **Lomer MC**, Thompson RP, Powell JJ. Fine and ultrafine particles of the diet: influence on the mucosal immune response and association with Crohn's disease. *Proc Nutr Soc* 2002; **61**: 123-130 [PMID: 12002786]

72 **Powell JJ**, Harvey RS, Ashwood P, Wolstencroft R, Gershwin ME, Thompson RP. Immune potentiation of ultrafine dietary particles in normal subjects and patients with inflammatory bowel disease. *J Autoimmun* 2000; **14**: 99-105 [PMID: 10648120 DOI: 10.1006/jaut.1999.0342]

73 **Evans SM**, Ashwood P, Warley A, Berisha F, Thompson RP, Powell JJ. The role of dietary microparticles and calcium in apoptosis and interleukin-1beta release of intestinal macrophages. *Gastroenterology* 2002; **123**: 1543-1553 [PMID: 12404229]

74 **Cui Y**, Liu H, Zhou M, Duan Y, Li N, Gong X, Hu R, Hong M, Hong F. Signaling pathway of inflammatory responses in the mouse liver caused by TiO2 nanoparticles. *J Biomed Mater Res A* 2011; **96**: 221-229 [PMID: 21105171 DOI: 10.1002/jbm.a.32976]

75 **Khan HA**, Abdelhalim MA, Alhomida AS, Al Ayed MS. Transient increase in IL-1β, IL-6 and TNF-α gene expression in rat liver exposed to gold nanoparticles. *Genet Mol Res* 2013; **12**: 5851-5857 [PMID: 24301954 DOI: 10.4238/2013.November.22.12]

76 **Chang H**, Ho CC, Yang CS, Chang WH, Tsai MH, Tsai HT, Lin P. Involvement of MyD88 in zinc oxide nanoparticle-induced lung inflammation. *Exp Toxicol Pathol* 2013; **65**: 887-896 [PMID: 23352990 DOI: 10.1016/j.etp.2013.01.001]

77 **Dhupal M**, Oh JM, Tripathy DR, Kim SK, Koh SB, Park KS. Immunotoxicity of titanium dioxide nanoparticles via simultaneous induction of apoptosis and multiple toll-like receptors signaling through ROS-dependent SAPK/JNK and p38 MAPK activation. *Int J Nanomedicine* 2018; **13**: 6735-6750 [PMID: 30425486 DOI: 10.2147/IJN.S176087]

78 **Park J**, Lim DH, Lim HJ, Kwon T, Choi JS, Jeong S, Choi IH, Cheon J. Size dependent macrophage responses and toxicological effects of Ag nanoparticles. *Chem Commun (Camb)* 2011; **47**: 4382-4384 [PMID: 21390403 DOI: 10.1039/c1cc10357a]

79 **Kim S**, Choi IH. Phagocytosis and endocytosis of silver nanoparticles induce interleukin-8 production in human macrophages. *Yonsei Med J* 2012; **53**: 654-657 [PMID: 22477013 DOI: 10.3349/ymj.2012.53.3.654]

80 **Triboulet S**, Aude-Garcia C, Armand L, Collin-Faure V, Chevallet M, Diemer H, Gerdil A, Proamer F, Strub JM, Habert A, Herlin N, Van Dorsselaer A, Carrière M, Rabilloud T. Comparative proteomic analysis of the molecular responses of mouse macrophages to titanium dioxide and copper oxide nanoparticles unravels some toxic mechanisms for copper oxide nanoparticles in macrophages. *PLoS One* 2015; **10**: e0124496 [PMID: 25902355 DOI: 10.1371/journal.pone.0124496]

81 **Bancos S**, Stevens DL, Tyner KM. Effect of silica and gold nanoparticles on macrophage proliferation, activation markers, cytokine production, and phagocytosis in vitro. *Int J Nanomedicine* 2014; **10**: 183-206 [PMID: 25565813 DOI: 10.2147/IJN.S72580]

82 **Chen Q**, Wang N, Zhu M, Lu J, Zhong H, Xue X, Guo S, Li M, Wei X, Tao Y, Yin H. TiO₂ nanoparticles cause mitochondrial dysfunction, activate inflammatory responses, and attenuate phagocytosis in macrophages: A proteomic and metabolomic insight. *Redox Biol* 2018; **15**: 266-276 [PMID: 29294438 DOI: 10.1016/j.redox.2017.12.011]

83 **Poon WL**, Alenius H, Ndika J, Fortino V, Kolhinen V, Meščeriakovas A, Wang M, Greco D, Lähde A, Jokiniemi J, Lee JC, El-Nezami H, Karisola P. Nano-sized zinc oxide and silver, but not titanium dioxide, induce innate and adaptive immunity and antiviral response in differentiated THP-1 cells. *Nanotoxicology* 2017; **11**: 936-951 [PMID: 28958187 DOI: 10.1080/17435390.2017.1382600]

84 **Yang EJ**, Kim S, Kim JS, Choi IH. Inflammasome formation and IL-1β release by human blood monocytes in response to silver nanoparticles. *Biomaterials* 2012; **33**: 6858-6867 [PMID: 22770526 DOI: 10.1016/j.biomaterials.2012.06.016]

85 **Lozano-Fernández T**, Ballester-Antxordoki L, Pérez-Temprano N, Rojas E, Sanz D, Iglesias-Gaspar M, Moya S, González-Fernández Á, Rey M. Potential impact of metal oxide nanoparticles on the immune system: The role of integrins, L-selectin and the chemokine receptor CXCR4. *Nanomedicine* 2014; **10**: 1301-1310 [PMID: 24650882 DOI: 10.1016/j.nano.2014.03.007]

86 **Zhu R**, Zhu Y, Zhang M, Xiao Y, Du X, Liu H, Wang S. The induction of maturation on dendritic cells by TiO2 and Fe(3)O(4)@TiO(2) nanoparticles via NF-κB signaling pathway. *Mater Sci Eng C Mater Biol Appl* 2014; **39**: 305-314 [PMID: 24863229 DOI: 10.1016/j.msec.2014.03.005]

87 **Olivares M**, Neef A, Castillejo G, Palma GD, Varea V, Capilla A, Palau F, Nova E, Marcos A, Polanco I, Ribes-Koninckx C, Ortigosa L, Izquierdo L, Sanz Y. The HLA-DQ2 genotype selects for early intestinal microbiota composition in infants at high risk of developing coeliac disease. *Gut* 2015; **64**: 406-417 [PMID: 24939571 DOI: 10.1136/gutjnl-2014-306931]

88 **Caminero A**, Galipeau HJ, McCarville JL, Johnston CW, Bernier SP, Russell AK, Jury J, Herran AR, Casqueiro J, Tye-Din JA, Surette MG, Magarvey NA, Schuppan D, Verdu EF. Duodenal Bacteria From Patients With Celiac Disease and Healthy Subjects Distinctly Affect Gluten Breakdown and Immunogenicity. *Gastroenterology* 2016; **151**: 670-683 [PMID: 27373514 DOI: 10.1053/j.gastro.2016.06.041]

89 **D'Argenio V**, Casaburi G, Precone V, Pagliuca C, Colicchio R, Sarnataro D, Discepolo V, Kim SM, Russo I, Del Vecchio Blanco G, Horner DS, Chiara M, Pesole G, Salvatore P, Monteleone G, Ciacci C, Caporaso GJ, Jabrì B, Salvatore F, Sacchetti L. Metagenomics Reveals Dysbiosis and a Potentially Pathogenic N. flavescens Strain in Duodenum of Adult Celiac Patients. *Am J Gastroenterol* 2016; **111**: 879-890 [PMID: 27045926 DOI: 10.1038/ajg.2016.95]

90 **Dudefoi W**, Moniz K, Allen-Vercoe E, Ropers MH, Walker VK. Impact of food grade and nano-TiO₂ particles on a human intestinal community. *Food Chem Toxicol* 2017; **106**: 242-249 [PMID: 28564612 DOI: 10.1016/j.fct.2017.05.050]

91 **Li J**, Yang S, Lei R, Gu W, Qin Y, Ma S, Chen K, Chang Y, Bai X, Xia S, Wu C, Xing G. Oral administration of rutile and anatase TiO₂ nanoparticles shifts mouse gut microbiota structure. *Nanoscale* 2018; **10**: 7736-7745 [PMID: 29658026 DOI: 10.1039/c8nr00386f]

92 **van den Brule S**, Ambroise J, Lecloux H, Levard C, Soulas R, De Temmerman PJ, Palmai-Pallag M, Marbaix E, Lison D. Dietary silver nanoparticles can disturb the gut microbiota in mice. *Part Fibre Toxicol* 2016; **13**: 38 [PMID: 27393559 DOI: 10.1186/s12989-016-0149-1]

93 **Javurek AB**, Suresh D, Spollen WG, Hart ML, Hansen SA, Ellersieck MR, Bivens NJ, Givan SA, Upendran A, Kannan R, Rosenfeld CS. Gut Dysbiosis and Neurobehavioral Alterations in Rats Exposed to Silver Nanoparticles. *Sci Rep* 2017; **7**: 2822 [PMID: 28588204 DOI: 10.1038/s41598-017-02880-0]

94 **Gokulan K**, Bekele AZ, Drake KL, Khare S. Responses of intestinal virome to silver nanoparticles: safety assessment by classical virology, whole-genome sequencing and bioinformatics approaches. *Int J Nanomedicine* 2018; **13**: 2857-2867 [PMID: 29844669 DOI: 10.2147/IJN.S161379]

World Journal of Clinical Cases

Submit a Manuscript: https://www.f6publishing.com

World J Clin Cases 2019 April 26; 7(8): 928-939

DOI: 10.12998/wjcc.v7.i8.928

ISSN 2307-8960 (online)

ORIGINAL ARTICLE

Retrospective Study

Optimal use of fielder XT guidewire enhances the success rate of chronic total occlusion percutaneous coronary intervention

Qian-Cheng Wang, Hai-Ruo Lin, Yuan Han, Hai Dong, Kai Xu, Shao-Yi Guan, Zhen-Huan Chen, Hui-Xin Hao, Jian-Ping Bin, Yu-Lin Liao, Quan-Min Jing

ORCID number: Qian-Cheng Wang (0000-0003-1085-9321); Hai-Ruo Lin (0000-0003-0413-3807); Yuan Han (0000-0002-8185-8388); Hai Dong (0000-0002-3135-8561); Kai Xu (0000-0002-5880-1922); Shao-Yi Guan (0000-0002-2866-3733); Zhen-Huan Chen (0000-0001-5819-3392); Hui-Xin Hao (0000-0001-5094-3515); Jian-Ping Bin (0000-0002-9561-1474); Yu-Lin Liao (0000-0001-5961-390X); Quan-Min Jing (0000-0002-8453-6667).

Author contributions: All authors helped to perform the study; Jing QM, Liao YL and Wang QC contributed to study conception and design; Jing QM, Wang QC, Dong H, Xu K, Guan SY and Han Y contributed to performing the procedures and collecting the data; Bin JP, Lin HR, Chen ZH and Hao HX contributed to interpreting the data and statistical analysis; Wang QC and Liao YL contributed to manuscript writing and made critical revision on the manuscript; All authors reviewed the manuscript and completed final approval.

Supported by the National Natural Science Foundation of China, No. 81570464 and No. 81770271; Special Fund for the Cultivation of College Students' Science and Technology Innovation in 2018, No. pdjha0095; and Municipal Planning Projects of Scientific Technology of Guangzhou, No. 201804020083.

Institutional review board statement: This study was reviewed and approved by the Ethics Committee of the General

Qian-Cheng Wang, Hai-Ruo Lin, Yuan Han, Zhen-Huan Chen, Hui-Xin Hao, Jian-Ping Bin, Yu-Lin Liao, Department of Cardiology, State Key Laboratory of Organ Failure Research, Nanfang Hospital, Southern Medical University, Guangzhou 510515, Guangdong Province, China

Qian-Cheng Wang, Hai Dong, Kai Xu, Shao-Yi Guan, Quan-Min Jing, Department of Cardiology, General Hospital of Northern Theater Command, Shenyang 110000, Liaoning Province, China

Corresponding author: Yu-Lin Liao, PhD, Professor, Department of Cardiology, State Key Laboratory of Organ Failure Research, Nanfang Hospital, Southern Medical University, 1838 Guangzhou Avenue North, Guangzhou 510515, Guangdong Province, China.
liao18@msn.com
Telephone: +86-20-62786294
Fax: +86-20-62786294

Abstract

BACKGROUND

Chronic total occlusion (CTO) is found in 18-31% of patients who undergo coronary angiography. Successful recanalization of CTOs is associated with reduced recurrent angina pectoris rates and increased long-term survival. Although the success rate of CTO percutaneous coronary intervention (CTO-PCI) has improved, CTO-PCI remains technically challenging. The Fielder XT guidewire was designed for CTO lesions. To validate whether the use of the guidewire increases the success rate, we compared the results of CTO-PCI with or without the guidewire. We hypothesized that the use of Fielder XT guidewire can increase the success rate of CTO-PCI.

AIM

To investigate whether the use of Fielder XT guidewire increases the final procedural success of CTO-PCI *via* the anterograde approach.

METHODS

Between January 2013 and December 2015, a retrospective study was conducted on 1230 consecutive patients with CTO who received PCI *via* the anterograde approach at the General Hospital of Northern Theater Command. The patients were divided into an XT Group (n = 686) and a no-XT Group (n = 544) depending on whether Fielder XT guidewire was used. Both groups were compared for clinical parameters, lesion-related characteristics, procedural outcomes and in-hospital complications. The data were statistically analyzed using Pearson's χ^2 test for categorical variables, and Students' t test was used to compare the

Hospital of Northern Theater Command.

Informed consent statement: Patients were not required to provide informed consent to participate in this study because the analyses used anonymous clinical data that were obtained after each patient had agreed to treatment based written consent.

Conflict-of-interest statement: The authors declare no conflicts of interest regarding this manuscript.

Manuscript source: Unsolicited manuscript

Received: January 30, 2019
Peer-review started: January 31, 2019
First decision: March 10, 2019
Revised: March 22, 2019
Accepted: April 9, 2019
Article in press: April 9, 2019
Published online: April 26, 2019

P-Reviewer: Abadi ATB, Aseni P, Elhamid SMA
S-Editor: Ji FF
L-Editor: Filipodia
E-Editor: Wu YXJ

quantitative data. Significant independent factors and a risk ratio with 95% confidence interval (CI) were assessed by multivariate logistic regression analysis.

RESULTS

In total, 1230 patients were recruited; 75.4% of the patients were male, and 55.8% of the patients were in the XT group. The overall success rate was 83.9%, with 87.8% in the XT group. Based on multivariate logistic regression analysis, factors positively associated with procedural success were the use of Fielder XT guidewire (P = 0.005, 95%CI: 1.172-2.380) and systolic blood pressure (P = 0.011, 95%CI: 1.003-1.022), while factors negatively associated with procedural success were blunt stump (P = 0.013, 95%CI: 1.341-11.862), male sex (P = 0.016, 95%CI: 0.363-0.902), New York Heart Association (NYHA) class (P = 0.035, 95%CI: 0.553-0.979), contrast amount (P = 0.018, 95%CI: 0.983-0.998) and occlusion time (P = 0.009, 95%CI: 0.994-0.999). No significant differences were found between the XT group and the no-XT group with respect to clinical parameters, lesion-related characteristics, coronary artery rupture [3 (0.4%) *vs* 8 (1.5%), P = 0.056], in-hospital death [2 (0.3%) *vs* 6 (1.1%), P = 0.079] or in-hospital target lesion revascularization [3 (0.4%) *vs* 7 (1.3%), P < 0.099]. However, there were significant differences between the groups with respect to success rate [602 (87.8%) *vs* 430 (79.0%), P < 0.001], procedure time [(74 ± 23) *vs* (83 ± 21), P < 0.001], stent length [(32.0 ± 15.8) *vs* (37.3 ± 17.6), P < 0.001], contrast amount [(148 ± 46) *vs* (166 ± 43), P < 0.001], post-PCI myocardial infarction [43 (6.3%) *vs* 59 (10.8%), P = 0.004], major adverse cardiovascular event [44 (6.4%) *vs* 57 (10.7%), P = 0.007], side branch loss [31 (4.5%) *vs* 44 (8.1%), P = 0.009], contrast-induced nephropathy [29 (4.2%) *vs* 40 (7.4%), P = 0.018] and no reflow [8 (1.2%) *vs* 14 (2.9%), P = 0.034].

CONCLUSION

The use of Fielder XT guidewire shortens the Procedure and increases the success rate of CTO-PCI, and is also associated with reduced complication rates.

Key words: Chronic total occlusion; Percutaneous coronary intervention; Anterograde wire escalation; Parallel wire technique; Fielder XT guidewire; Success rate

Core tip: This retrospective study aimed to investigate whether the use of Fielder XT guidewire can increase the final procedural success of chronic total occlusion-percutaneous coronary intervention *via* the anterograde approach. We found that the use of Fielder XT guidewire was positively associated with procedural success based on multivariate logistic regression analysis. We found no significant differences between the XT group and the no-XT group with respect to clinical parameters, lesion-related characteristics, coronary artery rupture, in-hospital death or in-hospital target lesion revascularization. However, we found significant differences between the groups with respect to success rate, procedure time, stent length, contrast amount and in-hospital complications.

Citation: Wang QC, Lin HR, Han Y, Dong H, Xu K, Guan SY, Chen ZH, Hao HX, Bin JP, Liao YL, Jing QM. Optimal use of fielder XT guidewire enhances the success rate of chronic total occlusion percutaneous coronary intervention. *World J Clin Cases* 2019; 7(8): 928-939
URL: https://www.wjgnet.com/2307-8960/full/v7/i8/928.htm
DOI: https://dx.doi.org/10.12998/wjcc.v7.i8.928

INTRODUCTION

Coronary chronic total occlusion (CTO), defined as a lesion with total occlusion exhibiting thrombolysis in myocardial infarction (TIMI) grade 0 flow in a native vessel for more than 3 mo, is found in 18%-31% of patients who undergo invasive coronary angiography[1,2]. Successful recanalization of CTOs has been shown to be associated with reduced risks of death, coronary artery bypass grafting[3], recurrent angina

pectoris[4] and increased long-term survival[5,6]. In addition, failure of CTO-percutaneous coronary intervention (CTO-PCI) is reported to be associated with higher subsequent mortality and more frequent major adverse cardiovascular events (MACE)[7]. Although experience and the introduction of new devices have improved the success rate of PCI[8], CTO-PCI is still technically challenging. The most common reason for CTO-PCI failure is the failure of the guidewire to cross the occlusion segment[9]. Recently, the Fielder XT guidewire was specifically designed for CTO lesions. It has a soft, tapered polymer-jacketed tip, and has been introduced and used worldwide.

To validate whether Fielder XT guidewire can increase the success rate of PCI in CTO lesions, we retrospectively compared data from 1230 consecutive patients with CTO who received PCI *via* the anterograde approach at our institution from January 2013 to December 2015. We hypothesized that the use of Fielder XT guidewire can increase the success rate of CTO-PCI *via* the anterograde approach.

MATERIALS AND METHODS

Study population

Between January 2013 and December 2015, 1230 consecutive patients with CTO who received PCI *via* the anterograde approach at the General Hospital of Northern Theater Command. The study protocol was approved by the local ethics committee, and all procedures were performed according to current international guidelines[10,11]. All patients provided written informed consent. We conducted a retrospective analysis of these 1230 patients.

Definitions

CTO was defined as a lesion with total occlusion exhibiting TIMI grade 0 flow in a native vessel for more than 3 mo. Estimation of the occlusion duration was based on the first onset of angina symptoms, prior history of myocardial infarction (MI) in the target vessel territory, or comparison with a prior angiogram. Procedural success was defined as angiographic success (final residual diameter stenosis < 20% and TIMI grade 3 flow following recanalization of the CTO). Clinical success was defined as successful PCI with the patient discharged alive.

Criteria for choice of donors

Patients were candidates for intervention if they had sufficient cardiac function to lie in the supine position for at least 2 h. To minimize confounding factors, only patients undergoing primary anterograde CTO-PCI whose target vessel was ≥ 2.5 mm in diameter were included in this study. Patients were excluded if they had more than one CTO treated during the same PCI procedure, or if there was no clear evidence for CTO duration ≥ 3 mo.

Study design

Based on the use of Fielder XT guidewire, the patients were divided into two groups: the XT group (n = 686) and the no-XT group (n = 544). Both groups were compared for clinical parameters, lesion-related characteristics, procedural outcomes and in-hospital complications.

CTO-PCI procedure

All interventional procedures were performed using standard techniques. The selection of arterial access depends on the characteristics of the target lesions. Generally, puncture of one of the right radial arteries or right femoral arteries was performed. If necessary, puncture of two arteries among the right radial artery, left radial artery, right femoral artery and left femoral artery were performed. We preferred the Amplatz Left guiding catheter when performing CTO-PCI of the right coronary artery, and we preferred the EBU or the Extra Backup guiding catheter when performing CTO-PCI of the left anterior descending (LAD) and left circumflex artery. The anterograde wire escalation (AWE) strategy was employed for anterograde crossing of the CTO. AWE was usually started with a soft (tip load = 0.8 g), tapered polymer-jacketed guidewire (such as Fielder XT, Asahi Intecc, Japan), a tapered polymer-jacketed guidewire (such as Pilot 50, Abbott, United States), a stiff guidewire (such as Miracle 6, Asahi Intecc), or a stiff, tapered guidewire (such as Conquest, Asahi Intecc).

AWE technique was always performed using an over-the-wire system (such as Finecross microcatheter, Terumo, Japan, or Corsair microcatheter, Asahi Intecc) to support the guidewire. A microcatheter allowed rapid exchange of guidewires, while maintaining wire position and improving guidewire torque response. Microcatheters

also improve support and enable dynamic alterations of the penetration power of the guidewire by changing the distance between the microcatheter tip and wire tip. Some of the preferred wires are able to cross the CTO lesions either directly or with the support of the over-the-wire system. If the first soft wire entered the subintimal space of the occlusion segment and failed to cross the CTO lesion, we upgraded to a stiff, tapered wire for crossing using the parallel wires technique. If the first wire could not enter the proximal cap of the CTO lesion, we used a higher-tip-load tapered wire to puncture the proximal cap and then downgraded to a softer, tapered polymer-jacketed guidewire to cross the occlusion. If the CTO had tortuous vessels or unclear vascular anatomy, the knuckle wire technique was usually attempted with a polymer-jacketed guidewire (such as Fielder XT or Pilot 50). Other techniques including the buddy wire technique, multiwire plaque crushing, subintimal tracking and reentry, and balloon jailing were also employed as required. All PCI procedures were performed by experienced interventionists who handled at least 50 cases of CTO-PCI annually.

Statistical analysis

Continuous variables are presented as the mean ± SD, and categorical data are presented as numbers (proportions). The data were statistically analyzed using Pearson's χ^2 test for categorical variables, and Students' t test was used to compare the quantitative data. Significant independent factors and risk ratio with 95% confidence interval (CI) were assessed by multivariate logistic regression analysis. Analyses were performed using SPSS software (version 21.0; SPSS Inc., Chicago, IL, United States), and $P < 0.05$ (2-sided) was considered statistically significant.

RESULTS

Patients

A total of 1230 patients aged from 31 to 88 years were enrolled, with 74.8% (898/1230) of the patients being male and 55.8% (686/1230) of the patients in the XT group. The overall success rate was 83.9% (1032/1230).

Arterial access

The right radial arterial access percentage is 38.4% (472/1230); the right femoral arterial access percentage is 6.3% (77/1230); the right and left radials arterial accesses percentage is 33.1% (407/1230); the right radial arterial and right femoral arterial accesses percentage is 17.1% (210/1230); the right and left femoral arterial accesses percentage is 5.2% (64/1230).

Parameters predicting the success of CTO-PCI

According to backward logistic regression analysis by Wald's method, the following factors were positively correlated with successful CTO-PCI: Use of Fielder XT guidewire ($P = 0.005$, 95%CI: 1.172-2.380) and systolic blood pressure ($P = 0.011$, 95%CI: 1.003-1.022), while factors negatively associated with procedural success were blunt stump ($P = 0.013$, 95%CI: 1.341-11.862), male sex ($P = 0.016$, 95%CI: 0.363-0.902), New York Heart Association (NYHA) class ($P = 0.035$, 95%CI: 0.553-0.979), contrast amount ($P = 0.018$, 95%CI: 0.983-0.998) and occlusion time ($P = 0.009$, 95%CI: 0.994-0.999) (Table 1).

Clinical characteristics in the two groups

Based on the use of Fielder XT guidewire, the patients were divided into two groups: The XT group ($n = 686$; 55.8%) and the no-XT group ($n = 544$; 44.2%). When clinical characteristics from the two groups were compared, we found no significant differences based on male sex ($P = 0.313$), age ($P = 0.062$), height ($P = 0.064$), body weight ($P = 0.645$), body mass index ($P = 0.112$), systolic blood pressure ($P = 0.146$), diastolic blood pressure ($P = 0.365$), hypertension ($P = 0.782$), diabetes mellitus ($P = 0.988$), previous stroke ($P = 0.521$), old MI ($P = 0.587$), previous PCI ($P = 0.431$), previous renal insufficiency ($P = 0.513$), smoking ($P = 0.325$), alcohol drinking ($P = 0.887$), left ventricular ejection fraction ($P = 0.587$), left ventricular end-diastolic diameter ($P = 0.559$), serum creatinine ($P = 0.577$), cardiothoracic ratio ($P = 0.089$), NYHA heart function class ($P = 0.643$) or age ≥ 65 years ($P = 0.585$) (Table 2).

Lesion-related characteristics in the two groups

The groups were further compared for lesion-related characteristics. The two groups did not differ significantly in terms of multivessel coronary artery disease ($P = 0.609$), lesion calcification ($P = 0.423$), tortuosity ($P = 0.124$), bridging collaterals ($P = 0.665$), blunt stump ($P = 0.787$), J-CTO score ($P = 0.077$), Rentrop class ($P = 0.686$), CTO vessel

Table 1 Parameters predicting success of chronic total occlusion-percutaneous coronary intervention

	β coefficient	Wald	Exp (β)	*P*-value	95%CI of OR
Clinical predictors					
Sex, male	-0.559	7.780	0.572	0.016	0.363~0.902
Systolic blood pressure	0.012	6.405	1.012	0.011	1.003~1.022
NYHA class	-0.307	4.445	0.735	0.035	0.553~0.979
Contrast amount	-0.009	5,555	0.991	0.018	0.983~0.998
Lesion-related predictors					
Occlusion time	-0.003	6.848	0.997	0.009	0.994~0.999
Blunt stump	-1.382	6.192	3.982	0.013	1.341~11.862
Use of Fielder XT	0.513	8.060	1.670	0.005	1.172~2.380
Constant	-5.668	0.127	0.003	0.722	

NYHA: New York Heart Association; CI: Confidence interval; OR: Odds ratio.

(P = 0.570), occlusion length (P = 0.876), or occlusion time (P = 0.796) (Table 3).

Procedural outcomes and in-hospital complications

When the procedural outcomes and in-hospital complications were compared between the two groups, there were no significant differences in coronary artery rupture [3 (0.4%) *vs* 8 (1.5%), P = 0.056], in-hospital death [2 (0.3%) *vs* 6 (1.1%), P = 0.079] or in-hospital target lesion revascularization (TLR) [3 (0.4%) *vs* 7 (1.3%), P < 0.099] (Table 4); however, there were significant differences with regard to success rate [602 (87.8%) *vs* 430 (79.0%), P < 0.001], procedure time [(74 ± 23) *vs* (83 ± 21), P < 0.001], stent length [(32.0 ± 15.8) *vs* (37.3 ± 17.6), P < 0.001], contrast amount [(148 ± 46) *vs* (166 ± 43), P < 0.001], post-PCI MI [43 (6.3%) *vs* 59 (10.8%), P = 0.004], MACE [44 (6.4%) *vs* 57 (10.7%), P = 0.007], side branch loss [31 (4.5%) *vs* 44 (8.1%), P = 0.009], contrast-induced nephropathy (CIN) [29 (4.2%) *vs* 40 (7.4%), P = 0.018] and no reflow [8 (1.2%) *vs* 14 (2.9%), P = 0.034] (Table 4).

DISCUSSION

This retrospective study investigated the use of Fielder XT guidewire in CTO-PCI *via* the anterograde approach. We focused on the relationship between the use of Fielder XT guidewire and the success rate of CTO-PCI, and evaluated the occurrence of in-hospital complications in two groups. The main novel findings of this study are as follows: (1) The use of Fielder XT guidewire contributes to increasing the success rate of CTO-PCI *via* the anterograde approach; and (2) The use of Fielder XT guidewire is associated with reduced rates of in-hospital complications and stent implantations.

The AWE technique is the most common strategy for CTO-PCI, and polymer-jacketed guidewires are most frequently used to implement this strategy. Although Karatasakis *et al*[12] recently reported that the use of stiff polymer-jacketed guidewires results in a high CTO crossing rate without increasing the incidence of MACE or perforation[12], we found that a soft, tapered polymer-jacketed Fielder XT (Figure 1) guidewire was also effective in crossing the occlusion. Consistent with our results, the Euro-CTO club has recommended starting with a soft (tip load < 1 g), tapered polymer-jacketed guidewire, not only because of high success rates but also because of the low risk of distal vessel damage if the wire fails to cross the lesion[13]. The existence of microchannels, which partly or completely connect from the proximal cap to the distal end of CTO lesions[14] (Figure 2A), has also been reported to predict procedural success[15]. Single wiring displays a high success rate as the initial PCI strategy for CTO of the LAD, and is generally performed with a tapered guidewire such as Fielder XT[16] (Figure 2B). The diameter of the Fielder XT guidewire is 230 μm, while the diameters of the microchannels range from 160 to 230 μm[14]. Therefore, it is reasonable to select Fielder XT as the initial guidewire. Additionally, microchannels frequently end at the sidewall of the coronary artery or connect to the side branches far proximal to the distal end of the CTO lesion. Some of these microchannels may run longitudinally through the lesion from the proximal to the distal lumen for up to 85% of the total length of the CTO (Figure 2A). The initial soft, tapered polymer-jacketed guidewire can easily enter the proximal cap through microchannels, but the wire

Table 2 Clinical characteristics in the two groups, *n* (%)

	Overall population, *n* = 1230	XTgroup, *n* = 686	No-XT group, *n* = 544	*P*-value
Sex, male	928 (75.4)	510 (74.3)	418 (76.8)	0.313
Age, yr	61.9 ± 10.3	62.4 ± 9.9	61.3 ± 10.8	0.062
Height, cm	169.5 ± 6.3	169.2 ± 6.3	169.9 ± 6.4	0.064
Body weight, kg	74.0 ± 10.0	74.4 ± 10.7	74.2 ± 10.0	0.645
Body mass index, kg/m^2	25.8 ± 3.2	26.0 ± 3.3	25.7 ± 3.1	0.112
SBP, mmHg	137.0 ± 20.8	137.7 ± 20.6	136.0 ± 21.0	0.146
DBP, mmHg	81.0 ± 12.9	81.3 ± 13.1	80.6 ± 12.7	0.365
Hypertension	765 (62.2)	429 (62.5)	336 (61.8)	0.782
Diabetes mellitus	405 (32.9)	226 (32.9)	179 (32.9)	0.988
Previous stroke	95 (7.7)	50 (7.3)	45 (8.3)	0.521
OMI	408 (33.2)	232 (33.8)	176 (32.4)	0.587
Previous PCI	328 (26.7)	189 (27.6)	139 (25.6)	0.431
PRI	119 (9.7)	63 (9.2)	56 (10.3)	0.513
Smoking	693 (56.3)	378 (55.1)	315 (57.9)	0.325
Alcohol drinking	445 (36.2)	247 (36.0)	198 (36.4)	0.887
LVEF, %	60.0 ± 9.0	60.0 ± 9.0	59.8 ± 8.6	0.587
LVEDd, mm	48.4 ± 6.3	48.5 ± 6.4	48.3 ± 6.2	0.559
Serum creatinine, μmol/L	73.0 ± 23.0	72.5 ± 23.9	71.8 ± 21.6	0.577
Cardiothoracic ratio, %	54.0 ± 6.0	53.8 ± 6.1	53.2 ± 6.0	0.089
NYHA heart function class				0.643
Class I	923 (75.0)	510 (74.3)	413 (75.9)	
Class II	247 (20.1)	144 (21.0)	103 (18.9)	
Class III	60 (4.9)	32 (4.7)	28 (5.1)	
Age ≥ 65 yr	532 (43.3)	292 (42.6)	240 (44.1)	0.585

Values represent the mean ± SD or number of patients and proportion (%). SBP: Systolic blood pressure; DBP: Diastolic blood pressure; OMI: Old myocardial infarction; PRI: Previous renal insufficiency; PCI: Percutaneous coronary intervention; LVEF: Left ventricular ejection fraction; LVEDd: Left ventricular end-diastolic diameter; NYHA: New York Heart Association.

frequently goes into the sidewall of the coronary artery and results in forming intimal dissection (Figure 2C). It may also go into the side branches of the occlusion segment (Figure 2D). In such situations, the parallel wire technique, which is based on a middle-hard guidewire with a tapered tip, is the best approach to solve the problem. First, the initial guidewire in the false lumen or side branch is left both as a marker and to obstruct the false channel. Second, a second tapered guidewire is used to trace the exact path as the first wire. After the tip of the second guidewire reaches the point where the first guidewire appeared to divert from the true lumen, the tip of the second guidewire is intentionally directed into the true lumen (Figure 2E and F). In this case, the second guidewire usually has a high crossing rate and a low side branch occlusion rate. If the second guidewire fails to enter the true lumen, the AWE strategy for CTO will usually involve switching from a middle-hard guidewire with a tapered tip to a stiff guidewire with a tapered tip. If the initial guidewire had already crossed the occlusion segment and entered the subintimal region of the distal cap (Figure 2G), an anterograde dissection reentry (ADR) strategy can be employed. This is usually attempted to minimize the length of the dissection by reentry into the distal true lumen using a stiff guidewire with a tapered tip immediately after the distal cap of the occlusion segment (Figure 2H). If an initial stiff guidewire has been used to puncture the proximal cap, it is important to downgrade to a soft, tapered polymer-jacketed guidewire, such as Fielder XT, to reduce the risk of perforation and increase the chance of tracking the vessel[17].

In the present study, we found that a strategy based on the initial use of Fielder XT guidewire significantly increased the success rate of CTO-PCI *via* the anterograde approach. This may have been partially attributable to the existence of microchannels with a diameter of approximately 160-230 μm in the CTO lesions. The number of microchannels has been reported to decrease with CTO maturation[18]. Other studies have reported that these channels can exist in loose tissues extending from the proximal to distal fibrous caps in CTOs of any age[19]. Thus, successful tracking of microchannels in loose tissue may be possible, even in very old CTOs[20]. Consistent

Table 3 Lesion-related characteristics in the two groups, *n* (%)

	Overall population, *n* = 1230	XT group, *n* = 686	No-XT group, *n* = 544	*P*-value
Multivessel CAD	530 (43.1)	300 (43.7)	230 (42.3)	0.609
LC	170 (13.8)	90 (13.1)	80 (14.7)	0.423
Tortuosity	105 (10.2)	57 (11.7)	48 (8.8)	0.124
Bridging collaterals	95 (7.7)	55 (8.0)	40 (7.4)	0.665
Blunt stump	107 (8.7)	61 (8.9)	46 (8.5)	0.787
J-CTO score				0.077
0	597 (48.5)	332 (48.4)	265 (48.7)	
1	507 (41.2)	282 (41.1)	225 (41.4)	
2	99 (8.0)	50 (7.3)	49 (9.0)	
3	23 (1.9)	19 (2.8)	4 (0.7)	
4	4 (0.3)	3 (0.4)	1 (0.2)	
Rentrop class				0.686
0	233 (18.9)	126 (18.4)	107 (19.7)	
1	220 (17.9)	117 (17.1)	103 (18.9)	
2	434 (35.3)	245 (35.7)	189 (34.7)	
3	343 (27.9)	198 (28.9)	145 (26.7)	
CTO vessel				0.570
LM	1 (0.1)	1 (0.1)	0 (0)	
LAD	545 (44.3)	302 (44.0)	243 (44.7)	
LCX	173 (14.1)	103 (15.0)	70 (12.9)	
RCA	511 (41.5)	280 (40.8)	231 (42.5)	
Occlusion length, mm	21.6 ± 14.8	21.5 ± 15.1	21.7 ± 14.5	0.876
Occlusion time, mo	82.3 ± 27.1	45.9 ± 60.0	45.0 ± 50.9	0.796

Values represent the mean ± SD or number of patients and proportion (%). CAD: Coronary artery disease; LC: Lesion calcification; J-CTO: Multicenter CTO Registry in Japan; rentrop class definition: Class 1, filling of side branches of the artery *via* collateral channels without visualization of the epicardial segment; Class 2, partial filling of the epicardial segment *via* collateral channels; Class 3, complete filling of the epicardial segment of the artery *via* collateral channels; CTO: Chronic total occlusion; LM: Left main artery; LAD: Left anterior descending artery; LCX: Left circumflex artery; RCA: Right coronary artery.

with these data, we found that the use of Fielder XT guidewire significantly increased the success rate of CTO-PCI, although there were no significant differences in occlusion time between the two groups.

Nevertheless, factors predicting the success or failure of CTO-PCI are context-dependent. In agreement with previous studies, we noted that blunt stump[21-24] was an independent predictor of the procedural success of CTO-PCI. In recent years, multiple scoring systems have been established to predict the procedural success, efficiency, and complications of CTO-PCI[21-26]. Both the multicenter CTO registry in Japan (J-CTO) and clinical- and lesion-related (CL) scores include blunt stump as the lesion-related predictor[21,23]. CTO with blunt stump is a major obstacle to successful intervention. If the proximal cap has a blunt morphology, the occlusion is often more mature[17]. Older occlusions usually have harder proximal caps and lack microchannels connected to the proximal cap, which prevent the initial soft, tapered polymer-jacketed guidewire from entering the proximal cap. Thus, the blunt stump of proximal cap is an obstacle to the procedural success of CTO-PCI[17]. In accordance with the results of previous studies, we also found that contrast amount, procedure time and cardiac function were independent predictors of procedural success. Algorithms also provide specific guidance, suggesting that operators should consider stopping a CTO procedure if the procedure time is > 3 h, or more than 3.7 mL × the estimated glomerular filtration rate of contrast has been used[17]. Systolic blood pressure is closely related to cardiac function, and systolic blood pressure was thus an independent predictor of procedural success in this study. Furthermore, females have lower J-CTO scores than males. The technical success rate is usually higher in females than in males[27], consistent with our observed outcomes.

In summary, we found in this study that the use of Fielder XT guidewire was associated with a relatively shorter procedure time and lower contrast amount, as Fielder XT guidewire could cross CTO lesions into the distal true lumen by microchannels. The amount of contrast media is closely related to the incidence of

Table 4 Procedural outcomes and in-hospital complications in the two groups

	Overall population, *n* = 1230	XTgroup, *n* = 686	No-XT group, *n* = 544	*P*-value
Stent length, mm	34.3 ± 16.8	32.0 ± 15.8	37.3 ± 17.6	< 0.001
Contrast amount, mL	156.1 ± 45.6	148 ± 46	166 ± 43	< 0.001
Side branch loss	75 (6.1)	31 (4.5)	44 (8.1)	0.009
CIN	69 (5.6)	29 (4.2)	40 (7.4)	0.018
Coronary artery rupture	11 (0.9)	3 (0.4)	8 (1.5)	0.056
No reflow	22 (1.9)	8 (1.2)	14 (2.9)	0.034
Post-PCI MI	102 (8.3)	43 (6.3)	59 (10.8)	0.004
In-hospital death	8 (0.7)	2 (0.3)	6 (1.1)	0.079
TLR	10 (0.8)	3 (0.4)	7 (1.3)	0.099
MACE	101 (8.3)	44 (6.4)	57 (10.7)	0.007
Success rate	1032 (83.9)	602 (87.8)	430 (79.0)	< 0.001
Procedure time, min	78 ± 23	74 ± 23	83 ± 21	< 0.001

Values represent the mean ± SD or number of patients and proportion (%). CIN: Contrast-induced nephropathy; MI: Myocardial infarction; PCI: Percutaneous coronary intervention; TLR: Target lesion revascularization; MACE: Major adverse cardiovascular event.

CIN, and several studies have shown that the volume of contrast media is an independent risk factor for the development of contrast-induced acute kidney injury[28-30]. We observed a similar outcome in which the volume of contrast media was positively associated with CIN incidence. We also found that the use of Fielder XT guidewire was associated with lower rates of in-hospital complications and stent implantation. Furthermore, the initial soft, tapered polymer-jacketed guidewire we used could cross the CTO lesion and reach the distal cap, with lower likelihoods of dissection and a smaller degree of hematoma than stiff guidewires. ADR based on the soft guidewire we used above could also ensure true lumen reentry once through the CTO segment, which decreased the length of the implanted stent and reduced side branch loss. Additionally, MI of perioperative caused by the occlusion of side branches after CTO-PCI was avoided.

In conclusion, the use of Fielder XT guidewire shortens the procedure and increases the success rate of CTO-PCI, and is also associated with reduced complication rates.

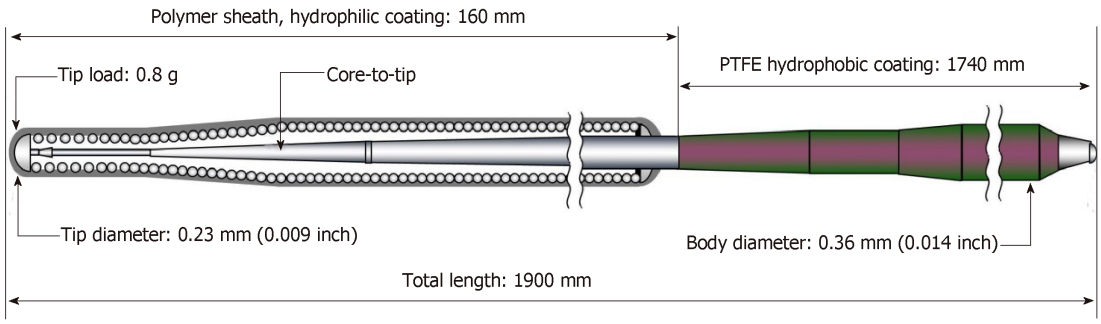

Figure 1 An illustrative image of the Fielder XT guidewire.

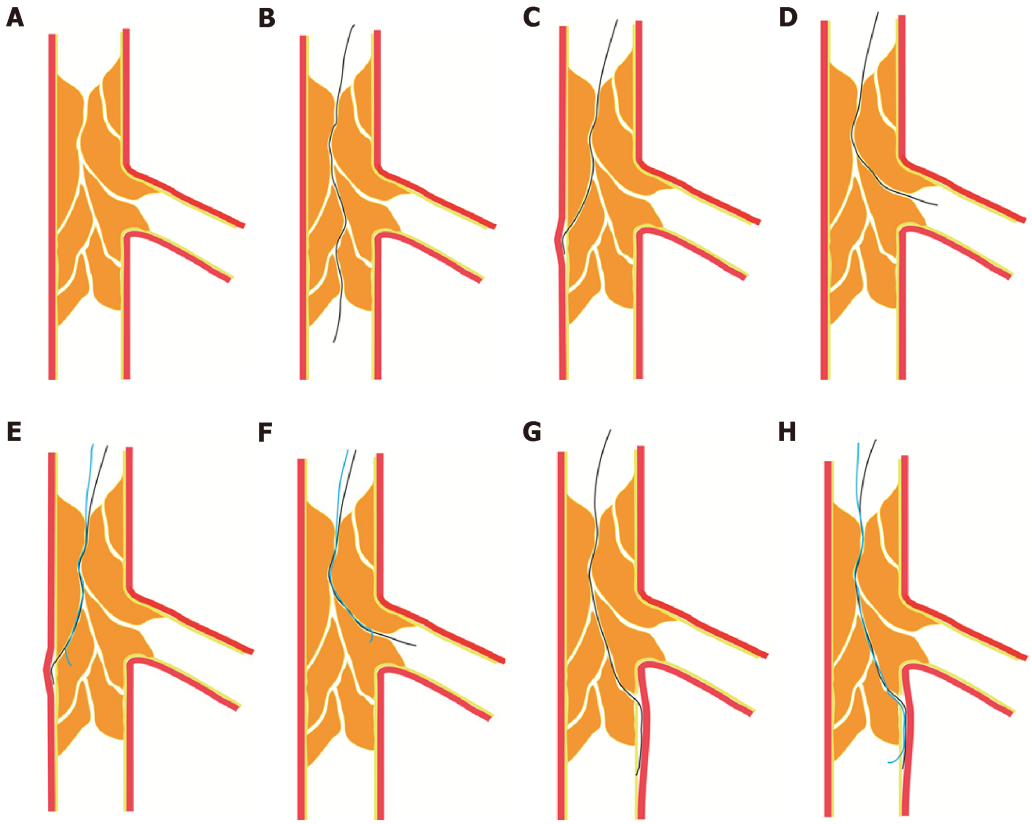

Figure 2 Fielder XT guidewires enter the chronic total occlusion lesions along the microchannels with different anatomical features. A: Microchannels partly or completely connecting from the proximal cap to the distal end of chronic total occlusion (CTO) lesion; B: A Fielder XT guidewire crossing the CTO lesion through microchannels; C: A Fielder XT guidewire entering the sidewall of the coronary artery and resulting in forming intimal dissection; D: A Fielder XT guidewire entering the side branch of the occlusion segment; E-F: After leaving the Fielder XT guidewire in the false lumen, tracing of a second tapered guidewire along the same pathway into the true lumen; G: A Fielder XT guidewire crossing the occlusion segment into the subintimal of the distal cap; H: A stiff guidewire with a tapered tip entering the distal true lumen after the distal cap.

ARTICLE HIGHLIGHTS

Research background

Chronic total occlusion (CTO) is found in 18%-31% of patients who undergo coronary angiography. Successful recanalization of CTOs has been shown to be associated with reduced recurrent angina pectoris rates and increased long-term survival. Although the success rate of CTO percutaneous coronary intervention (CTO-PCI) has improved, CTO-PCI remains technically challenging. The Fielder XT guidewire was designed for CTO lesions. To validate whether the use of the guidewire increases the success rate, we compared the results of CTO-PCI with or without the guidewire. We hypothesized that the use of Fielder XT guidewire can increase the success rate of CTO-PCI.

Research motivation

Although experience and the introduction of new devices have improved the success rates of PCI, CTO-PCI is still technically challenging. We thus wanted to validate whether the use of Fielder XT guidewire increases the success rate of CTO-PCI.

Research objectives
To investigate whether the use of Fielder XT guidewire increases the final procedural success of CTO-PCI *via* the anterograde approach.

Research methods
Between January 2013 and December 2015, a retrospective study was conducted on 1230 consecutive patients with CTO who received PCI *via* the anterograde approach at the General Hospital of Northern Theater Command. The patients were divided into an XT Group (n = 686) and a no-XT Group (n = 544) depending on whether Fielder XT guidewire was used. Both groups were compared for clinical parameters, lesion-related characteristics, procedural outcomes and in-hospital complications. The data were statistically analyzed using a Pearson's χ^2 test for categorical variables, and a Students' t test was used to compare the quantitative data. Significant independent factors and risk ratios with a 95% confidence interval (CI) were assessed by multivariate logistic regression analysis.

Research results
In total, 1230 patients were recruited; 75.4% of the patients were male, and 55.8% of the patients were in the XT group. The overall success rate was 83.9%, with 87.8% in the XT group. Based on multivariate logistic regression analysis, factors positively associated with procedural success were the use of Fielder XT guidewire (P = 0.005, 95%CI: 1.172-2.380) and systolic blood pressure (P = 0.011, 95%CI: 1.003-1.022), while factors negatively associated with procedural success were blunt stump (P = 0.013, 95%CI: 1.341-11.862), male sex (P = 0.016, 95%CI: 0.363-0.902), NYHA class (P = 0.035, 95%CI: 0.553-0.979), contrast amount (P = 0.018, 95%CI: 0.983-0.998) and occlusion time (P = 0.009, 95%CI: 0.994-0.999). No significant differences were found between the XT group and the no-XT group with respect to clinical parameters, lesion-related characteristics, coronary artery rupture [3 (0.4%) *vs* 8 (1.5%), P = 0.056], in-hospital death [2 (0.3%) *vs* 6 (1.1%), P = 0.079] or in-hospital target lesion revascularization [3 (0.4%) *vs* 7 (1.3%), P < 0.099]. However, there were significant differences between the groups with respect to success rate [602 (87.8%) *vs* 430 (79.0%), P < 0.001], procedure time [(74 ± 23) *vs* (83 ± 21), P < 0.001], stent length [(32.0 ± 15.8) *vs* (37.3 ± 17.6), P < 0.001], contrast amount [(148 ± 46) *vs* (166 ± 43), P < 0.001], post-PCI myocardial infarction [43 (6.3%) *vs* 59 (10.8%), P = 0.004], major adverse cardiovascular event [44 (6.4%) *vs* 57 (10.7%), P = 0.007], side branch loss [31 (4.5%) *vs* 44 (8.1%), P = 0.009], contrast-induced nephropathy [29 (4.2%) *vs* 40 (7.4%), P = 0.018] and no reflow [8 (1.2%) *vs* 14 (2.9%), P = 0.034].

Research conclusions
The use of Fielder XT guidewire shortens the procedure and increases the success rate of CTO-PCI, and is also associated with reduced complication rates.

Research perspectives
Larger multicenter studies are required to better understand the relationship between the use of Fielder XT series (such as Fielder XT, Fielder XT-R and Fielder XT-A) guidewires and the procedural success of CTO-PCI *via* anterograde, retrograde, or hybrid approaches.

REFERENCES

1 **Fefer P**, Knudtson ML, Cheema AN, Galbraith PD, Osherov AB, Yalonetsky S, Gannot S, Samuel M, Weisbrod M, Bierstone D, Sparkes JD, Wright GA, Strauss BH. Current perspectives on coronary chronic total occlusions: the Canadian Multicenter Chronic Total Occlusions Registry. *J Am Coll Cardiol* 2012; **59**: 991-997 [PMID: 22402070 DOI: 10.1016/j.jacc.2011.12.007]

2 **Jeroudi OM**, Alomar ME, Michael TT, El Sabbagh A, Patel VG, Mogabgab O, Fuh E, Sherbet D, Lo N, Roesle M, Rangan BV, Abdullah SM, Hastings JL, Grodin J, Banerjee S, Brilakis ES. Prevalence and management of coronary chronic total occlusions in a tertiary Veterans Affairs hospital. *Catheter Cardiovasc Interv* 2014; **84**: 637-643 [PMID: 24142769 DOI: 10.1002/ccd.25264]

3 **Warren RJ**, Black AJ, Valentine PA, Manolas EG, Hunt D. Coronary angioplasty for chronic total occlusion reduces the need for subsequent coronary bypass surgery. *Am Heart J* 1990; **120**: 270-274 [PMID: 2382608 DOI: 10.1016/0002-8703(90)90069-A]

4 **Christakopoulos GE**, Christopoulos G, Carlino M, Jeroudi OM, Roesle M, Rangan BV, Abdullah S, Grodin J, Kumbhani DJ, Vo M, Luna M, Alaswad K, Karmpaliotis D, Rinfret S, Garcia S, Banerjee S, Brilakis ES. Meta-analysis of clinical outcomes of patients who underwent percutaneous coronary interventions for chronic total occlusions. *Am J Cardiol* 2015; **115**: 1367-1375 [PMID: 25784515 DOI: 10.1016/j.amjcard.2015.02.038]

5 **Ivanhoe RJ**, Weintraub WS, Douglas JS, Lembo NJ, Furman M, Gershony G, Cohen CL, King SB. Percutaneous transluminal coronary angioplasty of chronic total occlusions. Primary success, restenosis, and long-term clinical follow-up. *Circulation* 1992; **85**: 106-115 [PMID: 1728439 DOI: 10.1161/01.CIR.85.1.106]

6 **Suero JA**, Marso SP, Jones PG, Laster SB, Huber KC, Giorgi LV, Johnson WL, Rutherford BD. Procedural outcomes and long-term survival among patients undergoing percutaneous coronary intervention of a chronic total occlusion in native coronary arteries: a 20-year experience. *J Am Coll Cardiol* 2001; **38**: 409-414 [PMID: 11499731 DOI: 10.1016/S0735-1097(01)01349-3]

7 **Prasad A**, Rihal CS, Lennon RJ, Wiste HJ, Singh M, Holmes DR. Trends in outcomes after percutaneous

coronary intervention for chronic total occlusions: a 25-year experience from the Mayo Clinic. *J Am Coll Cardiol* 2007; **49**: 1611-1618 [PMID: 17433951 DOI: 10.1016/j.jacc.2006.12.040]

8 **King SB**, Yeh W, Holubkov R, Baim DS, Sopko G, Desvigne-Nickens P, Holmes DR, Cowley MJ, Bourassa MG, Margolis J, Detre KM. Balloon angioplasty versus new device intervention: clinical outcomes. A comparison of the NHLBI PTCA and NACI registries. *J Am Coll Cardiol* 1998; **31**: 558-566 [PMID: 9502635 DOI: 10.1016/S0735-1097(97)10523-X]

9 **Sapontis J**, Christopoulos G, Grantham JA, Wyman RM, Alaswad K, Karmpaliotis D, Lombardi WL, McCabe JM, Marso SP, Kotsia AP, Rangan BV, Christakopoulos GE, Garcia S, Thompson CA, Banerjee S, Brilakis ES. Procedural failure of chronic total occlusion percutaneous coronary intervention: Insights from a multicenter US registry. *Catheter Cardiovasc Interv* 2015; **85**: 1115-1122 [PMID: 25557905 DOI: 10.1002/ccd.25807]

10 **Task Force on Myocardial Revascularization of the European Society of Cardiology (ESC) and the European Association for Cardio-Thoracic Surgery (EACTS);**. European Association for Percutaneous Cardiovascular Interventions (EAPCI), Wijns W, Kolh P, Danchin N, Di Mario C, Falk V, Folliguet T, Garg S, Huber K, James S, Knuuti J, Lopez-Sendon J, Marco J, Menicanti L, Ostojic M, Piepoli MF, Pirlet C, Pomar JL, Reifart N, Ribichini FL, Schalij MJ, Sergeant P, Serruys PW, Silber S, Sousa Uva M, Taggart D. Guidelines on myocardial revascularization. *Eur Heart J* 2010; **31**: 2501-2555 [PMID: 20802248 DOI: 10.1093/eurheartj/ehq277]

11 **Levine GN**, Bates ER, Blankenship JC, Bailey SR, Bittl JA, Cercek B, Chambers CE, Ellis SG, Guyton RA, Hollenberg SM, Khot UN, Lange RA, Mauri L, Mehran R, Moussa ID, Mukherjee D, Nallamothu BK, Ting HH; American College of Cardiology Foundation; American Heart Association Task Force on Practice Guidelines; Society for Cardiovascular Angiography and Interventions. 2011 ACCF/AHA/SCAI Guideline for Percutaneous Coronary Intervention. A report of the American College of Cardiology Foundation/American Heart Association Task Force on Practice Guidelines and the Society for Cardiovascular Angiography and Interventions. *J Am Coll Cardiol* 2011; **58**: e44-122 [PMID: 22070834 DOI: 10.1016/j.jacc.2011.08.007]

12 **Karatasakis A**, Tarar MN, Karmpaliotis D, Alaswad K, Yeh RW, Jaffer FA, Wyman RM, Lombardi WL, Grantham JA, Kandzari DE, Lembo NJ, Moses JW, Kirtane AJ, Parikh M, Garcia S, Doing A, Pershad A, Shah A, Patel M, Bahadorani J, Shoultz CA, Danek BA, Thompson CA, Banerjee S, Brilakis ES. Guidewire and microcatheter utilization patterns during antegrade wire escalation in chronic total occlusion percutaneous coronary intervention: Insights from a contemporary multicenter registry. *Catheter Cardiovasc Interv* 2017; **89**: E90-E98 [PMID: 27184465 DOI: 10.1002/ccd.26568]

13 **Sianos G**, Werner GS, Galassi AR, Papafaklis MI, Escaned J, Hildick-Smith D, Christiansen EH, Gershlick A, Carlino M, Karlas A, Konstantinidis NV, Tomasello SD, Di Mario C, Reifart N; EuroCTO Club. Recanalisation of chronic total coronary occlusions: 2012 consensus document from the EuroCTO club. *EuroIntervention* 2012; **8**: 139-145 [PMID: 22580257 DOI: 10.4244/EIJV8I1A21]

14 **Katsuragawa M**, Fujiwara H, Miyamae M, Sasayama S. Histologic studies in percutaneous transluminal coronary angioplasty for chronic total occlusion: comparison of tapering and abrupt types of occlusion and short and long occluded segments. *J Am Coll Cardiol* 1993; **21**: 604-611 [PMID: 8436741 DOI: 10.1016/0735-1097(93)90091-E]

15 **Baykan AO**, Gür M, Acele A, Şeker T, Quisi A, Kıvrak A, Yıldırım A, Uçar H, Akyol S, Çaylı M. Predictors of successful percutaneous coronary intervention in chronic total coronary occlusions. *Postepy Kardiol Interwencyjnej* 2016; **12**: 17-24 [PMID: 26966445 DOI: 10.5114/pwki.2016.56945]

16 **Nassar YS**, Boudou N, Dumonteil N, Lhermusier T, Carrie D. Guidewires used in first intentional single wiring strategy for chronic total occlusions of the left anterior descending coronary artery. *Heart Views* 2013; **14**: 56-61 [PMID: 23983909 DOI: 10.4103/1995-705X.115496]

17 **Harding SA**, Wu EB, Lo S, Lim ST, Ge L, Chen JY, Quan J, Lee SW, Kao HL, Tsuchikane E. A New Algorithm for Crossing Chronic Total Occlusions From the Asia Pacific Chronic Total Occlusion Club. *JACC Cardiovasc Interv* 2017; **10**: 2135-2143 [PMID: 29122129 DOI: 10.1016/j.jcin.2017.06.071]

18 **Munce NR**, Strauss BH, Qi X, Weisbrod MJ, Anderson KJ, Leung G, Sparkes JD, Lockwood J, Jaffe R, Butany J, Teitelbaum AA, Qiang B, Dick AJ, Wright GA. Intravascular and extravascular microvessel formation in chronic total occlusions a micro-CT imaging study. *JACC Cardiovasc Imaging* 2010; **3**: 797-805 [PMID: 20705258 DOI: 10.1016/j.jcmg.2010.03.013]

19 **Galassi AR**, Sianos G, Werner GS, Escaned J, Tomasello SD, Boukhris M, Castaing M, Büttner JH, Bufe A, Kalnins A, Spratt JC, Garbo R, Hildick-Smith D, Elhadad S, Gagnor A, Lauer B, Bryniarski L, Christiansen EH, Thuesen L, Meyer-Geßner M, Goktekin O, Carlino M, Louvard Y, Lefèvre T, Lismanis A, Gelev VL, Serra A, Marzà F, Di Mario C, Reifart N; Euro CTO Club. Retrograde Recanalization of Chronic Total Occlusions in Europe: Procedural, In-Hospital, and Long-Term Outcomes From the Multicenter ERCTO Registry. *J Am Coll Cardiol* 2015; **65**: 2388-2400 [PMID: 26046732 DOI: 10.1016/j.jacc.2015.03.566]

20 **Sumitsuji S**, Inoue K, Ochiai M, Tsuchikane E, Ikeno F. Fundamental wire technique and current standard strategy of percutaneous intervention for chronic total occlusion with histopathological insights. *JACC Cardiovasc Interv* 2011; **4**: 941-951 [PMID: 21939933 DOI: 10.1016/j.jcin.2011.06.011]

21 **Alessandrino G**, Chevalier B, Lefèvre T, Sanguineti F, Garot P, Unterseeh T, Hovasse T, Morice MC, Louvard Y. A Clinical and Angiographic Scoring System to Predict the Probability of Successful First-Attempt Percutaneous Coronary Intervention in Patients With Total Chronic Coronary Occlusion. *JACC Cardiovasc Interv* 2015; **8**: 1540-1548 [PMID: 26493246 DOI: 10.1016/j.jcin.2015.07.009]

22 **Opolski MP**, Achenbach S, Schuhbäck A, Rolf A, Möllmann H, Nef H, Rixe J, Renker M, Witkowski A, Kepka C, Walther C, Schlundt C, Debski A, Jakubczyk M, Hamm CW. Coronary computed tomographic prediction rule for time-efficient guidewire crossing through chronic total occlusion: insights from the CT-RECTOR multicenter registry (Computed Tomography Registry of Chronic Total Occlusion Revascularization). *JACC Cardiovasc Interv* 2015; **8**: 257-267 [PMID: 25700748 DOI: 10.1016/j.jcin.2014.07.031]

23 **Morino Y**, Abe M, Morimoto T, Kimura T, Hayashi Y, Muramatsu T, Ochiai M, Noguchi Y, Kato K, Shibata Y, Hiasa Y, Doi O, Yamashita T, Hinohara T, Tanaka H, Mitsudo K; J-CTO Registry Investigators. Predicting successful guidewire crossing through chronic total occlusion of native coronary lesions within 30 minutes: the J-CTO (Multicenter CTO Registry in Japan) score as a difficulty grading and time assessment tool. *JACC Cardiovasc Interv* 2011; **4**: 213-221 [PMID: 21349461 DOI: 10.1016/j.jcin.2010.09.024]

24 **Christopoulos G**, Kandzari DE, Yeh RW, Jaffer FA, Karmpaliotis D, Wyman MR, Alaswad K, Lombardi W, Grantham JA, Moses J, Christakopoulos G, Tarar MNJ, Rangan BV, Lembo N, Garcia S, Cipher D,

Thompson CA, Banerjee S, Brilakis ES. Development and Validation of a Novel Scoring System for Predicting Technical Success of Chronic Total Occlusion Percutaneous Coronary Interventions: The PROGRESS CTO (Prospective Global Registry for the Study of Chronic Total Occlusion Intervention) Score. *JACC Cardiovasc Interv* 2016; **9**: 1-9 [PMID: 26762904 DOI: 10.1016/j.jcin.2015.09.022]

25 **Morino Y**, Kimura T, Hayashi Y, Muramatsu T, Ochiai M, Noguchi Y, Kato K, Shibata Y, Hiasa Y, Doi O, Yamashita T, Morimoto T, Abe M, Hinohara T, Mitsudo K; J-CTO Registry Investigators. In-hospital outcomes of contemporary percutaneous coronary intervention in patients with chronic total occlusion insights from the J-CTO Registry (Multicenter CTO Registry in Japan). *JACC Cardiovasc Interv* 2010; **3**: 143-151 [PMID: 20170870 DOI: 10.1016/j.jcin.2009.10.029]

26 **Galassi AR**, Boukhris M, Azzarelli S, Castaing M, Marzà F, Tomasello SD. Percutaneous Coronary Revascularization for Chronic Total Occlusions: A Novel Predictive Score of Technical Failure Using Advanced Technologies. *JACC Cardiovasc Interv* 2016; **9**: 911-922 [PMID: 27085580 DOI: 10.1016/j.jcin.2016.01.036]

27 **Karatasakis A**, Iwnetu R, Danek BA, Karmpaliotis D, Alaswad K, Jaffer FA, Yeh RW, Kandzari DE, Lembo NJ, Patel M, Mahmud E, Lombardi WL, Wyman RM, Grantham JA, Doing AH, Toma C, Choi JW, Uretsky BF, Moses JW, Kirtane AJ, Ali ZA, Parikh M, Karacsonyi J, Rangan BV, Thompson CA, Banerjee S, Brilakis ES. The Impact of Age and Sex on In-Hospital Outcomes of Chronic Total Occlusion Percutaneous Coronary Intervention. *J Invasive Cardiol* 2017; **29**: 116-122 [PMID: 28089997]

28 **Nijssen EC**, Rennenberg RJ, Nelemans PJ, Essers BA, Janssen MM, Vermeeren MA, van Ommen V, Wildberger JE. [Prophylactic hydration to protect renal function from intravascular iodinated contrast material in patients at high risk of contrast-induced nephropathy (AMACING): a prospective, randomised, phase 3, controlled, open-label, non-inferiority trial]. *Ned Tijdschr Geneeskd* 2018; **161**: D1734 [PMID: 29328007 DOI: 10.1016/S0140-6736(17)30057-0]

29 **Mehran R**, Aymong ED, Nikolsky E, Lasic Z, Iakovou I, Fahy M, Mintz GS, Lansky AJ, Moses JW, Stone GW, Leon MB, Dangas G. A simple risk score for prediction of contrast-induced nephropathy after percutaneous coronary intervention: development and initial validation. *J Am Coll Cardiol* 2004; **44**: 1393-1399 [PMID: 15464318 DOI: 10.1016/j.jacc.2004.06.068]

30 **Rihal CS**, Textor SC, Grill DE, Berger PB, Ting HH, Best PJ, Singh M, Bell MR, Barsness GW, Mathew V, Garratt KN, Holmes DR. Incidence and prognostic importance of acute renal failure after percutaneous coronary intervention. *Circulation* 2002; **105**: 2259-2264 [PMID: 12010907 DOI: 10.1161/01.CIR.0000016043.87291.33]

World Journal of Clinical Cases

Submit a Manuscript: https://www.f6publishing.com

World J Clin Cases 2019 April 26; 7(8): 940-950

DOI: 10.12998/wjcc.v7.i8.940

ISSN 2307-8960 (online)

ORIGINAL ARTICLE

Observational Study

Association between ventricular repolarization variables and cardiac diastolic function: A cross-sectional study of a healthy Chinese population

Zhi-Dan Li, Xiao-Juan Bai, Lu-Lu Han, Wen Han, Xue-Feng Sun, Xiang-Mei Chen

ORCID number: Zhi-Dan Li (0000-0001-5558-2800); Xiao-Juan Bai (0000-0002-5919-7173); Lu-Lu Han (0000-0001-8021-8998); Wen Han (0000-0003-4410-3362); Xue-Feng Sun (0000-0003-1160-4371); Xiang-Mei Chen (0000-0002-8889-6360).

Author contributions: Li ZD analyzed the data and drafted the manuscript; Bai XJ designed the manuscript and approved the manuscript for final submission; Han LL and Han W measured some important parameters; Sun XF and Chen XM participated in the coordination of the study; all authors read and approved the final manuscript.

Supported by the National Basic Research Program of China, No. 973-Program #2007CB507405.

Institutional review board statement: The study was approved by the ethics committee of General Hospital of Chinese People's Liberation Army (Beijing, China).

Informed consent statement: All patients gave informed consent.

Conflict-of-interest statement: The authors declare no conflict of interest.

STROBE statement: The authors have read the STROBE Statement-checklist of items, and the manuscript was prepared and revised according to the STROBE Statement-checklist of items.

Zhi-Dan Li, Xiao-Juan Bai, Lu-Lu Han, Wen Han, Department of Gerontology and Geriatrics, Shengjing Hospital of China Medical University, Shenyang 110004, Liaoning Province, China

Xue-Feng Sun, Xiang-Mei Chen, Department of Kidney, General Hospital of Chinese People's Liberation Army, Beijing 100853, China

Corresponding author: Xiao-Juan Bai, PhD, Professor, Department of Gerontology and Geriatrics, Shengjing Hospital of China Medical University, 36 Sanhao Street, Shenyang 110004, Liaoning Province, China. xiaojuan_bai@126.com
Telephone: +86-24-62043437
Fax: +86-24-62043437

Abstract

BACKGROUND

Diastolic electromechanical couple, a well-described phenomenon in symptomatic heart failure, has not been well studied in healthy people. We hypothesized that ventricular repolarization variables, such as the QT interval, Tpeak-to-Tend (Tpe) interval and Tpe/QT ratio, are associated with cardiac diastolic function in the healthy Chinese population.

AIM

To assess the relationship between ventricular repolarization variables and cardiac diastolic function in apparently healthy Chinese individuals.

METHODS

This was a community-based cross-sectional study conducted in Shenyang, China. A total of 414 healthy subjects aged 35-91 years were enrolled. All subjects underwent standard 12-lead electrocardiography (ECG) and comprehensive echocardiography. ECG enabled the measurement of QT and Tpe intervals and Tpe/QT ratio. echocardiographic parameters, such as the ratio of mitral early diastolic inflow velocity (E) and late diastolic inflow velocity (A), E-wave deceleration time, left atrial volume (LAV) and LAV index, were measured to assess diastolic function. E/A < 0.75 was considered to indicate reduced diastolic function. ECG and echocardiography results were analyzed separately and in a blinded fashion. Correlation and regression analyses were applied to determine associations.

RESULTS

Manuscript source: Unsolicited manuscript

Received: December 26, 2018
Peer-review started: December 27, 2018
First decision: March 10, 2019
Revised: March 28, 2019
Accepted: April 9, 2019
Article in press: April 9, 2019
Published online: April 26, 2019

P-Reviewer: Barik R, Karatza AA, Kharlamov AN
S-Editor: Ji FF
L-Editor: A
E-Editor: Wu YXJ

Ventricular repolarization variables, such as the QTc interval (393.59 ± 26.74 *vs* 403.86 ± 33.56; $P < 0.001$), Tpe interval (72.68 ± 12.41 *vs* 77.26 ± 17.86; $P < 0.01$), Tpe_c interval (76.36 ± 13.53 *vs* 83.32 ± 21.25; $P < 0.001$) and Tpe/QT ratio (0.19 ± 0.03 *vs* 0.20 ± 0.04; $P < 0.01$), were significantly different between the normal diastolic function group and the reduced diastolic function group. Significant associations were found between repolarization variables and diastolic function. After adjusting for all other possible confounders, the QTc and Tpe_c intervals were significantly associated with the E/A ratio ($P = 0.008$; $P = 0.010$). In men, the QTc interval was associated with abnormal diastolic function, and compared to the third QTc tertile, in the second QTc tertile, the odds ratio was 0.257 (95%CI: 0.102–0.649; $P = 0.004$).

CONCLUSION
Repolarization variables are associated with cardiac diastolic function even in healthy people. Moderate levels of the QTc interval exert a protective effect on diastolic dysfunction in men.

Key words: QT interval; Tpeak-to-Tend interval; Diastolic dysfunction; Ventricular repolarization; Electrocardiography

Core tip: A community-based cross-sectional study conducted to assess the relationship between ventricular repolarization variables and cardiac diastolic function in apparently healthy Chinese individuals. We observed an independent association between ventricular repolarization variables and cardiac diastolic function parameters, and moderate levels of the QTc interval tend to have a protective effect on diastolic dysfunction in men. Electromechanical coupling may represent a relationship between heterogeneity of repolarization and abnormal myocardial mechanics.

Citation: Li ZD, Bai XJ, Han LL, Han W, Sun XF, Chen XM. Association between ventricular repolarization variables and cardiac diastolic function: A cross-sectional study of a healthy Chinese population. *World J Clin Cases* 2019; 7(8): 940-950
URL: https://www.wjgnet.com/2307-8960/full/v7/i8/940.htm
DOI: https://dx.doi.org/10.12998/wjcc.v7.i8.940

INTRODUCTION

Heart failure (HF) is a complex and increasingly common syndrome that affects over 23 million patients worldwide[1]. Approximately half of patients with HF present with diastolic dysfunction, and asymptomatic diastolic dysfunction is present in 21% of the population[2]. Asymptomatic diastolic dysfunction may be present for a significant period of time before developing into symptomatic HF. The latency between dysfunction and symptoms represents the best time for using effective diagnostics and therapies[3]. Therefore, the mechanisms underlying diastolic dysfunction need to be more extensively studied.

Growing evidence demonstrates that the pathologies of diastolic dysfunction and systolic dysfunction are different. Some studies have reported that electrical repolarization abnormalities are associated with declining diastolic function, suggesting that diastolic electromechanical coupling represents a unifier linking diastolic dysfunction, calcium handling, and repolarization abnormalities with the development of symptomatic HF[4]. The QT interval is the most commonly used parameter in the electrocardiographic (ECG) assessment of repolarization by physicians in clinical practice. The Tpeak-to-Tend (Tpe) interval, defined as the time interval between the peak and the end of the T wave, is proposed as a readily available ECG measurement of the dispersion of ventricular repolarization. The Tpe/QT ratio is used to predict cardiac arrhythmias. Previous studies have evaluated the QT and Tpe intervals as potential mechanistic contributors to diastolic dysfunction in specific populations[5-8]. Wilcox *et al*[5] found QTc prolongation was independently associated with diastolic dysfunction in patients with clinical suspicion of HF. Another study by Khan *et al*[6] confirmed that a prolonged QTc interval was a

useful tool for predicting diastolic dysfunction. In addition, Sauer *et al*[7] showed that increased Tpe interval was associated with both resting and exercise-induced diastolic dysfunction. However, the subjects of the studies above were all patients with risk factors of HF, and risk factors such as hypertension and diabetes mellitus may influence both heart structure and heart function and are powerful potential confounders of electromechanical coupling. Thus, the aim of this study was to assess the relationship between ventricular repolarization variables, such as the QT interval, Tpe interval and Tpe/QT ratio, and diastolic function in an apparently healthy Chinese population and determine whether measuring repolarization variables may provide information valuable for predicting cardiac diastolic function in healthy people.

MATERIALS AND METHODS

Study population

The subjects who participated in this community-based cross-sectional study were recruited from a healthy Han Chinese population between 2007 and 2008. There were the following register criteria: (1) Age older than 35 years; (2) Being healthy by self-evaluation; (3) Having the ability to care for themselves and perform activities associated with daily living independently and without difficulty; (4) Having the ability to provide informed consent and self-reported data. Subjects with cardiovascular disease, hypertension [defined as a systolic blood pressure (SBP) ≥ 140 mmHg or a diastolic blood pressure (DBP) ≥ 90 mmHg and/or an antihypertensive medication requirement], diabetes (defined as a fasting plasma glucose > 7.0 mmol/L or an insulin or oral hypoglycemic medication requirement), and other chronic diseases were excluded from the study. The subjects who provided the informed consent conducted physical examination or laboratory tests. After excluding persons with an abnormal physical examination or laboratory results, 414 healthy subjects (186 men and 228 women) were included in the study. This study was approved by the Ethics Committee of China Medical University.

Clinical measurements and laboratory tests

The participants underwent a clinical examination and completed a detailed questionnaire at the time of enrollment. Before they were examined, the subjects rested for 10-15 min in a temperature-controlled environment. Physical parameters, including height and weight, were measured with a digital scale while the participants were wearing light clothing and no shoes on a digital scale. Blood pressure was measured using a manual stethoscope and a sphygmomanometer with an adjustable cuff. Two measurements were performed 2 min apart, and the average of the two measurements was calculated. Body mass index (BMI) was calculated as the mass in kilograms divided by height in meters squared, and body surface area (BSA) was calculated according to the following formula: BSA (m^2) = 0.0061 × height (cm) + 0.0128 × weight (kg) - 0.1529.

Blood samples were collected from the subjects between 8:00 and 9:00 am after the subjects had fasted for at least 10 h overnight. Blood biochemical parameters, including triglycerides (TG), total cholesterol (TC), high-density lipoprotein cholesterol (HDL-C-C), low-density lipoprotein (LDL-C), fasting blood glucose (FBG) and serum creatinine (SCr) levels, were assayed on-site at the medical laboratory of the study center.

ECG

All subjects underwent a 12-lead ECG recorded at a paper speed of 25 mm/sec and a voltage of 10 mm/mV by a standard ECG system. For ECG analysis, we performed manual measurements of the values with a digital caliper using a computer program. The QT interval was measured between the QRS onset and the end of the T wave, and the Tpe interval was measured from the peak of the T wave to the end of the T wave. The QT interval and the Tpe interval were corrected separately for heart rate using the Bazett formula[9]. We also calculated the Tpe/QT and Tpe/QTc ratios. All measurements were performed in lead V5[10]. In cases in which lead V5 could not be used for the analysis, leads V4 and V6 (in that order) were utilized. ECG measurements were performed by a single trained reader who was blinded to the echocardiographic results.

Echocardiography

All subjects underwent a complete M-mode, two-dimensional and pulsed-wave (PW) Doppler echocardiographic examination using a Philips iE33 Ultrasound System, and all echocardiographic measurements were obtained according to published

guidelines[11,12]. PW Doppler was performed in the apical 4-chamber view to obtain data pertaining to mitral inflow velocities and time intervals. The primary measurements performed during this procedure included measurements of mitral early diastolic inflow velocity (E), late diastolic inflow velocity (A), the E/A ratio, and E-wave deceleration time (DT). We used the apical four-chamber views to measure left atrial anterior-posterior diameter (LA-AP-D), left atrial medial-lateral diameter (LA-ML-D) and left atrial superior-inferior diameter (LA-SI-D). The left atrial volume (LAV) was computed by the equation 4π/3(LA-SI-D/2)(LA-AP-D/2)(LA-ML-D/2) according to the ellipsoid model, and the left atrial volume index (LAVI) was calculated as the LAV in milliliters divided by the BSA in meters squared. According to the American Society of Echocardiography guidelines[12], in this study, E/A < 0.75 was considered to be reduced diastolic function.

Statistical analysis

The Kolmogorov-Smirnov test was used for all analyses of normally distributed data. All continuous data were normally distributed and were expressed as the means ± SDs. The differences in these variables between different groups were examined using the independent-samples t-test. Categorical variables were expressed as the number {(percentile) [*n*(%)]}, and comparative analyses of different groups were performed using the chi-square (χ^2) test. Simple correlation analyses were performed by calculating Pearson's coefficients for the relationships between two variables. Multiple linear regression analyses were performed to adjust for possible confounding variables. The following three models were used: An un-adjusted model, a model adjusted only for age, and a model adjusted for age, BMI, SBP, DBP, TG, TC, HDL-C, LDL-C, FBG and SCr. Binary logistic regression was reformed to investigate the associations between abnormal diastolic function and the levels of QTc and Tpe_c. The subjects were categorized into tertiles (1-3) for QTc and Tpe_c, with tertile 3 showing the highest levels of QTc and Tpe_c. The following two models were applied: A model adjusting for age and a model adjusting for age, BMI, SBP, DBP, TG, TC, HDL-C, LDL-C, FBG and SCr. All statistical analyses were performed using SPSS 19.0 statistical software (SPSS, Chicago, IL, United States), and a *P* value < 0.05 was considered statistically significant.

RESULTS

Clinical, electrocardiographic and echocardiographic characteristics

A total of 414 subjects (186 men) were assessed in this study, and the mean age was 55 ± 14 years old. Subjects were divided into two groups based on their E/A values (one group with E/A ≥ 0.75 and the other with E/A < 0.75). The differences in the clinical, ECG and echocardiographic characteristics between the groups with normal and reduced E/A ratios are shown in Table 1. Age, BMI, SBP, DBP and SCr were significantly higher in subjects with a reduced E/A ratio (*P* < 0.01). Furthermore, there were several ECG-related differences between the two groups: The RR interval, QTc interval, Tpe interval, Tpe_c interval and Tpe/QT ratio were higher in those with E/A < 0.75 than in those with E/A ≥ 0.75 (*P* < 0.01). All echocardiographic parameters were significantly different between the two groups (*P* < 0.05).

Correlation analysis between electrocardiographic repolarization variables and other variables

Table 2 shows the Pearson correlation coefficients for the relationships between ECG repolarization variables and other variables. All the repolarization variables except the Tpe/QTc ratio were significantly associated with age (*P* < 0.05) and all except the QT interval were associated with BMI (*P* < 0.05). Moreover, the QTc interval was significantly associated with SBP, TC and LDL-C (*P* < 0.05). The Tpe interval was significantly associated with HDL-C (*P* < 0.05). The Tpe_c interval was significantly associated with HDL-C and LDL-C (*P* < 0.05).The Tpe/QT ratio was significantly associated with HDL-C, LDL-C and SCr (*P* < 0.05). The Tpe/QTc ratio was significantly associated with HDL-C and SCr (*P* < 0.01). With regard to the echocardiographic diastolic parameters, the E/A ratio was negatively and significantly correlated with QTc, Tpe and Tpe_c intervals and Tpe/QT ratio (*P* < 0.01). E was negatively correlated with the Tpe_c interval and the Tpe/QT ratio (*P* < 0.05). A was positively correlated with all the repolarization variables except the Tpe/QTc ratio (*P* < 0.01). DT was positively correlated with the QT interval and the Tpe/QTc ratio (*P* < 0.05). LAV was positively correlated with all the repolarization variables except the Tpe/QT ratio (*P* < 0.05). LAVI was positively correlated with QTc and Tpe intervals (*P* < 0.01).

Table 1 Clinical, electrocardiography and echocardiographic characteristics based on their E/A ratio

	All subjects (*n* = 414)	E/A ≥ 0.75 (*n* = 300)	E/A < 0.75 (*n* = 114)	*P*-value
Age (yr)	55.21 ± 14.18	55.25 ± 13.20	69.62 ± 11.05	< 0.001
Male *n* (%)	186 (44.9%)	124 (41.3%)	62 (55.4%)	0.017
BMI (kg/m^2)	23.68 ± 3.00	23.41 ± 2.93	24.37 ± 3.08	0.004
SBP (mmHg)	125.64 ± 12.69	123.05 ± 12.68	132.43 ± 9.93	< 0.001
DBP (mmHg)	75.97 ± 8.84	74.92 ± 8.97	78.73 ± 7.87	< 0.001
TG (mmol/L)	1.38 ± 1.10	1.39 ± 1.18	1.36 ± 0.84	0.840
TC (mmol/L)	5.23 ± 1.05	5.22 ± 1.08	5.26 ± 0.98	0.722
HDL-C (mmol/L)	1.64 ± 0.41	1.65 ± 0.40	1.62 ± 0.44	0.440
LDL-C (mmol/L)	2.90 ± 0.75	2.88 ± 0.76	2.95 ± 0.70	0.448
FBG (mmol/L)	5.55 ± 0.49	5.54 ± 0.48	5.60 ± 0.53	0.248
SCr (μmol/L)	64.37 ± 14.46	62.72 ± 13.23	68.71 ± 16.58	< 0.001
PR interval (ms)	157.08 ± 23.73	156.36 ± 24.18	158.97 ± 22.50	0.302
RR interval (ms)	905.53 ± 126.29	915.40 ± 118.32	879.56 ± 142.52	0.010
QT interval (ms)	372.81 ± 30.07	371.45 ± 29.49	376.39 ± 31.40	0.136
QTc interval (ms)	393.52 ± 29.44	393.59 ± 26.74	403.86 ± 33.56	< 0.001
Tpe interval (ms)	73.94 ± 14.25	72.68 ± 12.41	77.26 ± 17.86	0.003
Tpe$_c$ interval (ms)	78.27 ± 16.30	76.36 ± 13.53	83.32 ± 21.25	< 0.001
Tpe/QT	0.20 ± 0.03	0.19 ± 0.03	0.20 ± 0.04	0.004
Tpe/QTc	0.19 ± 0.03	0.19 ± 0.03	0.19 ± 0.03	0.160
E (cm/s)	74.36 ± 17.83	80.27 ± 16.20	58.82 ± 11.49	< 0.001
A (cm/s)	75.07 ± 19.21	68.75 ± 16.70	91.69 ± 15.07	< 0.001
E/A	1.07 ± 0.41	1.23 ± 0.36	0.64 ± 0.08	< 0.001
MV-DT (ms)	162.78 ± 35.15	159.43 ± 31.14	171.60 ± 42.92	0.002
LAV (mL)	33.16 ± 9.73	32.30 ± 9.70	35.42 ± 9.48	0.003
LAVI (mL/m^2)	19.83 ± 5.31	19.38 ± 5.29	21.01 ± 5.22	0.005
LVEF (%)	62.54 ± 4.71	62.86 ± 4.47	61.68 ± 5.21	0.023

BMI: Body mass index; SBP: Systolic blood pressure; DBP: Diastolic blood pressure; TG: Triglyceride; TC: Total cholesterol; HDL-C-C: High-density lipoprotein cholesterol; LDL-C: Low-density lipoprotein cholesterol; FBG: Fasting blood glucose; SCr: Serum creatinine; E: Early diastolic inflow velocity; A: Late diastolic inflow velocity; DT: E-wave deceleration time; LAV: Left atrial volume; LAVI: Left atrial maximum volume index; LVEF: Left ventricular ejection fraction.

Associations between electrocardiographic repolarization variables and echocardiographic diastolic function parameters

Table 3 shows the results of the multiple linear regression analyses, in which echocardiographic diastolic function parameters served as the dependent variables, and ECG repolarization variables served as the independent variables. After adjusting for all other possible confounders, A and E/A ratio were significantly associated with QTc and Tpe$_c$ intervals and the Tpe/QT ratio, and A was also significantly associated with the Tpe interval. LAV and LAVI showed significant and independent associations with the QTc interval, and LAV was also significantly associated with the QT interval. DT was significantly associated with the QT interval.

Table 4 shows the binary logistic regression analyses performed using reduced diastolic function as the dependent variable and cut-off values of the QTc and Tpe$_c$ interval as the independent variables. In men, the odds ratio in subjects with reduced diastolic function was 2.715 (95%CI: 1.356–5.432; $P < 0.001$) for longer QTc interval after adjustment for age, compared to the subjects in normal QTc interval. This association was still significant after adjustment for all other variables, and the odds ratio was 2.567 (95%CI: 1.227–5.370; $P = 0.012$). In women, the QTc interval was not correlated with reduced diastolic function. With regard to the Tpe$_c$ interval, in men, compared to the third Tpe$_c$ tertile, in the Tpe$_c$ second tertile, the odds ratio approached statistical significance (0.423; 95%CI: 0.175–1.022; $P = 0.056$) after adjustment for all other variables.

Table 2 Correlation analysis between electrocardiography repolarization variables and other variables

	QT (ms)	QTc (ms)	Tpe (ms)	Tpe_c (ms)	Tpe/QT	Tpe/QTc
Age (yr)	0.223[b]	0.281[b]	0.167[b]	0.169[b]	0.109[a]	0.090
BMI (kg/m^2)	0.073	0.109[a]	0.119[a]	0.124[a]	0.120[a]	0.100[a]
SBP (mmHg)	0.082	0.167[b]	0.059	0.089	0.049	0.004
DBP (mmHg)	-0.031	0.029	-0.034	-0.008	-0.005	-0.036
TG (mmol/L)	-0.02	0.028	0.058	0.073	0.086	0.058
TC (mmol/L)	0.009	0.115[a]	0.054	0.094	0.071	0.020
HDL-C (mmol/L)	-0.061	-0.067	-0.132[b]	-0.122[a]	-0.140[b]	-0.130[b]
LDL-C (mmol/L)	-0.046	0.155[b]	0.088	0.127[a]	0.098[a]	0.042
FBG (mmol/L)	-0/089	0.080	0.015	0.074	0.081	0.001
SCr (μmol/L)	-0/013	-0.055	0.089	0.068	0.123[a]	0.146[b]
E (cm/s)	0.051	-0.093	-0.072	-0.121[a]	-0.138[b]	-0.060
A (cm/s)	0.152[b]	0.324[b]	0.189[b]	0.237[b]	0.157[b]	0.079
E/A	-0.070	-0.288[b]	-0.155[b]	-0.223[b]	-0.175[b]	-0.067
DT (ms)	0.244[b]	-0.028	0.073	-0.047	-0.039	0.102[a]
LAV (mL)	0.312[b]	0.209[b]	0.157[b]	0.099[a]	0.038	0.100[a]
LAVI (mL/m^2)	0.354	0.255[b]	0.148[b]	0.091	0.002	0.062

P-values are from analysis of variance:
[a]Significant difference ($P < 0.05$);
[b]Significant difference ($P < 0.01$). BMI: Body mass index; SBP: Systolic blood pressure; DBP: Diastolic blood pressure; TG: Triglyceride; TC: Total cholesterol; HDL-C-C: High-density lipoprotein cholesterol; LDL-C: Low-density lipoprotein cholesterol; FBG: Fasting blood glucose; SCr: Serum creatinine; E: Early diastolic inflow velocity; A: Late diastolic inflow velocity; DT: E-wave deceleration time; LAV: Left atrial volume; LAVI: Left atrial maximum volume index.

DISCUSSION

The most important findings of the present study are the associations between ventricular repolarization variables and cardiac diastolic function in a population of healthy adults. These relationships remained significant even after correction for other potential confounders.

The ECG QT interval is one of the ventricular repolarization variables most commonly used by physicians in clinical practice. Previous studies have demonstrated the existence of a relationship between a prolonged QT interval and abnormal myocardial mechanical function among patients with inherited long QT syndrome (LQTS), which has historically been considered a purely electrical disease[13-15]. In recent years, clinicians have become increasingly interested in the association between the QT interval and echocardiographic parameters representing diastolic function in patients with suspected HF, hypertension, and diabetes mellitus and have obtained data supporting the idea that there is a correlation between diastolic dysfunction and the QT interval[5,8,16]. However, diseases such as hypertension and diabetes mellitus influence both heart structure and heart function and are powerful potential confounders of electromechanical coupling measurements. The present community-based study included apparently healthy subjects selected from a Chinese population without hypertension, diabetes, cardiovascular disease, or other chronic diseases and thus excluded potential confounders. We found an independent linear association between the QTc interval and echocardiographic diastolic parameters. Moreover, this study also demonstrates that moderate levels of QTc exert a protective effect on diastolic dysfunction in healthy men. To the best of our knowledge, this is the first study to demonstrate an association between QTc interval levels and diastolic function in a healthy population. Possible explanations for this finding include the possibility that the link between electrical repolarization and diastolic mechanics may be commonly mediated by the effects of calcium handing[4]. Previous studies have also described a U-shaped association between the QTc interval and risk of death[17,18]. Therefore, it is biologically plausible that there is an optimum for the dispersion of ventricular repolarization and that the risk of diastolic dysfunction is increased at both ends of the spectrum. However, sex-related differences in the association between QTc interval levels and diastolic function remain to be explored.

Table 3 Relationship between electrocardiography repolarization variables and echocardiographic diastolic parameters using a stepwise multiple regression model

	Model 1		Model 2		Model 3	
	Beta	*P*-value	Beta	*P*-value	Beta	*P*-value
QT interval (ms)						
A (cm/s)	0.152	0.002	0.033	0.435	0.028	0.504
DT (ms)	0.244	< 0.001	0.194	< 0.001	0.182	< 0.001
LAV (mL)	0.312	< 0.001	0.271	< 0.001	0.248	< 0.001
QTc interval (ms)						
A (cm/s)	0.324	< 0.001	0.186	< 0.001	0.178	< 0.001
E/A	-0.288	< 0.001	-0.131	0.001	-0.105	0.008
LAV (mL)	0.209	< 0.001	0.152	0.002	0.105	0.019
LAVI (mL/m^2)	0.255	< 0.001	0.181	< 0.001	0.142	0.003
Tpe (ms)						
A (cm/s)	0.189	< 0.001	0.102	0.015	0.099	0.016
E/A	-0.155	0.002	-0.057	0.153	-0.035	0.355
LAV (mL)	0.157	0.001	0.119	0.014	0.167	0.120
LAVI (mL/m^2)	0.148	0.003	0.098	0.039	0.080	0.086
Tpe$_c$ (ms)						
E (cm/s)	-0.121	0.014	-0.062	0.185	-0.032	0.489
A (cm/s)	0.237	< 0.001	0.150	< 0.001	0.143	< 0.001
E/A	-2.223	< 0.001	-0.126	0.002	-0.098	0.010
LAV (mL)	0.099	0.045	0.059	0.233	0.015	0.749
Tpe/QT						
E (cm/s)	-0.138	0.005	-0.100	0.030	-0.066	0.152
A (cm/s)	0.157	0.001	0.099	0.017	0.097	0.018
E/A	-0.175	< 0.001	-0.111	0.005	-0.083	0.028
Tpe/QTc						
DT (ms)	0.102	0.038	0.078	0.101	0.072	0.139
LAV (mL)	0.100	0.041	0.079	0.100	0.037	0.388

E: Early diastolic inflow velocity; A: Late diastolic inflow velocity; DT: E-wave deceleration time; LAV: Left atrial volume; LAVI: Left atrial maximum volume index. Model 1: Unadjusted model; Model 2: Adjusted for age; Model 3: Fully adjusted for age, gender, body mass index, systolic blood pressure, diastolic blood pressure, triglyceride, total cholesterol, high-density lipoprotein cholesterol, low-density lipoprotein cholesterol, fasting blood glucose and serum creatinine. Standardized coefficients and *P*-values were the outcomes of the regression analyses.

Tpe is the interval between the peak of the T wave and the end of the T wave. The Tpe interval is usually viewed as representative of the difference in repolarization times between subendocardial and subepicardial myocardial cells and has been proposed to reflect the transmural cardiac repolarization expressed through surface 12 ECG[4]. Multiple recent studies have demonstrated that Tpe interval plays an important role as a potential ECG biomarker for predicting arrhythmia risk and cardiovascular death[19-21]. Furthermore, some studies have evaluated the Tpe interval as a potential mechanism that contributes to mechanical dysfunction in patients with overt or suspected HF[7,22]. In the present population-based study, we found a significant linear association between ECG Tpe and Tpe$_c$ intervals and the echocardiographic E/A ratio and A wave. These findings add to the growing literature supporting the notion that electromechanical coupling of dispersion of repolarization is a potential mechanism of diastolic dysfunction. It is interesting to note that the Tpe$_c$ interval was more strongly correlated with diastolic function parameters in this study, compared to the Tpe interval. The basis for this result is unclear and is beyond the scope of the current study. In the present study, we found that in men, compared to the third Tpe$_c$ tertile, in the Tpe$_c$ second tertile, the odds ratio approached statistical significance (0.423; 95%CI: 0.175–1.022; P = 0.056) after adjustment for all other variables. Moderate Tpe$_c$ levels tend to have a protective effect on diastolic dysfunction in men. A large population study found U-shaped associations between the Tpe interval and the risks of all-cause and cardiovascular

Table 4 Association of E/A ratio within tertiles of QTc and Tpe_c using binary logistic regression model

	Tertile 1				Tertile 2				Tertile 3
	Model 1		Model 2		Model 1		Model 2		
	OR (95%CI)	*P*-value	OR (95%CI)	*P*-value	OR (95%CI)	*P*-value	OR (95%CI)	*P*-value	OR
Tertiles of QTc									
Men (*n* = 186)	0.604 (0.272-1.342)	0.216	0.763 (0.317-1.836)	0.545	0.210 (0.087-0.506)	0.001	0.257 (0.102-0.649)	0.004	1 (ref)
Women (*n* = 228)	0.527 (0.176-1.579)	0.253	0.982 (0.284-3.396)	0.977	1.230 (0.539-2.806)	0.624	1.480 (0.574-3.815)	0.417	1 (ref)
Tertiles of Tpe_c									
Men (*n* = 186)	0.890 (0.397-1.996)	0.777	0.980 (0.404-2.372)	0.963	0.465 (0.204-1.061)	0.069	0.423 (0.175-1.022)	0.056	1 (ref)
Women (*n* = 228)	0.483 (0.188-1.242)	0.131	0.477 (0.162-1.404)	0.179	0.487 (0.204-1.160)	0.104	0.532 (0.200-1.416)	0.206	1 (ref)

Model 1: Adjusted for age; Model 2: Fully adjusted for age, gender, body mass index, systolic blood pressure, diastolic blood pressure, triglyceride, total cholesterol, high-density lipoprotein cholesterol, low-density lipoprotein cholesterol, fasting blood glucose and serum creatinine. OR values and *P*-value were the outcome of binary logistic regression using abnormal diastolic function as the dependent variable.

mortality, atrial fibrillation, and HF[19]. Therefore, similar to the QTc interval, there may be an optimum for the dispersion of cardiac repolarization, and the risk of cardiovascular outcomes may be increased at both ends of the spectrum. Further investigations are necessary to confirm and improve the present findings.

The Tpe/QT ratio is a novel ventricular repolarization variable that is used to predict cardiac arrhythmias[23]. Some studies have suggested the applicability of Tpe/QT ratio as a potentially important index of arrhythmogenesis in congenital and acquired channelopathies[23,24]. Furthermore, some studies have evaluated the Tpe/QT ratio as a potential ECG biomarker for predicting arrhythmia risk and cardiovascular death[25-27]. In the present study, we found an inverse linear association between the Tpe/QT ratio and the E/A ratio. However, the Tpe/QTc ratio was not associated with any echocardiographic diastolic function parameters after adjustment for several important potential confounders. The basis for this finding in unclear, and additional studies are required.

Our results should not be interpreted to suggest that repolarization variables measured on surface ECG can be used to screen for diastolic dysfunction on echocardiography. Furthermore, our current understanding of the role of ventricular repolarization in the development or progression of HF is limited. Rather, our findings provide evidence showing that ventricular repolarization parameters may be used as markers of asymptomatic mild diastolic dysfunction. Epidemiological studies suggest that there is a latent phase during which diastolic dysfunction is present and progresses in severity before the symptoms of HF arise[28]. This asymptomatic phase represents a potential time to intervene and thereby prevent symptomatic HF. The latency between dysfunction and symptoms represents the best time for using effective diagnostics and therapies. Identifying a pharmacological intervention to restore repolarization to a more normal state may be a novel target for therapy.

The present study had several limitations that require discussion. First, this research is part of a cross-sectional study, and it is therefore difficult to demonstrate cause-effect relationships between ventricular repolarization variables and cardiac diastolic function. A longitudinally designed study is required to confirm the current findings. Second, the subjects included in this study were recruited from communities in northern China. Therefore, the findings in the study are not representative of the general population. Third, a relatively low number of subjects were included in the study, and the proportion of women (55.1%) was higher than that of men (44.9%). Fourth, we chose to report the QT and Tpe intervals corrected for heart rate (QTc and Tpe_c) using the Bazett formula. The Bazett formula undercorrects the QT interval at lower heart rates and overcorrects it at higher heart rates[29]. However, the Bazett formula is the formula that is most often used in research or clinical practice. Fifth, several important parameters, including LV mass and QRS durations, were not measured in this study but may affect ventricular repolarization variables[30]. Further studies are needed to confirm and improve upon the findings of the present study.

In conclusion, this study reveals that even in healthy people, ventricular repolarization variables are linearly associated with cardiac diastolic function parameters. Furthermore, moderate levels of the QTc interval tend to have a protective effect on diastolic dysfunction in men. Electromechanical coupling may represent a relationship between heterogeneity of repolarization and abnormal

myocardial mechanics. A longitudinal study should be performed in the future to confirm the findings of the current study.

ARTICLE HIGHLIGHTS

Research background

Asymptomatic diastolic dysfunction present for a significant period of time before developing into symptomatic heart failure (HF), and diastolic electromechanical coupling may represent a unifier linking diastolic dysfunction, calcium handling, and repolarization abnormalities with the development of symptomatic HF. We assessed the relationship between ventricular repolarization variables, such as the QT interval, Tpe interval and Tpe/QT ratio, and diastolic function in an apparently healthy Chinese population through a community-based cross-sectional study.

Research motivation

Some studies have reported that electrical repolarization abnormalities are associated with declining diastolic function in patients with suspected HF, hypertension, and diabetes mellitus. However, diseases such as hypertension and diabetes mellitus influence both heart structure and heart function and are powerful potential confounders of electromechanical coupling measurements. Therefore, this study hopes to determine whether measuring repolarization variables may provide information valuable for predicting cardiac diastolic function in healthy people.

Research objectives

The research objective of this study was to explore the relationship between ventricular repolarization variables and cardiac diastolic function in apparently healthy Chinese individuals.

Research methods

We retrospectively analyzed 414 healthy subjects aged 35-91 years who were enrolled between September 2007 and June 2008. All subjects underwent standard 12-lead electrocardiography (ECG) and comprehensive echocardiography. ECG and echocardiography results were analyzed separately and in a blinded fashion. Correlation and regression analyses were applied to determine associations. This study is a community-based cross-sectional study.

Research results

Our research found that even in healthy people, ventricular repolarization variables are associated with cardiac diastolic function parameters. Furthermore, moderate levels of the QTc interval tend to have a protective effect on diastolic dysfunction in men.

Research conclusions

Repolarization variables are associated with cardiac diastolic function even in healthy people. Electromechanical coupling may represent a relationship between heterogeneity of repolarization and abnormal myocardial mechanics.

Research perspectives

We observed an independent association between ventricular repolarization variables and cardiac diastolic function in a community-based cross-sectional study. However, a relatively low number of subjects were included in the study, and the cross-sectional study has its own shortcomings. A longitudinally designed study is required to confirm the current findings.

REFERENCES

1 **Lloyd-Jones D**, Adams RJ, Brown TM, Carnethon M, Dai S, De Simone G, Ferguson TB, Ford E, Furie K, Gillespie C, Go A, Greenlund K, Haase N, Hailpern S, Ho PM, Howard V, Kissela B, Kittner S, Lackland D, Lisabeth L, Marelli A, McDermott MM, Meigs J, Mozaffarian D, Mussolino M, Nichol G, Roger VL, Rosamond W, Sacco R, Sorlie P, Stafford R, Thom T, Wasserthiel-Smoller S, Wong ND, Wylie-Rosett J; American Heart Association Statistics Committee and Stroke Statistics Subcommittee. Executive summary: heart disease and stroke statistics--2010 update: a report from the American Heart Association. *Circulation* 2010; **121**: 948-954 [PMID: 20177011 DOI: 10.1161/CIRCULATIONAHA.109.192666]

2 **Jeong EM**, Dudley SC. Diastolic dysfunction. *Circ J* 2015; **79**: 470-477 [PMID: 25746522 DOI: 10.1253/circj.CJ-15-0064]

3 **Halley CM**, Houghtaling PL, Khalil MK, Thomas JD, Jaber WA. Mortality rate in patients with diastolic dysfunction and normal systolic function. *Arch Intern Med* 2011; **171**: 1082-1087 [PMID: 21709107 DOI: 10.1001/archinternmed.2011.244]

4 **Prenner SB**, Shah SJ, Goldberger JJ, Sauer AJ. Repolarization Heterogeneity: Beyond the QT Interval. *J Am Heart Assoc* 2016; **5**: pii: e003607 [PMID: 27130347 DOI: 10.1161/JAHA.116.003607]

5 **Wilcox JE**, Rosenberg J, Vallakati A, Gheorghiade M, Shah SJ. Usefulness of electrocardiographic QT interval to predict left ventricular diastolic dysfunction. *Am J Cardiol* 2011; **108**: 1760-1766 [PMID: 21907948 DOI: 10.1016/j.amjcard.2011.07.050]

6 **Khan HS**, Iftikhar I, Khan Q. Validity of Electrocardiographic QT Interval in Predicting Left Ventricular Diastolic Dysfunction in Patients with Suspected Heart Failure. *J Coll Physicians Surg Pak* 2016; **26**: 353-

356 [PMID: 27225136]
7 **Sauer A**, Wilcox JE, Andrei AC, Passman R, Goldberger JJ, Shah SJ. Diastolic electromechanical coupling: association of the ECG T-peak to T-end interval with echocardiographic markers of diastolic dysfunction. *Circ Arrhythm Electrophysiol* 2012; **5**: 537-543 [PMID: 22467673 DOI: 10.1161/CIRCEP.111.969717]
8 **Jani Y**, Kamberi A, Xhunga S, Pocesta B, Ferati F, Lala D, Zeqiri A, Rexhepi A. The influence of type 2 diabetes and gender on ventricular repolarization dispersion in patients with sub-clinic left ventricular diastolic dysfunction. *Am J Cardiovasc Dis* 2015; **5**: 155-166 [PMID: 26550530]
9 **Luo S**, Michler K, Johnston P, Macfarlane PW. A comparison of commonly used QT correction formulae: the effect of heart rate on the QTc of normal ECGs. *J Electrocardiol* 2004; **37** Suppl: 81-90 [PMID: 15534815 DOI: 10.1016/j.jelectrocard.2004.08.030]
10 **Castro-Torres Y**, Carmona-Puerta R, Katholi RE. Ventricular repolarization markers for predicting malignant arrhythmias in clinical practice. *World J Clin Cases* 2015; **3**: 705-720 [PMID: 26301231 DOI: 10.12998/wjcc.v3.i8.705]
11 **Nagueh SF**, Smiseth OA, Appleton CP, Byrd BF, Dokainish H, Edvardsen T, Flachskampf FA, Gillebert TC, Klein AL, Lancellotti P, Marino P, Oh JK, Alexandru Popescu B, Waggoner AD; Houston, Texas; Oslo, Norway; Phoenix, Arizona; Nashville, Tennessee; Hamilton, Ontario, Canada; Uppsala, Sweden; Ghent and Liège, Belgium; Cleveland, Ohio; Novara, Italy; Rochester, Minnesota; Bucharest, Romania; and St. Louis, Missouri.. Recommendations for the Evaluation of Left Ventricular Diastolic Function by Echocardiography: An Update from the American Society of Echocardiography and the European Association of Cardiovascular Imaging. *Eur Heart J Cardiovasc Imaging* 2016; **17**: 1321-1360 [PMID: 27422899 DOI: 10.1093/ehjci/jew082]
12 **Nagueh SF**, Appleton CP, Gillebert TC, Marino PN, Oh JK, Smiseth OA, Waggoner AD, Flachskampf FA, Pellikka PA, Evangelisa A. Recommendations for the evaluation of left ventricular diastolic function by echocardiography. *Eur J Echocardiogr* 2009; **10**: 165-193 [PMID: 19270053 DOI: 10.1093/ejechocard/jep007]
13 **Leren IS**, Hasselberg NE, Saberniak J, Håland TF, Kongsgård E, Smiseth OA, Edvardsen T, Haugaa KH. Cardiac Mechanical Alterations and Genotype Specific Differences in Subjects With Long QT Syndrome. *JACC Cardiovasc Imaging* 2015; **8**: 501-510 [PMID: 25890583 DOI: 10.1016/j.jcmg.2014.12.023]
14 **Savoye C**, Klug D, Denjoy I, Ennezat PV, Le Tourneau T, Guicheney P, Kacet S. Tissue Doppler echocardiography in patients with long QT syndrome. *Eur J Echocardiogr* 2003; **4**: 209-213 [PMID: 12928025 DOI: 10.1016/s1525-2167(03)00011-8]
15 **Letsas KP**, Efremidis M, Kounas SP, Pappas LK, Gavrielatos G, Alexanian IP, Dimopoulos NP, Filippatos GS, Sideris A, Kardaras F. Clinical characteristics of patients with drug-induced QT interval prolongation and torsade de pointes: identification of risk factors. *Clin Res Cardiol* 2009; **98**: 208-212 [PMID: 19031039 DOI: 10.1007/s00392-008-0741-y]
16 **Mayet J**, Shahi M, McGrath K, Poulter NR, Sever PS, Foale RA, Thom SA. Left ventricular hypertrophy and QT dispersion in hypertension. *Hypertension* 1996; **28**: 791-796 [PMID: 8901825 DOI: 10.1161/01.HYP.28.5.791]
17 **Nielsen JB**, Graff C, Rasmussen PV, Pietersen A, Lind B, Olesen MS, Struijk JJ, Haunsø S, Svendsen JH, Køber L, Gerds TA, Holst AG. Risk prediction of cardiovascular death based on the QTc interval: evaluating age and gender differences in a large primary care population. *Eur Heart J* 2014; **35**: 1335-1344 [PMID: 24603310 DOI: 10.1093/eurheartj/ehu081]
18 **Zhang Y**, Post WS, Dalal D, Blasco-Colmenares E, Tomaselli GF, Guallar E. QT-interval duration and mortality rate: results from the Third National Health and Nutrition Examination Survey. *Arch Intern Med* 2011; **171**: 1727-1733 [PMID: 22025428 DOI: 10.1001/archinternmed.2011.433]
19 **Bachmann TN**, Skov MW, Rasmussen PV, Graff C, Pietersen A, Lind B, Struijk JJ, Olesen MS, Haunsø S, Køber L, Svendsen JH, Holst AG, Nielsen JB. Electrocardiographic Tpeak-Tend interval and risk of cardiovascular morbidity and mortality: Results from the Copenhagen ECG study. *Heart Rhythm* 2016; **13**: 915-924 [PMID: 26707793 DOI: 10.1016/j.hrthm.2015.12.027]
20 **Porthan K**, Viitasalo M, Toivonen L, Havulinna AS, Jula A, Tikkanen JT, Väänänen H, Nieminen MS, Huikuri HV, Newton-Cheh C, Salomaa V, Oikarinen L. Predictive value of electrocardiographic T-wave morphology parameters and T-wave peak to T-wave end interval for sudden cardiac death in the general population. *Circ Arrhythm Electrophysiol* 2013; **6**: 690-696 [PMID: 23881778 DOI: 10.1161/CIRCEP.113.000356]
21 **Rosenthal TM**, Stahls PF, Abi Samra FM, Bernard ML, Khatib S, Polin GM, Xue JQ, Morin DP. T-peak to T-end interval for prediction of ventricular tachyarrhythmia and mortality in a primary prevention population with systolic cardiomyopathy. *Heart Rhythm* 2015; **12**: 1789-1797 [PMID: 25998895 DOI: 10.1016/j.hrthm.2015.04.035]
22 **Sauer AJ**, Selvaraj S, Aguilar FG, Martinez EE, Wilcox JE, Passman R, Goldberger JJ, Freed BH, Shah SJ. Relationship between repolarization heterogeneity and abnormal myocardial mechanics. *Int J Cardiol* 2014; **172**: 289-291 [PMID: 24447740 DOI: 10.1016/j.ijcard.2013.12.232]
23 **Gupta P**, Patel C, Patel H, Narayanaswamy S, Malhotra B, Green JT, Yan GX. T(p-e)/QT ratio as an index of arrhythmogenesis. *J Electrocardiol* 2008; **41**: 567-574 [PMID: 18790499 DOI: 10.1016/j.jelectrocard.2008.07.016]
24 **Yamaguchi M**, Shimizu M, Ino H, Terai H, Uchiyama K, Oe K, Mabuchi T, Konno T, Kaneda T, Mabuchi H. T wave peak-to-end interval and QT dispersion in acquired long QT syndrome: a new index for arrhythmogenicity. *Clin Sci* (Lond. *)* 2003; **105**: 671-676 [PMID: 12857349 DOI: 10.1042/CS20030010]
25 **Aslan MM**, Atici A. Assessment of increased risk of arrhythmia in advanced age pregnancies. *Pak J Med Sci* 2018; **34**: 687-690 [PMID: 30034440 DOI: 10.12669/pjms.343.14313]
26 **Kuzu F**. The effect of type 2 diabetes on electrocardiographic markers of significant cardiac events. *Pak J Med Sci* 2018; **34**: 626-632 [PMID: 30034428 DOI: 10.12669/pjms.343.14562]
27 **Karakulak UN**, Yilmaz OH, Tutkun E, Gunduzoz M, Ercan Onay E. Comprehensive Electrocardiographic Analysis of Lead Exposed Workers: An Arrhythmic Risk Assessment Study. *Ann Noninvasive Electrocardiol* 2017; **22** [PMID: 27282320 DOI: 10.1111/anec.12376]
28 **Redfield MM**, Jacobsen SJ, Burnett JC, Mahoney DW, Bailey KR, Rodeheffer RJ. Burden of systolic and diastolic ventricular dysfunction in the community: appreciating the scope of the heart failure epidemic. *JAMA* 2003; **289**: 194-202 [PMID: 12517230 DOI: 10.1016/S0022-0248(01)00919-8]
29 **Mozos I**. The link between ventricular repolarization variables and arterial function. *J Electrocardiol* 2015; **48**: 145-149 [PMID: 25444569 DOI: 10.1016/j.jelectrocard.2014.11.008]

30 **Oikarinen L**, Nieminen MS, Viitasalo M, Toivonen L, Jern S, Dahlöf B, Devereux RB, Okin PM; LIFE Study Investigators. QRS duration and QT interval predict mortality in hypertensive patients with left ventricular hypertrophy: the Losartan Intervention for Endpoint Reduction in Hypertension Study. *Hypertension* 2004; **43**: 1029-1034 [PMID: 15037560 DOI: 10.1161/01.HYP.0000125230.46080.c6]

World Journal of Clinical Cases

Submit a Manuscript: https://www.f6publishing.com

World J Clin Cases 2019 April 26; 7(8): 951-960

DOI: 10.12998/wjcc.v7.i8.951

ISSN 2307-8960 (online)

CASE REPORT

Non-invasive home lung impedance monitoring in early post-acute heart failure discharge: Three case reports

Edita Lycholip, Eglė Palevičiūtė, Ina Thon Aamodt, Ragnhild Hellesø, Irene Lie, Anna Strömberg, Tiny Jaarsma, Jelena Čelutkienė

ORCID number: Edita Lycholip (0000-0001-6451-7787); Eglė Palevičiūtė (0000-0003-4758-7833); Ina Thon Aamodt (0000-000290989646); Ragnhild Helleso (0000-0002-7757-6521); Irene Lie (0000-0002-04617812); Anna Strömberg (0000-0002-4259-3671); Tiny Jaarsma (0000-0002-4197-4026); Jelena Čelutkienė (0000-0003-3562-9274).

Author contributions: Lycholip E and Čelutkienė J were involved in diagnostics, treatment and follow-up of the patients; Lycholip E, Čelutkienė J, Palevičiūtė E, Strömberg A, Lie I, Aamodt IT, Hellesø R and Jaarsma T interpreted the patients' data and drafted the manuscript; Lycholip E and Čelutkienė J prepared the figures; all authors contributed to writing and editing the manuscript for important intellectual content; all authors have read and approved the final manuscript.

Supported by the NordForsk " Nordic Programme on Health and Welfare" , No. 76015.

Informed consent statement: Written informed consent forms were obtained from these patients for participating in the "Nordic Programme on Health and Welfare." Copies of the written consent forms are available for review by the Editor of this journal.

Conflict-of-interest statement: The authors declare that they have no conflict of interests.

CARE Checklist (2016) statement:

Edita Lycholip, Eglė Palevičiūtė, Jelena Čelutkienė, Clinic of Cardiac and Vascular Diseases, Institute of Clinical Medicine, Faculty of Medicine, Vilnius University, Vilnius 03101, Lithuania

Edita Lycholip, Eglė Palevičiūtė, Jelena Čelutkienė, Center of Cardiology and Angiology, Vilnius University Hospital Santaros Klinikos, Vilnius 08661, Lithuania

Ina Thon Aamodt, Faculty of Medicine, Institute of Health and Society, Department of Nursing Science, University of Oslo, Oslo 0318, Norway

Ina Thon Aamodt, Irene Lie, Center for Patient-Centered Heart and Lung Research, Department of Cardiothoracic Surgery, Oslo University Hospital, Oslo 0420, Norway

Ragnhild Hellesø, Departamento of Nursing Science, Institute of Health and Society, University of Oslo, Oslo 0318, Norway

Anna Strömberg, Department of Medical and Health Sciences, Linkoping University, Linkoping 58185, Sweden

Tiny Jaarsma, Department of Social and Welfare Studies, Linkoping University, Norrkoping 58185, Sweden

Corresponding author: Edita Lycholip, PhD, Chief Nurse, Center of Cardiology and Angiology, Vilnius University Hospital Santaros Klinikos, Santariskiu-2, Vilnius 08661, Lithuania. edita.lycholip@santa.lt
Telephone: +370-688-62459
Fax: +370-5250-1742

Abstract

BACKGROUND

Patients discharged after hospitalization for acute heart failure (AHF) are frequently readmitted due to an incomplete decongestion, which is difficult to assess clinically. Recently, it has been shown that the use of a highly sensitive, non-invasive device measuring lung impedance (LI) reduces hospitalizations for heart failure (HF); it has also been shown that this device reduces the cardiovascular and all-cause mortality of stable HF patients when used in long-term out-patient follow-ups. The aim of these case series is to demonstrate the potential additive role of non-invasive home LI monitoring in the early post-discharge period.

CASE SUMMARY

All authors have read the CARE checklist (2016) and prepared and revised the manuscript in accordance with the CARE checklist (2016).

Manuscript source: Unsolicited manuscript

Received: December 20, 2018
Peer-review started: December 20, 2018
First decision: January 12, 2019
Revised: February 15, 2019
Accepted: February 26, 2019
Article in press: February 26, 2019
Published online: April 26, 2019

P-Reviewer: Iacoviello M, Rostagno C
S-Editor: Ji FF
L-Editor: A
E-Editor: Wu YXJ

We present a case series of three patients who had performed daily LI measurements at home using the edema guard monitor (EGM) during 30 d after an episode of AHF. All patients had a history of chronic ischemic HF with a reduced ejection fraction and were hospitalized for 6–17 d. LI measurements were successfully made at home by patients with the help of their caregivers. The patients were carefully followed up by HF specialists who reacted to the values of LI measurements, blood pressure, heart rate and clinical symptoms. LI reduction was a more frequent trigger to medication adjustments compared to changes in symptoms or vital signs. Besides, LI dynamics closely tracked the use and dose of diuretics.

CONCLUSION

Our case series suggests non-invasive home LI monitoring with EGM to be a reliable and potentially useful tool for the early detection of congestion or dehydration and thus for the further successful stabilization of a HF patient after a worsening episode.

Key words: Heart failure; Home monitoring; Lung impedance; Case report; Pulmonary congestion

Core tip: The monitoring of lung impedance (LI) using the edema guard monitor (EGM) seems to be a very sensitive tool for detecting an early increase in lung fluid volume. Non-invasive daily monitoring of LI with the EGM consistently reflects the changes in the dose of diuretics and responds to other treatment adjustments. The titration of the diuretic dose, according to LI values, may optimize patient stabilization in the early post-discharge period.

Citation: Lycholip E, Palevičiūtė E, Aamodt IT, Hellesø R, Lie I, Strömberg A, Jaarsma T, Čelutkienė J. Non-invasive home lung impedance monitoring in early post-acute heart failure discharge: Three case reports. *World J Clin Cases* 2019; 7(8): 951-960
URL: https://www.wjgnet.com/2307-8960/full/v7/i8/951.htm
DOI: https://dx.doi.org/10.12998/wjcc.v7.i8.951

INTRODUCTION

Hospital readmissions are a challenge in the care of heart failure (HF) patients. Readmissions are stressful for patients and families and, at the same time, might have financial consequences for health care organizations. The Hospital Readmissions Reduction Program was recently established in the United States. This program involved a public reporting of hospitals' 30-d risk-standardized readmission rates and applied financial penalties for hospitals with higher readmissions. The results of such a health care policy show that focusing mainly on the financial part of health care may significantly worsen patient care and outcomes[1,2]. In the first 30 d, the patients seem to be most vulnerable for rehospitalization; therefore, extra attention during this time period is warranted.

The impedance-HF trial revealed that the use of lung impedance (LI) measurements for the guidance of the preemptive treatment of patients with chronic HF reduced all-cause and HF hospitalizations by 39% and 55%, respectively[3]. In that study, measurements of LI were done using the highly sensitive, non-invasive device edema guard monitor (EGM). The EGM is based on an algorithm calculating the chest wall impedance, which is the preponderant component of the total electrical thoracic impedance. The subtraction of the chest wall impedance from the latter yields the net LI, which is the impedance of interest. Decreasing LI values represent the increase of lung fluid[1]. In previous reports, EGM was used only in the hospital or during regular outpatient clinic visits. Since EGM seems to be very sensitive to evolving pulmonary congestion, we hypothesized that it could be an accurate tool for the cautious titration of the doses of medicines, especially diuretics, ensuring a smooth and swift transition to follow-up care[3,4].

We present a case series of three patients after an episode of acute heart failure

(AHF), who had autonomously performed daily home LI measurements using the EGM during a 1-month follow up period. The aim of this case series is to demonstrate the potential additive role of non-invasive LI monitoring with EGM in patient stabilization in the early post-discharge period.

The technique of LI measurements and patient monitoring

The measurements were done with the help of the patients' caregivers once every day at the same time, attaching three EGM electrodes on the front and three EGM electrodes on back side of the chest wall, repeating the measurements 3 times (Figure 1). The LI values were being daily reported to a HF nurse via phone call or SMS, along with arterial blood pressure (BP), heart rate (HR) and body weight. Two patients performed all 30 measurements (100%) and one 29 d out of 30 (96.7%). Echocardiography and laboratory tests were performed before discharge and 1 month later.

CASE SERIES PRESENTATION

We present three patients suffering from ischemic HF with a reduced ejection fraction, who were urgently hospitalized because of signs and symptoms of decompensation.

Chief complaints

At admission patients complained of progressing AHF symptoms: dyspnea at mild physical exertion or at rest, fatigue, palpitations and dizziness.

History of present illness

All patients had a history of chronic ischemic HF with a reduced ejection fraction for several years.

History of past illness

Patients' past illnesses are shown in Table 1.

Personal and family history

Patients' demographic characteristics are presented in Table 1; family history was unremarkable.

Physical examination upon admission

At admission physical examination of the patients revealed normal BP, tachycardia, leg edema, fine crackles in the lungs. In Patient 2 several paroxysms of ventricular tachycardia were seen on electrocardiogram, led by cold sweat, extreme weakness and decrease of BP.

Laboratory examinations

Laboratory tests parameters are summarized in Table 2.

Imaging examinations

Echocardiographic parameters are shown in Table 2.

FINAL DIAGNOSIS

Based on clinical symptoms, signs and objective findings, acute decompensated HF was diagnosed in all patients.

TREATMENT

During hospitalization, patients were treated medically according to the ESC guidelines (Table 2). In Patient 2, several paroxysms of ventricular tachycardia were documented with a subsequent implantation of a biventricular defibrillator; Patient 3 was additionally treated with an implantation of drug-eluting stents in the left main and 2 other coronary arteries. Given the severe systolic dysfunction, mitral regurgitation, pulmonary hypertension and anticipated long duration of stenting, coronary intervention in Patient 3 was protected with extracorporeal membrane oxygenation. The dynamics of laboratory, echocardiographic parameters, LI, weight and discharge HF medications are presented in Table 2.

During the course of 30 d follow-up in all three patients, the dosages of medications were adjusted remotely with telephone calls or during four unplanned visits to the

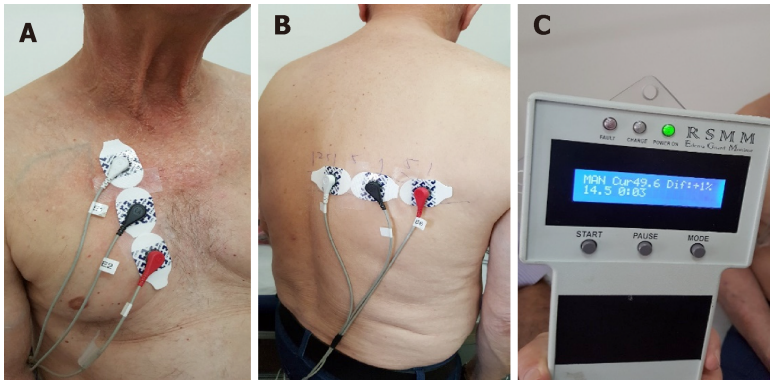

Figure 1 The technique of lung impedance measurements. A: Three electrodes were placed vertically on the front right side of the chest, 4.5 cm from the midline of the sternum with the upper electrode attached precisely under the clavicle; B: Another set of 3 electrodes was placed on the back along the horizontal line crossing the low edge of the right scapula, with the most leftward electrode placed at the crossing point of the horizontal line with the spine; C: The LI measurement result was displayed as a number on the screen.

outpatient department.

OUTCOME AND FOLLOW-UP

The patients were asked to come for additional assessments due to deteriorating symptoms, and for laboratory assessments when an electrolyte imbalance or a worsening renal function were suspected. All patients were discharged in a better functional status, but they still remained in functional class III per the New York Heart Association classification.

Case 1: The dependence of LI values on diuretic intake

Torasemide 50 mg was prescribed in Patient 1 every other day during the first week. There were 5 d when the patient did not take torasemide at all. Figure 1 illustrates the high dependence of the LI value on the use of a diuretic: each missed diuretic dose has caused the mean drop of LI value by 9 points, or 9.5% (maximal LI value was 97.8 Ω, minimal 82.6 Ω). The concomitant fluctuation of the patient's weight was negligible, ranging between 0 and 500 g, mostly decreasing (Figure 2).

Case 2: The adjustment of treatment in relation to the LI measurement

For Patient 2, the decrease of LI by -9% and -18%, compared with the initial LI, was twice treated by increasing the dose of torasemide from 50 to 100 mg daily. During the follow-up period, the Patient 2's weight fluctuated between 103.3 to 105.7 kg. In 4 d, when LI had decreased the most, the patient's weight increased by 200 g (0.2%) averagely, as compared with the previous day (Figure 3).

Case 3: Dehydration and congestion reflected by LI changes

In Patient 3, the LI value at discharge was 101.8 Ω, while during the next 3 d, it was high and still increasing (101- > 112- > 117Ω; +15%), pointing to decreasing lung fluid, yet the patient felt poorly. The patient reported a shortness of breath at rest and during night. On the 4th d, the patient was invited to an unscheduled cardiologist visit; acute renal failure with hyperkalemia and hypochloremia were diagnosed. The patient was readmitted for 3 d and treated with intravenous fluid and electrolyte infusion. An acute kidney injury was likely associated with contrast-induced damage after the complex percutaneous coronary procedure. Subsequently, during a three-day period (from the 17th to the 20th of the month), Patient 3 gained 800 g in weight, felt increased dyspnea on the 20th and 21st d in parallel with a decrease of LI. The negative dynamics of NT-proBNP on the 30th d were concordant with a gradual progressive decline of LI during the follow-up (Figure 4).

The correlation between weight changes and LI decrease

In Patient 1 and Patient 3, clinically relevant inverse correlations (a decrease of LI and an increase in weight) were found. LI had decreased 1 d before the increase of weight of Patient 1 with a cross-correlation coefficient equal to -0.738 ($P < 0.001$); in Patient 3, LI and weight has had the maximum cross-correlation at the same day with a coefficient of -0.830 ($P < 0.001$).

Table 1 Patients' demographics, medical history and length of hospital stay

	Patient 1	Patient 2	Patient 3
Age	66	62	83
Gender	Male	Male	Female
Medical history			
Arterial hypertension	+	+	+
Kidney disease	+	+	+
Myocardial infarction	+	+	+
Revascularization	+	+	+
Atrial fibrillation	-	+	-
Implanted devices	Biventricular pacemaker	Biventricular defibrillator	-
Length of stay (d)	6	17	15

In the course of a 30 d-follow-up, the dosages of medications were adjusted remotely via telephone calls reacting to the changes in symptoms, BP, HR or LI in all three patients. The patients were asked to come for four unplanned visits to the outpatient department when the symptoms had been deteriorating, LI had decreased but an electrolyte imbalance or a worsening renal function had been concomitantly suspected. Among other clinical parameters, the values of LI were the main triggers for adjusting treatment, especially for the dosage of diuretics (Table 3).

DISCUSSION

A variety of tools that quantify changes in lung fluid content have been evaluated to aid in the early detection of impending HF exacerbation, but in clinical practice, the prediction of pulmonary congestion is still a challenge. Invasive hemodynamic monitoring of PA pressure using a permanently implanted pressure sensor and the titration of diuretics according to pressure values have been reported to decrease hospitalizations for acute HF during 6 mo[5]. Monitoring of LI is also possible through the use of OptiVol feature and implanted cardioverter defibrillator or biventricular pacemaker.Although adding OptiVol alerts to HF management in observational studies was shown to improve patient prognosis as well, the positive predictive value for HF exacerbations was found to be only moderate[6,7].

The main disadavantages of these techniques are invasiveness, relatively high cost and inapplicability on a routine basis. Non-invasive transthoracic impedance (TI) measurements are associated with chest congestion, as fluid increases the electrical conductivity of the tissue[8,9]. The use of conventional electrical TI equipment for monitoring pulmonary congestion was found to be insufficiently sensitive and did not guarantee reliable monitoring of lung fluid content in the individual patient[10]. This may be explained by the fact that TI consists of the target net LI, which is only a small fraction of the overall TI, plus the high impedance of the chest walls.

In this case series, we report three patients with acute HF, who were monitored with the help of the EGM – a highly sensitive, non–invasive, LI measuring device. An arrangement of three electrodes on each side of the chest allows additional electrical circuits between electrodes, which enables calculation of the chest wall impedance and its subtraction from TI; this approach increases the sensitivity of the device to measure changes in lung fluid content by approximately 25 times[3]. As a result, preemptive treatment of an evolving pulmonary congestion can be initiated very early, a therapeutic policy that has proven its effectiveness in patients with ST elevation myocardial infarction[11]. Our experience with these patients suggests the EGM to be a practical tool that can be used for monitoring of lung fluid, especially while adjusting the dose of diuretics. We have applied a threshold of approximately 10% for reduction of LI (from the initial value measured on discharge) for therapy adjustment. This value is based on previous publications showing the LI dynamics during HF hospitalization and our own experience[12,13] The presented example of Patient 1 clearly illustrates a high dependence of the LI value on the use of diuretics, reflecting an increase in congestion following after the day when the medication was not taken.

Importantly, the measurement of LI with the EGM at home requires the help of a caregiver to attach electrodes to the chest. Though not technically difficult, this dependence on family members may be considered a disadvantage of the method. An

Table 2 The dynamics of laboratory tests, echocardiography parameters, lung impedance, weight and medications throughout 30 d

Characteristics	Patient 1		Patient 2		Patient 3	
	Discharge	After 30 d	Discharge	After 30 d	Discharge	After 30 d
Laboratory tests						
NT-proBNP (ng/L)	109	179	3485	2061	2927	5398
Troponin I (ng/L)	13.5	15.4	50.2	20.8	168.0	25.1
Potassium (mmol/L)	5.2	6.3	4.7	4.0	5.1	4.2
Sodium (mmol/L)	139	138	139	139	137	143
Chlorine (mmol/L)	100	95	101	98	98	103
Creatinine (mkmol/L)	133	282	96	103	111	118
eGFR (mL/min per 1.73 m^2)	48	19	73	68	40	37
Echocardiography						
LV diastolic diameter (mm)	59	56	76	76	71	71
LV ejection fraction 2D (%)	29	27	20	28	23	30
LV ejection fraction 3D (%)	26	29	19	25	35	23
Cardiac output (L/min) 2D	3.1	3.43	4.14	4.68	4.1	3.9
Cardiac output (L/min) 3D	1.7	2.2	4.4	4	4.3	2.2
LV stroke volume 2D (mL)	36	47	41	52	48	58
PCWP (by Nagueh, mmHg)	9.34	12.7	21.0	17	13.0	8.2
Global longitudinal 2D strain (%)	-7	-8.8	-6	-3.6	-6.2	-7.7
Right ventricular diameter (cm)	3.3	3.8	5.2	5.3	2.3	1.9
RV S′ (cm/s)	9	11	7	10	15	14
TAPSE (cm)	1.7	1.9	0.6	1.6	2.1	1.9
RV FAC (%)	32.3	35	16.6	28.8	49.6	74.8
Lung impedance (Ω)	88.6	93.0	107.9	97.1	101.8	88.1
Weight (kg)	80	81.3	104	105	60.0	61.8
Medicatio						
Percentage of target dose of beta-blocker	25%	50 %	100 %	100%	25%	25%
Percentage of target dose of ACEI	100%	100%	12.5%	25%	50%	25%
Percentage of target dose of Spironolactone	50%	-	50%	100%	100%	-
Torasemide daily dose (mg)	50 mg (e.s.d.)	10 mg	50 mg	100 mg	25 mg	10 mg

NT-proBNP: N-terminal pro B-type natriuretic peptide; eGFR: Estimated glomerular filtration rate; LV: Left ventricular; PCWP: Pulmonary capillary wedge pressure; RV S′: Systolic velocity of tricuspid valve; TAPSE: Tricuspid annular plain systolic excursion; FAC: Fractional area change; ACEI: Angiotensin-converting enzyme inhibitor.

essential aspect is the availability of healthcare professional who daily accepts and reacts to LI values. Considering data on reduction of HF hospitalizations using this kind of congestion monitoring[3], financial savings with EGM may be highly significant due to the relatively low cost of the device and regular service.

Significant fluctuations of LI were noticed in all these cases; moreover, the LI change was the most important trigger for medication adjustment compared to standard monitoring variables, such as BP, HR, symptoms and markers of renal function. Though the monitoring of weight changes caused by fluid retention is routinely recommended for HF patients[13], several studies showed that many episodes of worsening HF did not appear to be associated with weight gain. For example, in a case-control study 54% of patients hospitalized due to AHF gained ≤ 1 kg during the month prior to admission[14]. This suggests that volume overload incompletely characterizes the pathophysiology of AHF and redistribution of volume may also contribute to the development of signs and symptoms of congestion[15,16].

These cases illustrate that LI measurements may represent a more sensitive method for the evaluation of fluid retention compared to weight and subjective symptoms. In two out of these three patients, we found a clinically and statistically significant correlation (lag -1; 0) of weight increase with the drop of LI. It was shown previously that the sensitivity of LI for HF hospitalization and the ambulatory adjustment of diuretics was twice as high as of body weight (83.3% *vs* 43.9%), and the unexplained detection rate per patient-year was 1.6 *vs* 4.8, respectively[17]. The case of Patient 3 illustrates that the LI measurements can sometimes even reflect excessive

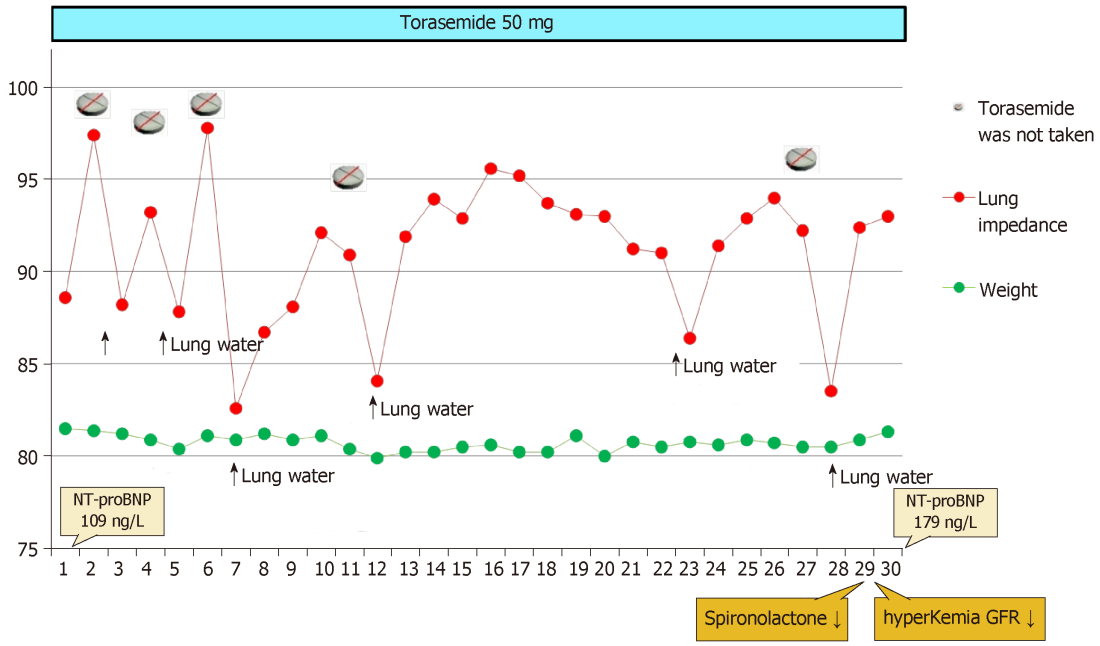

Figure 2 The dynamics of lung impedance, weight and diuretic dose for Patient 1. The N-terminal pro B-type natriuretic peptide level was not high at the day of discharge, but the patient had clear signs and symptoms of congestive heart failure (HF) on admission (shortness of breath, bilateral rales in the lungs, leg edema, poor left ventricular function on echocardiography). HF with reduced ejection fraction developed after an acute myocardial infarction more than 4 years ago; then, his BNP was 2611 ng/L, but 2 years after, it had reduced to the level of 200 ng/L. NT-proBNP: N-terminal pro B-type natriuretic peptide; GFR: Glomerular filtration rate.

dehydration, assisting in the detection of not only an under- but also over-dosage of diuretics.

CONCLUSION

Our first experience with taking LI measurements using the EGM implies the high sensitivity and potential clinical utility of this tool consistently reflected the changes in the dose of diuretics. Non-invasive daily monitoring of LI may become an important component of successful transitions from acute to stable phases of HF, but more clinical experience is needed in order to find the best algorithms for the reactions of health care professionals to different LI changes.

Table 3 Triggers for treatment adjustments reacting to clinical and monitoring parameters

Trigger	Intervention	Frequency of intervention, times
Symptoms (weakness)	Hospitalization because of revealed renal failure, hyperkalemia	1
High HR	Increasing the dose of beta-blockers	3
	Administration of Ivabradine	1
Uncontrolled BP	Increasing the dose of ACE inhibitors	1
Electrolyte imbalance	Increasing the dose of Spironolactone and decreasing the dose of Torasemide	1
LI decrease	Increasing the dose of beta-blockers and Spironolactone	1
	Increasing the dose of ACE inhibitors and beta-blockers	1
	Increasing the dose of Torasemide	5
Weight gain	-	0

HR: Heart rate; BP: Blood pressure; LI: Lung impedance; ACE: Angiotensin-converting enzyme.

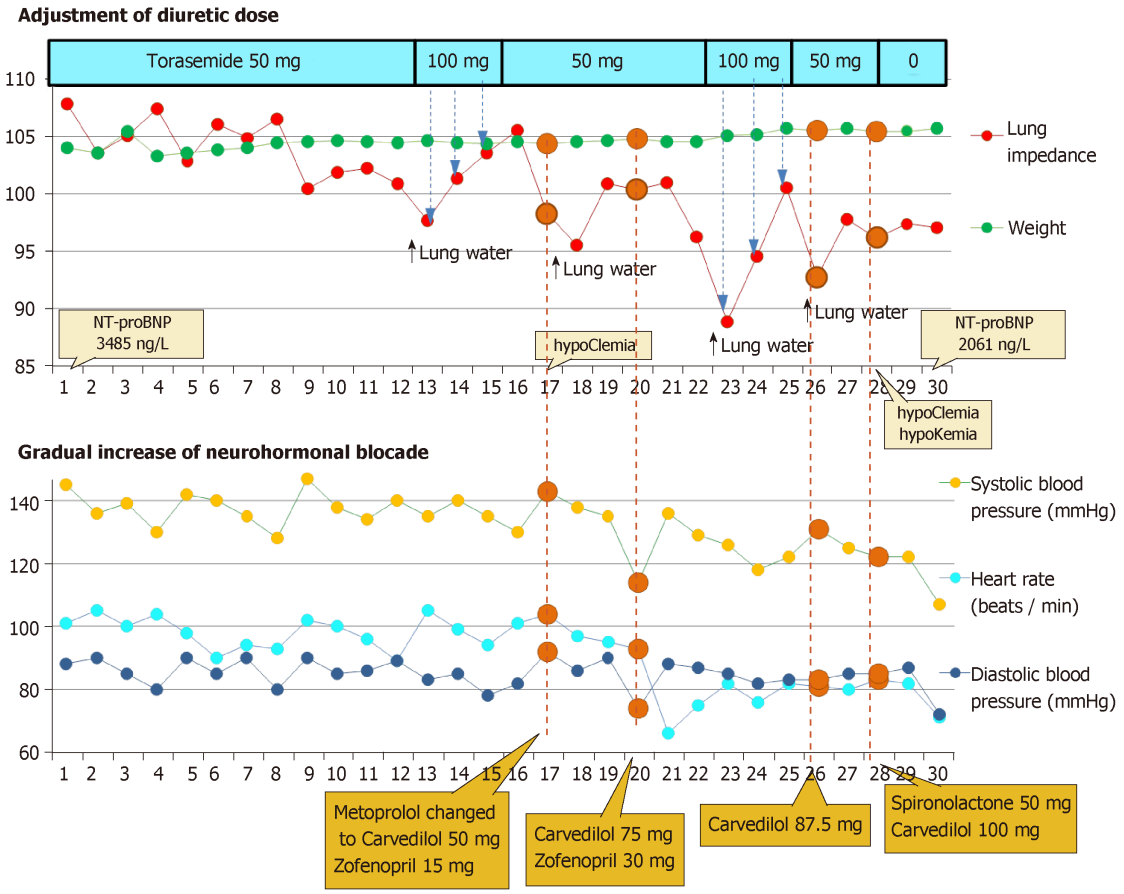

Figure 3 The dynamics of lung congestion, weight, hemodynamics and medication dosage for Patient 2. NT-proBNP: N-terminal pro B-type natriuretic peptide.

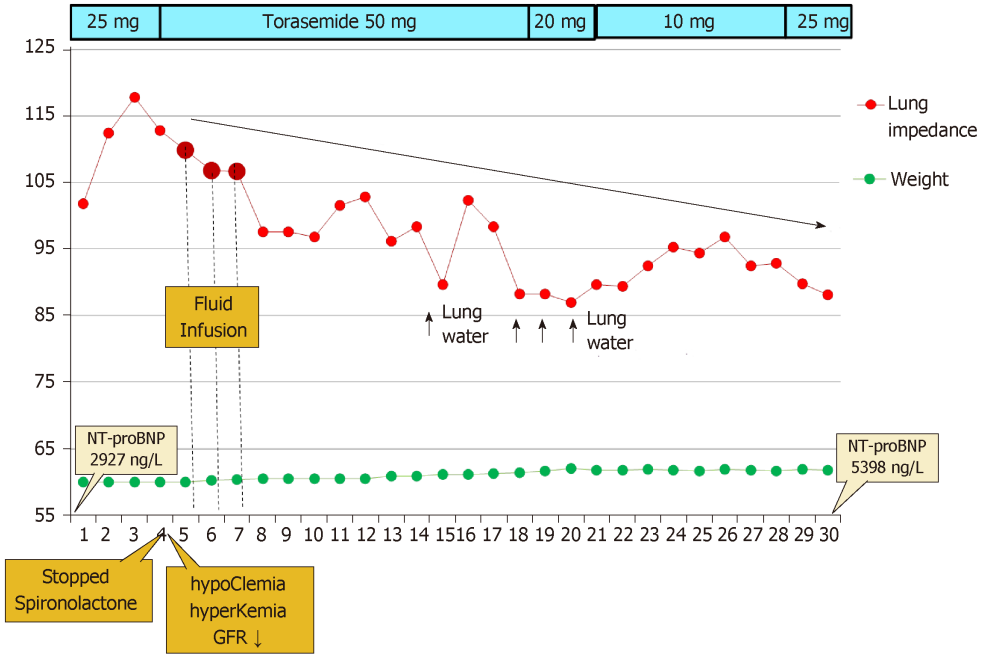

Figure 4 The dynamics of lung congestion, weight and diuretic dose for Patient 3 (in this figure, the legend is different than the others (LI). NT-proBNP: N-terminal pro B-type natriuretic peptide; GFR: Glomerular filtration rate.

REFERENCES

1 **Gupta A**, Allen LA, Bhatt DL, Cox M, DeVore AD, Heidenreich PA, Hernandez AF, Peterson ED, Matsouaka RA, Yancy CW, Fonarow GC. Association of the Hospital Readmissions Reduction Program Implementation With Readmission and Mortality Outcomes in Heart Failure. *JAMA Cardiol* 2018; **3**: 44-53 [PMID: 29128869 DOI: 10.1001/jamacardio.2017.4265]

2 **Čerlinskaitė K**, Hollinger A, Mebazaa A, Cinotti R. Finding the balance between costs and quality in heart failure: a global challenge. *Eur J Heart Fail* 2018; **20**: 1175-1178 [PMID: 29673007 DOI: 10.1002/ejhf.1195]

3 **Shochat MK**, Shotan A, Blondheim DS, Kazatsker M, Dahan I, Asif A, Rozenman Y, Kleiner I, Weinstein JM, Frimerman A, Vasilenko L, Meisel SR. Non-Invasive Lung IMPEDANCE-Guided Preemptive Treatment in Chronic Heart Failure Patients: A Randomized Controlled Trial (IMPEDANCE-HF Trial). *J Card Fail* 2016; **22**: 713-722 [PMID: 27058408 DOI: 10.1016/j.cardfail.2016.03.015]

4 **Shochat M**, Shotan A, Blondheim DS, Kazatsker M, Dahan I, Asif A, Shochat I, Frimerman A, Rozenman Y, Meisel SR. Derivation of baseline lung impedance in chronic heart failure patients: use for monitoring pulmonary congestion and predicting admissions for decompensation. *J Clin Monit Comput* 2015; **29**: 341-349 [PMID: 25193676 DOI: 10.1007/s10877-014-9610-6]

5 **Abraham WT**, Adamson PB, Bourge RC, Aaron MF, Costanzo MR, Stevenson LW, Strickland W, Neelagaru S, Raval N, Krueger S, Weiner S, Shavelle D, Jeffries B, Yadav JS; CHAMPION Trial Study Group. Wireless pulmonary artery haemodynamic monitoring in chronic heart failure: a randomised controlled trial. *Lancet* 2011; **377**: 658-666 [PMID: 21315441 DOI: 10.1016/S0140-6736(11)60101-3]

6 **Catanzariti D**, Lunati M, Landolina M, Zanotto G, Lonardi G, Iacopino S, Oliva F, Perego GB, Varbaro A, Denaro A, Valsecchi S, Vergara G; Italian Clinical Service Optivol-CRT Group. Monitoring intrathoracic impedance with an implantable defibrillator reduces hospitalizations in patients with heart failure. *Pacing Clin Electrophysiol* 2009; **32**: 363-370 [PMID: 19272067 DOI: 10.1111/j.1540-8159.2008.02245.x]

7 **Conraads VM**, Tavazzi L, Santini M, Oliva F, Gerritse B, Yu CM, Cowie MR. Sensitivity and positive predictive value of implantable intrathoracic impedance monitoring as a predictor of heart failure hospitalizations: the SENSE-HF trial. *Eur Heart J* 2011; **32**: 2266-2273 [PMID: 21362703 DOI: 10.1093/eurheartj/ehr050]

8 **Larsen FF**, Mogensen L, Tedner B. Transthoracic electrical impedance at 1 and 100 kHz--a means for separating thoracic fluid compartments? *Clin Physiol* 1987; **7**: 105-113 [PMID: 3568579 DOI: 10.1111/j.1475-097X.1987.tb00152.x]

9 **Cuba-Gyllensten I**, Gastelurrutia P, Riistama J, Aarts R, Nuñez J, Lupon J, Bayes-Genis A. A novel wearable vest for tracking pulmonary congestion in acutely decompensated heart failure. *Int J Cardiol* 2014; **177**: 199-201 [PMID: 25499378 DOI: 10.1016/j.ijcard.2014.09.041]

10 **Packer M**, Abraham WT, Mehra MR, Yancy CW, Lawless CE, Mitchell JE, Smart FW, Bijou R, O'Connor CM, Massie BM, Pina IL, Greenberg BH, Young JB, Fishbein DP, Hauptman PJ, Bourge RC, Strobeck JE, Murali S, Schocken D, Teerlink JR, Levy WC, Trupp RJ, Silver MA; Prospective Evaluation and Identification of Cardiac Decompensation by ICG Test (PREDICT) Study Investigators and Coordinators. Utility of impedance cardiography for the identification of short-term risk of clinical decompensation in stable patients with chronic heart failure. *J Am Coll Cardiol* 2006; **47**: 2245-2252 [PMID: 16750691 DOI: 10.1016/j.jacc.2005.12.071]

11 **Shochat M**, Shotan A, Blondheim DS, Kazatsker M, Dahan I, Asif A, Shochat I, Rabinovich P, Rozenman

Y, Meisel SR. Usefulness of lung impedance-guided pre-emptive therapy to prevent pulmonary edema during ST-elevation myocardial infarction and to improve long-term outcomes. *Am J Cardiol* 2012; **110**: 190-196 [PMID: 22482863 DOI: 10.1016/j.amjcard.2012.03.009]

12 **Lycholip E**, Čelutkienė J. Doctoral dissertation: Telemonitoring technologies for heart failure patients: opinions of professionals, patient-reported outcomes and measurements of lung impedance. 2018: 46-49. Available from: http://www.lmb.lt/nr-36-spalio-1-7-d/

13 **Ponikowski P**, Voors AA, Anker SD, Bueno H, Cleland JG, Coats AJ, Falk V, González-Juanatey JR, Harjola VP, Jankowska EA, Jessup M, Linde C, Nihoyannopoulos P, Parissis JT, Pieske B, Riley JP, Rosano GM, Ruilope LM, Ruschitzka F, Rutten FH, van der Meer P; Authors/Task Force Members; Document Reviewers. 2016 ESC Guidelines for the diagnosis and treatment of acute and chronic heart failure: The Task Force for the diagnosis and treatment of acute and chronic heart failure of the European Society of Cardiology (ESC). Developed with the special contribution of the Heart Failure Association (HFA) of the ESC. *Eur J Heart Fail* 2016; **18**: 891-975 [PMID: 27207191 DOI: 10.1002/ejhf.592]

14 **Mullens W**, Damman K, Harjola VP, Mebazaa A, Brunner-La Rocca HP, Martens P, Testani JM, Tang WHW, Orso F, Rossignol P, Metra M, Filippatos G, Seferovic PM, Ruschitzka F, Coats AJ. The use of diuretics in heart failure with congestion - a position statement from the Heart Failure Association of the European Society of Cardiology. *Eur J Heart Fail* 2019; **21**: 137-155 [PMID: 30600580 DOI: 10.1002/ejhf.1369]

15 **Dovancescu S**, Pellicori P, Mabote T, Torabi A, Clark AL, Cleland JGF. The effects of short-term omission of daily medication on the pathophysiology of heart failure. *Eur J Heart Fail* 2017; **19**: 643-649 [PMID: 28295907 DOI: 10.1002/ejhf.748]

16 **Chaudhry SI**, Wang Y, Concato J, Gill TM, Krumholz HM. Patterns of weight change preceding hospitalization for heart failure. *Circulation* 2007; **116**: 1549-1554 [PMID: 17846286 DOI: 10.1161/CIRCULATIONAHA.107.690768]

17 **Al-Chekakie MO**, Bao H, Jones PW, Stein KM, Marzec L, Varosy PD, Masoudi FA, Curtis JP, Akar JG. Addition of Blood Pressure and Weight Transmissions to Standard Remote Monitoring of Implantable Defibrillators and its Association with Mortality and Rehospitalization. *Circ Cardiovasc Qual Outcomes* 2017; **10** [PMID: 28506978 DOI: 10.1161/CIRCOUTCOMES.116.003087]

World Journal of Clinical Cases

Submit a Manuscript: https://www.f6publishing.com

World J Clin Cases 2019 April 26; 7(8): 961-971

DOI: 10.12998/wjcc.v7.i8.961

ISSN 2307-8960 (online)

CASE REPORT

Bilateral adrenocortical adenomas causing adrenocorticotropic hormone-independent Cushing's syndrome: A case report and review of the literature

Yu-Lin Gu, Wei-Jun Gu, Jing-Tao Dou, Zhao-Hui Lv, Jie Li, Sai-Chun Zhang, Guo-Qing Yang, Qing-Hua Guo, Jian-Ming Ba, Li Zang, Nan Jin, Jin Du, Yu Pei, Yi-Ming Mu

ORCID number: Yu-Lin Gu (0000-0002-0795-8268); Wei-Jun Gu (0000-0001-8690-645X); Jing-Tao Dou (0000-0002-7079-8674); Zhao-Hui Lu (0000-0002-2291-4773); Jie Li (0000-0003-1786-0245); Sai-Chun Zhang (0000-0001-9668-2971); Guo-Qing Yang (0000-0002-7896-6572); Qing-Hua Guo (0000-0003-2840-2354); Jian-Ming Ba (0000-0002-5019-4064); Li Zang (0000-0001-9969-8039); Nan Jin (0000-0002-8595-449X); Jin Du (0000-0001-8387-9724); Yu Pei (0000-0002-3269-9835); Yi-Ming Mu (0000-0002-3344-3540).

Author contributions: Gu WJ treated the patient, collected the data, and reviewed the manuscript; Gu YL analyzed the data and drafted the manuscript; Zhang SC was involved in nursing care of the patient and made substantial contributions to case report conception and design, and data acquisition, analysis, and interpretation; LJ performed the histological examination; Lv ZH, Yang GQ, Guo QH, Ba JM, Zang L, Jin N, Du J, and Pei Y made substantial contributions to case report conception and design and data acquisition, analysis, and interpretation, and revised the manuscript critically for important intellectual content; Dou JT and Mu YM were the superior advisors, and they gave final approval of the version to be published, and agreed to be accountable for all aspects of the work in ensuring that questions related to the accuracy or integrity

Yu-Lin Gu, Wei-Jun Gu, Jing-Tao Dou, Zhao-Hui Lv, Sai-Chun Zhang, Guo-Qing Yang, Qing-Hua Guo, Jian-Ming Ba, Li Zang, Nan Jin, Jin Du, Yu Pei, Yi-Ming Mu, Department of Endocrinology, Chinese People's Liberation Army General Hospital, Beijing 100853, China

Jie Li, Department of Pathology, Chinese People's Liberation Army General Hospital, Beijing 100853, China

Corresponding author: Wei-Jun Gu, MD, PhD, Assistant Professor, Department of Endocrinology, Chinese People's Liberation Army General Hospital, Beijing 100853, China.
guweijun301@163.com
Telephone: +86-010-55499301
Fax: +86-010-68168631

Abstract

BACKGROUND

Adrenocorticotropic hormone (ACTH)-independent Cushing's syndrome (CS) is mostly due to unilateral tumors, with bilateral tumors rarely reported. Its common causes include primary pigmented nodular adrenocortical disease, ACTH-independent macronodular adrenal hyperplasia, and bilateral adrenocortical adenomas (BAAs) or carcinomas. BAAs causing ACTH-independent CS are rare; up to now, fewer than 40 BAA cases have been reported. The accurate diagnosis and evaluation of BAAs are critical for determining optimal treatment options. Adrenal vein sampling (AVS) is a good way to diagnose ACTH-independent CS.

CASE SUMMARY

A 31-year-old woman had a typical appearance of CS. The oral glucose tolerance test showed impaired glucose tolerance and obviously increased insulin and C-peptide levels. Her baseline serum cortisol and urine free cortisol were elevated and did not show either a circadian rhythm or suppression with dexamethasone administration. The peripheral 1-deamino-8-D-arginine-vasopressin (DDVAP) stimulation test showed a delay of the peak level, which was 1.05 times as high as the baseline level. Bilateral AVS results suggested the possibility of BAAs. Abdominal computed tomography showed bilateral adrenal adenomas with atrophic adrenal glands (right: 3.1 cm × 2.0 cm × 1.9 cm; left: 2.2 cm × 1.9 cm × 2.1 cm). Magnetic resonance imaging of the pituitary gland demonstrated normal findings. A left adenomectomy by retroperitoneoscopy was performed first,

of any part of the work are appropriately investigated and resolved. All authors read and approved the final manuscript.

Informed consent statement: All study participants, or their legal guardian, provided written informed consent prior to study enrollment. And written informed consent was obtained from the patient for publication of this report and any accompanying images. The study was reviewed and approved by the Chinese People's Liberation Army General Hospital Institutional Review Board.

Conflict-of-interest statement: The authors declare that they have no conflicts of interest.

CARE Checklist (2016) statement: The authors have read the CARE Checklist (2016), and the manuscript was prepared and revised according to the CARE Checklist (2016).

Manuscript source: Unsolicited manuscript

Received: December 2, 2018
Peer-review started: December 3, 2018
First decision: January 26, 2018
Revised: January 31, 2018
Accepted: February 26, 2019
Article in press: February 26, 2019
Published online: April 26, 2019

P-Reviewer: Lalli E, Aseni P
S-Editor: Dou Y
L-Editor: Wang TQ
E-Editor: Wu YXJ

followed by resection of the right-side adrenal mass 3 mo later. Biopsy results of both adenomas showed cortical tumors. Evaluations of ACTH and cortisol showed a significant decrease after left adenomectomy but could still not be suppressed, and the circadian rhythm was absent. Following bilateral adenomectomy, this patient has been administered with prednisone until now, all of her symptoms were alleviated, and she had normal blood pressure without edema in either of her lower extremities.

CONCLUSION
BAAs causing ACTH-independent CS are rare. AVS is of great significance for obtaining information on the functional state of BAAs before surgery.

Key words: Bilateral adrenocortical adenomas; Adrenocorticotropic hormone-independent Cushing's syndrome; Adrenal venous sampling; Case report

Core tip: Bilateral adrenocortical adenomas (BAAs) causing adrenocorticotropic hormone (ACTH)-independent Cushing syndrome (CS) are rare; up to now, fewer than 40 BAA cases have been reported. The accurate diagnosis and evaluation of BAAs are critical for determining optimal treatment options. We report a rare case of BAAs causing ACTH-independent CS, which was diagnosed by adrenal vein sampling (AVS) and computed tomography before surgery. The patient underwent a bilateral retroperitoneoscopy adenomectomy and glucocorticoid replacement therapy. Our case indicates that AVS is of great significance for obtaining information on the functional state of BAAs before surgery.

Citation: Gu YL, Gu WJ, Dou JT, Lv ZH, Li J, Zhang SC, Yang GQ, Guo QH, Ba JM, Zang L, Jin N, Du J, Pei Y, Mu YM. Bilateral adrenocortical adenomas causing adrenocorticotropic hormone-independent Cushing's syndrome: A case report and review of the literature. *World J Clin Cases* 2019; 7(8): 961-971
URL: https://www.wjgnet.com/2307-8960/full/v7/i8/961.htm
DOI: https://dx.doi.org/10.12998/wjcc.v7.i8.961

INTRODUCTION

Inappropriate exposure to excessive concentrations of free glucocorticoids results in Cushing's syndrome (CS)[1], with the clinical features of centripetal obesity, moon face, hirsutism, plethora, and striae, among others. The excess of glucocorticoid comes from endogenous or exogenous sources[2]. Endogenous causes of CS are rare. The incidence rates of CS are estimated to be 2 to 3 cases per million people per year in Europe and 10-15 cases per million people per year in America[3]. Some studies have revealed that subclinical hypercortisolism is significantly more possible in patients with bilateral incidentalomas[4]. Endogenous CS can be divided into adrenocorticotropic hormone (ACTH)-independent and -dependent forms. ACTH-independent CS is mostly due to unilateral tumors, with bilateral tumors rarely reported. Its main causes include ACTH-independent macronodular adrenal hyperplasia (AIMAH), primary pigmented nodular adrenocortical disease (PPNAD), and bilateral adrenocortical adenomas (BAAs) or carcinomas[5,6]. BAAs causing ACTH-independent CS are rare; up to now, fewer than 40 BAA cases have been reported. The accurate diagnosis and evaluation of BAAs are critical for determining optimal treatment options. Herein, we report a Chinese patient with BAAs, who was diagnosed with ACTH-independent CS by adrenal vein sampling (AVS) and computed tomography (CT).

CASE PRESENTATION

Chief complaints

A 31-year-old woman, who complained of gaining body weight, red face, moon face,

bruising, and menstrual irregularity for two years, presented to our outpatient department.

History of present illness

The patient's symptoms started two years ago with weight gain, red face, moon face, bruising, and menstrual irregularity.

History of past illness

She was diagnosed with hypertension a month ago and was medicated with nifedipine delayed-release tablets (II) 40 mg twice a day. Her family history was negative.

Physical examination

Physical examination revealed centripetal obesity, moon face, buffalo hump, thin skin, hirsutism, acne, striae on her abdomen, arms, and legs, and edema of both lower extremities. The height of this patient was 159 cm, and her body weight was 73.5 kg. Her blood pressure was 130/100 mmHg, with a pulse of 84 beats per minute.

Laboratory examinations

Her blood counts were within the normal limits, and she had no serum electrolytes disorders. The biochemical data showed dyslipidemia. The oral glucose tolerance test showed impaired glucose tolerance (IGT) and obviously increased insulin and C-peptide levels. The endocrinological data showed elevated cortisol (761.0 nmol/L) and 24-h urine free cortisol (UFC) (1650.7 nmol/L) and the absence of a circadian rhythm and a non-suppression response to dexamethasone (dexamethasone 0.5 mg every 6 h for 2 d and 2 mg every 6 h for 2 d) administration (Table 1).

Imaging examinations

Abdominal CT showed bilateral adrenal adenomas with atrophic adrenal glands (right: 3.1 cm × 2.0 cm × 1.9 cm; left: 2.2 cm × 1.9 cm × 2.1 cm), which were enhanced homogeneously with contrast material (Figure 1). A magnetic resonance imaging (MRI) scan of the pituitary gland demonstrated normal findings.

Further diagnostic work-up

The patient was further evaluated with 1-deamino-8-D-arginine-vasopressin (DDVAP). The peripheral DDVAP stimulation test showed a baseline ACTH level of 6.9 pmol/L, and ACTH reached a peak level (7.26 pmol/L) at 90 min after stimulation, which was 1.05 times as high as the baseline level (Table 2). Then, we performed bilateral AVS to examine if the two adenomas were cortisol-secreting. Bilateral AVS results were as follows: the left-side adrenal vein (LAV)-to-peripheral vein (PV) cortisol gradient was 16.00; the right-side AV (RAV)-to-PV gradient was 8.29; and the ratio of the LAV cortisol-to-left side aldosterone (ALD) gradient to the RAV cortisol-to-right side ALD gradient was 1.23 (Table 3).

MULTIDISCIPLINARY EXPERT CONSULTATION

Jing-Tao Dou, MD, PhD, Professor and Chief, Department of Endocrinology, Chinese PLA General Hospital

It is important to know which side is functioning, which is hard to determine by imaging. We can do bilateral AVS to examine if the two adenomas are cortisol-secreting.

Ju-Ming Lu, MD, PhD, Professor and Chief, Department of Endocrinology, Chinese PLA General Hospital

BAAs often: (A) occur in mid-aged females; (B) have varying clinical symptoms; (C) are a kind of ACTH-independent CS, with hypercortisolism, absence of serum cortisol diurnal rhythm, and elevated UFC, though ACTH is in the normal range; (D) are 2.0-3.5 cm in diameter on CT; and (F) have normal finding in MRI of the pituitary. We should determine the source of ACTH, and testing the rhythm of ACTH-F is important.

Yong Song, MD, PhD, Assistant Professor, Department of Urology, Chinese PLA General Hospital

The patient should undergo surgical treatment twice separately after obtaining the result of bilateral AVS.

Table 1 Endocrinological study at different periods of bilateral adrenocortical adenomas

		Baseline			Low-dose dexam test	High-dose dexam test
		00:00 h	08:00 h	16:00 h		
Before the operation	ACTH (pmol/L)	4.26	4.13	3.62	3.51	4.1
	F (nmol/L)	606.42	761	618.08	579.34	689.18
	UFC (nmol/L)	1650.7	-	-	3073.5	2122.6
After unilateral operation	ACTH (pmol/L)	7.84	7.86	7.7	9.28	-
	F (nmol/L)	391.78	440.08	455.65	414.36	-
	UFC (nmol/L)	1024.9	-	-	1117	-
After bilateral operations	ACTH (pmol/L)	4.66	4.86	3.66	4.93	-
	F (nmol/L)	<25.7	<25.7	<25.7	<25.7	-
	UFC (nmol/L)	-	<25.7	-	-	-

Reference range: ACTH at 8 AM, <10.12 pmol/L; F at 8 AM, 198.7-797.5 nmol/L; 4 PM: 85.3-459.6 nmol/L; 0 AM: 0-165.7 nmol/L; UFC: 98.0-500.1 nmol/24 h; dexam: Dexamethasone; ACTH: Adrenocorticotropic hormone; F: Cortical; UFC: Urine free cortisol.

FINAL DIAGNOSIS

The final diagnosis was ACTH-independent CS and BAAs.

TREATMENT

A left adenomectomy by retroperitoneoscopy was performed on June 21, 2016. Irregular gray yellow tissue that measured 3.5 cm × 2.5 cm × 1 cm was observed on the left side. The cut surface was solid and golden yellow in color. Histologically, a single well-encapsulated adrenocortical tumor was observed in the adrenal gland. The Weiss score was 1. The immunohistochemistry results revealed MelanA(+), CgA(-), Syn(+), Ki-67(+2%), Inhibin-a(+), CK(-), and S-100(spotty+) (Figure 2A, 2B and Figure 3). Resection of the right-side adrenal mass was performed 3 mo later. The biopsy revealed nodular tissue on the right side measuring 2 cm × 1.8 cm × 1.5 cm. The cut surface was golden yellow in color. The Weiss score was 1. The immunohistochemistry results revealed MelanA(+), CgA(-), Syn(+), Ki-67(+2%), Inhibin-a(+), CK(-), S-100(spotty +) (Figure 2C, 2D and Figure 4).

OUTCOME AND FOLLOW-UP

Evaluations of ACTH and cortisol showed a significant decrease after the surgery. All of her symptoms were alleviated, and she had normal blood pressure and no edema in either of her lower extremities. She was administered with prednisone 20 mg once a day for half a month, which was then tapered to 15 mg once a day for a month and 5 mg twice a day, and finally 2.5 mg twice a day. The last follow-up was on June 5, 2017, at which point all of her symptoms and signs have been alleviated (Figure 5).

DISCUSSION

Our case was confirmed as ACTH independency based on: (1) Very low plasma ACTH with increased serum cortisol level; (2) Unresponsiveness to a high-dose dexamethasone suppression test; (3) Unresponsiveness to a DDVAP stimulation test; and (4) MRI scan of the pituitary gland demonstrated normal findings; however, CT showed bilateral adrenal adenomas with atrophic adrenal glands. According to the tests above, ACTH-independent CS was diagnosed. Cases of ACTH-independent CS associated with adrenocortical adenoma are secondary to unilateral adrenocortical adenomas in approximately 90% of cases[7]. In contrast, bilateral cortisol-secreting tumors are a rare cause of CS[8].

As we know, the possibilities of bilateral adrenal space-occupying lesion are mainly: (1) BAAs; (2) Carcinomas; (3) PPNAD; and (4) AIMAH. Markedly enlarged bilateral hyperplastic adrenal glands with multiple macronodules up to 5 cm in diameter are a characteristic histopathological feature of AIMAH[1]. This disorder may

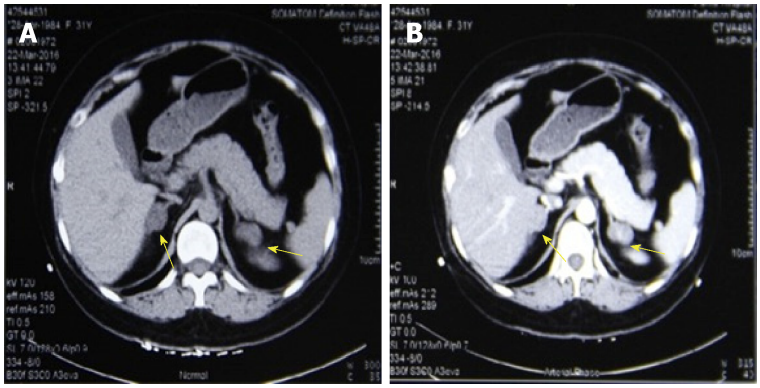

Figure 1 Abdominal computed tomography images. Abdominal computed tomography images show bilateral adrenal adenomas with atrophic adrenal glands. Arrows indicate tumors with a low density (right, 3.1 cm × 2.0 cm × 1.9 cm; left, 2.2 cm × 1.9 cm × 2.1 cm). Tumors are homogeneously enhanced in the presence of contrast material.

be associated with other receptors besides ACTH, which are expressed in the adrenal cortex ectopically, such as gastric inhibitory polypeptide, luteinizing hormone/human chorionic gonadotropin and others[9,10]. PPNAD is another bilateral adrenal hyperplastic disease; CT scan shows bilateral small discrete nodules between 2 and 5 mm in size without overall enlargement of the glands. The possible mechanism may be a novel mutation in the type lα regulatory subunit of the protein kinase A (*PRKAR1A*) gene: p.E17X (c.49G>T), which confirms that the diagnosis of PPNAD could be one component of Carney complex[11]. While carcinoma seems much more aggressive, with a heavier and larger mass, it is always complicated with severe hypertension, masculinization, hypokalemia, or alkalosis. On CT scan, the tumor is generally bigger than 5 cm in diameter, with heterogeneous enhancement with contrast agent[12]. BAAs were first reported by CHAPELL in 1963[13]. To the best of our knowledge, fewer than 40 BAAs cases have been reported. BAAs are the most significant feature of this case.

The mechanism of BAAs is unclear. Some studies have revealed that steroidogenic enzymes, such as P450scc, 3β-HSD, P450c21, P450c17, and P450c11, are intensely expressed in the compact cells of the adenoma, while their expression profiles are negative in the adjacent non-neoplastic cortex. At the same time, the histological features may differ between two adenomas[14,15]. It is difficult to distinguish between functioning or nonfunctioning adrenal cortical masses by the imaging characteristics on CT scanning[1]. AVS is a helpful method to distinguish between these conditions. The compound 6 beta-(131I)-iodomethyl-19-norcholesterol (NP-59) is another possible means for evaluating the function of an adenoma; however, NP-59 scintigraphy is never a common imaging modality in China. AVS provides important information concerning the laterality of excessive ALD, but it also has advantages compared with adrenal scintigraphy and CT in the diagnosis of CS and BAAs[16,17]. However, only a few cases have been reported with the use of AVS in the diagnosis of BAAs before surgery. According to the Mayo Clinic[16], AV-to-PV cortisol gradient greater than 6.5 is more likely to be a cortisol-secreting adenoma. In our case, the gradient of LAV-to-PV cortisol was 16, and the RAV-to-PV cortisol gradient was 8.2. The "ALD-corrected" high-side to low-side AV cortisol gradient was 2.3 or greater, which is consistent with autonomous cortisol secretion from predominantly one adrenal gland; a gradient of 2.0 or less indicates bilateral cortisol hypersecretion. The ratio of L/R of our patient was 1.23, less than 2.0. All of these pieces of evidence indicated that the hypersecretion of cortisol might originate from both adrenal glands. The first case of BAAs in China was reported in the medical literature by our team[18]. However, the AVS technique was not available at that time; therefore, we could not determine which side was functioning before the surgery.

Extirpation of the functioning adenoma is the optimal choice for bilateral CS adenomas[19]. AVS is a useful accessory examination before surgery to design a surgical plan that makes much more sense. Some authors believe that if AVS is unavailable, the larger of the two adenomas should be removed first, and then further management should be determined according to the postoperative hormone tests. However, at least 5 years of follow-up examinations is required, because the contralateral adrenal adenoma might have clinically significant endocrine function later[1,8]. Bilateral adenomas generally appear at the same time, but there has been a report of an adenoma appearing 9 years after the contralateral surgery[8]. In our case, the bilateral adenomas were both functioning; we resected the left one first because of

Table 2 The results of peripheral 1-deamino-8-D-arginine-vasopressin stimulation test

Time	ACTH (pmol/L)	F (nmol/L)
-15 min	6.88	640.24
0 min	6.97	624.03
15 min	6.7	637.87
30 min	6.59	590.82
45 min	6.59	625.47
60 min	7.19	598.56
90 min	7.26	524.71
120 min	6.68	577.39

Normally, adrenocorticotropic hormone (ACTH) peaks between 15 min and 30 min after the infusion of DDAVP, while this patient had delayed peaking. Cushing disease is suspected if the peak level of ACTH is over 1.5 times much more than the baseline level. We can definitely diagnose it as Cushing disease if it is over 3 times. This patient's ratio was 1.05, therefore it is not Cushing disease[30]. ACTH: Adrenocorticotropic hormone; F: Cortisol.

its thriving function on AVS. Three months later, we removed the right adenoma. When bilateral adrenal tumors are considered, a unilateral or bilateral adenoma resection is a better choice if functional adrenal tissue can be preserved to avoid acute adrenal insufficiency or lifelong steroid replacement. However, how much residual adrenal tissue is required for adequate adrenal function has not been much known[18]. Brauckhoff estimated that preservation of approximately one-third of the entire adrenal gland could provide sufficient function[20]. Several authors have advocated preserving the adrenal vein, because adequate venous preservation may be important for maintaining the functionality of the remnant tissue[21,22]. But, in most cases, impaired adrenocortical function is likely caused by atrophy of the normal adrenal tissue. Few studies have demonstrated the feasibility of a partial adenomectomy for BAAs. Glucocorticoid therapy has to be employed to maintain the balance of water and electrolyte metabolism after surgery. Some studies have reported that long-term inadequate corticosteroid replacement therapy might provoke pituitary ACTH-producing hyperplasia adenoma[23-26]. Therefore, proper use of corticosteroids is significantly important. It has been suggested that corticosteroid replacement therapy can be divided into several doses (for example, it can be divided equally into three doses a day, taken at 9:00, 14:00, and 20:00 or 2/3 of a total dose in the morning and 1/3 in the early afternoon)[27].

Based on the reported cases, the clinical characteristics of BAAs could be summarized as: (1) Mainly occurring in mid-aged females; (2) Varying clinical symptoms, though most patients visit hospital because of typical symptoms; (3) Being a kind of ACTH-independent CS, with hypercortisolism, absence of serum cortisol diurnal rhythm, elevated UFC, and no suppression of serum cortisol after low-dose or high-dose dexamethasone suppression testing, while ACTH cannot be tested or is in the normal range, resulting in no reaction to the ACTH stimulation test; (4) Probably different pathological features and functioning state; (5) Bilateral well-encapsulated adenomas of 2.0 cm - 3.5 cm in diameter on the CT scan, with the presence of single or numerous nodules[19,28]; and (6) Normal findings of the MRI of the pituitary[19]. It has been reported that except for glucocorticoids, BAAs could also secrete mineralocorticoids and androgen[29]. In our patients, the plasma renin activity, the ALD concentration, the ALD-to-renin ratio, and the urine epinephrine and dopamine levels were in the normal range, while norepinephrine was only elevated slightly.

CONCLUSION

When patients present with bilateral adrenal lesions, it is crucial to make a definitive diagnosis before operation since various treatments are prescribed for different causes. Few cases of BAAs diagnosed using AVS have been reported. Our case indicates that AVS might be useful for obtaining differential diagnoses in such cases. Once considering BAAs, it is not recommended that bilateral adenomas be removed simultaneously. Hormone replacement therapy may be needed for fear of adrenal insufficiency, and the tapered discontinuation of the replacement therapy is necessarily slow.

Table 3 The results of bilateral adrenal vein sampling

	LAV	RAV	L/R	PV
ACTH (pmol/L)	8.50	8.73	/	9.10
F (nmol/L)	11093.75	5746.61	14.86	693.38
ALD (ng/dL)	13.95	8.90	/	5.0
F/ALD	795	645	1.23	/

An AV-to-PV cortisol gradient greater than 6.5 is consistent with a cortisol-secreting adenoma. In our case, the LAV-to-PV cortisol gradient was 16, and the RAV-to-PV cortisol gradient was 8.2. The "aldosterone-corrected" high-side to low-side AV cortisol gradient was 2.3 or greater, consistent with autonomous cortisol secretion predominantly from one adrenal gland; a gradient of 2.0 or less indicates bilateral cortisol hypersecretion. The ratio of L/R of our patient was 1.23, less than 2.0. All of these pieces of evidence indicated that the hypersecretion of cortisol might originate from both adrenal glands[17]. ACTH: Adrenocorticotropic hormone; F: Cortisol; LAV: Left side adrenal vein; RAV: Right side adrenal vein; L/R: (left side adrenal vein cortisol/ left side aldosterone): (right side adrenal vein cortisol/right side aldosterone); PV: Peripheral vein; ALD: Aldosterone; F/ALD: Cortisol/aldosterone.

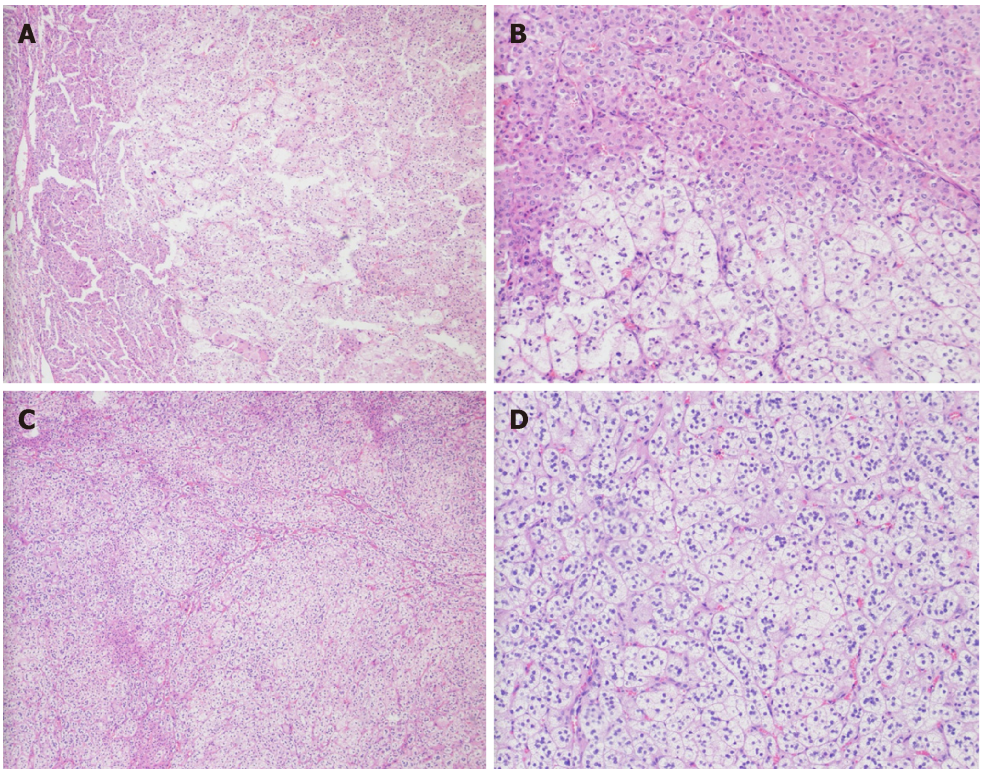

Figure 2 Histological characteristics of the adenomas (Hematoxylin-eosin staining). A-D: The left (A: ×40, B: ×100) and right (C: ×40, D: ×100) adenomas comprised both clear cells and compact cells.

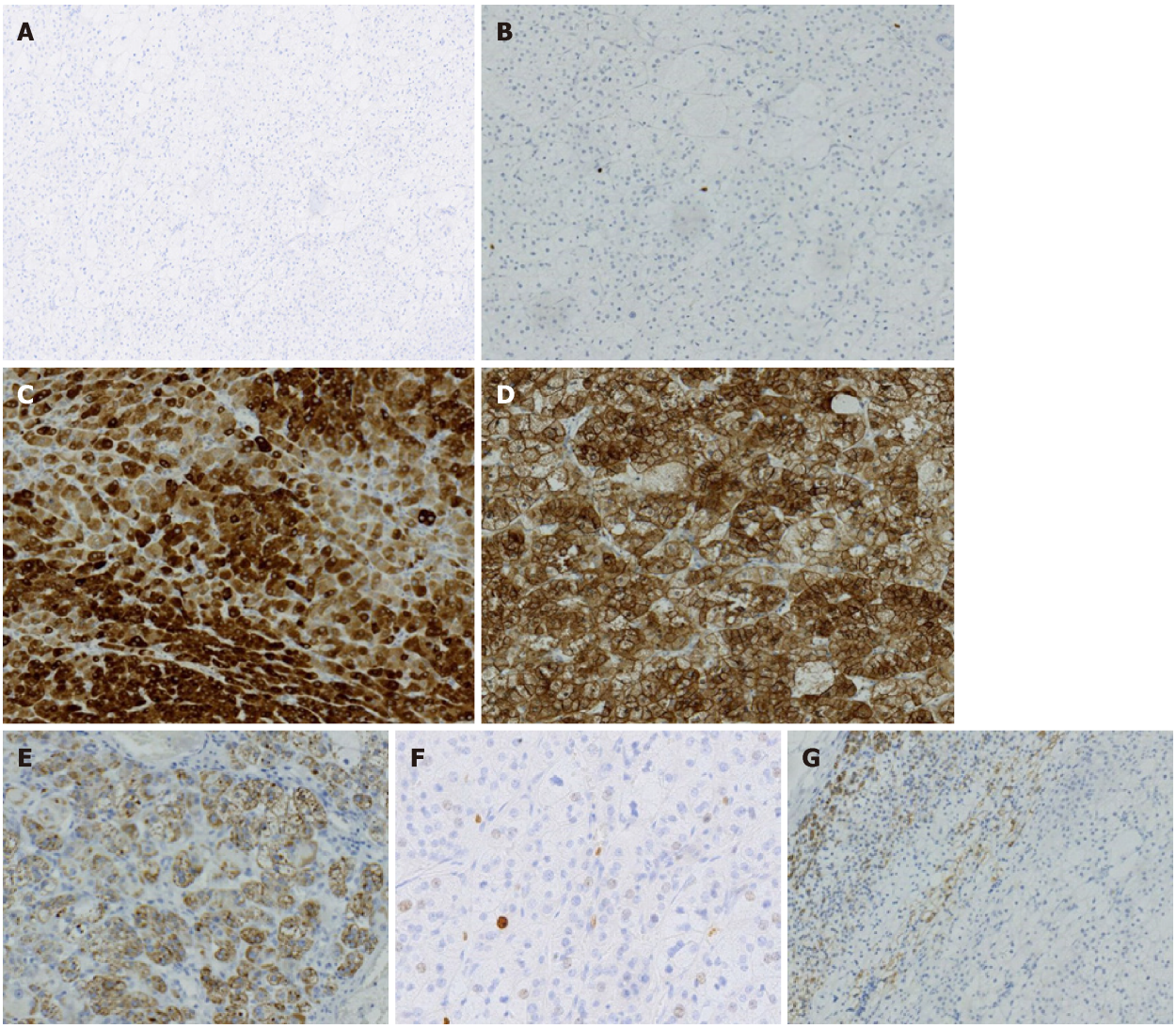

Figure 3 Immunohistochemical staining of the left adrenal adenoma (×100). A and B: Areas negative for chromogranin A (CgA) (A) and cytokeratin (CK) (B); C-E: Tumor cells exhibiting strong staining for inhibin (C), synaptophysin (Syn) (D), and MelanA (E); F and G: Most parts of the tumor showed a proliferation index < 2% (F) and spotty positivity for S100 (G).

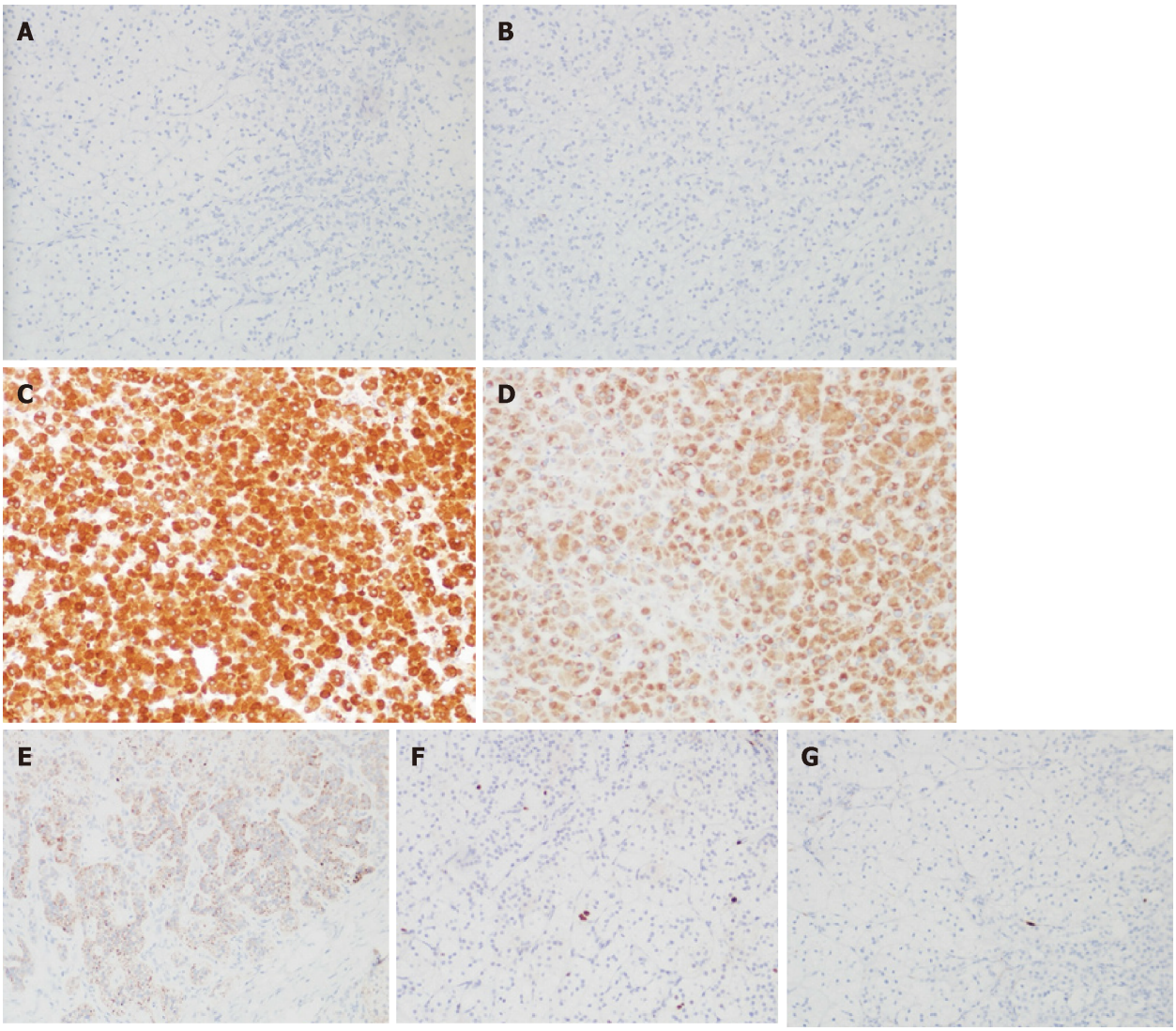

Figure 4 Immunohistochemical staining of the right adrenal adenoma (×100). Areas negative for chromogranin A (CgA) (A) and cytokeratin (CK) (B), where some tumor cells exhibited positive staining for inhibin (C), synaptophysin (Syn) (D), and MelanA (E). Most parts of the tumor show a proliferation index < 2% (F) and spotty positivity for S100 (G).

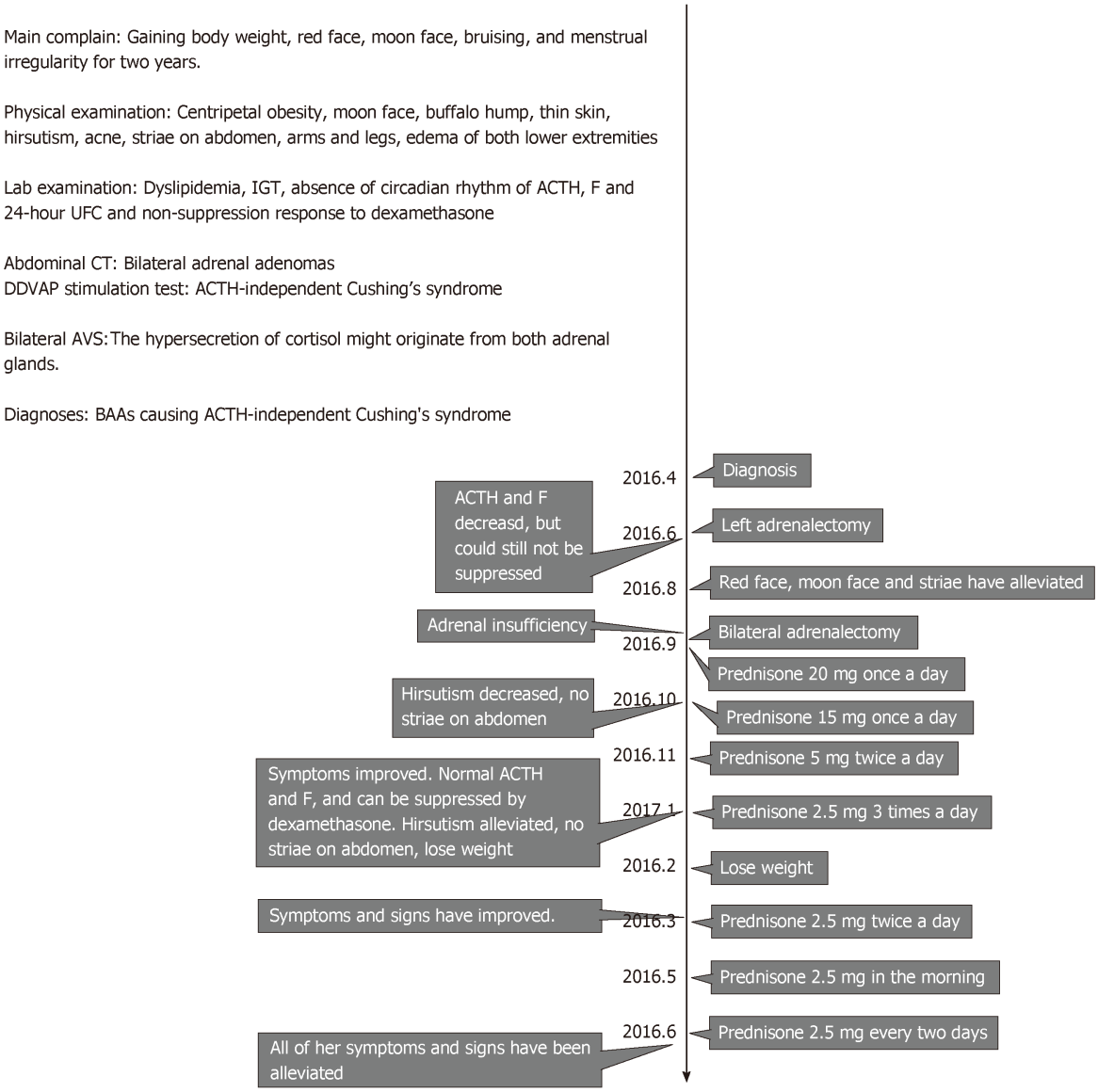

Figure 5 The timeline of this case report.

ACKNOWLEDGEMENTS

The authors thank all of the treatment groups of the Chinese People's Liberation Army General Hospital.

REFERENCES

1 **Li Z**, Zhu Y, Kong C, Yin L, Gao Z, Zhao W, Gong D. Corticotropin-independent Cushing's syndrome in patients with bilateral adrenal masses. *Urology* 2011; **77**: 417-421 [PMID: 21167562 DOI: 10.1016/j.urology.2010.09.045]
2 **Melmed S**, Polonsky KS, Larsen PR, Kronenberg H. Williams textbook of endocrinology. 13th ed. Elsevier Health Sciences, Philadelphia. 2015; 507
3 **Guaraldi F**, Salvatori R. Cushing syndrome: maybe not so uncommon of an endocrine disease. *J Am Board Fam Med* 2012; **25**: 199-208 [PMID: 22403201 DOI: 10.3122/jabfm.2012.02.110227]
4 **Vassiliadi DA**, Ntali G, Vicha E, Tsagarakis S. High prevalence of subclinical hypercortisolism in patients with bilateral adrenal incidentalomas: a challenge to management. *Clin Endocrinol (Oxf)* 2011; **74**: 438-444 [PMID: 21175735 DOI: 10.1111/j.1365-2265.2010.03963.x]
5 **Newell-Price J**, Bertagna X, Grossman AB, Nieman LK. Cushing's syndrome. *Lancet* 2006; **367**: 1605-1617 [PMID: 16698415 DOI: 10.1016/S0140-6736(06)68699-6]
6 **Nieman LK**, Biller BM, Findling JW, Newell-Price J, Savage MO, Stewart PM, Montori VM. The diagnosis of Cushing's syndrome: an Endocrine Society Clinical Practice Guideline. *J Clin Endocrinol Metab* 2008; **93**: 1526-1540 [PMID: 18334580 DOI: 10.1210/jc.2008-0125]

7 **Nieman LK**. Cushing's syndrome. Endocrinology. 4th ed. Philadelphia. 2001; 1691-1720
8 **Tung SC**, Wang PW, Huang TL, Lee WC, Chen WJ. Bilateral adrenocortical adenomas causing ACTH-independent Cushing's syndrome at different periods: a case report and discussion of corticosteroid replacement therapy following bilateral adrenalectomy. *J Endocrinol Invest* 2004; **27**: 375-379 [PMID: 15233560 DOI: 10.1007/BF03351066]
9 **Lacroix A**, Bolté E, Tremblay J, Dupré J, Poitras P, Fournier H, Garon J, Garrel D, Bayard F, Taillefer R. Gastric inhibitory polypeptide-dependent cortisol hypersecretion--a new cause of Cushing's syndrome. *N Engl J Med* 1992; **327**: 974-980 [PMID: 1325608 DOI: 10.1056/NEJM199210013271402]
10 **Reznik Y**, Allali-Zerah V, Chayvialle JA, Leroyer R, Leymarie P, Travert G, Lebrethon MC, Budi I, Balliere AM, Mahoudeau J. Food-dependent Cushing's syndrome mediated by aberrant adrenal sensitivity to gastric inhibitory polypeptide. *N Engl J Med* 1992; **327**: 981-986 [PMID: 1325609 DOI: 10.1056/NEJM199210013271403]
11 **Mineo R**, Tamba S, Yamada Y, Okita T, Kawachi Y, Mori R, Kyo M, Saisho K, Kuroda Y, Yamamoto K, Furuya A, Mukai T, Maekawa T, Nakamura Y, Sasano H, Matsuzawa Y. A Novel Mutation in the type Iα Regulatory Subunit of Protein Kinase A (PRKAR1A) in a Cushing's Syndrome Patient with Primary Pigmented Nodular Adrenocortical Disease. *Intern Med* 2016; **55**: 2433-2438 [PMID: 27580546 DOI: 10.2169/internalmedicine.55.6605]
12 **Zhang ZP**, Liu M, Zhu SC, Wan B. 4 cases report of adrenocortical carcinoma and literature review. *Zhongguo Yixue Zazhi* 2016; **51**: 62-65
13 **Chappell AG**. Cushing's Syndrome due to Bilateral Adrenal Adenomata. *Proc R Soc Med* 1963; **56**: 165-166 [PMID: 19994207]
14 **Nomura K**, Saito H, Aiba M, Iihara M, Obara T, Takano K. Cushing's syndrome due to bilateral adrenocortical adenomas with unique histological features. *Endocr J* 2003; **50**: 155-162 [PMID: 12803235]
15 **Tamura H**, Sugihara H, Minami S, Emoto N, Shibasaki T, Shuto Y, Shimizu K, Gomi Y, Sasano H, Wakabayashi I. Cushing's syndrome due to bilateral adrenocortical adenomas with different pathological features. *Intern Med* 1997; **36**: 804-809 [PMID: 9392354 DOI: 10.2169/internalmedicine.36.804]
16 **Young WF**, du Plessis H, Thompson GB, Grant CS, Farley DR, Richards ML, Erickson D, Vella A, Stanson AW, Carney JA, Abboud CF, Carpenter PC. The clinical conundrum of corticotropin-independent autonomous cortisol secretion in patients with bilateral adrenal masses. *World J Surg* 2008; **32**: 856-862 [PMID: 18074172 DOI: 10.1007/s00268-007-9332-8]
17 **Yasuda A**, Seki T, Ito K, Takagi A, Watanabe D, Nakamura N, Hanai K, Terachi T, Maekawa T, Sasano H, Fukagawa M. A rare case of Cushing's syndrome due to bilateral adrenocortical adenomas. *Tokai J Exp Clin Med* 2014; **39**: 158-165 [PMID: 25504201]
18 **Yang GQ**, Lu JM. A case report of Cushing's syndrome due to bilateral adrenocortical adenomas. *Zhonghua Neifenmidaixie Zazhi* 2001; **17**: 188-189
19 **Domino JP**, Chionh SB, Lomanto D, Katara AN, Rauff A, Cheah WK. Laparoscopic partial adrenalectomy for bilateral cortisol-secreting adenomas. *Asian J Surg* 2007; **30**: 154-157 [PMID: 17475590 DOI: 10.1016/S1015-9584(09)60152-4]
20 **Brauckhoff M**, Gimm O, Thanh PN, Bär A, Ukkat J, Brauckhoff K, Bonsch T, Dralle H. Critical size of residual adrenal tissue and recovery from impaired early postoperative adrenocortical function after subtotal bilateral adrenalectomy. *Surg* 2003; **134**: 1020-1027 [DOI: 10.1016/j.surg.2003.08.005]
21 **Janetschek G**, Finkenstedt G, Gasser R, Waibel UG, Peschel R, Bartsch G, Neumann HP. Laparoscopic surgery for pheochromocytoma: adrenalectomy, partial resection, excision of paragangliomas. *J Urol* 1998; **160**: 330-334 [PMID: 9679871 DOI: 10.1016/S0022-5347(01)62886-6]
22 **Neumann HP**, Reincke M, Bender BU, Elsner R, Janetschek G. Preserved adrenocortical function after laparoscopic bilateral adrenal sparing surgery for hereditary pheochromocytoma. *J Clin Endocrinol Metab* 1999; **84**: 2608-2610 [PMID: 10443647 DOI: 10.1210/jcem.84.8.5872]
23 **Clayton R**, Burden AC, Schrieber V, Rosenthal FD. Secondary pituitary hyperplasia in Addison's disease. *Lancet* 1977; **2**: 954-956 [PMID: 72291 DOI: 10.1016/S0140-6736(77)90891-1]
24 **Jara-Albarran A**, Bayort J, Caballero A, Portillo J, Laborda L, Sampedro M, Cure C, Mateos JM. Probable pituitary adenoma with adrenocorticotropin hypersecretion (corticotropinoma) secondary to Addison's disease. *J Clin Endocrinol Metab* 1979; **49**: 236-241 [PMID: 222793 DOI: 10.1210/jcem-49-2-236]
25 **Krautli B**, Müller J, Landolt AM, von Schulthess F. ACTH-producing pituitary adenomas in Addison's disease: two cases treated by transsphenoidal microsurgery. *Acta Endocrinol (Copenh)* 1982; **99**: 357-363 [PMID: 6280426 DOI: 10.1530/acta.0.0990357]
26 **Scheithauer BW**, Kovacs K, Randall RV. The pituitary gland in untreated Addison's disease. A histologic and immunocytologic study of 18 adenohypophyses. *Arch Pathol Lab Med* 1983; **107**: 484-487 [PMID: 6309113]
27 **Groves RW**, Toms GC, Houghton BJ, Monson JP. Corticosteroid replacement therapy: twice or thrice daily? *J R Soc Med* 1988; **81**: 514-516 [PMID: 3184107 DOI: 10.1177/014107688808100906]
28 **Zheng KW**, Li HZ, Zhang XB. Cushing's syndrome from bilateral adenocortical adenomas (a report of 4 cases and literature review). *Xiandai Miniaowaike Zazhi* 2014; **19**: 513-516
29 **Oki K**, Yamane K, Sakashita Y, Kamei N, Watanabe H, Toyota N, Shigeta M, Sasano H, Kohno N. Primary aldosteronism and hypercortisolism due to bilateral functioning adrenocortical adenomas. *Clin Exp Nephrol* 2008; **12**: 382-387 [PMID: 18543063 DOI: 10.1007/s10157-008-0064-3]
30 **Mao JF**, Chai XF, Liu LP, Chen S, Wang ZX, Lu L, and Lu ZL. Desmopressin stimulation test for the differential diagnosis of ACTH dependent Cushing syndrome. *Zhongguo Shiyongneike Zazhi* 2014; **34**: 1000-1003 [DOI: 10.7504/nk2014090403]

World Journal of Clinical Cases

Submit a Manuscript: https://www.f6publishing.com

World J Clin Cases 2019 April 26; 7(8): 972-983

DOI: 10.12998/wjcc.v7.i8.972

ISSN 2307-8960 (online)

CASE REPORT

Two case reports and literature review for hepatic epithelioid angiomyolipoma: Pitfall of misdiagnosis

Jia-Xi Mao, Fei Teng, Cong Liu, Hang Yuan, Ke-Yan Sun, You Zou, Jia-Yong Dong, Jun-Song Ji, Jun-Feng Dong, Hong Fu, Guo-Shan Ding, Wen-Yuan Guo

ORCID number: Jia-Xi Mao (0000-0001-5006-6153); Fei Teng (0000-0001-9076-8862); Cong Liu (0000-0001-6432-0511); Hang Yuan (0000-0002-7023-9995); Ke-Yan Sun (0000-0002-7909-2029); You Zou (0000-0002-5462-9395); Jia-Yong Dong (0000-0002-6659-3553); Jun-Song Ji (0000-0002-1867-341X); Jun-Feng Dong (0000-0003-2257-5983); Hong Fu (0000-0003-0223-1905); Guo-Shan Ding (0000-0001-8917-969X); Wen-Yuan Guo (0000-0003-3313-3881).

Author contributions: Mao JX, Teng F, and Liu C contributed equally to this work; Mao JX and Teng F contributed to the concept and design of the study; Mao JX, Teng F, and Liu C drafted the manuscript; Yuan H, Sun KY, Zou Y, and Dong JF contributed to treatment of patients; Dong JY and Ji JS were involved in the acquisition, analysis, and interpretation of clinical data; Fu H, Ding GS, and Guo WY performed analysis and interpretation of pathologic data and were responsible for critical revision of the manuscript; Guo WY and Ding GS are the guarantors; All authors read and approved the final manuscript.

Supported by the National Science Foundation of China under Grant numbers, No. 81702923; and Outstanding Postgraduate Seedling Cultivation Fund of Naval Medical University.

Informed consent statement: Written informed consents were obtained from the two patients.

Jia-Xi Mao, Fei Teng, Cong Liu, Hang Yuan, Ke-Yan Sun, You Zou, Jia-Yong Dong, Jun-Song Ji, Jun-Feng Dong, Hong Fu, Guo-Shan Ding, Wen-Yuan Guo, Department of Liver Surgery and Organ Transplantation, Changzheng Hospital, Naval Medical University, Shanghai 200003, China

Corresponding author: Wen-Yuan Guo, MD, PhD, Associate Professor, Department of Liver Surgery and Organ Transplantation, Changzheng Hospital, Naval Medical University, 415 Fengyang Road, Huangpu District, Shanghai 200003, China. guowenyuan@smmu.edu.cn
Telephone: +86-21- 63276788
Fax: +86-21-63276788

Abstract

BACKGROUND

Hepatic epithelioid angiomyolipoma (HEAML) is a rare liver disease and is easily misdiagnosed. Enhanced recognition of HEAML is beneficial to the differential diagnosis of rare liver diseases.

CASE SUMMARY

We presented two cases of HEAML in Changzheng Hospital, Naval Medical University, and then collected and analyzed all reports about HEAML recorded in PubMed, MEDLINE, China Science Periodical Database, and VIP database from January 2000 to March 2018. A total of 409 cases of HEAML in 97 reports were collected, with a ratio of men to women of 1:4.84 and an age range from 12 years to 80 years (median 44 years). Among the patients with clinical symptoms mentioned, 61.93% (205/331) were asymptomatic, 34.74% (115/331) showed upper or right upper quadrant abdomen discomfort, while a few of them showed abdominal mass, gastrointestinal symptoms, low fever, or weight loss. The misdiagnosis rate of HEAML was as high as 40.34% (165/409) due to its nonspecific imaging findings. Most of the tumors were solitary and round in morphology, with clear boundaries. Ultrasound scan indicated low echo with internal nonuniformity and rich blood supply in most cases. Computer tomography/magnetic resonance imaging enhanced scan showed varied characteristics. The ratio of fast wash-in and fast wash-out, fast wash-in and slow wash-out, and delayed enhancement was roughly 4:5:1. A definite diagnosis of HEAML depended on the pathological findings of the epithelioid cells in lesions and the expression of human melanoma black 45, smooth muscle actin, melanoma antigen, and actin by immunohistochemical staining. HEAML had a relatively low malignant rate of 3.91%. However, surgical resection was the main

Conflict-of-interest statement: All authors have no conflict of interest related to the manuscript.

CARE Checklist (2016) statement: The authors have read the CARE Checklist (2013), and the manuscript was prepared and revised according to the CARE Checklist (2016).

Manuscript source: Unsolicited manuscript

Received: December 18, 2018
Peer-review started: December 19, 2018
First decision: January 18, 2019
Revised: February 10, 2019
Accepted: February 26, 2019
Article in press: February 26, 2019
Published online: April 26, 2019

P-Reviewer: Abenavoli L, Fujino Y, Gassler N, Hashimoto N, Nakano H
S-Editor: Wang JL
L-Editor: Filipodia
E-Editor: Wu YXJ

treatment for HEAML, due to the difficulty diagnosing before operation.

CONCLUSION
HEAML is a rare and easily misdiagnosed disease, and it should be diagnosed carefully, taking into account clinical course, imaging, pathological ,and immunohistochemical findings.

Key words: Hepatic epithelioid angiomyolipoma; Imaging; Pathology; Misdiagnosis; Potentially malignant; Case report

Core tip: Hepatic epithelioid angiomyolipoma (HEAML) is a rare and easily misdiagnosed disease, with a misdiagnosis rate as high as 40.34% and a relatively low malignant rate of 3.91%. In this work, we presented two cases of primary and secondary HEAML and analyzed the 409 cases of HEAML recorded in PubMed, MEDLINE, China Science Periodical Database, and VIP database from January 2000 to March 2018. This pooled analysis of HEAML, in view of clinical course, imaging, pathological and immunohistochemical findings, may provide a better understanding of HEAML.

Citation: Mao JX, Teng F, Liu C, Yuan H, Sun KY, Zou Y, Dong JY, Ji JS, Dong JF, Fu H, Ding GS, Guo WY. Two case reports and literature review for hepatic epithelioid angiomyolipoma: Pitfall of misdiagnosis. *World J Clin Cases* 2019; 7(8): 972-983
URL: https://www.wjgnet.com/2307-8960/full/v7/i8/972.htm
DOI: https://dx.doi.org/10.12998/wjcc.v7.i8.972

INTRODUCTION

Hepatic epithelioid angiomyolipoma (HEAML) is a rare subtype of hepatic angiomyolipoma (AML). It is a hepatic mesenchymal neoplasm with malignant potential that is primarily composed of epithelioid cells. Retrieved from major databases, a total of 409 cases of HEMAL have been reported with a misdiagnosis rate as high as 40.34% (165/409) due to its non-specific manifestations. Here we presented two cases of HEAML in Changzheng Hospital, Naval Medical University, Shanghai and made pooled analysis on the diagnosis and prognosis of HEAML. This work was performed in accordance with the Declaration of Helsinki and approved by the Institutional Ethics Committee of Changzheng Hospital. Written informed consents were obtained from the 2 patients for using their data for clinical research and publication.

CASE PRESENTATION

Case 1

History and physical examination: A 40-year-old female patient was admitted to hospital because "health examination revealed hepatic space-occupying lesion 1 wk ago". The patient had no obvious positive clinical manifestations and positive signs.

Diagnostic imaging: Ultrasound and computed tomography (CT) scan suggested a mass of 5 cm × 3 cm in the right lobe of liver (Figure 1A). The hepatitis B surface antigen and tumor markers, such as alpha fetoprotein (AFP), carcino-embryonic antigen (CEA), carbohydrate antigen (CA) 199, and CA125, were all negative.

Histopathology: The postoperative pathological diagnosis was HEAML (potentially malignant) (Figure 1B-C). Immunohistochemistry results were as follows: Antigen Ki67 (Ki67) (1% positive), human melanoma black 45 (HMB45) (positive in some cells), smooth muscle actin (SMA) (weak positive), soluble protein-100 (S100) (-), cluster of differentiation (CD) 34 (positive in vessels), calponin (++) (Figure 1D), estrogen receptor (positive in some cells) (Figure 1E), progesterone receptor (+) (Figure 1F), Keratin-pan (Kpan) (weak positive) (Figure 1G), epithelial membrane antigen (EMA) (-), vimentin (partially positive) (Figure 1H), neuron-specific enolase (-

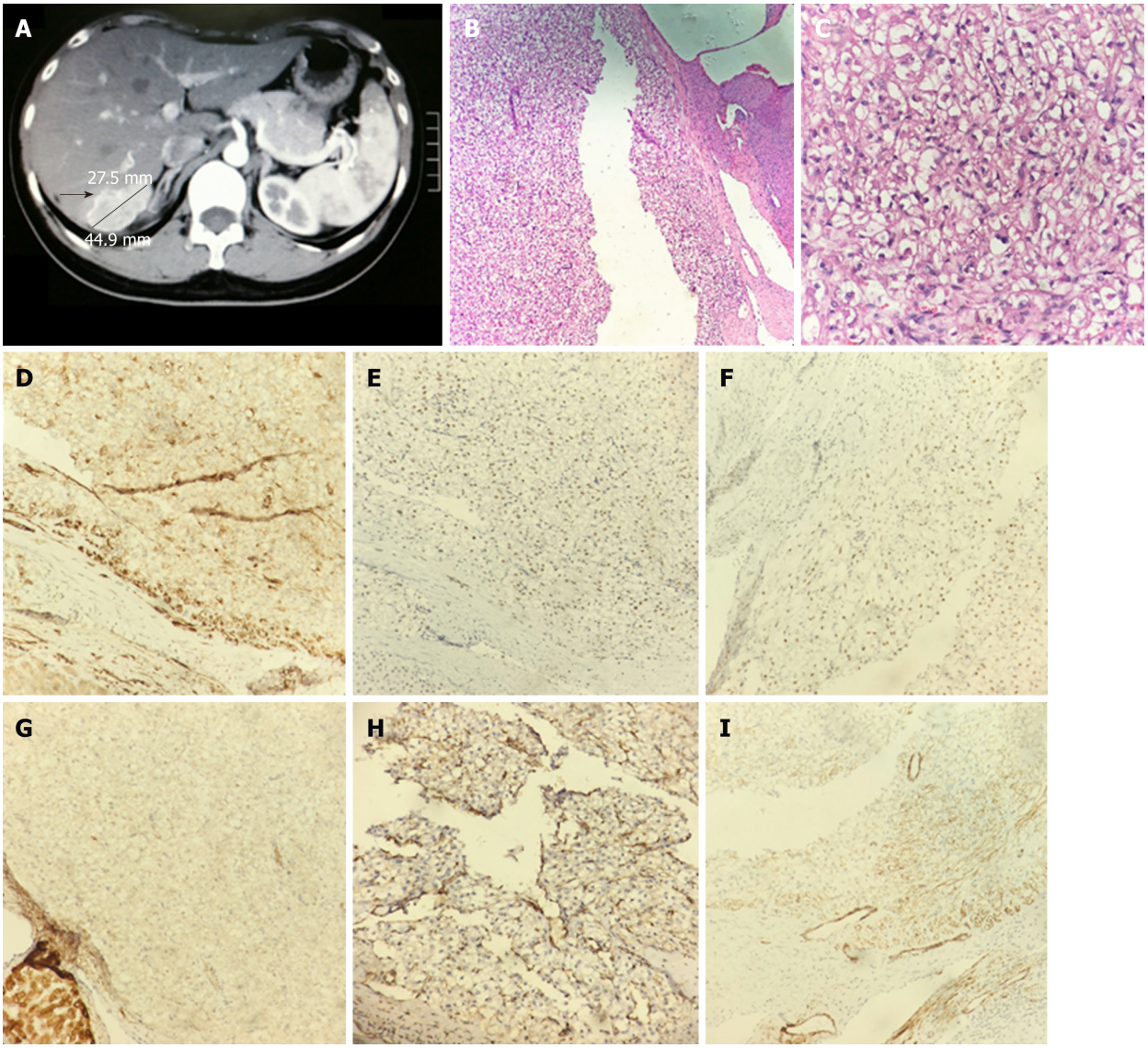

Figure 1 Imaging and pathological immunohistochemical findings of case 1. A: Computed tomography scan suggested a mass of 5 cm × 3 cm in the right lobe of liver; B, C: The postoperative pathological diagnosis was hepatic epithelioid angiomyolipoma (HE staining, B: × 100, C: × 400); D-I (× 200): Immunohistochemistry results were as follows: Calponin (++) (D); estrogen receptor (positive in some cells) (E); progesterone receptor (+) (F); K-pan (weak positive) (G); vimentin (partially positive) (H); and actin (partially positive) (I). HE: Hematoxylin and eosin.

), actin (partially positive) (Figure 1I), AFP (weak positive), and hepatocyte paraffin-1 (HepPar)-1 (-).

Case 2

History of illness: A 39-year-old female patient underwent left nephrectomy due to a left kidney space-occupying lesion in October, 2009. Postoperative pathological examination suggested epithelioid AML. In April 2010, abdominal CT revealed left retroperitoneal lymph node enlargement, which was biopsied afterwards by surgery. Pathological examination prompted a diagnosis of AML. The patient was treated by radiotherapy and high intensity focused ultrasound during the next few years but did not achieve a complete cure.

Imaging examination, histopathology: In routine review on 8 July 2014, ultrasound and CT scan revealed a mass with a maximum diameter of about 6 cm in liver. A CT-guided liver tumor puncture biopsy was performed (Figure 2A), and the pathological diagnosis suggested metastatic HEAML (Figure 2B-D). Immunohistochemistry results were as follows: Ki67 (1% positive), HMB45 (+), melanoma antigen (Melan-A) (+), SMA (+), S100 (-), EMA (-), vimentin (partially positive), AFP (-), and HepPar-1 (-). On 25 July 25 2014, chest CT revealed multiple micronodules in the right lung, the largest one of which was approximately 4 mm and located in the superior lobe.

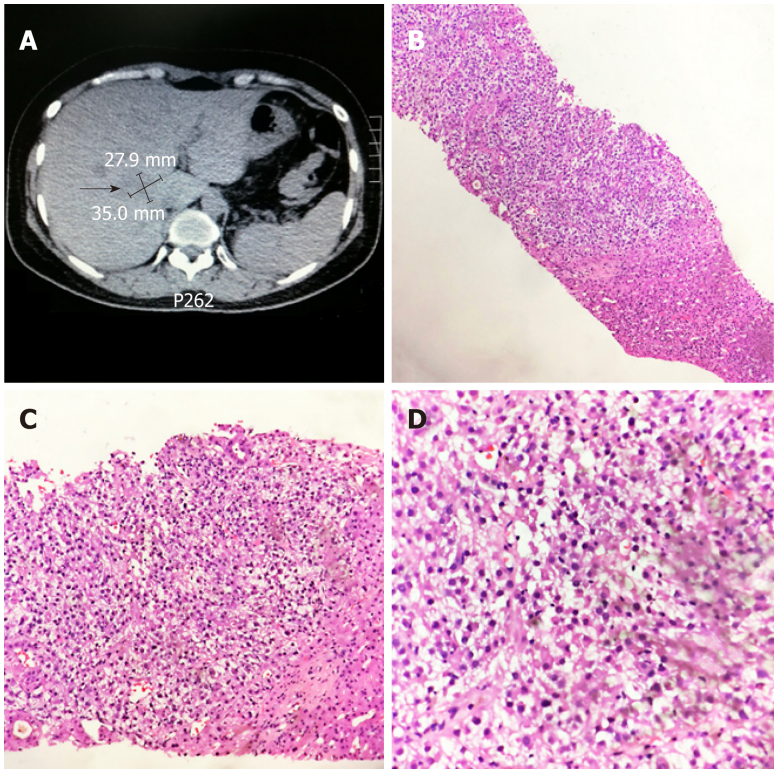

Figure 2 Computed tomography guided percutaneous liver tumor puncture and pathological findings of case 2. A: Computed tomography scan revealed a mass of 3.5 cm × 3.0 cm in liver; B-D: The pathological diagnosis suggested metastatic hepatic epithelioid angiomyolipoma (HE staining, B: × 100, C: × 200, D: × 400).

FINAL DIAGNOSIS

Case 1

The patient was diagnosed with primary HEAML.

Case 2

This patient was diagnosed as a secondary HEAML of renal origin.

TREATMENT

Case 1

The patient underwent liver resection on the third day after admission. During intraoperative exploration, a mass with medium texture and clear boundaries was found located in segment 6, protruding from the liver surface, while no satellite lesions were discovered.

Case 2

The patient underwent transcatheter arterial chemoembolization six times between 28 July 28 2014 and 10 March 2016. During that period, chest CT and abdominal magnetic resonance imaging (MRI) was performed repeatedly and confirmed the presence of bilateral lung nodules, liver space-occupying lesion, and retroperitoneal lymph node enlargement.

OUTCOME AND FOLLOW-UP

Case 1

The patient recovered well after surgery and was discharged on the postoperative day 9. There was no relapse during the 3 years of follow-up.

Case 2

The patient ultimately died on 15 October 2016 due to systemic metastasis of the tumor and multiple organ failure.

DISCUSSION

Literature review

General data: We collected all reports related to HEAML recorded in the PubMed, MEDLINE, China Science Periodical Database, and VIP database from January 2000 to March 2018. A total of 64 articles were enrolled into analysis after excluding 32 articles without valuable data and five articles with repeated data[1-64]. In total, there were 409 cases, of which 386 presented as single tumor and 23 presented as multiple tumors. The male to female ratio was 1:4.84, with 70 males and 339 females. The median age was 44 years old, ranging from 12 years to 80 years old. Of the patients with symptoms mentioned in articles, 61.93% (205/331) were asymptomatic when ultrasound or imaging examination discovered the tumors, while 34.74% (115/331) present with discomfort of the upper abdomen. Fourteen patients had a history of hepatitis B. Seven patients had tuberous sclerosis complex (TSC). The aminotransferases were abnormal in 4 patients. The CA199 level was elevated in 4 patients. Two patients had a history of breast cancer, while one patient was comorbid with cholangiocarcinoma and had elevated CA125 level. Two patients were comorbid with hepatic hemangioma, one patient was comorbid with gallstone disease, and one patient was comorbid with cirrhosis due to schistosomiasis.

The tumor was located in the right lobe in 181 cases, left lobe in 153 cases, and caudate lobe in 12 cases. The maximum diameter of the tumor ranged from 1 cm to 20 cm, with a median of 5.9 cm. Among the cases with tumor morphology described, tumors were round in 86 cases (85.15%) and lobular or irregular in 15 cases (14.85%), while tumors were well defined in 116 cases (84.67%) and ill-defined in 21 cases (15.33%).

Ultrasonography: Ultrasound usually indicated low echo on HEAML, with clear boundary, internal nonuniformity, and rich blood supply. A low echo halo presented in 27.66% cases (13/47). Contrast-enhanced ultrasonography revealed that all lesions appeared homogeneous hyperechoic during arterial phase, and most lesions appeared homogeneous isoechoic during portal and delayed phase (Table 1).

CT: HEAML mostly showed as slightly low density with nonuniformity on CT plain scan. The lesions were obviously or moderately enhanced in arterial phase, and the enhancement decreased during portal and delayed phase in most cases. The enhanced scan showed varied characteristics. The ratio of fast wash-in and fast wash-out, fast wash-in and slow wash-out, and delayed enhancement was roughly 4:5:1. The central vessel sign could be seen in 75.80% of the cases (119/157), and the early drainage veins, which returned into branches of hepatic vein or portal vein, could be seen in 61.48% of the cases (75/122). HEAML usually had no capsule. When the tumor was large enough, it might oppress the surrounding liver parenchyma to form an incomplete pseudocapsule (Table 2).

MRI: MRI scan usually suggested inhomogenous and low T1 weighted imaging (T1WI) signal and an increase in T2WI and diffusion weighted imaging (DWI) signal. Gadolinium ethoxybenzyl diethylenetriamine pentaacetic acid enhanced scan usually showed marked enhancement in the arterial phase, which was decreased during portal and delayed phase (Table 3).

Diagnosis and treatment: Preoperative diagnosis of HEAML was difficult. Among the 409 cases, 59 cases were preoperatively misdiagnosed as benign diseases, including 16 cases of focal nodular hyperplasia, 15 cases of hepatocellular adenoma (HCA), 11 cases of AML, five cases of hemangiomas, one case of hamartoma, and 11 cases of unclassified tumors. One hundred and four cases were misdiagnosed as malignant diseases, including 71 cases of hepatocellular carcinoma, one case of cholangiocarcinoma, five cases of metastatic cancer, three cases of mesenchymal tissue-derived tumors (angiosarcoma, liposarcoma, *etc*), and 24 cases of unclassified tumors. Another two cases were not diagnosed clearly preoperatively. The misdiagnosis rate was thus as high as 40.34% (165/409)[5-12,18-19,22-24,30-39,43-47,51-53,56,62-63]. Surgical resection was the main treatment for HEAML, due to the difficulty diagnosing before operation. For those not suitable for hepatectomy, ablation or interventional therapy could be the alternative treatment after puncture biopsy for pathological diagnosis.

Gross appearance: In general, the section of HEAML was incanus and grayish yellow or grayish red, and the texture was soft mostly. Most of the HEAML had no capsule, with clear or relatively clear boundaries. For HEAMLs, 40.27% (60/149) were accompanied by hemorrhage and necrosis, and 33.33% (23/69) were comorbid with fat lesions. Cystic degeneration occurred in 14.04% (16/114) of the tumors (Table 4).

Table 1 Ultrasound and contrast-enhanced ultrasonography of hepatic epithelioid angiomyolipoma

Items	Cases
Ultrasound	
Echo (low/mixed/high)	54/8/24
Internal uniformity (heterogeneity/homogeneity)	37/38
Boundary (clear/indistinct)	55/5
Hypoechoic halo (Y/N)	13/34
Blood supply (rich/abundant/rare)	22/6/7
Contrast-enhanced ultrasonography	
Arterial phase (high/middle/low)	15/0/0
Portal phase (high or slightly high/middle/low or slightly low)	4/8/3
Delay phase (high or slightly high/middle/low or slightly low)	3/7/5

Microscope appearance: Epithelioid tumor cells could be observed under the microscope and arranged irregularly in nodules or flaky structures, with relatively obvious atypia. Sometimes multinucleated giant cells and ganglion-like large cells could be observed. Generally, epithelioid tumor cells were round, polygonal, or short-spindle in shape and were radially distributed around thin-walled blood vessels or muscular arteries. The cytoplasm was abundant and slightly eosinophilic staining. Sometimes the cytoplasm was clear and contained adipose vacuoles. The centrally located nuclei were large, round, or oval in shape. The nucleoli were obvious and mitotic figures were rare.

Immunohistochemistry: Immunohistochemical examination revealed that the expressions of HMB45, SMA, Actin, Melan-A, macrophage marker 387, melanoma antigen recognized by T-cells 1, A103, *etc* were positive. The expressions of CD31, CD34 on vascular wall, vimentin, pp70S6K, and MyoD1 were positive in about half of the cases. In a few cases, the fat S-100, CD68, desmin, muscle specific actin, human myeloperoxidase (MPO), E-cadherin, and b-cadherin was positive or weakly positive. The Kpan, AFP, HepPar-1, EMA, CEA, CD117, and p53 was basically negative (Table 5). The Ki-67 expression ranged from < 1% to 15%, with a median of 1.96%.

Follow-up: The duration of follow-up was 2 mo to 180 mo, with a median of 31 mo. The rate of malignancy was 3.96% (16/409). Notably, among the 16 malignant cases, only 1 case was diagnosed potential malignancy on pathology, other cases were identified malignancy because of intrahepatic recurrence (6 cases) and distant metastases (9 cases). Among those metastatic cases, 2 cases were lung metastasis and 1 case was bone metastasis, while other cases were not specified the sites of metastasis. The time of postoperative relapse was 5 mo to 108 mo, with a median of 42.5 mo.

Discussion

Since Bonetti and colleagues first described AML in 1992, it has gradually been increasingly recognized as a relatively rare mesenchymal tumor. AML was most commonly found in the kidney and less often in the liver. Most patients with hepatic AML were female and asymptomatic, and the masses usually occurred in non-cirrhotic liver without serological abnormalities. In most cases, hepatic AML was discovered incidentally during regular health check-ups or examinations for other diseases. The pathogenesis of hepatic AML has not yet been clarified. There was an association with TSC in more than 50% of the AML in the kidney, but this association had been estimated to be only 5%-15% of the patients presenting with solitary liver tumors. In our review, TSC was found in 7 patients (1.7%), which might be under-estimated due to incomplete information. However, TSC was probably a risk factor for malignant behavior of epithelioid AML[65]. Histologically, it was composed of blood vessels, adipose tissue, and smooth muscle. Compared with typical AML, HEAML was histologically dominated by epithelioid cells and contained much less adipose cells.

HEAML occurred primarily in young and middle-aged females, with an average age of 45 years old at the time of diagnosis. The male to female ratio was about 1:4.84. Approximately two-thirds of patients were found to be asymptomatic on physical examination, while one-third of patients presented with discomfort or swelling pain of the epigastrium or right upper quadrant. A few patients presented with an abdominal mass, poor appetite, nausea and vomiting, anemia, fatigue, low fever,

Table 2 Preoperative computed tomography manifestations of hepatic epithelioid angiomyolipoma

Items	Cases
Computed tomography	
Plain scan phase	
Uniformity (uniform/non-uniform)	15/24
Density (low density/equidensity)	63/9
Arterial phase (Obvious uniform enhancement/apparent or moderate non-uniform enhancement)	54/53
Portal phase (obvious enhancement/enhancement reduction)	33/42
Delayed phase (sustained moderate enhancement/enhancement reduction)	23/30
Characteristic manifestations	
Central vessel sign (Y/N)	119/38
Early drainage veins (Y/N)	75/47
Enhancement mode (fast wash-in and fast wash-out/fast wash-in and slow wash-out/delayed enhancement)	67/83/15
Pseudocapsule (Y/N)	65/73

weight loss, changes in bowel habits, *etc*[1]. Patients usually had no hepatitis, cirrhosis, or family history of this type of tumor. The common tumor markers were almost all negative.

HEAML imaging findings included: (1) Most of the tumors were solitary and round in morphology, while a few were lobulated or irregular, with clear boundaries; (2) Ultrasound scan indicated low echo with internal nonuniformity, clear boundary, and rich blood supply in most cases, sometimes with low echo halo. Contrast-enhanced ultrasound showed that all lesions appeared homogeneous hyperechoic during arterial phase, and most lesions appeared homogeneous isoechoic during portal and delayed phase; (3) CT plain scan usually showed low density lesions, which was obviously or moderately enhanced in arterial phase, and the enhancement decreased during portal and delayed phase in most cases; (4) Most of the lesions were accompanied by central vessels and early drainage veins, which afflux into branches of the hepatic vein or portal vein; (5) The enhanced scan showed varied characte-ristics. The ratio of fast wash-in and fast wash-out, fast wash-in and slow wash-out, and delayed enhancement was roughly 4:5:1; (6) HEAML usually had no capsule. When the tumor was large enough, it might oppress the surrounding liver parenchyma to form an incomplete pseudocapsule. Recognizing the imaging features of no capsule, and hypervasularity with central punctiform or filiform vessels as a characteristic enhancement may distinguish Epi-HAML from other hepatic tumors[30]; and (7) MRI scan usually suggested inhomogenous and low T1WI signal, and increase in T2WI and DWI signal. Gadolinium ethoxybenzyl diethylenetriamine pentaacetic acid enhanced scan usually showed marked enhancement in arterial phase, which was decreased during portal and delayed phase.

The preoperative misdiagnosis rate was as high as 40.34% (165/409) because of the non-specific clinical and imaging manifestations of HEAML. It was necessary to differentiate with hepatocellular carcinoma, focal nodular hyperplasia, HCA, hemangiomas, and metastatic cancers when making diagnosis. Currently, the major treatment strategy was surgical resection. In general, HEAML had no capsule, but presented with clear boundaries. HEAML demonstrated expansive growth and squeezed the adjacent liver parenchyma. Internal hemorrhage and necrosis was more common than typical AML. The definitive diagnosis of HEAML depended on pathological findings of epithelioid cells in the lesions, and the immunohistochemical findings of melanoma specific markers (HMB45, Melan-A) and myogenic markers (SMA, muscle specific actin, Actin).

Most of the HEAMLs were benign, with a relatively low malignant rate of 3.91% (16/409). Notably, 15 cases of malignancy were identified because of intrahepatic recurrence or distant metastasis, while the pathological examination did not demonstrate malignancy distinctly on the first operation. The malignant HEAML mainly metastasize to the lung and bones and could involve multiple organs in severe cases. The median time of postoperative relapse was 42.5 mo. Therefore, periodic reexamination was needed to prevent recurrence, especially within 5 years after surgery, just like gastrointestinal tumors. In addition, the HEAML could be secondary, with primary lesions mostly originated from kidney. The second case reported in this article initially presented as retroperitoneal lymph node enlargement 1 year after renal EAML resection, and eventually exhibited liver and lung metastases 5 years after the surgery. Secondary HEAML has rarely been reported. Among the 17

Table 3 Preoperative magnetic resonance imaging and gadolinium ethoxybenzyl diethylenetriamine pentaacetic acid enhanced scan manifestations of hepatic epithelioid angiomyolipoma

Items	Cases
Magnetic resonance imaging	
T1WI	
Low, slightly low signal/equisignal/high signal	107/1/1
Slightly uniform/non-uniform	13/26
T2WI	
Slightly high signal/high signal	39/70
Slightly uniform/non-uniform	3/29
DWI	
Slightly high signal/high signal	13/51
Slightly uniform/non-uniform	4/15
Gd-EOB-DTPA	
Arterial phase	
Homogeneous enhancement/heterogeneous enhancement	29/21
Obvious enhancement/Medium enhancement	47/7
Portal phase	
Continuous enhancement/enhancement weakened	22/29
Delayed phase	
Continuous enhancement/enhancement weakened	1/2

T1WI: T1 weighted imaging; DWI: Diffusion weighted imaging; Gd-EOB-DTPA: Gadolinium ethoxybenzyl diethylenetriamine pentaacetic acid.

secondary cases reported[8,37,66-71], 5 cases turned to multiple metastases. Secondary HEAML had no significant differences from primary HEAML in terms of clinical manifestations, imaging findings, pathology, and immunohistochemistry.

Table 4 Gross appearance of hepatic epithelioid angiomyolipom

Items	Cases or manifestations
Section	Mostly incanus, grayish yellow or grayish red
Capsule (Y/N)	10/53
Boundary	Clear
Texture (slightly soft/medium/slightly dense)	65/6/18
Hemorrhage or necrosis (Y/N)	60/89
Fat lesions (Y/N)	23/46
Cystic degeneration (Y/N)	16/98

Table 5 Immunohistochemistry markers of hepatic epithelioid angiomyolipoma

Markers	Positive/weakly positive/negative (+/±/-)	Positive rate
HMB45	219/2/5	97.35%
S-100	19/5/63	24.71%
SMA	128/15/32	77.43%
MSA	4/10/1	60%
Actin	32/1/5	85.53%
Melan-A	91/1/22	80.70%
CD31	2/0/2	50%
CD34	38/0/34	52.78%
CD68	2/6/5	33.33%
CD117	0/0/13	0%
Vimentin	23/11/17	55.88%
Kpan	0/0/101	0%
HepPar-1	0/0/52	0%
MAC387	6/0/0	100%
EMA	0/0/30	0%
Desmin	0/20/30	20%
MART-1	24/0/1	96%
CEA	1/0/9	10%
AFP	0/1/66	0.75%
MPO	0/1/1	25%
p53	0/0/9	0%
E-cadherin, b-cadherin	0/1/4	10%
pp70S6K	1/2/1	50%
MyoD1	2/2/1	60%

HMB45: Human melanoma black 45; SMA: Smooth muscle actin; MSA: Muscle specific actin; Melan-A: Melanoma antigen; EMA: Epithelial membrane antigen; CEA: Carcino-embryonic antigen; AFP: Alpha fetoprotein; MPO: Human myeloperoxidase.

ACKNOWLEDGEMENTS

We thank the patients for their cooperation. We thank Dr. Qing-Zi Zhu (Department of Pathology, Changzheng Hospital) for supplying HEAML tissue.

REFERENCES

1 **Ma ZP**, Lin GS, Chen BY, Wang C, Zhou JJ. MRI and clinical analysis of hepatic epithelioid angiomyolipoma. *Zhonghua Shiyong Zhenduan Yu Zhiliao Zazhi* 2018; **32**: 172-175 [DOI: 10.13507/j.issn.1674-3474.2018.02.020]
2 **Lee SY**, Kim BH. Epithelioid angiomyolipoma of the liver: a case report. *Clin Mol Hepatol* 2017; **23**: 91-94 [PMID: 28301898 DOI: 10.3350/cmh.2017.0011]
3 **Yang XG**, Liu GJ, He ML, Hu YF, Tong QY, Qiu WJ. CT and MRI characteristics of hepatic epithelial

angiomyolipoma. *Shiyong Fangshexue Zazhi* 2017; **33**: 1545-1548 [DOI: 10.3969/j.issn.1002-1671.2017.10.013]
4 **Zhang J**, Wang C, Ma ZP. Manifestation of CT in epithelioid angiomyolipoma of liver. *Gandanyi Waike Zazhi* 2017; **29**: 123-127 [DOI: 10.11952/j.issn.1007-1954.2017.02.009]
5 **Tan Y**, Xie X, Lin Y, Huang T, Huang G. Hepatic epithelioid angiomyolipoma: clinical features and imaging findings of contrast-enhanced ultrasound and CT. *Clin Radiol* 2017; **72**: 339.e1-339.e6 [PMID: 27890423 DOI: 10.1016/j.crad.2016.10.018]
6 **Fan PL**, Wang WP, Mao F, Ji Y, Xu C, Ji ZB, Huang BJ. Ultrasound Characteristics of Hepatic Epithelioid Angiomyolipoma. *Zhongguo Chaosheng Yixue Zazhi* 2017; **33**: 147-149
7 **Liu J**, Zhang CW, Hong DF, Tao R, Chen Y, Shang MJ, Zhang YH. Primary hepatic epithelioid angiomyolipoma: A malignant potential tumor which should be recognized. *World J Gastroenterol* 2016; **22**: 4908-4917 [PMID: 27239117 DOI: 10.3748/wjg.v22.i20.4908]
8 **Ortiz S**, Tortosa F. Epithelioid angiomyolipoma of the liver: Clinicopathological correlation in a series of 4 cases. *Rev Esp Enferm Dig* 2016; **108**: 27-30 [PMID: 26765232]
9 **Liu W**, Meng Z, Liu H, Li W, Wu Q, Zhang X, E C. Hepatic epithelioid angiomyolipoma is a rare and potentially severe but treatable tumor: A report of three cases and review of the literature. *Oncol Lett* 2016; **11**: 3669-3675 [PMID: 27313680 DOI: 10.3892/ol.2016.4443]
10 **Fukuda Y**, Omiya H, Takami K, Mori K, Kodama Y, Mano M, Nomura Y, Akiba J, Yano H, Nakashima O, Ogawara M, Mita E, Nakamori S, Sekimoto M. Malignant hepatic epithelioid angiomyolipoma with recurrence in the lung 7 years after hepatectomy: a case report and literature review. *Surg Case Rep* 2016; **2**: 31 [PMID: 27037804 DOI: 10.1186/s40792-016-0158-1]
11 **Liu LN**, Xie LQ. Diagnosis of hepatic epithelioid angiomyolipoma: one case report and review of literature. *Yixue Yingxiangxue Zazhi* 2016; **26**: 753-755
12 **Wu RD**, Yang XF, Wang M, Zhou LS, Huang K, Fang ZN, Zhen KG, Feng ST. Hepatic Epithelioid Angiomyolipoma MSCT Findings. *Linchuang Fangshexue Zazhi* 2016; **35**: 395-398 [DOI: 10.13437/j.cnki.jcr.2016.03.023]
13 **Song X**, Xu SL, Xiao WB. CT and MRI manifestations of hepatic epithelioid angiomyolipomas. *Zhongguo Yixue Yingxiang Jishu* 2016; **32**: 87-90 [DOI: 10.13929/j.1003-3289.2016.01.023]
14 **Yu YH**, Wu JT, Wang SA. Imaging features of hepatic epithelioid angiomyolipoma. *Yiliao Weisheng Zhuangbei* 2016; **37**: 75-77 [DOI: 10.7687/j.ISSN1003-8868.2016.03.075]
15 **Huang SC**, Chuang HC, Chen TD, Chi CL, Ng KF, Yeh TS, Chen TC. Alterations of the mTOR pathway in hepatic angiomyolipoma with emphasis on the epithelioid variant and loss of heterogeneity of TSC1/TSC2. *Histopathology* 2015; **66**: 695-705 [PMID: 25234729 DOI: 10.1111/his.12551]
16 **Sun J**, Wang S, Chen W, Wu J. Gd-EOB-DTPA-enhanced and diffusion-weighted magnetic resonance findings in hepatic epithelioid angiomyolipoma: A case report. *Oncol Lett* 2015; **10**: 1145-1148 [PMID: 26622641 DOI: 10.3892/ol.2015.3368]
17 **Tang YQ**, Li JW, Ling WW, Ling L, Qiang LU, Yan L. Features of hepatic epithelioid angiomyolipoma on ultrasonography. *Zhongguo Yixue Yingxiang Jishu* 2015; **31**: 746-749 [DOI: 10.13929/j.1003-3289.2015.05.027]
18 **Mei HY**, Wang SY. Imaging diagnosis of epithelioid angiomyolipoma of liver. *Shiyong Yixue Yingxiang Zazhi* 2015; **2**: 154-156 [DOI: 10.16106/j.cnki.cn14-1281/r.2015.02.023]
19 **Wu QQ**, Chen ZQ. Imaging findings and pathologic correlation of hepatic epithelioid angiomyolipoma. *Yixue Yingxiangxue Zazhi* 2015; **4**: 662-665
20 **Zhang JW**, Xu PJ. Epithelioid Angiomyolipoma of the Liver: Analysis of Magnetic Resonance Imaging Features. *Zhongguo Yixue Jisuanji Chengxiang Zazhi* 2015; **21**: 124-128 [DOI: 10.19627/j.cnki.cn31-1700/th.2015.02.009]
21 **Barbier L**, Torrents J, Hardwigsen J. Hepatic angiomyolipoma: what management? *Acta Chir Belg* 2014; **114**: 139-142 [PMID: 25073214 DOI: 10.1080/00015458.2014.11680997]
22 **Dai CL**, Xue LP, Li YM. Multi-slice computed tomography manifestations of hepatic epithelioid angiomyolipoma. *World J Gastroenterol* 2014; **20**: 3364-3368 [PMID: 24696616 DOI: 10.3748/wjg.v20.i12.3364]
23 **Tajima S**, Suzuki A, Suzumura K. Ruptured hepatic epithelioid angiomyolipoma: a case report and literature review. *Case Rep Oncol* 2014; **7**: 369-375 [PMID: 24987358 DOI: 10.1159/000363690]
24 **Xu H**, Wang H, Zhang X, Li G. [Hepatic epithelioid angiomyolipoma: a clinicopathologic analysis of 25 cases]. *Zhonghua Bing Li Xue Za Zhi* 2014; **43**: 685-689 [PMID: 25567596]
25 **Zhao Y**, Ouyang H, Wang X, Ye F, Liang J. MRI manifestations of liver epithelioid and nonepithelioid angiomyolipoma. *J Magn Reson Imaging* 2014; **39**: 1502-1508 [PMID: 24129971 DOI: 10.1002/jmri.24291]
26 **Zhou Y**, Chen F, Jiang W, Meng Q, Wang F. Hepatic epithelioid angiomyolipoma with an unusual pathologic appearance: expanding the morphologic spectrum. *Int J Clin Exp Pathol* 2014; **7**: 6364-6369 [PMID: 25337292]
27 **Zhu H**, Zheng XL, Wei M, Center MI. MRI Diagnosis of Hepatic Epithelioid Angiomyolipoma. *Zhongguo CT He MRI Zazhi* 2014; **3**: 75-77 [DOI: 10.3969/j.issn.1672-5131.2014.03.21]
28 **Occhionorelli S**, Dellachiesa L, Stano R, Cappellari L, Tartarini D, Severi S, Palini GM, Pansini GC, Vasquez G. Spontaneous rupture of a hepatic epithelioid angiomyolipoma: damage control surgery. A case report. *G Chir* 2013; **34**: 320-322 [PMID: 24342160]
29 **Kang SL**, He B, Han D. One case: lipid-poor hepatic epithelioid angiomyolipoma of the male. *Shiyong Fangshexue Zazhi* 2013; **29**: 338-339
30 **Ji JS**, Lu CY, Wang ZF, Xu M, Song JJ. Epithelioid angiomyolipoma of the liver: CT and MRI features. *Abdom Imaging* 2013; **38**: 309-314 [PMID: 22610058 DOI: 10.1007/s00261-012-9911-5]
31 **Lo RC**. Epithelioid angiomyolipoma of the liver: a clinicopathologic study of 5 cases. *Ann Diagn Pathol* 2013; **17**: 412-415 [PMID: 23786777 DOI: 10.1016/j.anndiagpath.2013.04.009]
32 **Saito Y**, Shimada M, Utsunomiya T, Morine Y, Imura S, Ikemoto T, Mori H, Hanaoka J, Sugimoto K, Iwahashi S, Yamada S, Asanoma M, Ishibashi H. Hepatic epithelioid angiomyolipoma with arterioportal venous shunting mimicking hepatocellular carcinoma: report of a case. *J Med Invest* 2013; **60**: 262-266 [PMID: 24190045 DOI: 10.2152/jmi.60.262]
33 **Li FQ**, Qian HF, Zhu YM, Ding Y, Hu XH. Diagnosis of Hepatic Epithelioid Angiomyolipoma by MRI. *Yixue Yanjiu Zazhi* 2013; **42**: 164-167 [DOI: 10.3969/j.issn.1673-548X.2013.03.051]
34 **Wu ZJ**, Hua H, Chen JJ, Jiang G, Li XF, Li SK, Xu WJ. CT characteristics of hepatic epithelial angiomyolipoma. *Zhongguo Yixue Yingxiang Jishu* 2013; **29**: 84-87 [DOI: 10.13929/j.1003-3289.2013.01.043]

35 **Agaimy A**, Vassos N, Croner RS, Strobel D, Lell M. Hepatic angiomyolipoma: a series of six cases with emphasis on pathological-radiological correlations and unusual variants diagnosed by core needle biopsy. *Int J Clin Exp Pathol* 2012; **5**: 512-521 [PMID: 22949933]

36 **Limaiem F**, Korbi S, Lahmar A, Bouraoui S, Aloui S, Jedidi S, Miloudi N, Mzabi-Regaya S. A misleading hepatic tumour: epithelioid angiomyolipoma. *Acta Gastroenterol Belg* 2012; **75**: 443-445 [PMID: 23402089]

37 **Xie L**, Jessurun J, Manivel JC, Pambuccian SE. Hepatic epithelioid angiomyolipoma with trabecular growth pattern: a mimic of hepatocellular carcinoma on fine needle aspiration cytology. *Diagn Cytopathol* 2012; **40**: 639-650 [PMID: 21563318 DOI: 10.1002/dc.21703]

38 **Liu H**, Zhou BY, Lin H. Hepatic Epithelioid Angiomyolipoma One Case Report of Ultrasonography and Review of Literature. *Hanshao Jibing Zazhi* 2012; **19**: 34-37 [DOI: 10.3969/j.issn.1009-3257.2012.04.010]

39 **Liu JP**, Chen ZJ, Huang YY, Sun ZS, Lu CY. Imaging and pathological features of hepatic monotypic epithelioid angiomyolipoma. *Yixue Yingxiangxue Zazhi* 2012; **22**: 219-221 [DOI: 10.3969/j.issn.1006-9011.2012.02.025]

40 **Wang ZH**, Wu D, Hou J, Zhang LT, Kong QK. MRI diagnosis of epithelioid angiomyolipoma of liver. *Zhonghua Fangshexue Zazhi* 2012; **46**: 803-806 [DOI: 10.3760/cma.j.issn.1005-1201.2012.09.007]

41 **Zhang LP**, Tang BH, Li LC, Li FY, He YQ, Wu RG, Huang H, Huang DC. CT Features of Epithelioid Angiomyolipoma in Liver: Report of 2 Cases and Literature Review. *Linchuang Fangshexue Zazhi* 2012; **31**: 1805-1807

42 **Talati H**, Radhi J, Popovich S, Marcaccio M. Hepatic Epithelioid Angiomyolipoma: Case Series. *Gastroenterology Res* 2010; **3**: 293-295 [PMID: 27942312 DOI: 10.4021/gr273w]

43 **Ma HL**, Yang CB, Chen WB, Zhang WJ, Li L. Hepatic epithelioid angiomyolipoma: an analysis of two cases. *Shijie Huaren Xiaohua Zazhi* 2011; **19**: 1071-1074 [DOI: 10.11569/wcjd.v19.i10.1071]

44 **Zhang B**, LV ZL, Qin X, Peng MH, Peng T. Hepatic epithelioid angiomyolipoma: A case report and literature review. *Zhongguo Aizheng Fangzhi Zazhi* 2011; **3**: 120-125 [DOI: 10.3969/j.issn.1674-5671.2011.02.07]

45 **Wen MC**, Jan YJ, Li MC, Wang J, Lin A. Monotypic epithelioid angiomyolipoma of the liver with TFE3 expression. *Pathology* 2010; **42**: 300-302 [PMID: 20350230 DOI: 10.3109/00313021003631254]

46 **Fu LP**, Bao YW, Ji JS, Zhao ZW, Xu M, Wang ZF, Fan XX. Imaging Diagnosis of Epithelioid Angiomyolipoma of Liver. *Shiyong Fangshexue Zazhi* 2010; **26**: 973-976 [DOI: 10.3969/j.issn.1002-1671.2010.07.014]

47 **Alatassi H**, Sahoo S. Epithelioid angiomyolipoma of the liver with striking giant cell component: fine-needle aspiration biopsy findings of a rare neoplasm. *Diagn Cytopathol* 2009; **37**: 192-194 [PMID: 19156824 DOI: 10.1002/dc.20979]

48 **Yamasaki S**, Tanaka S, Fujii H, Matsumoto T, Okuda C, Watanabe G, Suda K. Monotypic epithelioid angiomyolipoma of the liver. *Histopathology* 2000; **36**: 451-456 [PMID: 10792487 DOI: 10.1046/j.1365-2559.2000.00848.x]

49 **Leenman EE**, Mukhina MS, Nasyrov AR. [Monophasic angiomyolipoma (PEComa) of the liver]. *Arkh Patol* 2009; **71**: 44-46 [PMID: 20131508]

50 **Xu PJ**, Shan Y, Yan FH, Ji Y, Ding Y, Zhou ML. Epithelioid angiomyolipoma of the liver: cross-sectional imaging findings of 10 immunohistochemically-verified cases. *World J Gastroenterol* 2009; **15**: 4576-4581 [PMID: 19777618 DOI: 10.3748/wjg.15.4576]

51 **Yuan Y**, Zhang J, Huang YN. One cases report of epithelioid angiomyolipoma (EAML) of liver. *Xiandai Zhongliu Yixue* 2009; **17**: 1776-1780

52 **Deng YF**, Lin Q, Zhang SH, Ling YM, He JK, Chen XF. Malignant angiomyolipoma in the liver: a case report with pathological and molecular analysis. *Pathol Res Pract* 2008; **204**: 911-918 [PMID: 18723294 DOI: 10.1016/j.prp.2008.06.007]

53 **Khalbuss WE**, Fischer G, Bazooband A. Imprint cytology of epithelioid hepatic angiomyolipoma: mimicry of hepatocellular carcinoma. *Acta Cytol* 2007; **51**: 670-672 [PMID: 17718152]

54 **Parfitt JR**, Bella AJ, Izawa JI, Wehrli BM. Malignant neoplasm of perivascular epithelioid cells of the liver. *Arch Pathol Lab Med* 2006; **130**: 1219-1222 [PMID: 16879028 DOI: 10.1043/1543-2165(2006)130[1219:MNOPEC]2.0.CO;2]

55 **Rouquie D**, Eggenspieler P, Algayres JP, Béchade D, Camparo P, Baranger B. [Malignant-like angiomyolipoma of the liver: report of one case and review of the literature]. *Ann Chir* 2006; **131**: 338-341 [PMID: 16386232 DOI: 10.1016/j.anchir.2005.11.014]

56 **Mizuguchi T**, Katsuramaki T, Nobuoka T, Nishikage A, Oshima H, Kawasaki H, Kimura S, Satoh M, Hirata K. Growth of hepatic angiomyolipoma indicating malignant potential. *J Gastroenterol Hepatol* 2004; **19**: 1328-1330 [PMID: 15482547 DOI: 10.1111/j.1440-1746.2004.03583.x]

57 **Tryggvason G**, Blöndal S, Goldin RD, Albrechtsen J, Björnsson J, Jónasson JG. Epithelioid angiomyolipoma of the liver: case report and review of the literature. *APMIS* 2004; **112**: 612-616 [PMID: 15601311 DOI: 10.1111/j.1600-0463.2004.apm1120909.x]

58 **Hino A**, Hirokawa M, Takamura K, Sano T. Imprint cytology of epithelioid angiomyolipoma in a patient with tuberous sclerosis. A case report. *Acta Cytol* 2002; **46**: 545-549 [PMID: 12040651 DOI: 10.1159/000326875]

59 **Lin Y**, Shi Q, Zhou X. Hepatic monotypic epithelioid angiomyolipoma:two cases report and review of literature. *Zhenduan Binglixue Zazhi* 2002; **9**: 281-276 [DOI: 10.1016/S0731-7085(02)00079-1]

60 **Mai KT**, Yazdi HM, Perkins DG, Thijssen A. Fine needle aspiration biopsy of epithelioid angiomyolipoma. A case report. *Acta Cytol* 2001; **45**: 233-236 [PMID: 11284309 DOI: 10.1159/000327280]

61 **Croquet V**, Pilette C, Aubé C, Bouju B, Oberti F, Cervi C, Arnaud JP, Rousselet MC, Boyer J, Calès P. Late recurrence of a hepatic angiomyolipoma. *Eur J Gastroenterol Hepatol* 2000; **12**: 579-582 [PMID: 10833105 DOI: 10.1097/00042737-200012050-00018]

62 **Dalle I**, Sciot R, de Vos R, Aerts R, van Damme B, Desmet V, Roskams T. Malignant angiomyolipoma of the liver: a hitherto unreported variant. *Histopathology* 2000; **36**: 443-450 [PMID: 10792486 DOI: 10.1046/j.1365-2559.2000.00891.x]

63 **Flemming P**, Lehmann U, Becker T, Klempnauer J, Kreipe H. Common and epithelioid variants of hepatic angiomyolipoma exhibit clonal growth and share a distinctive immunophenotype. *Hepatology* 2000; **32**: 213-217 [PMID: 10915726 DOI: 10.1053/jhep.2000.9142]

64 **Savastano S**, Piotto M, Mencarelli R, Spanio P, Rubaltelli L. [A monotypic variant of hepatic angiomyolipoma completely composed of perivascular epithelioid cells. A case]. *Radiol Med* 2000; **100**:

79-81 [PMID: 11109461]
65 **Klompenhouwer AJ**, Verver D, Janki S, Bramer WM, Doukas M, Dwarkasing RS, de Man RA, IJzermans JNM. Management of hepatic angiomyolipoma: A systematic review. *Liver Int* 2017; **37**: 1272-1280 [PMID: 28177188 DOI: 10.1111/liv.13381]
66 **Guo B**, Song H, Yue J, Li G. Malignant renal epithelioid angiomyolipoma: A case report and review of the literature. *Oncol Lett* 2016; **11**: 95-98 [PMID: 26870174 DOI: 10.3892/ol.2015.3846]
67 **Neofytou K**, Famularo S, Khan AZ. PEComa in a Young Patient with Known Li-Fraumeni Syndrome. *Case Rep Med* 2015; **2015**: 906981 [PMID: 25821471 DOI: 10.1155/2015/906981]
68 **Vicens RA**, Jensen CT, Korivi BR, Bhosale PR. Malignant renal epithelioid angiomyolipoma with liver metastasis after resection: a case report with multimodality imaging and review of the literature. *J Comput Assist Tomogr* 2014; **38**: 574-577 [PMID: 24887578 DOI: 10.1097/RCT.0000000000000101]
69 **Nese N**, Martignoni G, Fletcher CD, Gupta R, Pan CC, Kim H, Ro JY, Hwang IS, Sato K, Bonetti F, Pea M, Amin MB, Hes O, Svec A, Kida M, Vankalakunti M, Berel D, Rogatko A, Gown AM, Amin MB. Pure epithelioid PEComas (so-called epithelioid angiomyolipoma) of the kidney: A clinicopathologic study of 41 cases: detailed assessment of morphology and risk stratification. *Am J Surg Pathol* 2011; **35**: 161-176 [PMID: 21263237 DOI: 10.1097/PAS.0b013e318206f2a9]
70 **Sato K**, Ueda Y, Tachibana H, Miyazawa K, Chikazawa I, Kaji S, Nojima T, Katsuda S. Malignant epithelioid angiomyolipoma of the kidney in a patient with tuberous sclerosis: an autopsy case report with p53 gene mutation analysis. *Pathol Res Pract* 2008; **204**: 771-777 [PMID: 18547741 DOI: 10.1016/j.prp.2008.04.008]
71 **Lin WC**, Wang JH, Wei CJ, Pan CC, Chang CY. Malignant renal epithelioid angiomyolipoma with aggressive behavior and distant metastasis. *J Chin Med Assoc* 2003; **66**: 303-306 [PMID: 12908574]

World Journal of Clinical Cases

Submit a Manuscript: https://www.f6publishing.com

World J Clin Cases 2019 April 26; 7(8): 984-991

DOI: 10.12998/wjcc.v7.i8.984

ISSN 2307-8960 (online)

CASE REPORT

Diagnosis of follicular lymphoma by laparoscopy: A case report

Cheng Wei, Feng Xiong, Zhi-Chao Yu, De-Feng Li, Ming-Han Luo, Ting-Ting Liu, Ying-Xue Li, Ding-Guo Zhang, Zheng-Lei Xu, Hong-Tao Jin, Qi Tang, Li-Sheng Wang, Jian-Yao Wang, Jun Yao

ORCID number: Cheng Wei (0000-0002-6373-1826); Feng Xiong (0000-0002-4021-0817); Zhi-Chao Yu (0000-0001-5123-9191); De-Feng Li (0000-0003-3118-6840); Ming-Han Luo (0000-0002-5056-3421); Ting-Ting Liu (0000-0002-1533-5220); Ying-Xue Li (0000-0001-6350-612X); Ding-Guo Zhang (0000-0001-7728-9672); Zheng-Lei Xu (0000-0002-5413-7390); Hong-Tao Jin (0000-0003-4143-5169); Qi Tang (0000-0001-5708-2850); Li-Sheng Wang (0000-0002-7418-6114); Jian-Yao Wang (0000-0003-1568-4479); Jun Yao (0000-0002-3472-1602).

Author contributions: Wei C, Xiong F, and Yu ZC contributed equally to this work; Wei C designed and wrote the report; Xiong F and Yu ZC reviewed the manuscript for its intellectual content and revised the entire work; Li DF and Luo MH performed the histological assessments and evaluations; Wang LS, Wang JY, and Yao J reviewed the manuscript for its intellectual content; all authors have read and approved the final manuscript.

Supported by The National Natural Science Foundation of China, No. 81800489; and Technical Research and Development Project of Shenzhen, No. JCYJ20170307100538697.

Informed consent statement: The patient involved in this study gave written informed consent authorizing the use and disclosure of his protected health information.

Conflict-of-interest statement: The authors of this manuscript have no conflicts of interest to disclose.

Cheng Wei, Feng Xiong, Zhi-Chao Yu, De-Feng Li, Ming-Han Luo, Ting-Ting Liu, Ying-Xue Li, Ding-Guo Zhang, Zheng-Lei Xu, Hong-Tao Jin, Qi Tang, Li-Sheng Wang, Jun Yao, Department of Gastroenterology, Jinan University of Second Clinical Medical Sciences, Shenzhen Municipal People's Hospital, Shenzhen 518020, Guangdong Province, China

Jian-Yao Wang, Department of General Surgery, Shenzhen Children's Hospital, Shenzhen 518026, Guangdong Province, China

Corresponding author: Jun Yao, PhD, Doctor, Department of Gastroenterology, Jinan University of Second Clinical Medical Sciences, Shenzhen Municipal People's Hospital, 1017 East Gate Road, Shenzhen 518020, Guangdong Province, China. yj_1108@126.com
Telephone: +86-755-22943322
Fax: +86-755-25533497

Abstract

BACKGROUND

Over the past years, only few cases of follicular lymphoma diagnosed by laparoscopy have been reported in the world. Since follicular lymphoma related ascites often causes occult disease and lacks specific clinical manifestations, it is often difficult to identify the cause by routine laboratory tests and imaging methods. Diagnostic experience is not sufficient and more cases need to be accumulated for further analysis.

CASE SUMMARY

Ascites due to unknown reasons often causes problems for clinical diagnosis and treatment. In this paper, we report one case with ascites in whom the reason causing ascites was not identified through routine examination. Laparoscopic examination of the celiac lesions and histological examination of the lesions were performed and the final diagnosis was peritoneal follicular lymphoma.

CONCLUSION

Laparoscopic abdominal examination is of great significance for the definite diagnosis of ascites due to an unknown reason.

Key words: Follicular lymphoma; Laparoscopy; Ascites; Case report

Core tip: Over the past years, only few cases of follicular lymphoma diagnosed by laparoscopy have been reported in the world. Since follicular lymphoma related ascites often causes occult disease and lacks specific clinical manifestations, it is often difficult

CARE Checklist (2016) statement: The authors have read the CARE Checklist (2016), and the manuscript was prepared and revised according to the CARE Checklist (2016).

Manuscript source: Unsolicited manuscript

Received: October 19, 2018
Peer-review started: October 22, 2018
First decision: November 27, 2018
Revised: January 28, 2019
Accepted: February 18, 2019
Article in press: February 18, 2019
Published online: April 26, 2019

P-Reviewer: Abadi ATB, Yamamoto K
S-Editor: Ji FF
L-Editor: Wang TQ
E-Editor: Wu YXJ

to identify the cause by routine laboratory tests and imaging methods. Diagnostic experience is not sufficient and more cases need to be accumulated for further analysis.

Citation: Wei C, Xiong F, Yu ZC, Li DF, Luo MH, Liu TT, Li YX, Zhang DG, Xu ZL, Jin HT, Tang Q, Wang LS, Wang JY, Yao J. Diagnosis of follicular lymphoma by laparoscopy: A case report. *World J Clin Cases* 2019; 7(8): 984-991
URL: https://www.wjgnet.com/2307-8960/full/v7/i8/984.htm
DOI: https://dx.doi.org/10.12998/wjcc.v7.i8.984

INTRODUCTION

Ascites is a clinical manifestation of many diseases and can be due to a variety of causes. Any pathological condition that results in an intraperitoneal fluid volume of more than 200 mL is called ascites. Since ascites often causes occult disease and lacks specific clinical manifestations, it is often difficult to identify the cause by routine laboratory tests and imaging methods. There are many causes of ascites, and the most common causes are cardiovascular diseases, liver diseases, peritoneal diseases, kidney diseases, connective tissue diseases, and malignant tumors. Identifying the cause of ascites plays a crucial role in the treatment and prognosis of patients. Laparoscopic examination of the abdominal cavity can observe intraperitoneal lesions and allows the pathological biopsy. Using this method, the diagnostic positive rate is high, the trauma is small, and the risk is low. It is very important to diagnose ascites cases due to unknown reasons[1]. Our department used laparoscopic abdominal examination and diagnosed a case of ascites caused by follicular lymphoma. The relevant case data are summarized as follows.

CASE PRESENTATION

General information

The patient (male, 60 years old) was admitted to our department in May 2017.

Chief complaints

Abdominal bloating for one month.

History of present illness

The patient presented abdominal distension without obvious inducement 1 month ago, and was aware that the abdominal distension was more obvious in a few days, which affected breathing and daily life. During the course of the disease, the patient had no diarrhea, abdominal pain, nausea, vomiting, fearlessness, cold, fever, or other discomfort. The patient had been hospitalized in other hospital before. Routine examination of blood in other hospital showed that white blood cell count was 11.5 × 10^9/L, lymphocyte ratio was 11.3%, and eosinophil count was 39.4%. Immune-related tests showed IgG 38.94 g/L, IgE 7250 g/L, and IgM 0.4 6 g/L. Urine is negative for Bence Jones protein. A full abdominal-pelvic computed tomography (CT) plain scan and three-dimensional reconstruction examination showed: (1) Wide nodular thickening of the peritoneum and multiple soft tissue masses in the abdominal cavity (considering malignant tumors with peritoneal metastasis and multiple lymph node metastasis); (2) The right liver lobe low perfusion area which suggested a possibility of metastases; (3) Mucosal thickening of the gastric antrum (it is recommended to perform gastroscopy); (4) A large amount of peritoneal effusion; and (5) Small renal cysts. Gastroscopy showed chronic non-atrophic gastritis with erosion. During hospitalization in other hospital, symptomatic treatments including absorbing ascites and diuretic treatment were provided. In order to facilitate further treatment, this patient was admitted to our hospital as "ascites to be diagnosed". Since the onset of the disease, the patient had a systemic rash accompanied by pruritus, which was diagnosed as "eczema" in the other hospital and the effect of drug treatment was poor. In recent 1 mo, the patient had normal defecation and urine, and was mentally stable, with poor appetite, poor sleep, and a weight loss of 10 kg.

History of past illness

The patient had a medical history of "hypertension" for 3 yr, without regular drug

treatment, and denied a chronic medical history of diabetes, coronary heart disease, and other diseases, an infectious medical history of hepatitis and tuberculosis, a medical history of surgery, blood transfusion, and trauma, and a history of drug allergy. The patient's history of preventive inoculation was unknown.

Personal and family history

The patient had a drinking history of 20 yr, about 250 mL liquor daily, and had been sober for 3 yr. The rest of the personal and family history sections were unexceptional.

Physical examination upon admission

Admission examination showed stable vital signs, visible multiple skin rashes, and itchy skin lesions after pruritus in mucous membranes without obvious abnormalities in heart and lung examinations. Abdominal distention with frog-like ventral appearance was observed. No obvious abnormalities in the liver, kidney and spleen were observed. Shifting dullness was positive. There was no obvious edema in both lower limbs.

Laboratory examinations

After admission, the relevant examinations were performed. Routine blood tests showed that the white blood cell count was 7.89 × 10^9/L, eosinophils accounted for 22.4%, and absolute eosinophil count was 1.77 × 10^9/L. High-sensitivity CRP was 12.7 mg/L, and procalcitonin was 0.17 ng/L. Biochemical tests showed that serum potassium was 3.2 mmol/L, serum sodium was 132.0 mmol/L, total protein was 99.5 g/L, albumin was 37.3 g/L, globulin was 62 g/L, immunoglobulin G was 46.04 g/L, IgG1 was 19.5 g/L, IgG4 was 5.93 g/L, and IgG 2 and IgG 3 were normal. Erythrocyte sedimentation rate was 47 mm/h, CA125 was 983.90 U/mL, coagulation function, renal function, hepatitis B, hepatitis C, syphilis, HIV test, tuberculosis immune examination, ANA series, anti-ENA antibody spectrum, vasculitis series, and other tests showed no obvious abnormalities. Ascites examination showed that it was yellow in color, slightly turbid, and qualitatively positive for mucin; the number of cells in ascites was 9829/μL, and the number of nucleated cells was 5829/μL (polymorphonuclear cells accounted for 8.1%, and mononuclear cells accounted for 91.9%). The total protein was 62.2 g/L, albumin was 22.1 g/L, globulin was 40.1 g/L, and adenosine deaminase was 15.9 U/L. CDC examination showed that Schistosoma IgG antibody was positive. Ascites bacteria, fungi, anaerobes, and mycobacteria culture and smears were negative. Ascites cytology showed that the smear had mesothelial cells, phagocytes, a large number of lymphocytes, and a small number of eosinophils.

Specialist examination

After the patient was admitted to the hospital, we performed gastrointestinal endoscopy and multi-point biopsy of the gastrointestinal mucosa. Gastroscopy revealed chronic superficial gastritis. Biopsy was performed for the gastric fundus, gastric body, gastric antrum, duodenal bulb, and duodenum descending area. Pathological diagnosis was chronic superficial gastritis in the fundus (eosinophil count < 20/HPF [high-power fields]); chronic superficial gastritis with intestinal metaplasia in gastric body (eosinophil count < 20/HPF); chronic superficial gastritis and focal glandular epithelial metaplasia in the gastric antrum (eosinophil count < 20/HPF), and chronic inflammation in the duodenal bulb and descending area (eosinophil count < 20/HPF) (Figure 1). Colonoscopy showed no obvious abnormalities in the ileum and colon mucosa. Multi-point biopsy by colonoscopy was performed in the distal ileum, ascending colon, transverse colon, descending colon, sigmoid colon, and rectum. Pathological diagnosis was chronic inflammatory changes in mucus (eosinophil count < 20/HPF) (Figure 2). The smear showed mesothelial cells, phagocytic cells, a large number of lymphocytes, and a small amount of eosinophils (Figure 3). The routine examination failed to identify the cause. In order to further diagnose, the patient completed laparoscopy with full communication and informed consent of the patient and her family. The patient underwent intravenous general anesthesia and tracheal intubation. Under the umbilicus, a long observation hole of about 10 mm was constructed, and pneumoperitoneum was built with the pressure of 12-14 mmHg. A laparoscope was placed through the sheath for examination. According to the nature and location of the lesion, two additional holes were made as surgical operation holes. Under the laparoscope, we found that the abdominal cavity was scattered with a large number of nodular lesions. Part of the omentum resection was sent for pathological examination. Histopathology showed that there was diffuse lymphoid cell infiltration in omentum tissues. Thus, we consider lymphoproliferative disease. Immunohistochemistry showed that there was lymphoid tissue hyperplasia that was closely arranged in a follicular shape. No

typical cuff structure was observed. Focal follicular fusion was observed. Central cells and centroblasts (>15/HPF) were seen in the follicles. Thus, we considered follicular lymphoma (grade 3a, follicular type) (Figure 4). Immunohistochemistry results showed CD20 (+), 20/HPF CD10 (+), Bcl-6 (+), Bcl-2 (-), CD3 (-), CD38, IgG, IgG4 (follicle cell plasma +), Ki-67 (60%), and CK (-) (Figure 5). After operation, the patient had no complications such as bleeding or infection. The final diagnosis was peritoneal follicular lymphoma. The patient was immediately transferred to the local hematology department for further treatment. The patient was followed once a month for 11 mo. He had no ascites and was generally in good condition currently.

FINAL DIAGNOSIS

Follicular lymphoma.

TREATMENT

We diagnosed the patient with ascites due to follicular lymphoma. After consultation with the Department of Hematology, the patient was transferred to the local hospital for further treatment. Since the patient was transferred to a local hospital, and the patient and his family members did not clearly describe the specific treatment plan, the emphasis was placed on the integrated treatment of traditional Chinese and Western medicine in the local hospital.

OUTCOME AND FOLLOW-UP

After 11 mo of follow-up, the patient's current condition was stable, and follicular lymphoma conversion was avoided.

DISCUSSION

Ascites is a common clinical manifestation. Common causes include cirrhosis, tuberculous peritonitis, and malignant tumors in the abdominal cavity. Cases with intractable ascites and/or ascites due to unknown reasons often have poor clinical outcomes or recurrent attacks, causing pain and increased medical burden to patients[2,3]. For clinically unexplained ascites, it is difficult to identify the cause relying only on clinical symptoms, serology, ascites puncture, cytology, ascites culture, imaging examination. This case in this report belongs to refractory ascites of unknown origin. Analysis of routine examination results, we first ruled out the possibility of tuberculous ascites and ascites due to cardiovascular, liver, kidney, and connective tissue diseases. This is because PPD test was negative, and chest X-ray findings were negative. Based on the patient's history, there was no tuberculosis. Hepatitis B surface antigen was negative, rheumatoid immunity, and vasculitis were negative, and heart and kidney functions were normal. We also ruled out the possibility of eosinophilic gastroenteritis. The patient's blood routine examination showed a significant increase in the ratio of lymphocytes and eosinophils. The CT performed in other hospital indicated mucosal thickening in the gastric antrum. We have improved gastrointestinal endoscopy and multi-point biopsy of the gastrointestinal tract, but the gastrointestinal mucosa pathology suggested that the eosinophil count was less than 20/HPF. In addition, during the course of treatment, the patient has a large amount of ascites, and ascites repeatedly occurred after drainage or diuretics treatment. Because the therapeutic effect was poor, it was possible to consider tumoral ascites. However, cytology of ascites did not identify tumor cells. We have seen a large number of lymphocytes in the patient's ascites, and we still consider the possibility of lymphoma. At the same time, the patient's abdominal-pelvic CT examination showed that the peritoneum had extensive nodular thickening, and multiple intra-abdominal soft tissue masses, leading to the consideration of the malignant tumor, peritoneal metastasis, and multiple lymph node metastasis. Finally, we decided to give patients laparoscopy to further confirm the diagnosis. The abdominal cavity was scattered with the nodular lesions and tissues were collected for biopsy during operation. Pathology indicated lymphoproliferative disorders. Immunohistochemistry indicated follicular lymphoma (grade 3a, follicular type). Finally, the patient was diagnosed with follicular lymphoma. We diagnosed the patient with ascites due to follicular lymphoma. After consultation with the Department of Hematology, the patient was

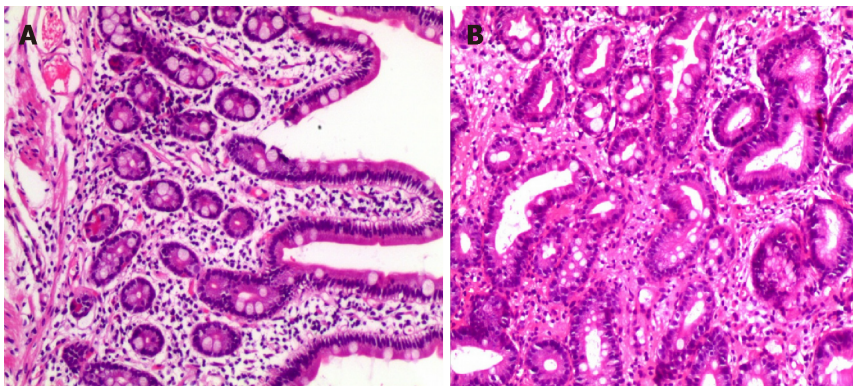

Figure 1 Pathological results of gastric biopsy. A: Visible mucosal glands are still well differentiated, with many lymphocytes and a small number of eosinophils infiltrating in the stroma observed under a light microscope (magnification, 100×); B: Mild intestinal metaplasia of mucosal glands and a small amount of interstitial lymphocyte, plasma cell, and eosinophil infiltration under a light microscope (magnification, 200×).

transferred to the local hospital for further treatment. After 11 mo of follow-up, the patient's current condition was stable, and follicular lymphoma conversion was avoided. In the diagnosis of follicular lymphoma-induced ascites, we had the following experience. First, the patient had large amounts of ascites with systemic skin pruritus and skin lesions, and there was no significant remission with common anti-histamine treatment. Second, blood tests suggested that eosinophils were elevated significantly; IgG and IgE levels were significantly elevated, especially IgE. Third, laparoscopy and the rapid diagnosis are of great value for the treatment and prognosis.

It has been reported that laparoscopy can increase the rate of diagnosis for ascites of unknown origin. Laparoscopy plays a critical role in diagnosing and differentially diagnosing ascites of unknown origin through biopsy of the lesion. In particular, laparoscopy has higher value for atypical cases[4,5]. First, abnormalities can be visually detected. It can observe the color, exudation, nodule, mass, and blood vessel distribution of the peritoneum in the parietal and visceral layers. Second, laparoscopic image enlargement function can detect miliary nodules with a diameter of 1-2 mm for small lesions with high resolution, while B-mode ultrasound, CT, and magnetic resonance imaging can only find lesions with a diameter of 1-2 cm or more. Third, it is highly targeted and has little damage. It can accurately take suspicious tissues to avoid damage to normal organs. Tissue biopsy can provide important evidence for treatment and prognosis.

When it is difficult to confirm the diagnosis through laboratory examinations and various imaging diagnostic techniques, laparoscopy shows its unique and accurate diagnostic effect, which can make up for the deficiencies of these examinations. Laparoscopic examination has fewer complications and less pain. It can not only directly observe normal organs and diseased tissues, but also can perform biopsy under direct vision and obtain evidence of medical examinations to assist treatment. Laparoscopy has been applied to the diagnosis of abdominal trauma, hepatitis, tuberculosis, ascites, abdominal masses, metastatic cancer in the abdominal cavity, and liver cancer. Laparoscopy can also be used for accurate staging of intra-abdominal malignancies, which can avoid unnecessary laparotomy.

Currently, there are very few peritoneal follicular lymphoma cases diagnosed by laparoscopy. Follicular lymphoma accounts for 22% of non-Hodgkin lymphomas in the world. The most common manifestation of follicular lymphoma is painless lymphadenopathy, typically characterized by multiple sites of lymphoid tissue invasion. Most patients do not have fever, night sweats, or weight loss[6,7]. A suitable biopsy evaluated by the hematology and pathology experts is sufficient to make a diagnosis of follicular lymphoma. Follicular lymphoma is one of malignant tumors that are most sensitive to chemotherapy and radiotherapy. Follicular lymphoma has a high rate of conversion to diffuse large B-cell lymphoma (7% per year).

About 40% of patients undergoing a repeat biopsy at some time during the course of the disease have been confirmed to have conversion, and almost all patients at the time of death had conversion. This conversion is often foreseen due to rapid lymph node growth and systemic symptoms such as fever, night sweats, and weight loss[8-10]. Laparoscopy is very useful for diagnosing ascites due to unexplained reasons, and it is sometimes important for determining the treatment plan for those patients and predicting the prognosis.

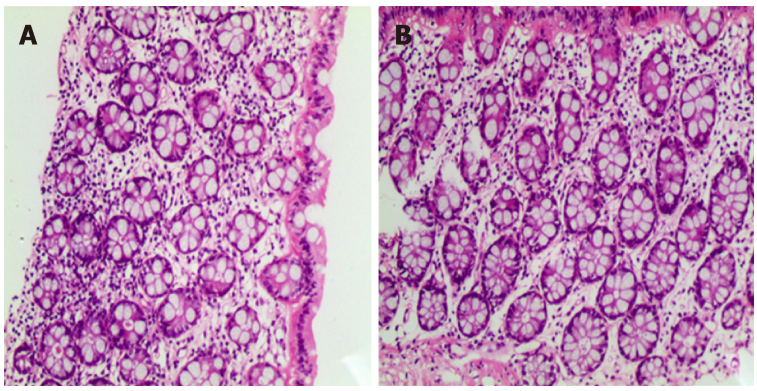

Figure 2 Pathological results of colon biopsy. A: The glandular differentiation is still good and there are many inflammatory cells infiltrating in the interstitial tissues (magnification, 100×); B: Large numbers of lymphocytes and a small amount of eosinophil infiltration (magnification, 200×).

CONCLUSION

Laparoscopic abdominal examination is of great significance for the definite diagnosis of ascites due to an unknown reason.

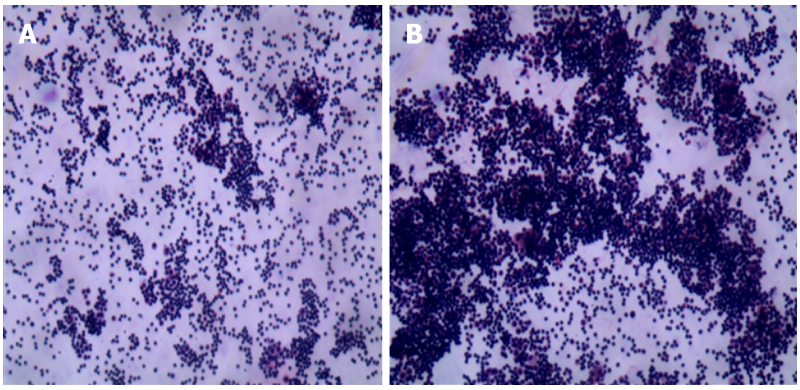

Figure 3 Cytology results of ascites. A: A large number of lymphocytes can be seen under a light microscope (magnification, 100×); B: A large number of lymphocytes are visible under a light microscope (magnification, 200×). The mesothelial cells, phagocytes, and a few eosinophils can be seen.

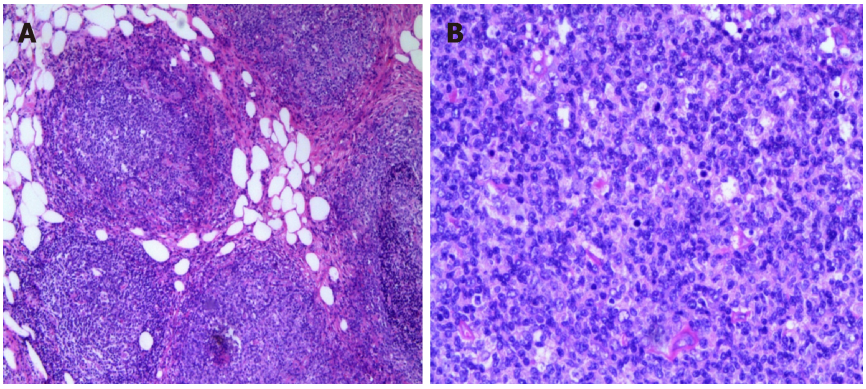

Figure 4 Omental histopathological examination. A: Lymphoid hyperplasia in omental adipose tissue; B: Some follicles were fused, and no typical cuff was observed. The follicular node was seen under a light microscope (magnification, 200×). The section consists of central cells and centroblasts, and the number of centroblasts is > 15/HPF.

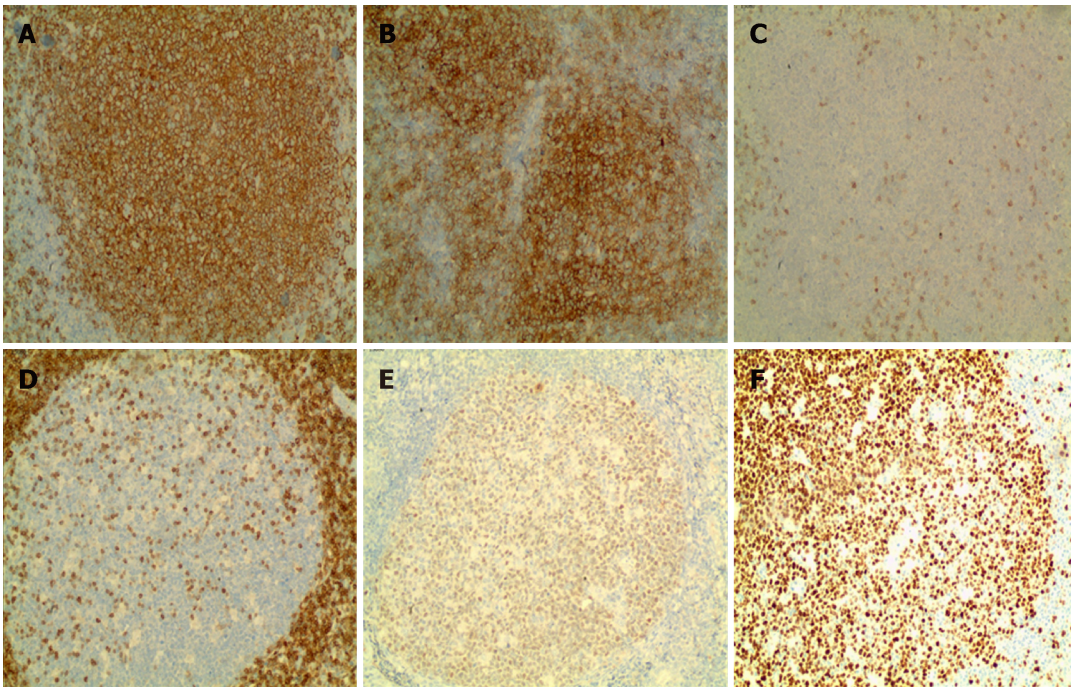

Figure 5 Results of omental immunohistochemistry (100×). A: Staining for CD20 is diffuse and strongly positive; B: Staining for CD10 is positive; C: Staining for CD3 is negative; D: Staining for Bcl-2 is negative; E: Staining for Bcl-6 is positive; F: Ki-67 positive rate is approximately 60%.

REFERENCES

1 **Bedioui H**, Ksantini R, Nouira K, Mekni A, Daghfous A, Chebbi F, Rebai W, Fteriche F, Jouini M, Kacem M, Ben Mami N, Filali A, Bensafta Z. Role of laparoscopic surgery in the etiologic diagnosis of exsudative ascites: a prospective study of 90 cases. *Gastroenterol Clin Biol* 2007; **31**: 1146-1149 [PMID: 18176376 DOI: 10.1016/S0399-8320(07)78354-9]

2 **ForŢofoiu MC**, Popescu DM, Pădureanu V, Dobrinescu AC, Dobrinescu AG, Mită A, Foarfă MC, Bălă VS, Muşetescu AE, Ionovici N, ForŢofoiu M. Difficulty in positive diagnosis of ascites and in differential diagnosis of a pulmonary tumor. *Rom J Morphol Embryol* 2017; **58**: 1057-1064 [PMID: 29250690]

3 **Caly WR**, Abreu RM, Bitelman B, Carrilho FJ, Ono SK. Clinical Features of Refractory Ascites in Outpatients. *Clinics (Sao Paulo)* 2017; **72**: 405-410 [PMID: 28792999 DOI: 10.6061/clinics/2017(07)03]

4 **Maeda S**, Yabuuchi J, Nobuta H, Makiishi T, Hirose K. Characteristics of Patients and Their Ascites Who Underwent Repeated Cell-Free and Concentrated Ascites Reinfusion Therapy. *Ther Apher Dial* 2015; **19**: 342-348 [PMID: 26386222 DOI: 10.1111/1744-9987.12343]

5 **Valle SJ**, Alzahrani NA, Alzahrani SE, Liauw W, Morris DL. Laparoscopic hyperthermic intraperitoneal chemotherapy (HIPEC) for refractory malignant ascites in patients unsuitable for cytoreductive surgery. *Int J Surg* 2015; **23**: 176-180 [PMID: 26475090 DOI: 10.1016/j.ijsu.2015.09.074]

6 **Seike T**, Inamura K, Okuno N, Asaumi Y, Takata Y, Okamura T, Matano S, Terahata S, Sakatoku K, Kawai H. [A case of gastric follicular lymphoma resected and diagnosed with laparoscopy and endoscopy cooperative surgery]. *Nihon Shokakibyo Gakkai Zasshi* 2017; **114**: 1996-2004 [PMID: 29109348 DOI: 10.11405/nisshoshi.114.1996]

7 **Prettyjohns M**, Hoskin P, McNamara C, Linch D; NICE non-Hodgkin Lymphoma Clinical Guideline Committee. The cost-effectiveness of immediate treatment or watch and wait with deferred chemotherapy for advanced asymptomatic follicular lymphoma. *Br J Haematol* 2018; **180**: 52-59 [PMID: 29076139 DOI: 10.1111/bjh.14990]

8 **Lackraj T**, Goswami R, Kridel R. Pathogenesis of follicular lymphoma. *Best Pract Res Clin Haematol* 2018; **31**: 2-14 [PMID: 29452662 DOI: 10.1016/j.beha.2017.10.006]

9 **Hess G**. The role of stem cell transplantation in follicular lymphoma. *Best Pract Res Clin Haematol* 2018; **31**: 31-40 [PMID: 29452664 DOI: 10.1016/j.beha.2017.10.009]

10 **Cheah CY**, Fowler NH. Novel agents for relapsed and refractory follicular lymphoma. *Best Pract Res Clin Haematol* 2018; **31**: 41-48 [PMID: 29452665 DOI: 10.1016/j.beha.2017.11.003]

World Journal of Clinical Cases

Submit a Manuscript: https://www.f6publishing.com

World J Clin Cases 2019 April 26; 7(8): 992-1000

DOI: 10.12998/wjcc.v7.i8.992

ISSN 2307-8960 (online)

CASE REPORT

Extranodal natural killer/T-cell lymphoma (nasal type) presenting as a perianal abscess: A case report

Yan-Ni Liu, Yong Zhu, Jia-Jun Tan, Guang-Shu Shen, Shu-Liang Huang, Chun-Gen Zhou, Shao-Hua Huangfu, Rui Zhang, Xiao-Bo Huang, Ling Wang, Qi Zhang, Bin Jiang

ORCID number: Yan-Ni Liu (0000-0002-8222-8951); Yong Zhu (0000-0003-3039-5413); Jia-Jun Tan (0000-0002-8944-1691); Guang-Shu Shen (0000-0003-0774-4953); Shu-Liang Huang (0000-0002-2760-0802); Chun-Gen Zhou (0000-0001-9111-7199); Shao-Hua Huangfu (0000-0002-4029-8759); Rui Zhang (0000-0002-3760-2174); Xiao-Bo Huang (0000-0002-9043-5651); Ling Wang (0000-0002-1967-844X); Qi Zhang (0000-0002-7048-6486); Bin Jiang (0000-0002-4622-9703).

Author contributions: Liu YN and Zhu Y contributed equally to this work; Liu YN, Tan JJ, Huangfu SH, Zhang R, Huang XB, and Wang L collected and analyzed the data, and drafted the manuscript; Shen GS and Zhang Q analyzed the results of diagnostic imaging; Huang SL and Zhou CG performed pathological evaluations; Liu YN, Zhu Y, and Jiang B wrote and revised the manuscript; all authors read and approved the final version of the manuscript.

Supported by the Nanjing Health Bureau Project, No. ZKX17034; Nanjing Traditional Chinese Medicine of Medical Conversion Base, No. ZHZD201802; and The 13th Five-Year Plan for Training Young Health Personnel in Nanjing, No. NWQR-201702.

Informed consent statement: The study was approved by the Medical Ethics Committee of The Nanjing Hospital of Chinese Medicine Affiliated to Nanjing University of Chinese Medicine,

Yan-Ni Liu, Chun-Gen Zhou, Rui Zhang, Xiao-Bo Huang, Ling Wang, Qi Zhang, Nanjing University of Chinese Medicine, Nanjing 210023, Jiangsu Province, China

Yong Zhu, Jia-Jun Tan, Shao-Hua Huangfu, Bin Jiang, Department of Colorectal Surgery, The Nanjing Hospital of Chinese Medicine Affiliated to Nanjing University of Chinese Medicine, Nanjing 2100022, Jiangsu Province, China

Guang-Shu Shen, Department of Pathology, The Nanjing Hospital of Chinese Medicine Affiliated to Nanjing University of Chinese Medicine, Nanjing 2100022, Jiangsu Province, China

Shu-Liang Huang, Department of Medical Imaging, The Nanjing Hospital of Chinese Medicine Affiliated to Nanjing University of Chinese Medicine, Nanjing 2100022, Jiangsu Province, China

Corresponding author: Bin Jiang, PhD, Chief Doctor, Director, National Center of Colorectal Disease, The Nanjing Hospital of Chinese Medicine Affiliated to Nanjing University of Chinese Medicine, Nanjing 2100022, Jiangsu Province, China. jbfirsth@aliyun.com
Telephone: +86-18951755051

Abstract

BACKGROUND

Extranodal natural killer (NK) T-cell lymphoma (ENKTL), nasal type is a rare subtype of extranodal non-Hodgkin lymphoma characterized by vascular damage and necrosis. The lesions usually present in the nasal cavity and adjacent tissues, however, the disease originates from the gastrointestinal or genitourinary tract in 25% of cases. Since rectal involvement in ENKTL is rare, rectal symptoms in the course of ENKTL are often misdiagnosed and considered to be related to benign diseases such as rectal fistula or perianal abscess.

CASE SUMMARY

We report the case of a 24-year-old Han Chinese female who initially presented with a perianal abscess that was subsequently diagnosed as nasal type ENKTL. Due to typical perianal pain, perianal abscess was diagnosed and surgical incision and drainage were performed. After recurrent, severe anal hemorrhages leading to hypovolemic shock and multiple surgeries, a diagnosis of ENKTL was made. The patient's condition gradually deteriorated, and she died shortly after initiation of chemotherapy.

CONCLUSION

and written informed consent was obtained from the family members of the patient.

Conflict-of-interest statement: All authors declare no conflict of interest.

CARE Checklist (2016) statement: This case report was written in accordance with the CARE (2016) guidelines.

Manuscript source: Unsolicited manuscript

Received: December 19, 2018
Peer-review started: December 19, 2018
First decision: January 19, 2019
Revised: February 21, 2019
Accepted: March 26, 2019
Article in press: March 26, 2019
Published online: April 26, 2019

P-Reviewer: Lazăr DC, Williams R
S-Editor: Gong ZM
L-Editor: Wang TQ
E-Editor: Wu YXJ

Systemic and neoplastic diseases should be included in the differential diagnosis of any potentially benign perianal abscess complicated with recurrent hemorrhages.

Key words: Extranodal natural killer T-cell lymphoma; Perianal abscess; Lymphoma; Rectal involvement; Case report

Core tip: The case highlights the need to include systemic and neoplastic diseases in the differential diagnosis of any potentially benign perianal abscess complicated with recurrent hemorrhages. A 24-year-old Han Chinese female, initially diagnosed with perianal abscess, underwent the surgical incision and drainage. The symptoms and the results of imaging, laboratory analysis, and colonoscopic biopsy were non-specific. After recurrent, severe anal hemorrhages leading to hypovolemic shock and multiple surgeries, a final diagnosis of extranodal natural killer/T cell lymphoma was made based on the result of histopathological examination. The patient's condition gradually deteriorated, and she died shortly after initiation of chemotherapy.

Citation: Liu YN, Zhu Y, Tan JJ, Shen GS, Huang SL, Zhou CG, Huangfu SH, Zhang R, Huang XB, Wang L, Zhang Q, Jiang B. Extranodal natural killer/T-cell lymphoma (nasal type) presenting as a perianal abscess: A case report. *World J Clin Cases* 2019; 7(8): 992-1000
URL: https://www.wjgnet.com/2307-8960/full/v7/i8/992.htm
DOI: https://dx.doi.org/10.12998/wjcc.v7.i8.992

INTRODUCTION

Extranodal nasal type NK/T-cell lymphoma (ENKTL), according to the 2016 revision of the World Health Organization classification of lymphoid neoplasms, is a type of invasive non-Hodgkin's lymphoma expressing NK cell (or less frequently T cell) markers. It is a rare disease that accounts for 2%-10% of malignant lymphomas and is most prevalent in Asia and South America[1]. It is most commonly observed in young and middle-aged males and the male to female ratio is about 2-4:1[2]. The nasal cavity is the most common primary site of ENKTL and adjacent tissues are often involved including the skin. Twenty-five percent of cases originate from extranasal tissues, including the gastrointestinal tract, lungs, skin, and testes. There have been only a few reports of ENKTL originating in the anorectal region.

Although the pathogenesis of ENKTL is not fully understood, it has been shown to be closely related to EBV infection[3,4]. The lesions are characterized by vascular invasion and destruction, significant necrosis, expression of cytotoxic molecules (*i.e.*, granzyme B, perforin, and T cell-restricted intracellular antigen-1 [TIA-1]), and Epstein-Barr virus (EBV) infection[5-8]. Typically, the cells are CD2 and CD56 positive, and surface CD3 negative[9-12]. Moreover, they are usually positive for cytotoxic molecules (such as granzyme B, TIA-1, and perforin), and negative for other T and NK cell-associated antigens, including CD4, CD5, CD8, CD16, and CD57[13-15].

While sinonasal ENKTL has a better prognosis than extranasal disease, its course is usually aggressive with rapid progression, and the prognosis is usually poor with a 5-year survival rate of approximately 30%[16] or even lower in more advanced stages[8,17,18]. Due to the non-specific symptoms, the disease is difficult to diagnose. Here we present a case of ENKTL in the rectum initially diagnosed and treated as a perianal abscess.

CASE PRESENTATION

Chief complaints

Anal discomfort for 22 d after surgery and fever for two days.

History of present illness

A 24-year-old female patient was admitted to our hospital for routine perianal abscess

incision and drainage surgery. The surgery was performed in January 2016. Thirteen days after the surgery, she was discharged in good condition. Twenty-two days after the discharge, the patient was readmitted to the hospital because of anal discomfort that started just after the discharge. Two days before readmission, the patient developed a fever.

History of past illness
The patient reported no past illnesses.

Personal and family history
The patient was previously healthy and her family history was unremarkable.

Physical examination upon admission
After admission, the doctor found that apart from a 2 cm surgical wound localized at the 6 o'clock position, a digital rectal examination revealed a prominent 3-4 cm lesion localized laterally from the surgical wound at the 7 o'clock position and extending upwards to the 11 o'clock position. Blood was present in the stool.

Laboratory examinations
Routine laboratory analysis showed leukocytosis with neutrophilia (white blood cells 16.12 × 10^9/L, 81.91% neutrophils); increased levels of inflammatory markers (C-reactive protein: 15.2 mg/L; prealbumin: 106.00 mg/L; albumin: 30.60 g/L; total protein: 48.20 g/L), cholinesterase (111.00 U/L), and creatine kinase (21.00 U/L).

Imaging examinations
Endorectal ultrasonography showed a hypoechoic area under the mucosa located 5 cm laterally from the 8-12 o'clock position of the anal margin in the anal canal. The mass was diagnosed as a submucosal infection. Enteroscopy showed hyperplasia and adhesions on the rectal mucosa at the margin of the perianal incision, which was diagnosed as proctitis. Biopsy samples were taken during endoscopy (Figure 1). Pathological examination revealed moderate to severe acute and chronic mucositis, inflammatory necrosis, and granulation tissue hyperplasia (Figure 2).

On days 3, 10, 16, and 23 of hospitalization, the patient underwent several anal exploration and hemostasis surgeries due to recurrent anal hemorrhage. The source of bleeding remained unidentified. Twenty-two days later, the patient was transferred to a secondary reference hospital for a laparoscopic assisted pelvic exploration and ileostomy. Excessive purulent secretions and necrotic tissue around the anus were observed in colonoscopy. In magnetic resonance imaging (MRI), thickening and edema of the rectum and external genital organs were observed along with multiple exudations and small lymph nodes around the rectum (Figure 3). After the surgery, continuous irrigations and drainage *via* an anal double cannula was performed. The patient was still feverish and suffered from very extensive, bloody discharge from the anus resulting in hypovolemic shock. Sigmoid colostomy with rectal and anal resection was suggested, but the patient did not consent to surgery and so after symptomatic treatment, she was discharged on request.

For the next 4 mo, the patient was treated conservatively in an outpatient clinic, however, the symptoms returned and the patient was readmitted to hospital. In addition to the perianal abscess, rectal vaginal fistula and inflammation of perianal tissue were diagnosed. On the seventh day of admission, the anorectal abscess was resected and the pelvic abscess was drained. A biopsy of the left inguinal lymph nodes was performed. Histopathological and immunohistochemical examinations showed the presence of CK (-), LCA (+), CD2 (+), CD3 (+), CD4 (-), CD5(-), CD8 (partial), CD56 (+), CD10 (-), CD20 (-), CD30 (partial), CD15 (-), CD79a (-), CD138 (-), CylinD1 (-), TIA (-), EMA (-), CD7 (-), granzyme B (+), perforin (+), and CD57 (-) cells that suggested a diagnosis of ENKTL (Figure 4). The Ki67 index was 65%.

Two weeks later, before the histopathological results were available, the patient was transferred to a tertiary reference hospital. The results of lymphocyte immunoassay are shown in Table 1.

FINAL DIAGNOSIS
A PET-CT scan performed after the transfer showed a thickened rectal wall, pathological mass in the perianal area with multiple exudations and gas in the peripheral fat space, enlarged spleen, pathological mass in the right nasal cavity, and thickened posterior wall of the trachea. In the scan range, the skin was irregularly thickened and high-density, subcutaneous shadows were visible (left neck, chest, abdomen, and left hip). Generalized lymphadenopathy (bilateral axillary, abdominal,

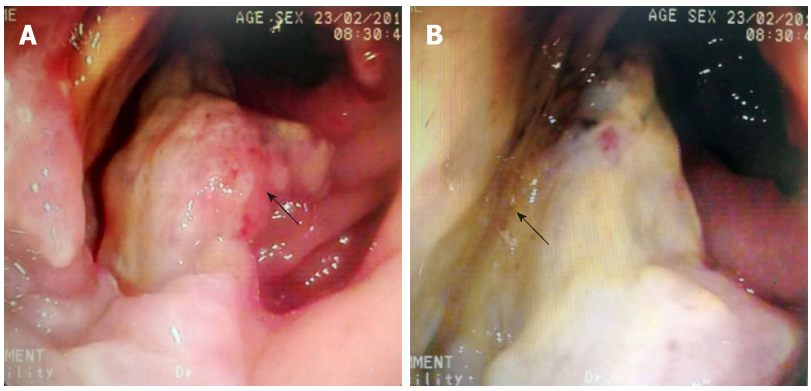

Figure 1 Colonoscopy images showing necrotic tissue and erosion at the edge of the anal margin (black arrows).

pelvic cavity, and left inguinal) was observed, in line with the diagnosis of lymphoma. In addition, signs of sinusitis and nodular foci of increased metabolism in left margin of L3 vertebral body and left iliac crest were visible (Figure 5). The images of nasopharyngeal biopsy were typical for ENKTL (Figure 6). Immunohistochemistry showed CD20 (-), CD3 (+), CD2 (+), CD56 (+), and TIA (+) cells with a Ki67 index of 90%. Fluorescent *in situ* hybridization showed the presence of EBV-encoded small RNAs (EBERs). A final diagnosis of stage IV ENKTL was made.

TREATMENT

Two weeks after the admission, COP chemotherapy was initiated (cyclophosphamide 1.3 g on day 1, vincristine 4 mg on day 1, and prednisone 50 mg b.i.d on days 1-5). However, on day 1, a massive anal hemorrhage resulting in hypovolemic shock occurred. As a result, chemotherapy was stopped and shock management including intravascular fluid therapy and blood transfusions were implemented. The patient's condition continued to deteriorate despite the treatment.

OUTCOME AND FOLLOW-UP

Three weeks later, the patient was transferred to Jiangbei People's Hospital for conservative maintenance therapy. Three days after the admission, continuous blood oozing from the anus was noted. Intravenous administration of a hemostatic agent (etamsylate and P-aminomethylbenzoic acid) was ineffective in stopping the bleeding. Coagulation panel showed activated partial thromboplastin time 58.40 s (reference value 20-40 s), fibrinogen 1.62 g/L (reference value 2-4 g/L), and D-dimer 2.94 μg/mL (reference value < 0.2 μg/mL). Because of suspected coagulopathy, daily infusions of red blood cells, cryoprecipitate, platelets, and plasma were introduced. Despite shock management, the patient's condition gradually deteriorated and she died 9 mo after presentation.

DISCUSSION

What could raise suspicion of ENKTL in a patient with typical symptoms of a common perianal abscess? The complicated postoperative course of the disease, including persistent fever and recurrent, massive anal hemorrhage resulting in hypovolemic shock not relieved after re-operation and antibiotic treatment, is not a typical course of perianal abscess and should prompt further diagnostic procedures[19]. However, as nasopharyngeal symptoms were not evident at the first admission and no abnormalities in imaging and routine laboratory analysis suggested a suspicion of systemic disease, malignancy was not included in the differential diagnosis at an early stage.

Pathological and immunohistochemical examinations of colonoscopy biopsies showed local inflammatory necrosis and inflammatory granulation tissue hyperplasia. This misleading result might be caused by the fact that routine colonoscopic biopsies are superficial and do not reach submucosal tissues potentially containing lymphoma

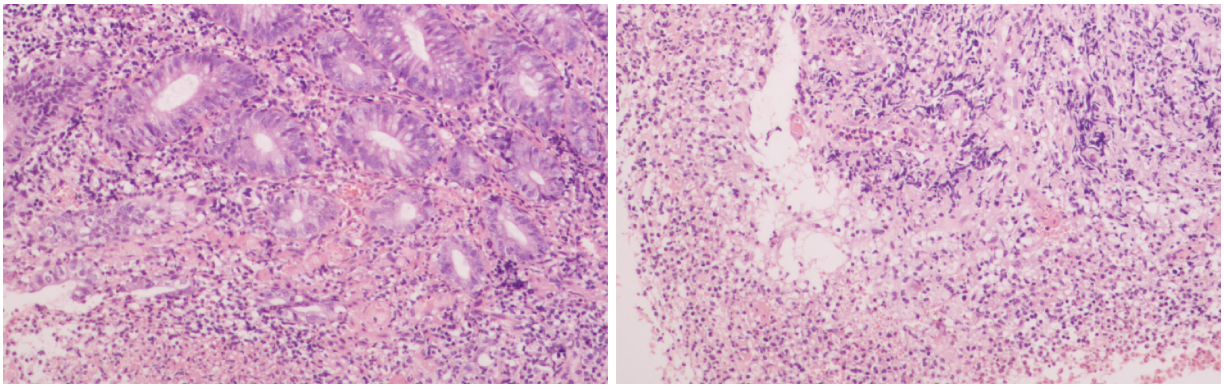

Figure 2 Histopathological examination showing moderate-severe acute and chronic inflammation with inflammatory necrosis and hyperplastic granulation tissue.

cells. Therefore, one could not suggest changing the primary diagnosis. In such cases, a deep tissue biopsy may improve the accuracy of the diagnosis.

In the anal canal, lymphoid tissue is accumulated around the anus where lymphoma cells may block the internal glands of the anus and cause perianal abscess formation. Therefore, in the cases of perianal disease with unexplained blood in the stool, fever, anemia, weight loss, and other systemic symptoms, timely biopsy may facilitate accurate diagnosis and allow initiation of adequate treatment[20,21]. In addition, full-body imaging can further reduce the risk of misdiagnosis.

Lymphoma cases presenting with a perianal abscess are very rare. Ninety percent of the anorectal abscesses are caused by acute infection of the anal glands. In the remaining cases, the abscess is formed as a result of other diseases such as inflammatory bowel disease, tuberculosis, or tumors. Gastrointestinal lymphoma is usually secondary to a wide range of lymph node diseases, and primary gastrointestinal lymphoma is relatively rare[22-24]. There are a few reports on lymphomas in the anorectal area, including ENKTL originating from the rectum. Kakimoto *et al*[25] reported a case of refractory ulcerative colitis presenting with colonic submucosal tumors histopathologically diagnosed as ENKTL. Valbuena *et al*[26] reported a case of a male who underwent rectal resection for clinical suspicion of carcinoma. After histopathologic examination, it was diagnosed as classical Hodgkin lymphoma (nodular sclerosis type) involving the rectum.

CONCLUSION

We present a rare case of fatal, disseminated ENKTL with rectal involvement in which a perianal abscess was initially suggested. Non-specific symptoms and results of imaging, laboratory analysis, and colonoscopic biopsy did not suggest systemic disease and consequently the final diagnosis was delayed. Therefore, a complicated course of surgical treatment, recurrent hemorrhages, and rapid deterioration of patient's condition should prompt further investigation, and systemic and neoplastic diseases should be included in the differential diagnosis of any potentially benign perianal abscess.

Table 1 Lymphocyte immunoassay results

	%
CD3	91.7
$CD3^+CD4^+$	49.8
$CD3^+CD8^+$	39.6
$CD3^+CD4^+/CD3^+CD8^+$	1.26
B cells	1.4
NK cells	5.1

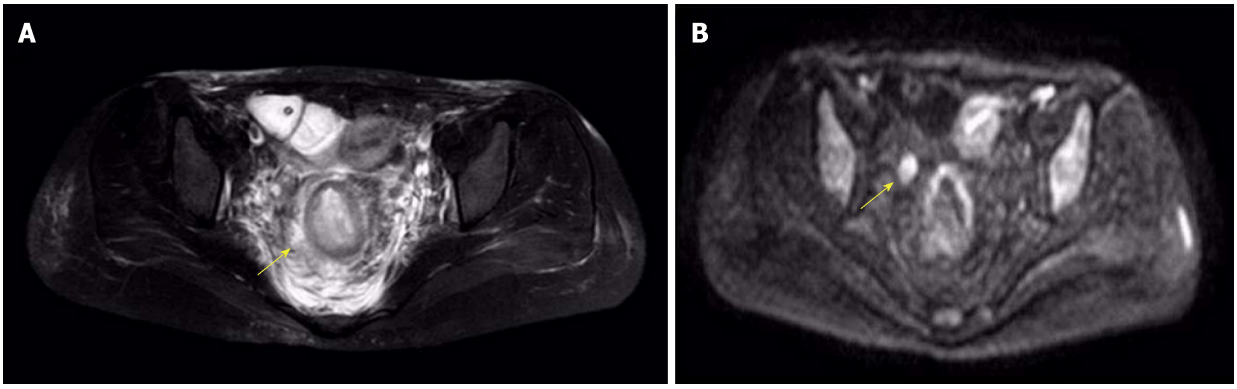

Figure 3 T2 liposuction magnetic resonance imaging demonstrated edema (A, yellow arrow) and enlarged lymph nodes (B, arrow) around the rectum on diffusion weighted imaging.

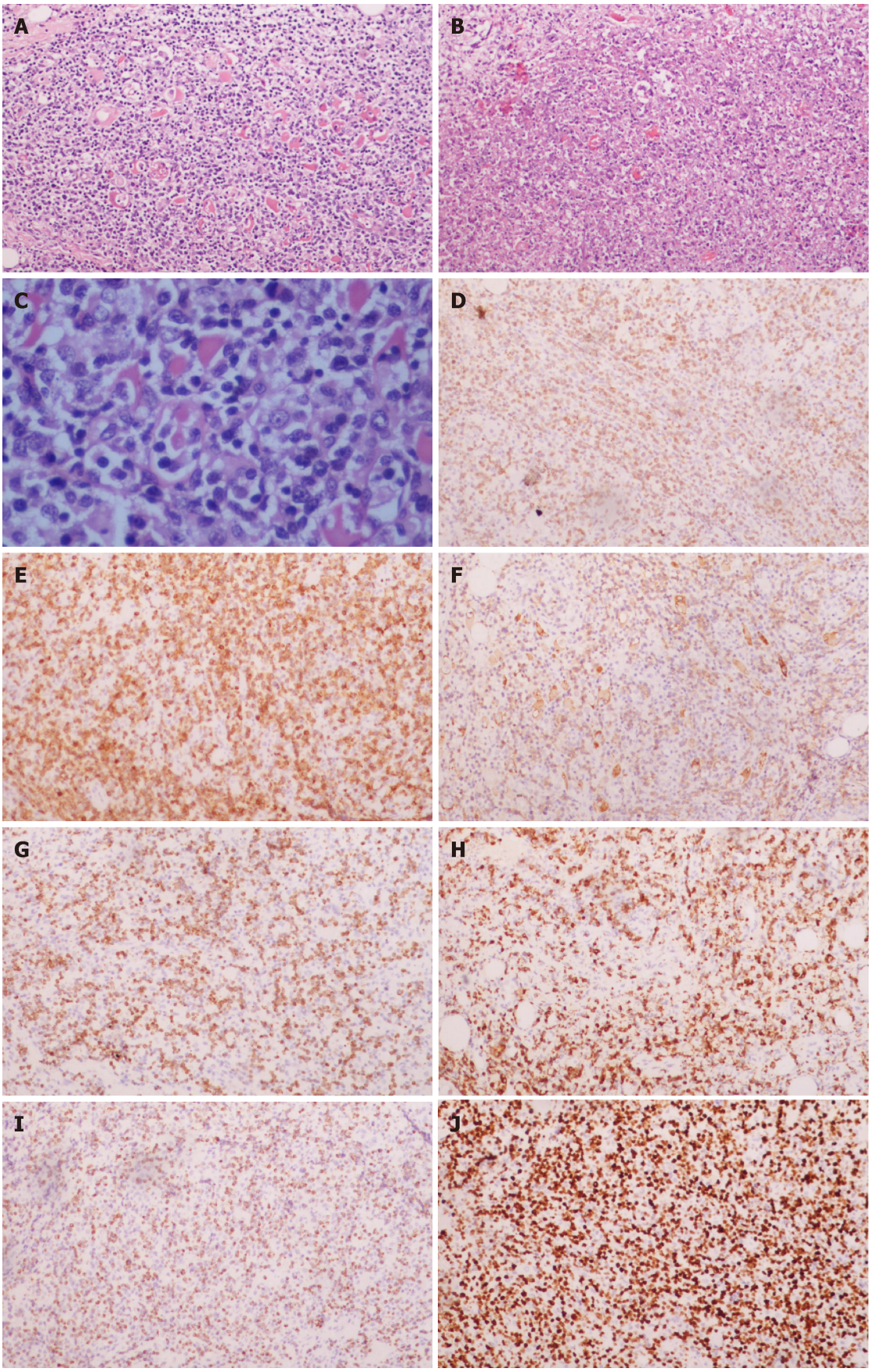

Figure 4 Histopathological and immunohistochemical examinations. A-C: Hematoxylin-eosin staining of tumor cells (A, 100× magnification, C, 400× magnification) and tumor-associated necrotic tissue (B, 100× magnification); D-J: immunohistochemical staining for CD2 (D), CD3 (E), CD56 (F), perforin (G), granzyme B (H), TIA-1 (I), and Ki-67 (J).

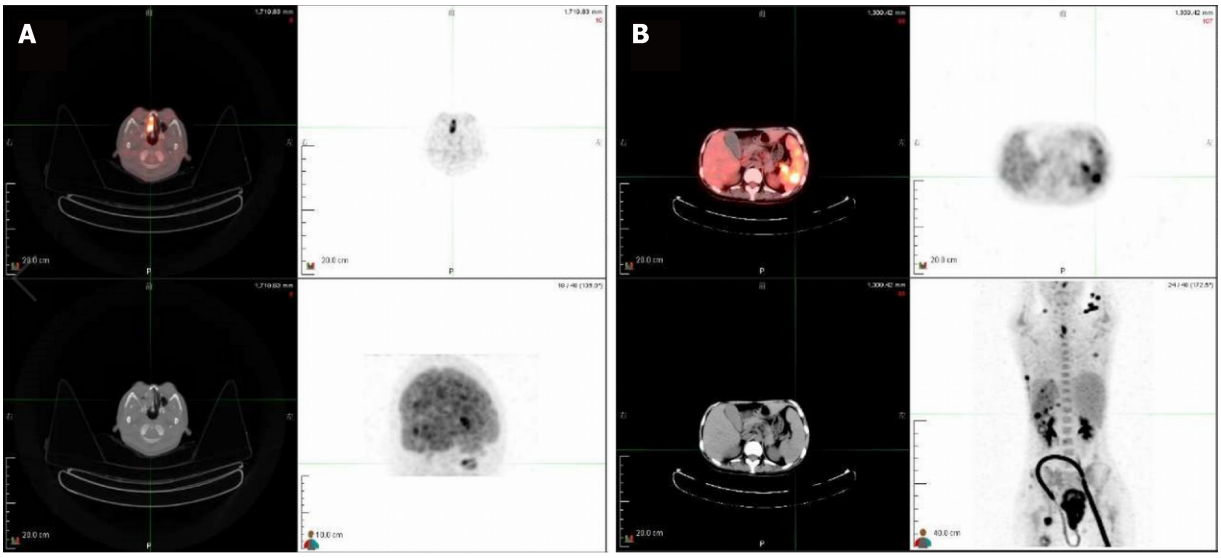

Figure 5 Positron emission tomography-computed tomography showing increased marker uptake in the kidneys (A) and nasopharyngeal area (B).

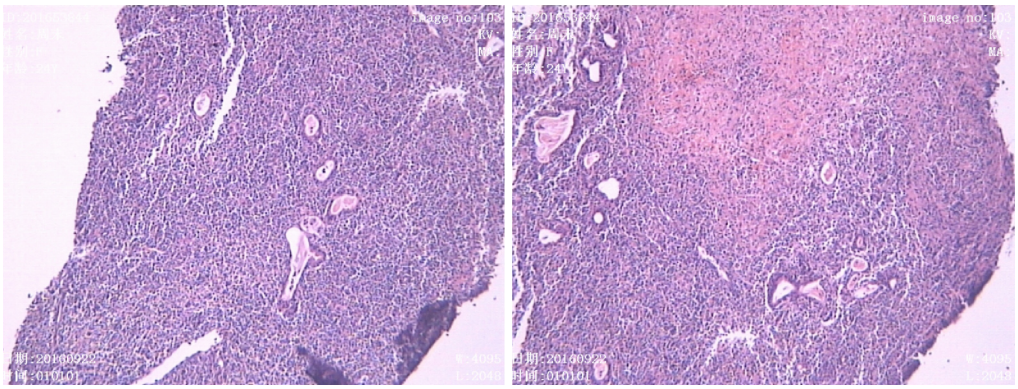

Figure 6 Small-to-moderate size lymphoid tissue hyperplasia with necrosis and apoptosis in nasal endoscopy biopsy.

REFERENCES

1 **Swerdlow SH**, Campo E, Pileri SA, Harris NL, Stein H, Siebert R, Advani R, Ghielmini M, Salles GA, Zelenetz AD, Jaffe ES. The 2016 revision of the World Health Organization classification of lymphoid neoplasms. *Blood* 2016; **127**: 2375-2390 [PMID: 26980727 DOI: 10.1182/blood-2016-01-643569]

2 **Li YX**, Fang H, Liu QF, Lu J, Qi SN, Wang H, Jin J, Wang WH, Liu YP, Song YW, Wang SL, Liu XF, Feng XL, Yu ZH. Clinical features and treatment outcome of nasal-type NK/T-cell lymphoma of Waldeyer ring. *Blood* 2008; **112**: 3057-3064 [PMID: 18676879 DOI: 10.1182/blood-2008-05-160176]

3 **Dobashi A**, Tsuyama N, Asaka R, Togashi Y, Ueda K, Sakata S, Baba S, Sakamoto K, Hatake K, Takeuchi K. Frequent BCOR aberrations in extranodal NK/T-Cell lymphoma, nasal type. *Genes Chromosomes Cancer* 2016; **55**: 460-471 [PMID: 26773734 DOI: 10.1002/gcc.22348]

4 **Sandell RF**, Boddicker RL, Feldman AL. Genetic Landscape and Classification of Peripheral T Cell Lymphomas. *Curr Oncol Rep* 2017; **19**: 28 [PMID: 28303495 DOI: 10.1007/s11912-017-0582-9]

5 **Tse E**, Kwong YL. Diagnosis and management of extranodal NK/T cell lymphoma nasal type. *Expert Rev Hematol* 2016; **9**: 861-871 [PMID: 27347812 DOI: 10.1080/17474086.2016.1206465]

6 **Au WY**, Weisenburger DD, Intragumtornchai T, Nakamura S, Kim WS, Sng I, Vose J, Armitage JO, Liang R; International Peripheral T-Cell Lymphoma Project. Clinical differences between nasal and extranasal natural killer/T-cell lymphoma: a study of 136 cases from the International Peripheral T-Cell Lymphoma Project. *Blood* 2009; **113**: 3931-3937 [PMID: 19029440 DOI: 10.1182/blood-2008-10-185256]

7 **Suzuki R**. Pathogenesis and treatment of extranodal natural killer/T-cell lymphoma. *Semin Hematol* 2014; **51**: 42-51 [PMID: 24468315 DOI: 10.1053/j.seminhematol.2013.11.007]

8 **Horwitz SM**, Ansell SM, Ai WZ, Barnes J, Barta SK, Choi M, Clemens MW, Dogan A, Greer JP, Halwani A, Haverkos BM, Hoppe RT, Jacobsen E, Jagadeesh D, Kim YH, Lunning MA, Mehta A, Mehta-Shah N, Oki Y, Olsen EA, Pro B, Rajguru SA, Shanbhag S, Shustov A, Sokol L, Torka P, Wilcox R, William B, Zain J, Dwyer MA, Sundar H. NCCN Guidelines Insights: T-Cell Lymphomas, Version 2.2018. *J Natl Compr Canc Netw* 2018; **16**: 123-135 [PMID: 29439173 DOI: 10.6004/jnccn.2018.0007]

9 **Li CC**, Tien HF, Tang JL, Yao M, Chen YC, Su IJ, Hsu SM, Hong RL. Treatment outcome and pattern of failure in 77 patients with sinonasal natural killer/T-cell or T-cell lymphoma. *Cancer* 2004; **100**: 366-375 [PMID: 14716773 DOI: 10.1002/cncr.11908]

10 **Huang YH**, Huang CT, Tan SY, Chuang SS. Primary gastric extranodal natural killer/T-cell lymphoma, nasal type, with acquisition of CD20 expression in the subcutaneous relapse: report of a case with literature review. *J Clin Pathol* 2015; **68**: 943-945 [PMID: 26142362 DOI: 10.1136/jclinpath-2015-203188]

11 **Yahalom J**, Illidge T, Specht L, Hoppe RT, Li YX, Tsang R, Wirth A; International Lymphoma Radiation Oncology Group. Modern radiation therapy for extranodal lymphomas: field and dose guidelines from the International Lymphoma Radiation Oncology Group. *Int J Radiat Oncol Biol Phys* 2015; **92**: 11-31 [PMID: 25863750 DOI: 10.1016/j.ijrobp.2015.01.009]

12 **Schorb E**, Finke J, Ferreri AJ, Ihorst G, Mikesch K, Kasenda B, Fritsch K, Fricker H, Burger E, Grishina O, Valk E, Zucca E, Illerhaus G. High-dose chemotherapy and autologous stem cell transplant compared with conventional chemotherapy for consolidation in newly diagnosed primary CNS lymphoma--a randomized phase III trial (MATRix). *BMC Cancer* 2016; **16**: 282 [PMID: 27098429 DOI: 10.1186/s12885-016-2311-4]

13 **Kim SJ**, Park S, Kang ES, Choi JY, Lim DH, Ko YH, Kim WS. Induction treatment with SMILE and consolidation with autologous stem cell transplantation for newly diagnosed stage IV extranodal natural killer/T-cell lymphoma patients. *Ann Hematol* 2015; **94**: 71-78 [PMID: 25082384 DOI: 10.1007/s00277-014-2171-4]

14 **Takata K**, Hong ME, Sitthinamsuwan P, Loong F, Tan SY, Liau JY, Hsieh PP, Ng SB, Yang SF, Pongpruttipan T, Sukpanichnant S, Kwong YL, Hyeh Ko Y, Cho YT, Chng WJ, Matsushita T, Yoshino T, Chuang SS. Primary cutaneous NK/T-cell lymphoma, nasal type and CD56-positive peripheral T-cell lymphoma: a cellular lineage and clinicopathologic study of 60 patients from Asia. *Am J Surg Pathol* 2015; **39**: 1-12 [PMID: 25188863 DOI: 10.1097/PAS.0000000000000312]

15 **Au WY**, Ma SY, Chim CS, Choy C, Loong F, Lie AK, Lam CC, Leung AY, Tse E, Yau CC, Liang R, Kwong YL. Clinicopathologic features and treatment outcome of mature T-cell and natural killer-cell lymphomas diagnosed according to the World Health Organization classification scheme: a single center experience of 10 years. *Ann Oncol* 2005; **16**: 206-214 [PMID: 15668271 DOI: 10.1093/annonc/mdi037]

16 **Vazquez A**, Khan MN, Blake DM, Sanghvi S, Baredes S, Eloy JA. Extranodal natural killer/T-Cell lymphoma: A population-based comparison of sinonasal and extranasal disease. *Laryngoscope* 2014; **124**: 888-895 [PMID: 24114591 DOI: 10.1002/lary.24371]

17 **Kirsch BJ**, Chang SJ, Le A. Non-Hodgkin Lymphoma Metabolism. *Adv Exp Med Biol* 2018; **1063**: 95-106 [PMID: 29946778 DOI: 10.1007/978-3-319-77736-8_7]

18 **Gill H**, Liang RH, Tse E. Extranodal natural-killer/t-cell lymphoma, nasal type. *Adv Hematol* 2010; **2010**: 627401 [PMID: 21234094 DOI: 10.1155/2010/627401]

19 **Wright WF**. Infectious Diseases Perspective of Anorectal Abscess and Fistula-in-ano Disease. *Am J Med Sci* 2016; **351**: 427-434 [PMID: 27079352 DOI: 10.1016/j.amjms.2015.11.012]

20 **Nelson RL**, Prasad ML, Abcarian H. Anal carcinoma presenting as a perirectal abscess or fistula. *Arch Surg* 1985; **120**: 632-635 [PMID: 3985803 DOI: 10.1001/archsurg.1985.01390290106019]

21 **Marti L**, Nussbaumer P, Breitbach T, Hollinger A. [Perianal mucinous adenocarcinoma. A further reason for histological study of anal fistula or anorectal abscess]. *Chirurg* 2001; **72**: 573-577 [PMID: 11383070 DOI: 10.1007/s001040170137]

22 **Primary gastrointestinal lymphomas**. *Lancet* 1977; **1**: 1191 [PMID: 68284 DOI: 10.1016/S0140-673677)92726-X]

23 **Inghirami G**, Chan WC, Pileri S; AIRC 5xMille consortium 'Genetics-driven targeted management of lymphoid malignancies'. Peripheral T-cell and NK cell lymphoproliferative disorders: cell of origin, clinical and pathological implications. *Immunol Rev* 2015; **263**: 124-159 [PMID: 25510275 DOI: 10.1111/imr.12248]

24 **Miyake MM**, Oliveira MV, Miyake MM, Garcia JO, Granato L. Clinical and otorhinolaryngological aspects of extranodal NK/T cell lymphoma, nasal type. *Braz J Otorhinolaryngol* 2014; **80**: 325-329 [PMID: 25183183 DOI: 10.1016/j.bjorl.2014.05.013]

25 **Kakimoto K**, Inoue T, Nishikawa T, Ishida K, Kawakami K, Kuramoto T, Abe Y, Morita E, Murano N, Toshina K, Murano M, Umegaki E, Egashira Y, Okuda J, Tanigawa N, Hirata I, Katsu K, Higuchi K. Primary CD56+ NK/T-cell lymphoma of the rectum accompanied with refractory ulcerative colitis. *J Gastroenterol* 2008; **43**: 576-580 [PMID: 18648746 DOI: 10.1007/s00535-008-2192-7]

26 **Valbuena JR**, Gualco G, Espejo-Plascencia I, Medeiros LJ. Classical Hodgkin lymphoma arising in the rectum. *Ann Diagn Pathol* 2005; **9**: 38-42 [PMID: 15692949 DOI: 10.1016/j.anndiagpath.2004.08.011]

World Journal of Clinical Cases

Submit a Manuscript: https://www.f6publishing.com

World J Clin Cases 2019 April 26; 7(8): 1001-1005

DOI: 10.12998/wjcc.v7.i8.1001

ISSN 2307-8960 (online)

CASE REPORT

Radiologic features of Castleman's disease involving the renal sinus: A case report and review of the literature

Xiao-Wan Guo, Xu-Dong Jia, Shan-Shan Shen, Hong Ji, Ying-Min Chen, Qian Du, Shu-Qian Zhang

ORCID number: Xiao-Wan Guo (0000-0002-8722-6680); Xu-Dong Jia (0000-0002-4193-1712); Shan-Shan Shen (0000-0001-9526-1227); Hong Ji (0000-0002-7949-4845); Ying-Min Chen (0000-0003-2413-3505); Qian Du (0000-0001-7274-949X); Shu-Qian Zhang (0000-0002-3750-382X).

Author contributions: Guo XW and Zhang SQ designed the research; Jia XD, Shen SS, Ji H, and Qian D collected and confirmed the data; Guo XW wrote the manuscript; Chen YM and Zhang SQ revised the manuscript.

Informed consent statement: Written informed consent was obtained from the patient for publication of this report.

Conflict-of-interest statement: All authors declare no conflicts of interest.

CARE Checklist (2016) statement: "Information for writing a case report" has been adopted.

Xiao-Wan Guo, Shan-Shan Shen, Hong Ji, Ying-Min Chen, Shu-Qian Zhang, Department of Radiology, Hebei General Hospital, Shijiazhuang 050051, Hebei Province, China

Xu-Dong Jia, Department of Urology, The Second Hospital of Hebei Medical University, Shijiazhuang 050051, Hebei Province, China

Qian Du, Department of Pathology, Hebei General Hospital, Hebei Province, Shijiazhuang 050051, Hebei Province, China

Corresponding author: Shu-Qian Zhang, MD, PhD, Chief Doctor, Doctor, Staff Physician, Department of Radiology, Hebei General Hospital, No. 348, Hepingxi Road, Xinhua District, Shijiazhuang 050051, Hebei Province, China. 1247225465@qq.com
Telephone: +86-311-85988016

Abstract

BACKGROUND

We present a rare case of plasma cell type of Castleman's disease (CD) involving only the right renal sinus in a 65-year-old woman with a duplex collecting system (DCS).

CASE SUMMARY

The patient presented with a right renal sinus lesion after renal ultrasonography. Subsequent abdominal enhanced computed tomography (CT) and magnetic resonance imaging (MRI) of the kidneys showed DCS and a soft tissue mass with mild enhancement at the lower right renal sinus. The lesion was suspected to be a malignant renal pelvic carcinoma. Hence, the patient underwent a right radical nephrectomy. Histological examination revealed hyperplastic lymphoid follicles in the renal sinus. A detailed review of the patient's CT and MRI images and a literature review suggested that the lesion was hypointense on T2-weighted images and hyperintense on diffusion-weighted image manifestations, and showed mild enhancement, which distinguished the plasma cell type of CD from many other renal sinus lesions. Furthermore, peripelvic soft tissue masses with a smooth internal surface of the renal pelvis were on imaging findings, which suggests that the urinary tract epithelial system is invulnerable and can be used to differentiate the plasma cell type of CD from malignant lymphoma with a focally growth pattern to some extent.

CONCLUSION

Preoperative diagnosis is often difficult in such cases, as plasma cell type of CD involving only the right kidney is exceedingly rare. However, heightened awareness of this disease entity and its radiographic presentations may alert one

Manuscript source: Unsolicited manuscript

Received: December 21, 2018
Peer-review started: December 23, 2018
First decision: January 12, 2019
Revised: January 31, 2019
Accepted: February 18, 2019
Article in press: February 18, 2019
Published online: April 26, 2019

P-Reviewer: Choi MR, Nechifor G, Ohashi N
S-Editor: Ji FF
L-Editor: Wang TQ
E-Editor: Wu YXJ

to consider this diagnosis.

Key words: Duplex collecting system; Castleman's disease; Plasma cell type; Renal sinus; Image; Case report

Core tip: We describe a rare case of plasma cell type of Castleman's disease (CD) involving only the right renal sinus in a 65-year-old woman with a duplex collecting system. The imaging findings and pathological features of CD involving the renal sinus are summarized in this literature review.

Citation: Guo XW, Jia XD, Shen SS, Ji H, Chen YM, Du Q, Zhang SQ. Radiologic features of Castleman's disease involving the renal sinus: A case report and review of the literature. *World J Clin Cases* 2019; 7(8): 1001-1005
URL: https://www.wjgnet.com/2307-8960/full/v7/i8/1001.htm
DOI: https://dx.doi.org/10.12998/wjcc.v7.i8.1001

INTRODUCTION

Castleman's disease (CD) is a rare benign lymphoproliferative disease, and its pathogenesis is still unclear. CD usually involves mediastinal lymph nodes. Extrathoracic presentations have rarely been described, with even fewer presentations in the kidneys. CD can be histologically classified into three types as follows: Hyaline vascular type, plasma cell type, and mixed type. Preoperative diagnosis by imaging examination is very difficult to differentiate the plasma cell type of CD from malignant lymphoma. Here, we report a case of plasma cell type CD with only renal sinuses involved. We hope to identify the imaging features that can help the preoperative qualitative diagnosis of this disease through a literature review. Our case is unique because it is the first report of CD presenting as sinus tumors in a patient with a duplex collecting system (DCS)

CASE PRESENTATION

Chief complaints

A 65-year-old woman showed right renal sinus lesions on renal ultrasonography performed as part of a healthy physical examination. Medical history was negative for symptoms of discomfort.

History of present illness

Her history was unremarkable.

Laboratory examinations

Laboratory findings showed mild liver dysfunction. Urinalysis findings were within normal limits, and urine cytology showed no evidence of malignancy. No obvious abnormality was found in other laboratory examinations. Normal blood flow to the left kidney and slightly decreased blood flow to the right kidney were noted on nephro-dynamic images.

Imaging examinations

DCS and a soft tissue mass with mild enhancement at the lower right renal sinus were detected after subsequent abdominal computed tomography (CT). Magnetic resonance imaging (MRI) revealed a homogeneous mass that was isointense on M3D Lava in-phase images and hypointense on T2-weighted images (T2WI). Diffusion-weighted images (DWI) showed a hyperintense mass (Figure 1).

FINAL DIAGNOSIS

The final diagnosis was CD of plasma cell type (Figure 2).

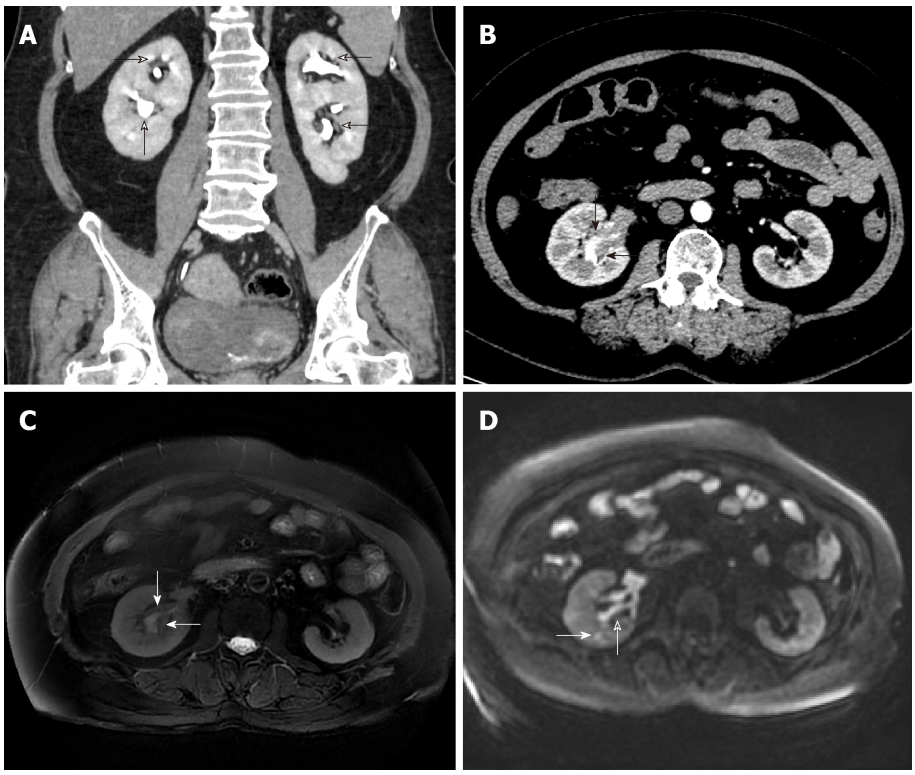

Figure 1 Plasma cell type of Castleman's disease involving the renal sinus and adjacent parenchyma in a 65-year-old woman. A: Coronal contrast-enhanced computed tomography (CT) image showing bilateral renal pelvis duplication; B: Axial contrast-enhanced CT image obtained at the renal hilum level shows mildly homogenous enhancement of a soft tissue mass in the right lower renal sinus; C: T2-weighted images (TR/TE, 10000/82.6) showing a soft tissue mass in the right renal sinus with slightly hypointense signals compared to that of the renal cortex; D: Diffusion-weighted images (b = 800 s/mm^2) showing that the mass (open arrow) is mildly hyperintense, and a hyperintensity lesion is in the renal parenchyma (solid arrow).

TREATMENT

The patient underwent a right radical nephrectomy. Histological examination revealed hyperplastic lymphoid follicles in the renal sinus and adjacent parenchyma. Immunohistochemical staining showed the following results: CD38 (+), CD138 (+), Kappa (+), Lambda (+), and CD21 (FDC+).

OUTCOME AND FOLLOW-UP

After treatment, thoracic and abdominal CT scans were used to determine whether the disease was multicentric. However, no enlarged lymph node or other lesions were found.

DISCUSSION

CD remains a rare and poorly understood disease characterized by massive growth of the lymphoid tissue. The renal sinus is an extremely unusual location for the manifestation of CD. The exact mechanism of CD in the renal sinus has not been reported thus far. Chronic low-grade inflammation, an immunodeficiency state, and autoimmunity have been proposed as probable mechanisms[1]. Patients with DCS are more susceptible to chronic inflammation, which is the probable cause of CD[2]. Our case supports chronic low-grade inflammation as a possible mechanism, although the exact cause of formation requires further study.

As far as we know, six articles on CD involving the renal sinus have been reported[3-8]. All lesions were confined to the renal sinus except in one case with a large range of lesions and retroperitoneal involvement. Six lesions in five cases were diagnosed as CD of plasma cell type, all of which were reported as case reports. Their imaging findings and pathological features are summarized in Table 1. In this table,

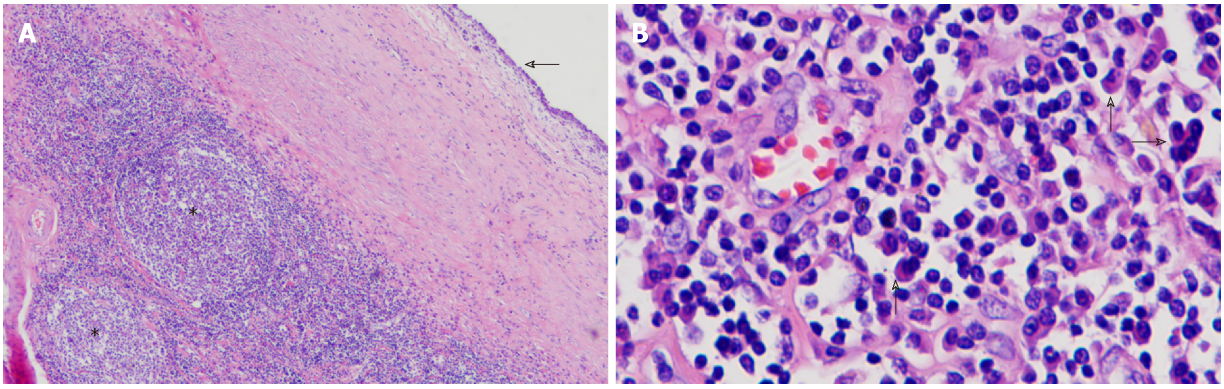

Figure 2 Histological examination of the right kidney in a 65-year-old woman. A: Photomicrograph (original magnification, 40×; hematoxylin-eosin staining) showing hyperplastic lymphoid follicles (asterisks) in renal sinus fat tissue below the normal renal pelvis (open arrow) in the lower right renal sinus; B: Interfollicular areas showing heavy staining.

the total number of patients with CD involvement of renal sinuses is six (seven lesions), including four males and two females, with an average age of 66 years. All of these patients presented homogeneous soft tissue density masses with mild enhancement, and the longest diameter less than 5 cm on CT image. Although the specific longest diameter of lesions was not given in some articles[4,5], the imaging data of lesions were given. Therefore, their size could be roughly obtained by comparison with the imaging data, in which the exact size of the lesions had been given. Four of these patients underwent MRI scans[4-6], showing isointense lesions on T1WI and hypointense lesions on T2WI, and two of these patients showed hyperintense lesions on DWI[4,5]. We believe that hypointensity on T2WI, hyperintensity on DWI manifestations, and mild enhancement can help us to distinguish the plasma cell type of CD from many renal sinus lesions, such as transitional cell carcinoma and renal sinus lymphoma. In most cases, the lesions of transitional cell carcinoma show high signal on T2WI, with unsmooth edges and hematuria as the most common clinical symptoms. However, it is still impossible to differentiate CD from renal sinus lymphoma by imaging alone. It also has lower signal intensity than a normal cortex with T1WI, and it is relatively iso- or hypointense in T2WI and hyperintense on DWI.

In Table 1, only one of the seven lesions showed complete occlusion of the collecting system[5], and the rest of the lesions showed slight dilatation of renal pelvis and calyces. Therefore, compensatory dilatation of the collecting duct system was considered to be caused by subcutaneous lymphocyte hyperplasia in the urinary tract. The pathology of three cases clearly indicated that the pelvic tumor was a benign lymphoproliferative lesion with widely scattered, hyperplastic lymphoid follicles, while the pelvic urothelium was intact, which was consistent with the smooth and nonfilling defect on the inner surface of the collection system from CT and MRI imaging[3,4]. Sheth *et al*[9] reported that the imaging findings of renal lymphoma are related to the tumor growth pattern. If malignant lymphocytes proliferate focally, single or multiple well-defined masses can be formed and adjacent urinary tract systems destroyed. However, if it follows an infiltrative growth pattern, then the size of the kidney may increase without damage to the basic structure, and the lesions may be quite small with ill-defined borders. Similar well-defined renal sinus masses have been found in reported cases. If they are considered renal sinus lymphoma, then their growth mode should be focal growth, which is bound to be accompanied by adjacent urinary tract destruction. In fact, three cases showed complete urinary tract epithelium under an electron microscope. Although the remaining four cases failed to provide pathological evidence, these cases all shared similar imaging features, which show smooth intrarenal pelvic lateral surfaces. Therefore, we speculated that the plasma cell type of CD, due to its benign hyperplasia of lymphoid pathological, may not show epithelial invasion like lymphoma. We believe the imaging findings of the plasma cell type of CD, showing peripelvic soft tissue masses and a smooth internal surface of the renal pelvis, suggest that the urinary tract epithelial system is invulnerable. It can be used to differentiate the plasma cell type of CD from malignant lymphoma with a focal growth pattern. However, it is just a speculation and more cases are needed to verify it. Since the treatment of CD is different from that of lymphoma, the preoperative diagnosis of CD involving renal sinus will affect the choice of clinical treatment.

Table 1 Clinicopathological and imaging characteristics of previously reported cases of plasma cell type of Castleman's disease with renal sinus involvement

Ref.	Jang *et al*[3]	Kin *et al*[4]	Nagahama *et al*[5]	Nishie *et al*[6]		Present
Sex	M	M	M	M	F	F
Age (yr)	64	59	79	70	65	62
Sinus	Left	Left	Left	Bilateral	Unilateral	Right
MRI						
T1WI	N/A	Isointense	Isointense	N/A	Isointense	Isointense
T2WI	N/A	Hypointense	Hypointense	N/A	Hypointense	Hypointense
DWI	N/A	Hyperintense	N/A	N/A	N/A	Hyperintense
CT size (cm)	2.5-4	N/A	N/A	3.0-4.5		2.8-4.5
Enhancement	Mild	Mild	Mild	Mild	Mild	Mild
Clear boundary	Yes	Yes	Yes	Yes	Yes	Yes
Hydronephrosis	Mild	Mild	Mild	Mild	Mild	Mild
Urothelium intact	Yes	Yes	N/A	N/A	N/A	Yes

M: Male; F: Female; N/A: Not available; Sinus: The lesion in the renal sinus; T2WI: T2-weighted images; DWI: Diffusion-weighted images; CT: Computed tomography; MRI: Magnetic resonance imaging; T1WI: T1-weighted images.

CONCLUSION

In conclusion, our case suggests that a patient with a DCS may have a risk of suffering CD due to his or her susceptibility to chronic inflammation, and imaging findings of the plasma cell type of CD, showing hypointensity on T2WI, hyperintensity on DWI, peripelvic soft tissue masses, and a smooth internal surface of the renal pelvis, are important to the preoperative diagnosis of CD of plasma cell type involving only the renal sinus.

REFERENCES

1 CASE RECORDS of the Massachusetts General Hospital: Case No. 40381. *N Engl J Med* 1954; **251**: 529-534 [PMID: 13203737 DOI: 10.1056/NEJM195409232511307]
2 **Fernbach SK**, Feinstein KA, Spencer K, Lindstrom CA. Ureteral duplication and its complications. *Radiographics* 1997; **17**: 109-127 [PMID: 9017803 DOI: 10.1148/radiographics.17.1.9017803]
3 **Jang SM**, Han H, Jang KS, Jun YJ, Lee TY, Paik SS. Castleman's disease of the renal sinus presenting as a urothelial malignancy: a brief case report. *Korean J Pathol* 2012; **46**: 503-506 [PMID: 23136580 DOI: 10.4132/KoreanJPathol.2012.46.5.503]
4 **Kim TU**, Kim S, Lee JW, Lee NK, Jeon UB, Ha HG, Shin DH. Plasma cell type of Castleman's disease involving renal parenchyma and sinus with cardiac tamponade: case report and literature review. *Korean J Radiol* 2012; **13**: 658-663 [PMID: 22977337 DOI: 10.3348/kjr.2012.13.5.658]
5 **Nagahama K**, Higashi K, Sanada S, Nezumi M, Itou H. [Multicentric Castleman's disease found by a renal sinus lesion: a case report]. *Hinyokika Kiyo* 2000; **46**: 95-99 [PMID: 10769797]
6 **Nishie A**, Yoshimitsu K, Irie H, Aibe H, Tajima T, Shinozaki K, Nakayama T, Kakihara D, Naito S, Ono M, Muranaka T, Honda H. Radiologic features of Castleman's disease occupying the renal sinus. *AJR Am J Roentgenol* 2003; **181**: 1037-1040 [PMID: 14500225 DOI: 10.2214/ajr.181.4.1811037]
7 **Nolan RL**, Banerjee A, Idikio H. Castleman's disease with vascular encasement and renal sinus involvement. *Urol Radiol* 1988; **10**: 173-175 [PMID: 3072749 DOI: 10.1007/bf02926523]
8 **Park JB**, Hwang JH, Kim H, Choe HS, Kim YK, Kim HB, Bang SM. Castleman disease presenting with jaundice: a case with the multicentric hyaline vascular variant. *Korean J Intern Med* 2007; **22**: 113-117 [PMID: 17616028 DOI: 10.3904/kjim.2007.22.2.113]
9 **Sheth S**, Ali S, Fishman E. Imaging of renal lymphoma: patterns of disease with pathologic correlation. *Radiographics* 2006; **26**: 1151-1168 [PMID: 16844939 DOI: 10.1148/rg.264055125]

Published By Baishideng Publishing Group Inc
7041 Koll Center Parkway, Suite 160, Pleasanton, CA 94566, USA
Telephone: +1-925-2238242
Fax: +1-925-2238243
E-mail: bpgoffice@wjgnet.com
Help Desk:https://www.f6publishing.com/helpdesk
https://www.wjgnet.com